

University of Alberta

MODEL-BASED CONTROL OF CATALYTIC REACTORS WITH REVERSE FLOW
OPERATION

by

Adrian Matias Fuxman ©

A thesis submitted to the Faculty of Graduate Studies and Research in partial fulfillment of the requirements for the degree of **Doctor of Philosophy**.

in

Chemical Engineering

Department of Chemical and Materials Engineering

Edmonton, Alberta
Fall 2008



Library and
Archives Canada

Published Heritage
Branch

395 Wellington Street
Ottawa ON K1A 0N4
Canada

Bibliothèque et
Archives Canada

Direction du
Patrimoine de l'édition

395, rue Wellington
Ottawa ON K1A 0N4
Canada

Your file Votre référence
ISBN: 978-0-494-46319-2
Our file Notre référence
ISBN: 978-0-494-46319-2

NOTICE:

The author has granted a non-exclusive license allowing Library and Archives Canada to reproduce, publish, archive, preserve, conserve, communicate to the public by telecommunication or on the Internet, loan, distribute and sell theses worldwide, for commercial or non-commercial purposes, in microform, paper, electronic and/or any other formats.

The author retains copyright ownership and moral rights in this thesis. Neither the thesis nor substantial extracts from it may be printed or otherwise reproduced without the author's permission.

AVIS:

L'auteur a accordé une licence non exclusive permettant à la Bibliothèque et Archives Canada de reproduire, publier, archiver, sauvegarder, conserver, transmettre au public par télécommunication ou par l'Internet, prêter, distribuer et vendre des thèses partout dans le monde, à des fins commerciales ou autres, sur support microforme, papier, électronique et/ou autres formats.

L'auteur conserve la propriété du droit d'auteur et des droits moraux qui protègent cette thèse. Ni la thèse ni des extraits substantiels de celle-ci ne doivent être imprimés ou autrement reproduits sans son autorisation.

In compliance with the Canadian Privacy Act some supporting forms may have been removed from this thesis.

Conformément à la loi canadienne sur la protection de la vie privée, quelques formulaires secondaires ont été enlevés de cette thèse.

While these forms may be included in the document page count, their removal does not represent any loss of content from the thesis.

Bien que ces formulaires aient inclus dans la pagination, il n'y aura aucun contenu manquant.

■+■
Canada

This thesis is dedicated to...

Natalia

Abstract

Dynamic operation of catalytic reactors has attracted increasing attention in recent years. The most successful application of this type of reactors is based on a reverse flow operation, where the dynamic operation improves the overall thermal efficiency of the system. The design and modeling of catalytic reactors with reverse flow operation has been thoroughly investigated; however, control of such systems is an area that has not received much attention. Issues such as the distributed nature of the state variables, the nonlinear dynamics and the unsteady-state operation make the formulation of a controller for this type of systems a challenging but interesting problem.

The goal of this thesis is twofold: firstly, the development of control strategies for catalytic reverse flow reactors is studied. Particular emphasis is put on the application of the reactor for mitigation of lean methane emissions. Secondly, the development of measures to quantify the nonlinearity in distributed parameter systems and, in particular, quasi-linear hyperbolic partial differential equations models. Such nonlinearity measures are intended for assessment of the suitability of linear control for such systems.

To formulate control strategies for catalytic flow reversal reactors (CFRR), optimal control techniques were used. On a practical side, a Model Predictive Control (MPC) scheme was employed. On a theoretical side, LQ-feedback control for infinite dimensional systems was used.

The control strategies were applied to a CFRR for the combustion of fugitive methane emissions. The CFRR technology has been successfully tested in underground coal mine applications, and its use in the oil and gas sector in Canada and around the world shows great promise. Outstanding issues to resolve include optimization of reactor design and development of suitable control strategies. It is expected that with the tools developed in this research, we will get closer to a successful control technique that can be used for a safe, stable and efficient operation of CFRR units.

One of the main issues in developing a control scheme for a catalytic reactor or any other distributed parameter system is the nonlinear dynamics. While published results in this area of quantification of process nonlinearity are limited to lumped parameter systems, this thesis focus on distributed parameter systems. Specifically, we look at means of open- and closed-loop nonlinearity quantification for systems modeled by quasi-linear hyperbolic partial differential equations.

Acknowledgements

I would like to express my gratitude to my supervisors, Dr. Fraser Forbes and Dr. Robert Hayes, whose expertise, understanding, and patience, made my years at the University of Alberta a great experience. I would like to thank them for giving me the opportunity to participate in various international conferences. I am specially thankful to Dr. Forbes, who gave me the opportunity to teach a senior undergraduate student course in the Chemical and Materials Engineering Department the University of Alberta.

A very special thanks goes out to Dr. Ilyasse Aksikas, without whose motivation and knowledge I would not have considered my involvement in the area of functional analysis and infinite dimensional systems. I would also like to express my gratitude to Rajab Litto for the excellent discussions about catalytic flow reversal reactors. I must also acknowledge Bob Burton for his patience and technical assistance with the computer systems.

Appreciation also goes out to the good friends that I made at the University of Alberta, Hailei Jiang, Ruoyu Cheng and Enayet Halim and my excellent officemates, Youtong Qi, Rumana Sharmin, Feng Huei and Xing Huan.

I would also like to thank Natalia for her invaluable support throughout all these years. Her words of support and her patience were key for me to finish this thesis. Lastly, I would like to thank my family, Miguel, Silvia, Diego and Ariel for their support and in particular, I must acknowledge my brother, Ariel, for his great advice throughout these years.

Contents

1	Introduction	1
1.1	Scope and Objectives	2
1.2	Thesis Outline	3
2	Modelling of Catalytic Flow Reversal Reactors	5
2.1	Global Warming and Methane Emissions	6
2.2	Combustion of Fugitive Methane Emissions	8
2.3	Background of Reverse Flow Operation of Catalytic Reactors	10
2.4	Applications of Reverse Flow Catalytic Reactors	11
2.5	Heat Recovery from Fugitive Methane Emissions	12
2.6	Mathematical Modelling	14
2.7	Reactor Configuration	15
2.8	Contributions	16
2.9	Modelling Reactor Dynamics	18
2.9.1	Heterogeneous Model	18
2.9.2	Pseudo-homogeneous Model	20
2.10	Classification of Partial Differential Equation Models	23
2.11	Computer Simulation	26
2.11.1	Model Validation	28
2.11.2	Parametric Analysis	28
2.11.3	Dynamical Analysis of the Heterogeneous Model	33
2.11.4	Validation of the Pseudo-Homogeneous Model	40
2.12	Empirical Modelling	43

2.13	Summary	46
3	Model Predictive Control of a Catalytic Flow Reversal Reactor	48
3.1	Model Predictive Control: Background	48
3.2	Model Predictive Control for Catalytic Flow Reversal Reactors	50
3.3	Contributions	54
3.4	Control Objectives	54
3.5	Selection of Controlled Variables	55
3.6	Selection of Manipulated Variables	57
3.7	MPC Controller Formulation	58
3.8	Method of Characteristics	59
3.8.1	2-Characteristics Model	62
3.8.2	1-Characteristic Model	64
3.8.3	MPC problem formulation	65
3.9	Controller Tuning	68
3.10	Numerical Simulations	70
3.10.1	Shrinking Horizon MPC with 2-Characteristics Internal Model	70
3.10.2	Receding Horizon MPC with 1-Characteristic Internal Model .	74
3.11	Dealing with Manipulated Variable Saturation	83
3.12	Summary	84
4	LQ-feedback Control of a Catalytic Flow Reversal Reactor	86
4.1	Introduction	87
4.2	Contributions	88
4.3	Background	88
4.3.1	Semigroup Theory	90
4.4	Stability Analysis of Infinite-Dimensional Systems	91
4.5	Linear Quadratic Regulator	92
4.5.1	LQ-Control of a Catalytic Flow Reversal Reactor	95
4.5.2	Dimensionless Model	95
4.5.3	Infinite Dimensional Linearized Model	97
4.6	Controller Design	99

4.7	Numerical Simulations	101
4.8	Summary	111
5	Open-Loop Nonlinearity Assessment for Hyperbolic PDE Models	113
5.1	Motivation	114
5.2	Introduction	114
5.3	Contributions	118
5.4	Nonlinearity Assessment based on Local Curvature	118
5.5	Classification of PDE systems	119
5.6	Open-Loop Nonlinearity Assessment for Hyperbolic PDE models . . .	120
5.6.1	Overall Measure of Curvature	130
5.7	Case Study: Plug-flow Reactor	131
5.8	Case Study: Catalytic Flow Reversal Reactor	137
5.9	Summary	141
6	Control Relevant Nonlinearity Assessment for Hyperbolic PDE Models	142
6.1	Introduction	143
6.2	Contributions	145
6.3	Control Relevant Nonlinearity Assessment of Hyperbolic PDE Models	146
6.4	Performance Sensitivity Measure	147
6.5	Case study: Chemical Tubular Reactor	153
6.6	Case study: Catalytic Flow Reversal Reactor	159
6.7	Summary	161
7	Conclusions and Recommendations	163
7.1	Conclusions	163
7.2	Recommendations	168
7.2.1	Modeling of Catalytic Flow Reversal Reactors	168
7.2.2	Control Design for CFRR units	168
7.2.3	Nonlinearity Assessment of Hyperbolic PDE	170

Bibliography	171
A Appendix A	181
A.1 Mathematical Model: Parameters	181
B Appendix B	186
B.1 Mathematical Background	186
B.2 Exponential Stability of a Linear Operator	189
B.3 LQ-Feedback Controller Formulation	190
C Appendix C	193
C.1 Feedback Control of Hyperbolic PDE Systems	193

List of Tables

2.1	Global atmospheric concentration, rate of concentration change, atmospheric lifetime and global warming potential of selected greenhouse gases.	7
2.2	Low (-1), mid-range (0) and high (+1) settings for the four factors. .	31
5.1	Model Parameters for the Tubular Reactor Model	132
A.1	Model Parameters used in the Heterogeneous Model of the Catalytic Reactor	181
A.2	Model Parameters used in the Pseudo-Homogeneous Model of the Catalytic Reactor	185
A.3	Model Coefficients	185

List of Figures

2.1	Illustration of the heat trap effect for reverse flow operation.	12
2.2	Illustration of various control measures for reverse flow catalytic reactor: (a) intermediate electrical heater, (b) intermediate heat exchanger, (c) hot or cold gas injection, (d) intermediate gas removal.	13
2.3	Pictures of different types of solid beds: ceramic monolith (left) and Denstone balls (right).	16
2.4	Pilot Reverse Flow Catalytic Reactor Unit.	17
2.5	Domain used to model the CFRR unit in COMSOL Multiphysics.	27
2.6	Comparison of the outputs from COMSOL (solid line) and FORTRAN (dashed line) simulators at $t = 5$ min for a reactor model without heat exchange in the open middle section. The initial conditions for both simulators are shown by the dashed-dot line.	29
2.7	Comparison of the outputs from COMSOL (solid line) and FORTRAN (dashed line) simulators at $t = 10$ min for a reactor model without heat exchange in the open middle section. The initial conditions for both simulators are shown by the dashed-dot line.	29
2.8	Comparison of the outputs from COMSOL (solid line) and FORTRAN (dashed line) simulators at $t = 5$ min for a reactor model with heat exchange in the open middle section. The initial conditions for both simulators are shown by the dashed-dot line.	30

2.9	Comparison of the outputs from COMSOL (solid line) and FORTRAN (dashed line) simulators at $t = 10$ min for a reactor model with heat exchange in the open middle section. The initial conditions for both simulators are shown by the dashed-dot line.	30
2.10	Stationary state mapping relating inlet reactant concentration Y_{f0} and mass extraction α to the maximum reactor temperature T_{max}	32
2.11	Stationary state mapping relating inlet superficial gas velocity $v_{s,in}$ and mass extraction α to the maximum reactor temperature.	33
2.12	Initial temperature distribution along the reactor centerline.	34
2.13	Evolution of the maximum and average temperature along the reactor centerline (top) and trajectory of the mass extraction from the reactor midsection (bottom).	35
2.14	Evolution of the temperature distribution along the reactor centerline.	35
2.15	Outlet methane conversion (top) and rate of energy removed from reactor midsection (E_{mid}) relative to the total energy fed to the reactor (E_{in}).	36
2.16	(Top) Evolution of the maximum and average temperature along the reactor centerline. (Bottom) trajectory of the inlet mole fraction of reactants.	37
2.17	(Top) Outlet methane conversion. (Bottom) Rate of energy removed from reactor midsection (E_{mid}) relative to the total energy fed to the reactor (E_{in}).	37
2.18	Evolution of the maximum and average temperature along the reactor centerline (top) and trajectory of the inlet superficial gas velocity (bottom).	38
2.19	Outlet methane conversion (top) and rate of energy removed from reactor midsection (E_{mid}) relative to the total energy fed to the reactor (E_{in}).	39
2.20	Start-up simulation for different switching times.	40

2.21	Outlet methane conversion (top) and rate of energy removed from reactor midsection (E_{mid}) relative to the total energy fed to the reactor (E_{in}).	40
2.22	Illustration of the CFRR unit used for simulation in the case studies. Inert Sections: solid support without any catalyst material; Active Section: solid support with a catalyst material	41
2.23	Distribution of the Peclet number along the reactor centerline. Solid line: Pe_m ; dashed-dot line Pe_h . Operating conditions: $v_{sin} = 0.3 m \cdot s^{-1}$, $T_{f0} = 298 K$, $Y_{f0} = 0.5 \%$ and $\alpha = 1$	42
2.24	Temperature difference between fluid and solid phase along the reactor centerline. Operating conditions: $v_{sin} = 0.3 m \cdot s^{-1}$, $T_{f0} = 298 K$, $Y_{f0} = 0.5 \%$ and $\alpha = 1$	43
2.25	Comparison between 1-D pseudo-homogeneous (dashed-dot line) model and 2-D heterogeneous model (solid line). Operating conditions: $v_{sin} = 0.3 m \cdot s^{-1}$, $T_{f0} = 298 K$, $Y_{f0} = 0.5 \%$, $\alpha = 1$ and $T_{cycle} = 10$ min.	44
2.26	2-D plot of the axial and radial temperature distribution T_s at the stationary state at the end of the semi-cycle and full cycle for $T_{cycle} = 20$ min (flow direction is indicated by the arrows).	44
2.27	2-D plot of the axial and radial temperature distribution T_s at the stationary state at the end of the semi-cycle and full cycle for $T_{cycle} = 10$ min (flow direction is indicated by the arrows).	45
3.1	Basic concept of Model Predictive Control	49
3.2	Initial curve \mathcal{J} and a characteristic \mathcal{C} on the integral surface \mathcal{S}	60
3.3	Illustration of the computation of future state variables using the method of characteristics	63
3.4	Spatial distribution of the temperature along the reactor centerline at stationary state. Solid line: temperature distribution at the beginning of the forward direction. Dashed line: temperature distribution at the beginning of the reverse direction.	71

3.5	Top: trajectory of the maximum (dashed-dot line) and average temperature (solid line) along the reactor centerline. Set-point trajectory is indicated by a dotted-line. Middle: trajectory of the disturbance, i.e. Y_{f0} . Bottom: trajectory of the manipulated variable $\alpha = u$	73
3.6	a) Trajectory of the maximum and average temperature along the reactor centerline; b) trajectory of the inlet mole fraction of reactant and c) trajectory of the manipulated variable, u . The dotted line in a) indicates the maximum allowable temperature.	76
3.7	a) Trajectory of the maximum and b) average temperature along the reactor centerline. c) Trajectory of the inlet mole fraction of reactant. d) Trajectory of the manipulated variable, $u = \alpha$. The dotted line in a) indicates the maximum allowable temperature. Solid lines: closed-loop simulation of MPC with maximum temperature constraint; dashed lines: closed-loop simulation of MPC without maximum temperature constraint.	78
3.8	Top: reactant conversion at $z/L = 1$. Bottom: ratio of the heat extracted from the reactor midsection and the total energy fed to the reactor.	79
3.9	a) Trajectory of the maximum temperature and b) trajectory of the average temperature. c) Trajectory of the disturbance (inlet gas velocity). c) Trajectory of the manipulated variable $\alpha = u$. The dotted-line in a) indicates the maximum allowable value for the temperature.	80
3.10	Top: reactant conversion at $z/L = 1$. Bottom: ratio of the heat extracted from the reactor midsection and the total energy fed to the reactor.	80
3.11	a) Trajectory of the maximum and average temperature for the set-point trajectory indicated by the dashed-line. The dotted-line indicates the maximum allowable value for the temperature. b) Trajectory of the manipulated variable $\alpha = u$	81

3.12	Top: reactant conversion at $z/L = 1$. Bottom: ratio of the heat extracted from the reactor midsection and the total energy fed to the reactor.	82
4.1	Top: temperature distributions at stationary state (solid lines) and initial temperature distribution for closed-loop numerical simulations (dashed-lines). Bottom: spatial distribution of the manipulated variable in the forward and reverse flow direction.	102
4.2	LQ-feedback function ψ for $w(z) = 1$ and $r(z) = 10$	103
4.3	Closed-loop distribution of the temperature along the reactor centerline.	104
4.4	Distribution of the difference between the current temperature and the temperature at stationary state, T_{ss}	105
4.5	Evolution of the the manipulated variable spatial profile along the reactor centerline.	106
4.6	Trajectory of the maximum temperature along the axis of the reactor for open- and closed-loop simulations.	106
4.7	Evolution of the closed-loop temperature distribution along the axis of the reactor for step disturbances in the inlet mole fraction of reactant	107
4.8	Evolution of the open-loop temperature distribution along the axis of the reactor for step disturbances in the inlet mole fraction of reactant	108
4.9	Closed-loop distribution of the temperature along the reactor centerline with suboptimal controller, $u_{sub}(t)$	108
4.10	Trajectory of the manipulated variable with suboptimal controller, $u_{sub}(t)$	109
4.11	Trajectory of the maximum temperature along the axis of the reactor for different cases.	109
4.12	Closed-loop distribution of the temperature along the reactor centerline with suboptimal controller, $u_{sub}(t)$ and mole fraction disturbance.	110
4.13	Trajectory of the manipulated variable with suboptimal controller, $u_{sub}(t)$	110

5.1	Illustration of the input/output specification.	121
5.2	Representation of the structure of \mathbf{A}_r . Each face represents the Hessian of the i^{th} coordinate of the rotated space.	129
5.3	Scale fused or measuring the extent of nonlinearity. The steady-locus is approximated by a surface of constant curvature $1/c$ where c is the RMS curvature.	131
5.4	3-dimensional plot of the steady-state locus for equally spaced input $u_0 \in \{260, 280, \dots, 440\}$	132
5.5	2-dimensional steady-state locus for equally spaced input $u_0 \in \{260, 280, \dots, 440\}$	133
5.6	Tangential curvature for $y = [x_1(z = 1), x_2(z = 1)]^T$	134
5.7	Normal curvature for $y = [x_1(z = 1), x_2(z = 1)]^T$	135
5.8	Distribution of the tangential curvature for $y = [x_1(z_0), x_2(z_0)]^T$ at three different operating conditions.	135
5.9	Distribution of the normal curvature for $y = [x_1(z_0), x_2(z_0)]^T$ at three different operating conditions.	136
5.10	Closed-loop trajectories of $y = x_2(z = 1)$ for set-point changes about three different operating points.	136
5.11	Steady-state locus for $z = 0.65L$ and for equally spaced input values: $\alpha_0 \in \{0.8, 0.82, \dots, 1\}$. x_1 represents the mole fraction Y and x_2 represents the reactor temperature T	137
5.12	Steady-state locus for $z = 0.4L$ and for equally spaced input values: $\alpha_0 \in \{0.8, 0.82, \dots, 1\}$. x_1 represents the mole fraction Y and x_2 represents the reactor temperature T	138
5.13	Tangential curvature for $y = [x_1(z = 0.4L), x_2(z = 0.4L)]^T$ (dashed-line) and $y = [x_1(z = 0.65L), x_2(z = 0.65L)]^T$ (solid-line).	139
5.14	Normal curvature for $y = [x_1(z = 0.4L), x_2(z = 0.4L)]^T$ (dashed-line) and $y = [x_1(z = 0.65L), x_2(z = 0.65L)]^T$ (solid-line).	139
5.15	Spatial distribution of the tangential and normal curvature for $y = [x_1(z_0), x_2(z_0)]^T$ at $u_0 = 0.9$	140

6.1	Equilibrium profiles of a) x_2^{ss} , b) x_1^{ss} , c) u^{ss} , for selected operating conditions: $u^{ss}(z) = 300K$ (dashed line), $u(z) = 360K$ (dashed-dot line) and $u(z) = 440K$ (solid line).	155
6.2	First order sensitivity for selected operating conditions: $u(z) = 300K$ (dotted line), $u(z) = 350K$ (dashed-dot line) and $u(z) = 400K$ (solid line). Top-left figure: $\frac{\partial x_1}{\partial x_{1,0}}$ vs. <i>time</i> ; top-right figure: $\frac{\partial x_1}{\partial x_{2,0}}$ vs. <i>time</i> ; bottom-left figure: $\frac{\partial x_2}{\partial x_{1,0}}$ vs. <i>time</i> ; bottom-right figure: $\frac{\partial x_2}{\partial x_{2,0}}$ vs. <i>time</i>	156
6.3	Second order sensitivity for selected operating conditions: $u(z) = 300K$ (dotted line), $u(z) = 350K$ (dashed-dot line) and $u(z) = 400K$ (solid line). Top-left figure: $\frac{\partial^2 x_2}{\partial x_{1,0}^2}$ vs. <i>time</i> ; top-right figure: $\frac{\partial^2 x_2}{\partial x_{1,0} \partial x_{2,0}}$ vs. <i>time</i> ; bottom-left figure: $\frac{\partial^2 x_2}{\partial x_{2,0} \partial x_{1,0}}$ vs. <i>time</i> ; bottom-right figure: $\frac{\partial^2 x_2}{\partial x_{2,0}^2}$ vs. <i>time</i>	157
6.4	RMSPSM for selected operating conditions.	158
6.5	Closed-loop temperature at $z/L = 1$ for $\tilde{\mathbf{x}}_0 = [0.01, 10]^T$ with linear (dashed line) and non-linear control (solid line).	158
6.6	RMSPSM vs. operating condition (T_j) for the case where one (circles), five (diamonds) and ten (crosses) heat exchangers are used to control the reactor system.	159
6.7	First and second order sensitivity for $u_{ss} = 0.92$ at three different spatial points along the axis of the reactor.	160
6.8	RMSPSM for selected operating conditions for the CFRR unit.	161

Nomenclature

Adimensional numbers

Gz Graetz number,

Nu Nusselt number,

Pe Peclet number,

Pr Prandtl number,

Re Reynolds number,

Sc Schmidt number,

Sh Sherwood number,

Greek Letters

α ratio $v_s/v_{s,in}$,

ϵ porosity,

μ effectiveness factor,

$\bar{\epsilon}$ perturbation parameter ,

ρ density,

τ_c time length of a semi-cycle,

Θ Performance Sensitivity Measure,

Ξ steady-state locus,

Subscripts

a axial direction,

f fluid phase,

r radial direction,

s solid phase,

eff effective value,

in inlet conditions,

Symbols

ΔH_R enthalpy of reaction,

\mathbf{I} identity matrix,

\mathcal{H} Hilbert space,

\bar{M} average molecular mass,

a_v surface area per unit volume,

C molar concentration ,

C_p heat capacity,

D dispersion or diffusion coefficient,

E activation energy ,

h heat transfer coefficient,

H_c control horizon,

H_p prediction horizon,

k	thermal conductivity,
k_m	mass transfer coefficient,
k_∞	first order rate constant,
L	linear operator,
L_c	characteristic length,
N	nonlinear operator,
n	spatial discretization,
P	pressure,
Q	gas flow rate,
R	internal radius of the reactor ,
r	independent variable (radial spatial direction),
R_g	gas constant,
$S(t)$	strongly continuous semigroup,
T	temperature,
t	independent variable (time) ,
T_s	sampling time,
T_{cycle}	full cycle time ,
v_s	superficial velocity,
Y	mole fraction,
z	independent variable (axial spatial direction),

Abbreviations

CFRR Catalytic Flow Reversal Reactor,
CMM Coal Mine Methane,
DPS Distributed Parameter System,
GHG Green House Gases,
GWP Global Warming Potential,
LQ Linear Quadratic,
MPC Model Predictive Control,
PDF Partial Differential Equation,
PSM Performance Sensitivity Measure,
QP Quadratic Programming,
RMSPSM Root Mean Squared Performance Sensitivity Measure,

1

Introduction

Chemical reactors have traditionally been operated at steady state; however, there are a large number of applications in which dynamic operation of the reactors provides significant advantages over steady-state operation. Transition from the usual steady-state mode of continuous processes towards forced unsteady-state conditions (dynamic operation) has been discussed in chemical engineering literature since the beginning of the 1960s (Matros and Bunimovich, 1996).

Reverse flow operation of a catalytic reactor is an example of forced unsteady-state conditions which creates an advantageous energetic effect by exploiting the reactor dynamics. The basic mode of operation does not include forced oscillations of inlet gas temperature or composition but rather comprises periodic reversal of cold gas flow to a preheated catalyst bed. The scope of possible applications of the technique includes both exothermic processes, such as sulfur dioxide oxidation for sulphuric acid production, or methanol synthesis and endothermic processes like hydrocarbons dehydrogenation. A number of publications relate to purification of volatile organic compounds, as well as nitrogen oxides and SO_2 .

Increasing world-wide concerns about global warming and greenhouse emissions has brought researchers to look for advanced solutions and techniques to mitigate harmful

emissions. One such solution includes the use of catalytic reverse flow reactors for combustion of fugitive methane emissions. Large amounts of methane are liberated daily from coal mines, biomass landfills and oil and gas transportation facilities, among others. Of all greenhouse gases, methane makes the second largest contribution to global warming. The reduction of methane emissions would therefore have a positive impact on the environment. Potentially, fugitive methane emissions can be used for energy generation; however, they often have low or fluctuating concentration of fuel value components that hinders their use in conventional fuel burners.

1.1 Scope and Objectives

The objective of this thesis is to develop control formulations for catalytic reactors with reverse flow operation. To assist in the formulation and testing of suitable control schemes, we develop a computer simulator that allows accurate simulation of process operation under different reactor configurations and operating conditions. Mathematical models that approximate the behavior of the catalytic reactor are also developed for control design. Computer implementation issues of the models are discussed in detail.

From a systems point of view, catalytic reactors belong to the nonlinear distributed parameter system's type. Although the core of the control theory has been developed for lumped parameter systems with linear dynamics, formulating a controller for a nonlinear distributed parameter system is an area of intensive research in the process control community.

A wide range of methods have been used to lump distributed parameter systems and obtain a system that is amenable to classical control techniques for lumped parameter systems. In this thesis, we studied the formulation of a model predictive controller for a reverse flow catalytic reactor using the method of characteristics. The method of characteristics is a technique that explores the geometric properties of the underlying distributed parameter system. In addition to the method of characteristics, we studied control techniques that use an infinite dimensional representation of the underlying reactor system.

Although there exist a wide range of *nonlinear* control techniques that can be used to formulate a controller for the resulting lumped or infinite dimensional system, these techniques are mathematically more involved than their linear counterparts. The classical control design approach for nonlinear systems is to linearize the system's model around a desired operating point and then use the resulting linear model for control formulation. In this thesis, we develop a measure of open-loop nonlinearity to quantify gain nonlinearity and locate operating regions where nonlinearity is significant. This aspect of nonlinearity can be used as preliminary information for the design of a control system. Moreover, we develop a closed-loop measure of nonlinearity to assess whether or not linear control techniques for (hyperbolic) distributed parameter systems provide a significant advantage over nonlinear control techniques. The measures of nonlinearity are applied to a chemical tubular reactor and a catalytic flow reversal reactor.

1.2 Thesis Outline

To enable easy travel through the thesis, each chapter begins with an abstract giving the reader an overall picture of the material presented therein.

Chapter 2 introduces the concept of catalytic flow reversal reactor and its application for combustion of lean methane emissions for mitigation of greenhouse gases. In this chapter, a computer simulator of a pilot catalytic reactor unit is developed to have high fidelity numerical simulations of the reactor dynamics. The simulator has been an invaluable tool in this thesis to understand the dynamic behaviour and develop simplified models for control design. The simulator has also been useful for optimal design studies at the University of Alberta and CANMET Energy Technology Centre, Varennes, Canada.

Chapter 3 deals with the control of catalytic flow reversal reactors for stable operation. During normal operation, the reactor unit is subject to disturbances in the inlet reactant concentration and inlet gas velocity. High concentrations may lead to instability by overheating and deactivation of the combustion reaction. Low concentrations can lead to extinction of the reaction. In this chapter, we aim at

developing a control scheme that keeps the reactor operating at stable conditions. The formulation of a model predictive control scheme is studied in this chapter.

Chapter 4 deals with the control of catalytic flow reversal reactors for optimal operation from a theoretical point of view. Linear optimal control techniques for infinite dimensional systems are used to formulate a controller for the catalytic flow reversal reactor. The theory of infinite dimensional systems is a complex one and it requires an important mathematical background; however, it provides a systematic way to formulate a controller without neglecting the distributed nature of the underlying system.

Chapter 5 studies the effect of process nonlinearity to aid in the selection of a suitable control technique for distributed parameter systems. A measure of nonlinearity is developed to quantify the magnitude of open-loop process nonlinearity in hyperbolic partial differential equation models. A plug flow reactor and a catalytic reverse flow reactor are used to show the application of the proposed nonlinearity measure.

In Chapter 6, a performance sensitivity measure is developed to study the effect of process nonlinearity in closed-loop *linear* control performance of hyperbolic distributed parameter systems. A plug flow reactor and a catalytic reverse flow reactor are used to show the application of the proposed measure and to study its significance for analysis and control design.

Conclusions to this work appear in Chapter 7 giving an overall summary and drawing inferences based on the overall work reported in this thesis. Future directions to the research are proposed towards the end of the chapter.

2

Modelling of Catalytic Flow Reversal Reactors

In this chapter, the reader is introduced to the concept of catalytic reactors with reverse flow operation and the application of the reactors to the combustion of lean methane streams. A computer simulator of the catalytic reactor is developed to yield high fidelity numerical simulations of the reactor dynamics and to understand the dynamic behaviour of the reactor system. To assist in the formulation and testing of suitable control schemes for catalytic reactors with reverse flow operation, simplified mathematical models are developed to approximate the dynamic behaviour of the catalytic reactor. The models include a sufficient level of detail to assure that they can be used for simulation of process operation and control design. Numerical simulations of open-loop operation are used to analyze reactor dynamics to develop a control scheme.

2.1 Global Warming and Methane Emissions

Global warming and its negative effects on the environment are capturing increasing attention from the scientific community and the public in general. The detailed causes of global warming in recent decades is an active field of research, but the scientific consensus identifies elevated levels of greenhouse gases due to human activity as the main influence.

Greenhouse gases create an atmospheric greenhouse effect. The greenhouse effect in the earth's atmosphere is primarily a function of the concentration of water, carbon dioxide (CO_2), methane (CH_4) and other trace gases in the atmosphere that absorb terrestrial radiation leaving the surface earth (Agency, 2007). Changes in the atmospheric concentrations of these greenhouse gases can alter the balance of energy transfers between the atmosphere, space, land and oceans. Holding everything constant, increasing greenhouse gas concentrations in the atmosphere will produce a net increase in the absorption of energy by the earth.

Greenhouse gases such as carbon dioxide, methane and nitrous oxide (N_2O) are continuously emitted to and removed from the atmosphere by natural processes. Anthropogenic activities, however, can cause additional quantities of these and other greenhouse to be emitted or sequestered, thereby changing their global average atmospheric concentrations. Atmospheric concentrations of the most important greenhouse gases along with their rates of growth are given in Table 2.1 (Agency, 2007).

To quantify the effect of different greenhouse gases in the atmosphere, there exists two scales. The first scale, the atmospheric lifetime, describes how long it takes to restore the system equilibrium following a small increase of the gas in the atmosphere. The second scale is the global warming potential (GWP). The GWP depends on both the efficiency of the gas molecules as greenhouse gas and its atmospheric lifetime. GWP is measured relative to the same mass of CO_2 and evaluated for a specific time scale. The atmospheric lifetime and global warming potential for the most important greenhouse gases is given in Table 2.1.

Domestic legislative efforts concentrate on raising fuel economy standards, capping

Table 2.1: Global atmospheric concentration, rate of concentration change, atmospheric lifetime and global warming potential of selected greenhouse gases.

Atmospheric Variable	CO ₂	CH ₄	N ₂ O	SF ₆
Pre-Industrial atmospheric concentration ^a	280 ppm	0.722 ppm	0.270 ppm	0 ppt
Atmospheric concentration ^b	376.7 ppm	1.756 ppm	0.319 ppm	5.4 ppt
Rate of conc. change ^c	1,610 ppm/yr	0.005 ppm/yr	0.0007 ppm/yr	0.23 ppt/yr
Atmospheric lifetime	50-200 ^d	12 ^e	114 ^e	3,200
GWP ^f	1	21	310	23,900

^a The pre-industrial period is considered as the time preceding the year 1750.

^b Concentrations measured in 2004.

^c Rate is calculated over the period 1990 to 2004 for CO₂, CH₄, and N₂; 1996 to 2004 for SF₆.

^d No single lifetime can be defined for CO₂ because of the different rates of uptake by different removal processes.

^e The lifetime has been defined as an 'adjustment time' that takes into account the indirect effect of the gas on its own residence time.

^f 100-year time horizon.

CO₂ emissions from power plants, and investing in alternative energy sources. Recommendations to consumers also focus on CO₂ by encouraging the public to buy fuel-efficient cars and appliances and to minimize their use. Unfortunately, the governments around the world and the environmental community have focused its efforts almost exclusively on abating carbon dioxide emissions.

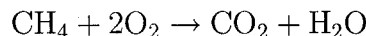
The focus solely on CO₂ is fueled in part by misconceptions. It is true that human activity produces vastly more CO₂ than all other greenhouse gases put together. However, this does not mean it is responsible for most of the earth's warming. Many other greenhouse gases trap heat far more powerfully than CO₂, some of them tens of thousands of times more powerfully, see Table 2.1.

By far the most important non-CO₂ greenhouse gas is methane. Methane is responsible for nearly as much global warming as all other non-CO₂ greenhouse gases combined. While atmospheric concentrations of CO₂ have risen by about 31% since pre-industrial times, methane concentrations have more than doubled.

With methane emissions causing nearly half of the planets human-induced warming, methane reduction must be a priority. Methane is produced by a number of sources, including coal mines, landfills and oil and gas transmission facilities.

2.2 Combustion of Fugitive Methane Emissions

Methane combustion leads to the generation of carbon dioxide through the following chemical reaction:



Methane has a global warming potential of 21 times that of carbon dioxide, that is, one tonne of methane has a GHG warming potential of 21 tonnes of CO₂ based on a 100 year life analysis. The reduction of methane emissions would therefore have a large positive impact on the reduction of GHG emissions. Although the combustion of one mole of methane yields one mole of carbon dioxide, equivalent carbon dioxide emissions will be reduced by a factor of about 20.

Globally, agriculture is a prominent source of methane along with underground coal mining and gas and oil production facilities. Worldwide coal mine methane

Sec. 2.2 Combustion of Fugitive Methane Emissions

(CMM) emissions make up approximately 8% of the world's anthropogenic methane emissions, which in turn comprise 17% of all anthropogenic greenhouse gas emissions (Shi and Agnew, 2006). In the year 2000, methane emissions from mine ventilation air alone was over 237 *Mtonnes* CO₂-equivalent (EPA, July 2003). Moreover, underground mining is by far the most important source of fugitive mine methane, and approximately 70% of all coal mining related emissions are from underground ventilation air (Moore *et al.*, June 1998).

Canada's primary source of methane gas emissions are fugitive emission, which come from natural gas and petrochemical production and transmission (Hayes, 2004). The oil and gas industry accounts for about 15% of the total methane emissions, which amounts to about 47 *Mtonnes/year* (987 *Mtonnes/year* of CO₂ equivalent), according to (Moore *et al.*, June 1998) based on 1990/1992 data. Overall, it has been estimated that fugitive methane emissions account for about 50% of the GHG emissions of the conventional oil and gas sector in Canada. Estimates by Environment Canada give for the year 2000 a total GHG emissions of 726 M tonnes of CO₂ equivalent. About 5.2% of 726 M tonnes of CO₂ equivalent are fugitive methane emissions from the oil and gas sector (1.8 *Mtonnes* of fugitive methane annually). Canada is responsible for about 2% of the world emissions of GHG.

Methane fugitive emissions are typically dilute (0.1-1.5 v/v%) and at ambient temperature and pressure. At low concentrations and flow rates it becomes difficult to combust methane using conventional methods. Methane, being a stable compound, requires a high temperature to initiate the combustion reaction. A significant amount of energy would be required to bring the dilute methane gas to a sufficiently high temperature to sustain combustion.

Currently, there are two options for the combustion of fugitive methane emissions. The first one, and most common, is the homogeneous combustion using flares. This method of eliminating fugitive emissions has been used for many years, as it can be cost effective; however, flaring has its drawbacks. It requires high temperatures of combustion, which can lead to producing harmful substances such as NO_x, another pollutant of significant concern. At low concentrations of emissions, flaring has the additional drawback that additional energy supply may be required to assist with

Sec. 2.3 Background of Reverse Flow Operation of Catalytic Reactors

flaring of emissions. In addition, flaring is not well tolerated by the public and government policies usually treat flaring negatively. Homogeneous combustion is best conducted when methane concentration is above 5% (Kushwaha, 2003).

The second method for combustion of methane emissions the catalytic combustion. This is a flameless combustion process that uses a solid catalyst to promote the reaction. Catalytic combustion requires relatively low inlet temperatures when compared to homogeneous combustion. Low concentration of methane can be combusted without the use of any additional energy supply. The low temperatures required for the combustion result in lower NO_x emission. Catalytic combustion is limited by the inlet gas temperature and catalyst activity (Hayes and Kolaczkowski, 1997).

Combustion of fugitive methane emissions in a catalytic reactor seems to be the best options; however, typical conditions involve lean streams at ambient temperature. To increase the temperature of the feed gas, a pre-heating step is usually employed before the combustion reaction. Preheating methods include external heat sources and the use of the thermal mass of the reactor by periodically reversing the flow direction. The former method can be associated with additional cost of fuel. The main advantage of the second option of periodic flow reversal is that the energy released by the reaction can be stored in the reactor solid bed and used to preheat the cold inlet stream and any remaining energy can be removed and used for secondary processes such as heating or power generation.

2.3 Background of Reverse Flow Operation of Catalytic Reactors

Reverse flow operation of catalytic reactors is an example of forced unsteady-state (dynamic) operation of a reactor unit that creates a beneficial energetic effect due to appropriate use of whole reactor dynamics (Matros and Bunimovich, 1996).

For exothermic reactions, the main advantage of the reverse-flow operation is that the solid bed is used not only to accelerate the chemical reaction but also as a heat exchanger and heat accumulation media (heat sink). The solid bed collects and

transfer the stored energy of the reaction to a cooler inlet gas. This makes it possible to provide continuous auto-thermal operation without external gas preheating in advance of the catalyst bed (Matros and Bunimovich, 1996).

Reverse flow operation of catalytic reactors is an attractive technology for treatment of diluted gases which have an adiabatic temperature rise of about 15 °C to 20 °C. According to Matros and Bunimovich (1996), the technology has been commercialized for processes involving the catalytic incineration of noxious organic industrial waste gases, SO₂ oxidation and NO_x reduction. Although most of the applications of reverse-flow operation are devoted to exothermic reactions, reverse-flow operation has also been used for endothermic and combined endothermic and exothermic catalytic reactions.

The principle of operation of a catalytic reactor with reverse-flow operation is illustrated in 2.1 (Hayes, 2004). Figure 2.1(a) illustrates a reactor temperature profile that might be observed in a standard unidirectional flow operation for a combustion reaction. If a temperature pattern, shown in Figure 2.1(a) and (b) is established, the reverse flow operation can then be used to take advantage of the high temperatures near the reactor exit to pre-heat the reactor feed. A quasi-steady state operation may be achieved in which the reactor temperature profile has a maximum value near the centre of the reactor, which slowly oscillates as the feed is switched between the two ends of the reactor, as shown in Figure 2.1 (c-e). The quasi-steady state operation will be referred to in this thesis as *stationary state*.

2.4 Applications of Reverse Flow Catalytic Reactors

Reverse flow catalytic reactors have been proposed for mitigation of lean methane emissions from coal mines and natural gas transmission facilities (Hayes, 2004).

Unlike coalbed methane, which has a concentration of 50 – 90%(v/v) methane, ventilation air in underground coal mines around the world generally contain methane at concentrations below 1.0 percent. Mine operators allow the release of methane, in the ventilation air, to the atmosphere without attempting to capture and use it.

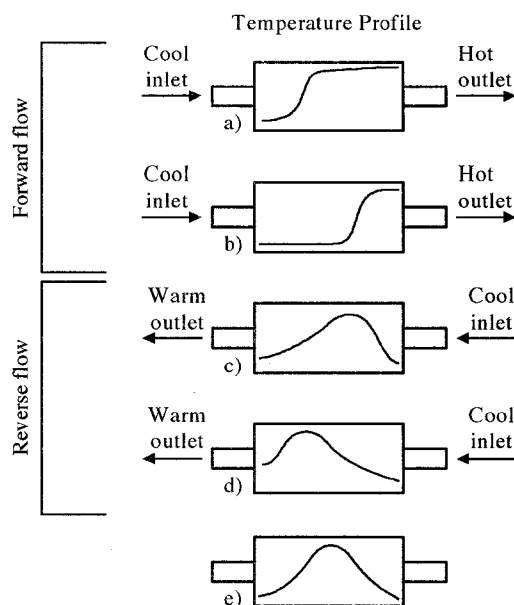


Figure 2.1: Illustration of the heat trap effect for reverse flow operation.

Sources of methane emissions also include solution gas venting (natural gas found in crude oil in underground reservoirs), upstream oil and gas production facilities and leaks in natural gas transmission facilities such as pipelines and compressor stations. In natural gas transmission facilities, the gas experiences pressure loss as it flows through the pipelines, and the gas must be periodically recompressed in compressor station. Methane emissions in compressor stations can be grouped into three sources. One source comprises emissions of methane resulting from incomplete combustion in engines. Another source of emissions includes leaks in valves, flanges and other equipment located within the compressor building; whilst the third source results from instrument venting (Hayes, 2004).

2.5 Heat Recovery from Fugitive Methane Emissions

Large amounts of methane are liberated from coal mines and gas transmission facilities. Potentially, these gases can be used for energy generation; however, they often have low or fluctuating concentration of fuel value components. It is possible to use catalytic flow reversal reactors to create an economically attractive process

Sec. 2.5 Heat Recovery from Fugitive Methane Emissions

by exploiting the heat from the combustion of methane vented from either coal gas mines or gas transmission facilities. Although many of the design issues have been thoroughly investigated, control of the catalytic units is an area that requires extensive research to develop a control scheme that guarantees operationally stable conditions and maximum heat recovery.

Different control measures can be used to achieve stable operating conditions. Figure 2.2 show possible process types with intermediate heat exchange. Energy recovery can be accomplished by passing hot reactant gas through one or more intermediate coolers or by withdrawal of part of the gas from reactor center, see Figure 2.2 b) and d). In cases of low inlet reactant concentration, operationally stable

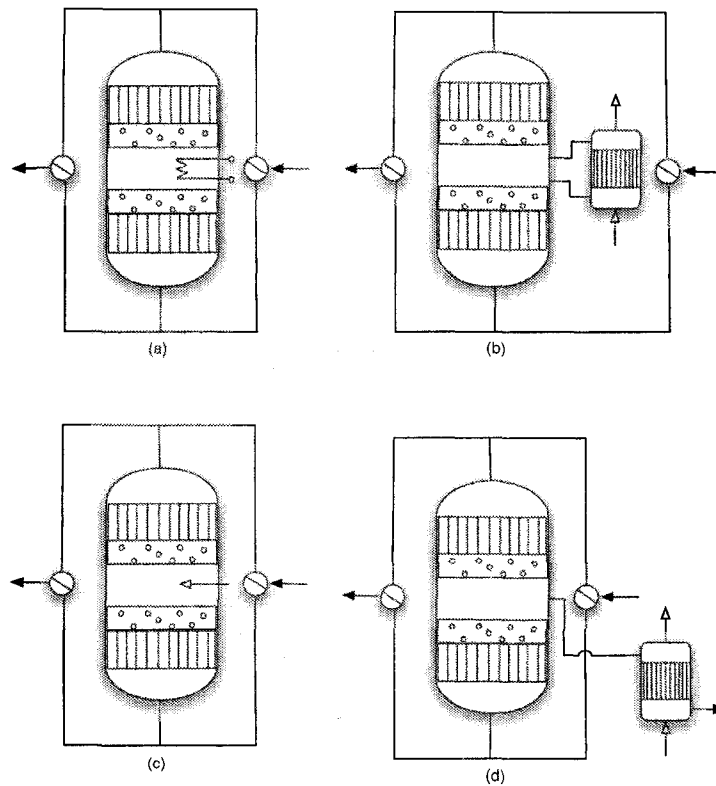


Figure 2.2: Illustration of various control measures for reverse flow catalytic reactor: (a) intermediate electrical heater, (b) intermediate heat exchanger, (c) hot or cold gas injection, (d) intermediate gas removal.

conditions can be obtained by gas preheating between two packed beds. The reactor can be configured with an electrical heater, fuel burner, or hot gas injection into the reactor center, see Figure 2.2 a) and c).

2.6 Mathematical Modelling

To model the dynamic behaviour of a catalytic reactor with reverse flow operation, a suitable model for a catalytic reactor with unidirectional flow is required. Then, the behaviour of the reverse flow catalytic reactor can be modelled by setting the initial conditions of each semi-cycle equal to the solution of the previous semi-cycle. Starting from a given initial profile of the state variables in the system, $x^0(0, z)$, the initial condition for each subsequent semi-cycle depend on the preceding:

$$x^{j+1}(0, l) = x^j(\tau_s, L - z), \quad (2.1)$$

where $j = 1, 2, \dots$ is the number of semi-cycles and L is the total length of the reactor unit.

The mathematical modelling of catalytic reactors with unidirectional flow is widely discussed in the literature. Good references include (Hayes and Kolaczkowski, 1997; Levenspiel, 1998; Fogler, 2005). Extensive investigation of catalytic flow reversal reactors, including numerical simulations and experimental analysis, have been performed and reviewed by Matros and Bunimovich (1996) and others.

Various models were proposed to represent the dynamic behaviour of CFRR units. The main difference between the models depends on the way that heat dissipation is modeled. Heat dissipation, by means of axial heat conductivity, interphase heat transfer, or heat transfer inside a catalyst pellet and radial diffusion of heat leads to a diversity of possible models. Each model is developed according to the specific reactor under study.

For example, Eigenberger and Nieken (1988) and Matros (1989) used a one-dimensional pseudo-homogeneous model. In pseudo-homogeneous models, it is considered that the solid temperature and concentrations are the same as the fluid ones. Gawdzik and Rakowski (1988), Bhatia (1991), Gupta and S.K. (1991) proposed a one-dimensional heterogeneous model to account for the gas/solid temperature difference but neglected the axial diffusion terms. In heterogeneous models, the gas and solid interface is assumed to be a discontinuity and separate mole and energy balances are written for the solid and fluid phases (Hayes and Kolaczkowski, 1997). Sapundzhiev *et al.* (1990) used a heterogeneous model that included the axial

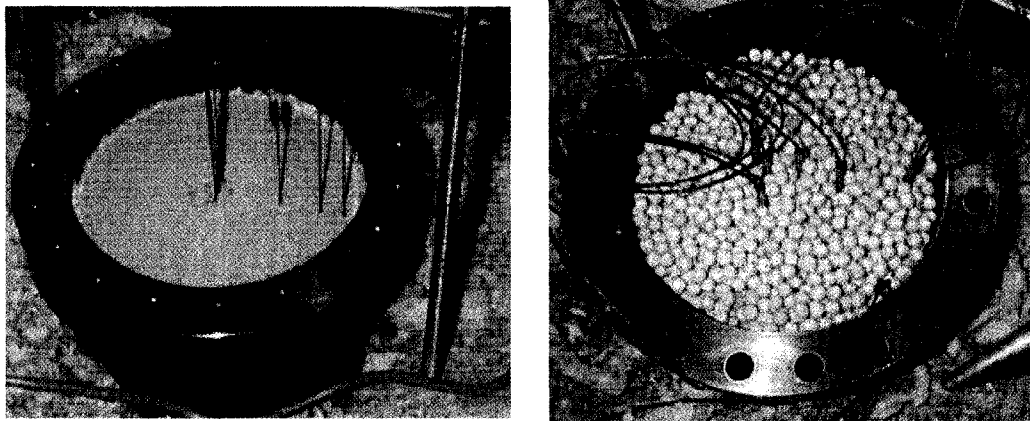
diffusion terms. Heterogeneous model with diffusion terms is now the most adopted model for simulation and design, see for example Marin *et al.* (2005). At a higher complexity level, Sapundzhiev *et al.* (1988) developed a two-dimensional heterogeneous model including radial diffusions and heat and mass transfer between the phases. Sapundzhiev *et al.* (1988) and Van de Beld and Westerterp (1996) added a heat balance term for the reactor wall since its heat capacity can be significant. They also suggested that, due to the presence of a thick layer of insulation, a considerable heat buffer can be created and the performance of a model might be improved by considering its heat capacity. In Aube and Sapoundjiev (2000) and Salomons *et al.* (2004), a two-dimensional heterogeneous model which included the effect of the reactor wall and insulation was simulated and validated.

In the next sections, the development of a mathematical model, the implementation of the model in a computer simulator and the analysis of the simulation results to aid in the formulation and testing of suitable control schemes for the catalytic reactor unit are presented.

2.7 Reactor Configuration

The distinctive feature of reverse flow catalytic reactors is the solid material inside the reactor. The solid can be either formed by particles or be structured, see Figure 2.3. The advantage of structured or monolithic supports in catalytic processes are well known (Marin *et al.*, 2005): low pressure drop, greater mechanical strength, better mass transfer, minimal 'channelling' across the bed in uniform monoliths. In reverse flow reactors, the boundaries of the catalyst bed are replaced by inert packing material. In this way, the temperature in the reactor can be elevated with a reduction of the quantity of catalyst needed. The reactor is usually surrounded by a thick insulation layer that keeps the accumulated energy within the reactor.

A set of on-off valves is used to regulate the fluid flow direction. A picture and schematic of the a pilot reverse flow reactor that is used in this thesis as the reactor "*to be controlled*" is shown in Figure 2.4. The pilot reactor unit is currently in operation at CANMET Energy Technology Centre, Varennes, Canada,



Structured bed.

Particle bed.

Figure 2.3: Pictures of different types of solid beds: ceramic monolith (left) and Denstone balls (right).

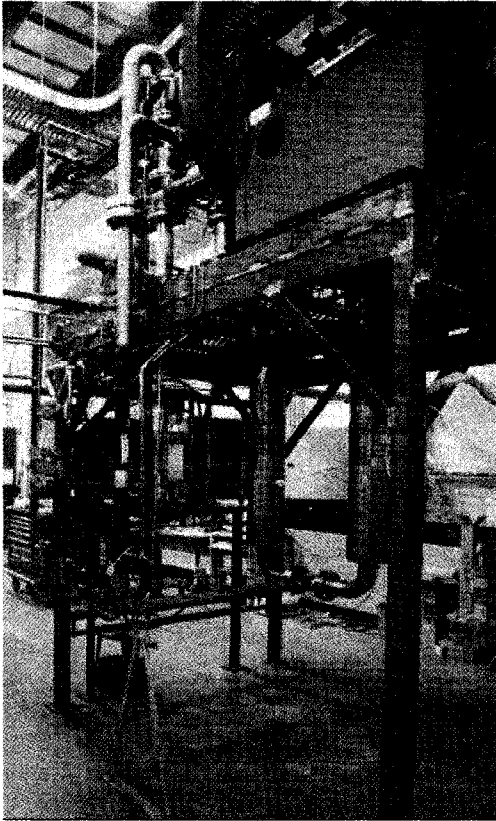
2.8 Contributions

Having introduced the catalytic reverse flow reactor for combustion of lean methane emissions, this section presents the main contributions of Chapter 2.

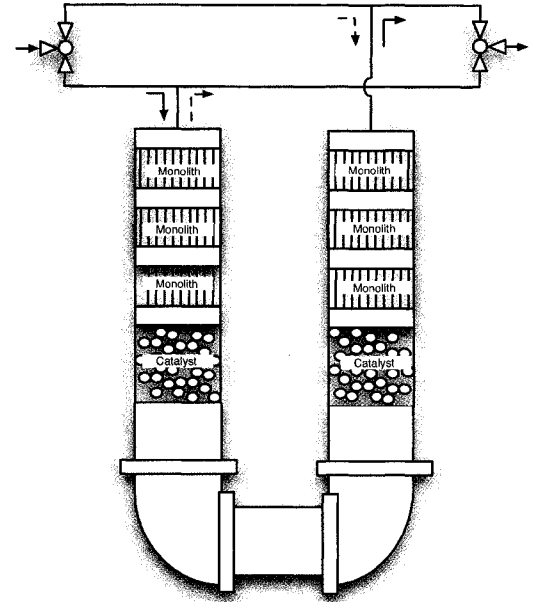
Analysis of process dynamics and formulation of control algorithms for a CFRR unit, like any other chemical reactor unit, can be performed effectively by developing a mathematical model of the process. Mathematical models are usually implemented in a computer to perform extensive numerical simulations to learn about the dynamic behaviour of the process.

(Salomons *et al.*, 2004) presented a high fidelity model and a computer simulator developed in FORTAN 95 for the pilot scale CFRR unit in Figure 2.4. In this chapter, we present details of the implementation of the high fidelity model in COMSOL Multiphysics finite element modelling package and the MATLAB framework. This computer program provides a convenient and *fast* modelling platform for implementation of control strategies. The model outputs were validated against the earlier model used in Salomons *et al.* (2004).

Simulations of open-loop reactor system behaviour are presented and used to aid in the formulation of a suitable control scheme in subsequent chapters. The reactor



Reactor Picture.



Reactor Schematic.

Figure 2.4: Pilot Reverse Flow Catalytic Reactor Unit.

simulator was also used to perform parametric studies of the main process variables (Litto *et al.*, 2006) and to develop low fidelity models that can adequately capture the dynamic (this thesis) and stationary state (Devals *et al.*, 2006) behaviour of the reactor system.

Devals *et al.* (2006) used the reactor simulator and a statistical design of experiments (DOE) to investigate and model the combustion of methane in the CFRR. More precisely, they modeled the stationary state of the maximum temperature and outlet methane concentration. The model was based on a 3-level full factorial design involving as factors the methane inlet concentration, the switching time, mass extraction and the gas superficial velocity.

In this chapter, a low fidelity 1-dimensional pseudo-homogeneous model is developed and validated against the high fidelity model developed in COMSOL

Multiphysics. The low fidelity model captures sufficient process dynamics and is used in the next chapters as an integral part of two control schemes.

2.9 Modelling Reactor Dynamics

The dynamics of the catalytic flow reversal reactor can be described by partial differential equations (PDE's) derived from mass and energy balances. With the pilot scale unit shown Figure 2.4 in mind, Aube and Sapoundjiev (2000) and Salomons *et al.* (2004) introduced a high fidelity dynamic model that is presented in the next section and is used throughout this thesis to represent the actual pilot unit to be controlled.

2.9.1 Heterogeneous Model

A 2-spatial dimension (2-D) heterogeneous model for the catalytic flow reversal reactor in Figure 2.4 can be developed on the basis of material and energy balances giving two material balances and two energy balances (Salomons *et al.*, 2004). The material and energy balance equations are given by :

Mole Balance:

Fluid Phase:

$$\frac{1}{r} \frac{\partial}{\partial r} \left(r D_{r,eff} C_f \frac{\partial Y_{CH_4,f}}{\partial r} \right) + \frac{\partial}{\partial z} \left(D_{a,eff} C_f \frac{\partial Y_{CH_4,f}}{\partial z} \right) - v_s C_f \frac{\partial Y_{CH_4,f}}{\partial z} - k_m a_v C_f (Y_{CH_4,f} - Y_{CH_4,s}) = 0 \quad (2.2)$$

$$\text{Boundary Conditions: } \begin{cases} Y_{CH_4,f} = Y(t) & \text{at } z = 0, \\ \frac{\partial Y_{CH_4,f}}{\partial z} = 0 & \text{at } z = L, \\ \frac{\partial Y_{CH_4,f}}{\partial r} = 0 & \text{at } r = 0, \\ \frac{\partial Y_{CH_4,f}}{\partial r} = 0 & \text{at } r = R. \end{cases}$$

Solid Phase:

$$k_m a_v C_f (Y_{CH_4,f} - Y_{CH_4,s}) = (1 - \varepsilon) \eta (-R_{CH_4}) \quad (2.3)$$

Energy Balance:

Fluid Phase:

$$\frac{1}{r} \frac{\partial}{\partial r} \left(r k_{rf,eff} \frac{\partial T_f}{\partial r} \right) + \frac{\partial}{\partial z} \left(k_{af,eff} \frac{\partial T_f}{\partial z} \right) - v_s \rho_f C_{p,f} \frac{\partial T_f}{\partial z} + h a_v (T_s - T_f) = 0 \quad (2.4)$$

$$\text{Boundary Conditions: } \begin{cases} T_f = T(t) & \text{at } z = 0, \\ \frac{\partial T_f}{\partial z} = 0 & \text{at } z = L, \\ \frac{\partial T_f}{\partial r} = 0 & \text{at } r = 0, \\ k_{rf,eff} \frac{\partial T_f}{\partial r} \Big|_{r=R^-} = k_{s,r} \frac{dT_s}{dr} \Big|_{r=R^+} & \text{at } r = R. \end{cases}$$

Solid Phase:

$$(1 - \varepsilon) \rho_s C_{p,s} \frac{\partial T_s}{\partial t} = \frac{1}{r} \frac{\partial}{\partial r} \left(r k_{rs,eff} \frac{\partial T_s}{\partial r} \right) + \frac{\partial}{\partial z} \left(k_{as,eff} \frac{\partial T_s}{\partial z} \right) + h a_v (T_f - T_s) + (1 - \varepsilon) \Delta H_R \eta (-R_{CH_4}) \quad (2.5)$$

$$\text{Boundary Conditions: } \begin{cases} \frac{\partial T_s}{\partial z} = 0 & z = 0, \\ \frac{\partial T_s}{\partial z} = 0 & z = L, \\ \frac{\partial T_s}{\partial r} = 0 & r = 0, \\ k_{rs} \frac{\partial T_s}{\partial r} = h_e (T_s - T_\infty) & r = R + \delta. \end{cases}$$

$$\text{Initial Conditions: } \{ T_s = T_s(z) \quad t = 0$$

where Y_f represents the mole fraction of CH_4 in the fluid phase, Y_s the mole fraction of CH_4 in the solid phase, T_f the temperature of the fluid phase and T_s the temperature of the solid phase. A description of the model parameters is given in Appendix A.

It is noted that for the inlet conditions, Dirichlet conditions of constant temperature and concentration were imposed for the fluid phase equations. Although strictly speaking Dankwerts type conditions are required with axial diffusion, the lack

of significant axial diffusion in the inlet sections of the inert sections makes the assumption of Dirichlet conditions reasonable at a reduction in complexity (Salomons *et al.*, 2004).

The parameters in equations (2.2) and (2.4) show a common feature of catalytic reactors, that is, the heat capacity of the solid phase is commonly three orders of magnitude higher than that for the gas. Taking this into account, heat accumulation in the gas phase is excluded from the reactor model.

For process simulation and design, the model in (2.2) to (2.5) is recommended because it represents, with a high degree of accuracy, the complex behaviour observed in the pilot CFRR unit for combustion of methane emissions.

To achieve stable operation of the CFRR unit, a controller needs to be designed. The formulation of a controller requires simpler models that can approximate the dynamic behaviour of the process. From a process control point of view, the models should be easy to use for control design and yet be detailed enough to capture the essential process dynamics. Simple models inevitably neglect some phenomena, either physical or chemical, but the neglected information is, in general, expected to be compensated for by the feedback usually used in control systems.

In the next section, we present a simple model, *i.e.* a 1-D pseudo-homogeneous model that is used in subsequent chapters to formulate control systems for the CFRR unit.

2.9.2 Pseudo-homogeneous Model

A simplified model is developed in this section to approximate the dynamic behaviour of the catalytic reactor. The model is based on the plug-flow pseudo-homogeneous model assumptions, that is, axial dispersion is neglected and the process variables in the fluid phase, T_f and Y_f , are the same as those in the solid phase, T_s and Y_s , respectively. The model includes terms for heat and mass transfer by flow convection and reaction kinetics but neglects the diffusion phenomena. The basic equations for

the mass and energy balances are:

$$\epsilon \frac{\partial Y}{\partial t} + \frac{\alpha v_{s,in}}{L} \frac{\partial Y}{\partial z} = -k_0 \exp\left(\frac{-E}{R_g T}\right) Y \quad (2.6)$$

$$\eta \frac{\partial T}{\partial t} + \frac{\alpha v_{s,in} \rho}{L} \frac{\partial T}{\partial z} = (-\Delta H_r) k_0 C \exp\left(\frac{-E}{R_g T}\right) Y \quad (2.7)$$

where the parameters k_0 , η and ρ are given by $k_0 = (1-\epsilon)\mu_{eff}k_\infty$, $\eta = \rho_s(1-\epsilon)Cp_s$ and $\rho = \rho_f Cp_f$, and with the boundary conditions given, for $t \geq 0$, by:

$$\begin{aligned} Y(0, t) &= Y_{in} \\ T(0, t) &= T_{in}. \end{aligned} \quad (2.8)$$

Y and T are the mole fraction of methane and temperature, respectively; $v_{s,in}$ is the inlet superficial velocity, α is the ratio of the actual superficial flow velocity and the inlet superficial flow velocity ($\alpha = v_s/v_{s,in}$). α is used to represent the fraction of gas removed from the reactor. Other model parameters are: ϵ , bed porosity; E , activation energy; μ_{eff} , catalyst efficiency, C_p , heat capacity and ρ , density (subscript s is used to indicate solid material and f to indicate fluid properties). Values for the model parameters are given in Appendix A The initial conditions are given, for $0 \leq z \leq 1$ by:

$$\begin{aligned} Y(z, 0) &= Y_0, \\ T(z, 0) &= T_0. \end{aligned} \quad (2.9)$$

The fluid in the reactor is treated as an ideal gas: $\rho_f = \frac{P\bar{M}}{R_g T}$ and $C = \frac{P}{R_g T}$. Any pressure drop in the reactor is neglected and it is considered that the density of the fluid phase is constant and is evaluated at the inlet conditions.

A common feature of packed-bed reactors is that the heat capacity of solid catalyst is commonly three orders of magnitude higher than that of the fluid phase. Therefore, the system of equations (2.6) and (2.7) possesses an inherent two-time scale property, that is, the dynamic behaviour that results from the mole balance equation is much faster than the temperature dynamics. This implies that Y is the fast variable, while T is the slow variable. For catalytic combustion of methane, the mole fraction dynamics is typically three orders of magnitude faster than the temperature dynamics. The mole fraction dynamics is only significant for a short period of time that proceeds each flow reversal and comprises approximately a residence time of the gas within the reactor. For typical processing of large volumes of lean methane streams, the gas

residence time is about a few seconds; however, this time is usually small compared to the flow reversal or switch time (typically of the order of minutes). This leads to the assumption that the mass balance in the fluid phase is at quasi-steady state and the accumulation term in the gas phase is excluded from the model; however, such approximation requires the analysis of the stability of the fast dynamics.

Following the procedure used in Christofides (2000), we obtain a singularly perturbed representation of the process, where the partition of the fast and slow variables is consistent with the dynamic characteristics of the process. A perturbation parameter $\bar{\epsilon}$ is defined as:

$$\bar{\epsilon} = \frac{\epsilon}{\eta}$$

Setting $\bar{t} = \frac{t}{\eta}$, $x_1 = Y$, $x_2 = T$, the system of equations (2.6) and (2.7) can be written in the following singularly perturbed form:

$$\bar{\epsilon} \frac{\partial x_1}{\partial \bar{t}} + \frac{\alpha v_{s,in}}{L} \frac{\partial x_1}{\partial z} = -k_0 \exp\left(\frac{-E}{R_g x_2}\right) x_1 \quad (2.10)$$

$$\frac{\partial x_2}{\partial \bar{t}} + \frac{\alpha v_{s,in} \rho}{L} \frac{\partial x_2}{\partial z} = (-\Delta H_r) k_0 C \exp\left(\frac{-E}{R_g x_2}\right) x_1 \quad (2.11)$$

Performing a two-time-scale decomposition of the system (2.10) and (2.11), the fast subsystem takes the form:

$$\frac{\partial x_1}{\partial \bar{\tau}} + \frac{\alpha v_{s,in}}{L} \frac{\partial x_1}{\partial z} = -k_0 \exp\left(\frac{-E}{R_g x_2}\right) x_1 \quad (2.12)$$

where $\bar{\tau} = \frac{\bar{t}}{\bar{\epsilon}}$ and x_1 depends only on the spatial variable z .

As shown in Christofides (2000), the fast dynamics are exponentially stable, and thus they can be neglected from the model if the objective is to model the long time behaviour of the system. The resulting equation used to model the fast dynamics is:

$$Y(t, z) = Y(t, 0) \exp\left(\int_0^z \left(\frac{-L}{\alpha v_{s,in}}\right) k_0 \exp\left(\frac{-E}{R_g T}\right) dz\right) \quad (2.13)$$

2.10 Classification of Partial Differential Equation Models

For solution of the reactor model equations for simulation and control design, it is important to classify the system of PDE used to model the reactor unit. Depending on the type of PDE that model the system, there exist different analytical techniques and numerical approximations to solve the system of PDE. Generally, a PDE model for a distributed parameter system is of the form:

$$F(z_1, \dots, z_n, x, x_{z_1}, \dots, x_{z_n}, x_{z_1 z_2}, \dots, u_1, \dots, u_m) = 0, \quad (2.14)$$

where $\mathbf{z} = (z_1, \dots, z_n)$ are independent variables such as time and position, x is a dependent variable of (z_1, \dots, z_n) , u is the manipulated variable, $x_{z_1} = \frac{\partial x}{\partial z_1}$, $x_{z_1 z_2} = \frac{\partial^2 x}{\partial z_1 \partial z_2}$, etc. The order of equation (2.14) is the order of the highest derivative occurring in the equation. Moreover, the equation is considered linear if it depends linearly on the states x and its derivatives; if all derivatives of x occur linearly with coefficients depending only on \mathbf{z} , then the equation is semilinear; and if the highest order derivatives of x occur linearly with coefficients depending on \mathbf{z} , u , and lower order derivatives of x , then the equation is quasilinear.

First-order and second-order PDE can be classified into hyperbolic, parabolic and elliptic equations. For first order PDE, consider the following quasi-linear system

$$\mathbf{A}(z, t, \mathbf{x}) \frac{\partial \mathbf{x}}{\partial t} + \mathbf{B}(z, t, \mathbf{x}) \frac{\partial \mathbf{x}}{\partial z} = \mathbf{c}(z, t, \mathbf{x}), \quad (2.15)$$

where we assume that \mathbf{A} is nonsingular. Without loss of generality, we consider that $\mathbf{A} = \mathbf{I}$ and

$$\frac{\partial \mathbf{x}}{\partial t} + \mathbf{B}(z, t, \mathbf{x}) \frac{\partial \mathbf{x}}{\partial z} = \mathbf{c}(z, t, \mathbf{x}). \quad (2.16)$$

Characterization of the system of first order PDE is obtained by the following definition (Mattheij *et al.*, 2005):

Definition 2.10.1 *The system (2.16) is called hyperbolic in (z, t, \mathbf{x}) if there exists a real diagonal matrix $\mathbf{\Lambda}(z, t, \mathbf{x})$ and a nonsingular matrix $\mathbf{T}(z, t, \mathbf{x})$ such that*

$$\mathbf{T}(z, t, \mathbf{x}) \mathbf{B}(z, t, \mathbf{x}) = \mathbf{\Lambda}(z, t, \mathbf{x}) \mathbf{T}(z, t, \mathbf{x}). \quad (2.17)$$

In this definition $\mathbf{\Lambda}(z, t, \mathbf{x}) = \text{diag}(\lambda_1(z, t, \mathbf{x}), \lambda_2(z, t, \mathbf{x}), \dots, \lambda_m(z, t, \mathbf{x}))$ and $\mathbf{T}(z, t, \mathbf{x})$ is the matrix of corresponding left eigenvectors.

For PDE with higher-order derivatives the classification may be reduced to first order systems. Consider the second order linear equation

$$a \frac{\partial^2 x}{\partial t^2} + b \frac{\partial^2 x}{\partial t \partial z} + c \frac{\partial^2 x}{\partial z^2} + d \frac{\partial x}{\partial t} + e \frac{\partial x}{\partial z} = f, \quad (2.18)$$

where the coefficients a, b, \dots, e are assumed constant and where the right hand side f possible depends on z, t and x . The independent variable z is a space coordinate, whereas t is either time or a space coordinate. Introducing the variables

$$p = \frac{\partial x}{\partial t}, \quad q = \frac{\partial x}{\partial z}, \quad (2.19)$$

we obtain the linear system

$$\begin{bmatrix} a & 0 \\ 0 & 1 \end{bmatrix} \frac{\partial}{\partial t} \begin{bmatrix} p \\ q \end{bmatrix} + \begin{bmatrix} b & c \\ -1 & 0 \end{bmatrix} \frac{\partial}{\partial z} \begin{bmatrix} p \\ q \end{bmatrix} = \begin{bmatrix} f - dp - eq \\ 0 \end{bmatrix}. \quad (2.20)$$

Clearly, this system is of the form of (2.15) with the coefficients matrices given by

$$\mathbf{A} = \begin{bmatrix} a & 0 \\ 0 & 1 \end{bmatrix}, \quad \mathbf{B} = \begin{bmatrix} b & c \\ -1 & 0 \end{bmatrix} \quad (2.21)$$

In the following, we assume that $a \neq 0$, so that \mathbf{A} is nonsingular. We look for a transformation matrix \mathbf{S} that can diagonalise the matrix

$$\mathbf{B}\mathbf{A}^{-1} = \begin{bmatrix} \frac{b}{a} & c \\ \frac{-1}{a} & 0 \end{bmatrix} \quad (2.22)$$

This will succeed if the characteristic equation

$$\det(\mathbf{B}\mathbf{A}^{-1} - \lambda \mathbf{I}) = \lambda^2 - \frac{b}{a} \lambda + \frac{c}{a} = 0 \quad (2.23)$$

has two different real roots. Consequently, system (2.20) is hyperbolic if $b^2 - 4ac > 0$. If $b^2 - 4ac = 0$, we have only one "double" characteristic; in fact no \mathbf{S} and $\mathbf{\Lambda}$ exist. If finally, $b^2 < 4ac$, there are no real characteristic values at all. This leads to the following definition (Mattheij *et al.*, 2005):

Definition 2.10.2 *The PDE (2.18) is called*

1. *hyperbolic*, if $b^2 - 4ac > 0$;
2. *parabolic*, if $b^2 - 4ac = 0$;
3. *elliptic*, if $b^2 - 4ac < 0$;

For quasilinear or fully nonlinear second-order equations, a similar classification can be made by linearization of the highest-order derivatives; but the resulting type (hyperbolic, parabolic, or elliptic) may depend upon the particular solution being considered. Higher-order systems can be decomposed into one or a combination of the three (Shang, 2002).

Classification of the type of PDE model is essential for the selection of a suitable method of solution. In general, it is not possible to find an analytical solution of a PDE system; thus some approximation is required. The main difference in the techniques used to approximate PDE equations is the method used to discretize the equations.

The most popular method to approximate PDE is the *finite difference* method. In this method, the PDE is discretized in space by replacing each spatial derivative in the equations by a discretization (usually from a truncated Taylor Series). The finite difference method is simple and easy to use. The method works well for problems with simple geometries and smoothly varying parameters. The main drawback of the method is that a high number of discretization points may be necessary to achieve satisfactory accuracy, which may require considerable computational effort (Dochain *et al.*, 1992).

In contrast to the finite difference method, where the PDE itself is discretized, there are *modal or pseudo-modal decomposition* techniques where the solution of the PDE is discretized. Modal decomposition techniques rely on the existence of basis functions such that the solution of the PDE can be written as a linear combination of the basis functions. Modal decomposition technique works well for parabolic PDE with linear spatial operator where the basis functions are obtained from the eigenfunctions of the linear spatial operator and the eigenvalues of the spatial operator are not bunched together (Ray, 1981); however, this technique relies on the existence and knowledge of the eigenvalues and eigenfunctions. For practical problems, the

determination of the eigenfunctions is not a simple task (Shang, 2002). For complex cases, the eigenfunctions can be obtained by using Karhunen-Loeve decomposition, which aims at obtaining empirical eigenfunctions from experimental or numerical data of a system.

In general, modelling of catalytic reactors leads to a system of PDE of parabolic or hyperbolic type. Parabolic PDEs are the result of modelling the chemical phenomena as well as the physical phenomena, including convection and diffusion transport phenomena. There exist several different methods to obtain a numerical solution of a parabolic PDE system, see for example (Lapidus, 1962; Hayes and Kolaczkowski, 1997; Grasselli and Pelinovsky, 2008).

Hyperbolic PDEs are the result of modelling the chemical phenomena as well as the convection transport phenomena. For hyperbolic type of PDE, the method of characteristics is often used as an analytical solution method. This method uses special curves in the time-space plane, called characteristic curves, along which the solution of the partial differential equation is reduced to the integration of an ordinary differential equation. For hyperbolic PDE systems with a single characteristic, the method gives a system of ODEs that exactly describes the original distributed parameter system (Shang, 2002). There exist different numerical methods to obtain the solution of hyperbolic PDE systems, but the most popular ones are based on finite differences, *i.e.* backwards difference or upwind scheme, a first approximation of the Taylor series expansion, and Lax-Wendroff scheme, second order approximation in the Taylor series expansion, (Morton and Mayers, 1994)

2.11 Computer Simulation

The mathematical model given in equations (2.2) to (2.5) was implemented using COMSOL Multiphysics, and executed using a Matlab framework. COMSOL Multiphysics is a simulation package for the simulation of physical process described by partial differential equations (PDE). The package employs the the finite element method to solve the PDE system and allows for entering coupled systems of PDE. COMSOL Multiphysics offers a well-managed interface to MATLAB and its toolboxes

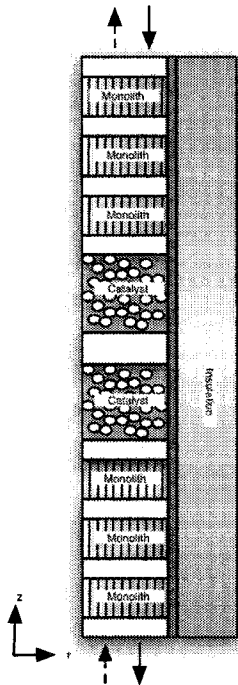


Figure 2.5: Domain used to model the CFRR unit in COMSOL Multiphysics.

for a large variety of programming, preprocessing and postprocessing possibilities. The combined software was highly useful for sensitivity analysis of the CFRR unit and simulation of closed-loop behaviour under a set of different control schemes.

The first step towards the implementation of the model is to define the different domains, each of which have a different set of PDEs and model parameters. The domain used to model the CFRR unit is illustrated in Figure 2.5. The domain includes the different materials used in the pilot scale reactor, that is 6 monolith sections separated by an open gap (to allow gas mixing), 2 packed-bed sections with the catalyst material which are separated by an open section, a stainless steel wall and an external insulation. The total length of the reactor is 2.73 m.

Each 2-D domain is discretized using triangular elements and Lagrange quadratic shape functions are used to interpolate the function to be solved at the discrete nodes within the elements.

2.11.1 Model Validation

The 2-D heterogeneous model in equations (2.2) to (2.5) was validated against experimental data in Salomons *et al.* (2004) through simulation using a computer code written in FORTRAN 95 language. To corroborate the validity of the simulation results obtained from the 2-D heterogeneous model implemented in COMSOL Multiphysics, we compared the outputs of the FORTRAN code and those from using the COMSOL package.

We chose the following operating conditions,

$$v_s = 0.21 \text{ m} \cdot \text{s}^{-1}$$

$$T_{in} = 298 \text{ K}$$

$$Y_{in} = 0.8 \%$$

to validate the outputs. Figures 2.6 and 2.7 show the temperature of the fluid phase of both simulators with unidirectional flow and no heat exchange to the reactor wall along the central open section. We observe a negligible difference between the output of both simulators. The same results were obtained for the other independent variables, i.e., T_s , Y_f , Y_s . When heat exchange is allowed at the central open section, the spatial temperature distributions differ slightly, see Figures 2.8 and 2.9.

The way the heat transfer is modelled at the fluid-wall boundary along the central open section is the only difference between the two simulators. After several simulations using different operating conditions, it was concluded that the way that the heat transfer was modeled in the COMSOL simulator, see the boundary conditions used in (2.4), gives the correct results.

2.11.2 Parametric Analysis

To gain insight into the behaviour of the pilot reactor unit, the COMSOL simulator was used in Litto *et al.* (2006) to perform a parametric study to analyze the effects of cycle time, velocity, reactor diameter, insulation thickness, thermal mass and thermal conductivity of the inert sections, on the transient behaviour of the reactor. Emphasis was placed on the effects of geometry from a scale-up perspective.

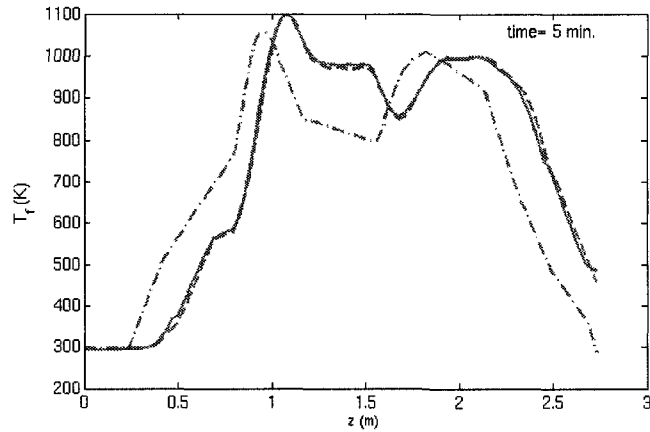


Figure 2.6: Comparison of the outputs from COMSOL (solid line) and FORTRAN (dashed line) simulators at $t = 5$ min for a reactor model without heat exchange in the open middle section. The initial conditions for both simulators are shown by the dashed-dot line.

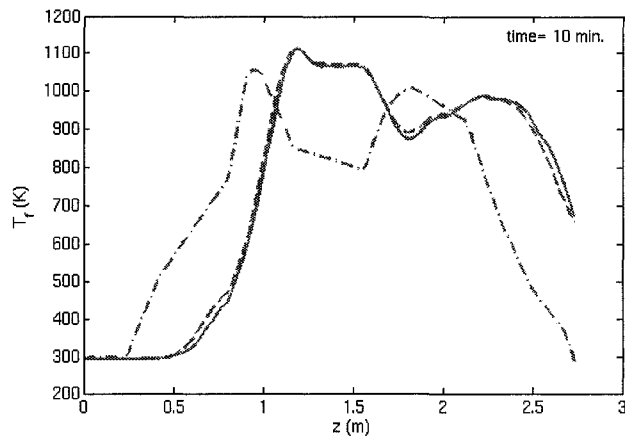


Figure 2.7: Comparison of the outputs from COMSOL (solid line) and FORTRAN (dashed line) simulators at $t = 10$ min for a reactor model without heat exchange in the open middle section. The initial conditions for both simulators are shown by the dashed-dot line.

From the numerical simulations obtained by Litto *et al.* (2006), it was observed that the thermal stability of the the reactor was maintained for longer times when the thermal mass (product of density and heat capacity) of the inert sections was highest, while thermal conductivity has only a minor effect on reactor temperature. It was also observed that, provided that complete conversion is achieved, the highest reactor temperature was achieved with the highest switch time.

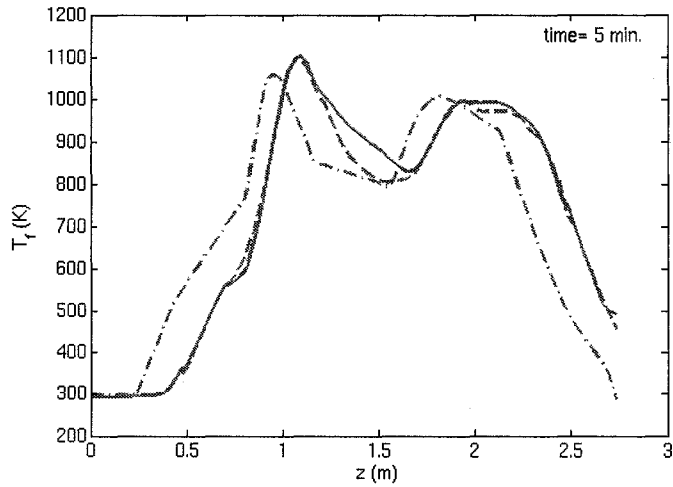


Figure 2.8: Comparison of the outputs from COMSOL (solid line) and FORTRAN (dashed line) simulators at $t = 5$ min for a reactor model with heat exchange in the open middle section. The initial conditions for both simulators are shown by the dashed-dot line.

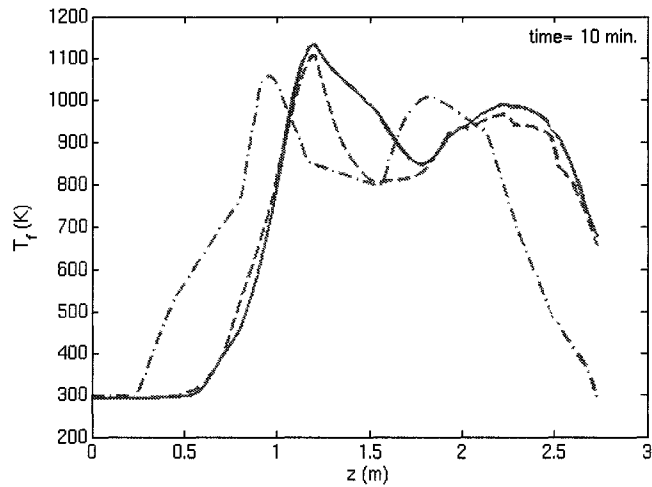


Figure 2.9: Comparison of the outputs from COMSOL (solid line) and FORTRAN (dashed line) simulators at $t = 10$ min for a reactor model with heat exchange in the open middle section. The initial conditions for both simulators are shown by the dashed-dot line.

The insulation was observed to not only prevent heat loss to the environment, but also to provide additional thermal mass. Moreover, the insulation effect was observed to lead to higher reactor temperature up to a maximum thickness. With increasing

reactor diameters, the radial temperature profiles became flatter, and the insulation effect diminished, leading to higher centreline temperatures.

In Devals *et al.* (2006), the COMSOL simulator was used to study the impact on the methane conversion and the maximum temperature in the reactor of key process parameters such as the methane inlet concentration, the gas superficial velocity and the switching time. A three-level full factorial design was built to investigate the impact of the key process parameters. A three-level design means that k factors are considered, each at 3 levels. These are (usually) referred to as low, intermediate and high levels. These levels are numerically expressed as -1, 0, and +1. A three-level designs can model possible curvature in the response function.

The model is given by:

$$\begin{aligned}
 Y = & a_0 + \sum_{i=1}^4 a_i V_i + \sum_{i=1}^4 a_{ii} V_i^2 + \sum_{i<j} a_{ij} V_i V_j + \sum_{i<j} a_{ijj} V_i V_j^2 + \\
 & \sum_{i<j} a_{iij} V_i^2 V_j + \sum_{i<j} a_{iiij} V_i^2 V_j^2
 \end{aligned} \tag{2.24}$$

where Y stands for the maximum temperature T_{max} or the methane conversion rate X . The coefficients a in this equation, which were computed using Statistica (from StatSoft), are given in Table A.3 for T_{max} and X . V_1 , V_2 , V_3 and V_4 correspond to the methane inlet concentration, the switching time, the inlet gas superficial velocity and the coefficient α respectively, but in their adimensional form (values between -1 and 1), see Table 2.2.

Table 2.2: Low (-1), mid-range (0) and high (+1) settings for the four factors.

Factor	1	0	1
Methane inlet concentration, V_1 ($\%v/v$)	0.2	0.75	1.3
Switching time, V_2 (s)	300	600	900
Gas superficial velocity, V_3 ($m \cdot s^{-1}$)	0.3	0.525	0.75
α , V_4	0.8	0.9	1.0

The model that relates the maximum reactor temperature and the key process parameters can be used to predict stable stationary state operational conditions. Figure 2.10 shows the stationary state mapping relating inlet reactant concentration

and mass extraction to the maximum reactor temperature. Figure 2.11 shows the stationary state mapping relating inlet superficial gas velocity and mass extraction to the maximum reactor temperature. The range of values for each variable in the mappings cover typical operating values used for the catalytic reactor with reverse flow operation for combustion of lean methane streams, i.e.:

$$Y_{f0} = 0.1 - 1.5\%$$

$$v_{s,in} = 0.1 - 1 \text{ m} \cdot \text{s}^{-1}$$

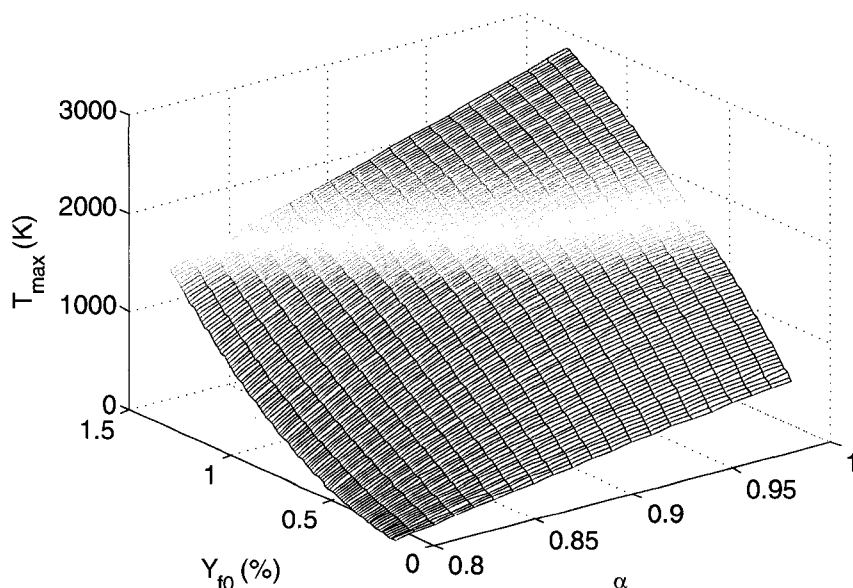


Figure 2.10: Stationary state mapping relating inlet reactant concentration Y_{f0} and mass extraction α to the maximum reactor temperature T_{max} .

Results based on a full factorial design involving the methane inlet concentration, the gas superficial velocity and the switching time has revealed that this technique is efficient in predicting with, fair accuracy, the behaviour of the CFRR for various sets of parameters, and that it therefore shows promise for: 1) the determination of an operating window leading to a stable periodic steady-state operation regime; and 2) the optimization of the CFRR with respect for instance to the amount of heat extracted. By stable operational conditions, we mean conditions that maintain the temperature above the extinction temperature of the reaction and below a critical value to avoid overheating or deactivation of the catalyst.

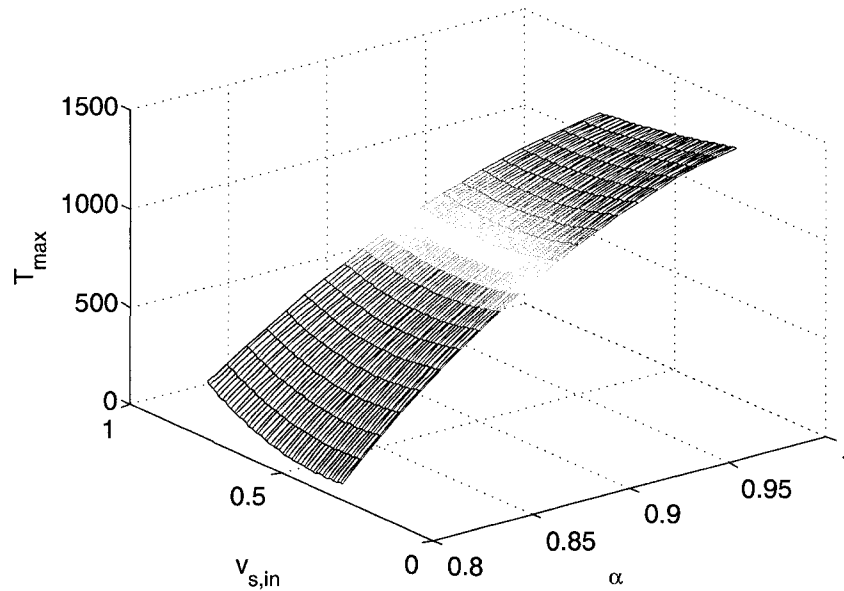


Figure 2.11: Stationary state mapping relating inlet superficial gas velocity $v_{s,in}$ and mass extraction α to the maximum reactor temperature.

The model in (2.24) is used in the next chapter as part of the control scheme developed for the pilot scale reactor unit to predict stationary state conditions.

2.11.3 Dynamical Analysis of the Heterogeneous Model

For design and scale-up of the reactor system, prediction of the system stationary state is usually desired; however, for control of the reactor system, understanding the dynamic behaviour of the system is of great importance.

We begin by simulating the 2-D heterogeneous model to evaluate the dynamic behaviour of the key variables that are most likely to be considered disturbances during normal process operation. We study the dynamics of the temperature spatial distribution along the axis of the reactor, the maximum and average temperature in the reactor for different amounts of gas extraction from the reactor mid-section, inlet reactant concentration, inlet gas velocity and frequency of flow reversal.

Using the following operating conditions

$$v_s = 0.3 \text{ m} \cdot \text{s}^{-1}$$

$$T_{in} = 298 \text{ K}$$

$$Y_{in} = 0.01 \%$$

and the initial temperature distribution shown in Figure 2.12, the evolution of the reactor variables of interest were evaluated.

The dynamic behaviour of the reactor to changes in the heat extraction is shown first. Figure 2.13 (top) shows the evolution maximum temperature and the average temperature in the reactor for a trajectory of the gas extraction, α , given in Figure 2.13 (bottom). The gas flow rate removed from the midsection of the reactor (Q) can be calculated from the following relation:

$$Q = v_{s,in} A (1 - \alpha) \quad (2.25)$$

The reactor temperature spatial distribution is shown in Figure 2.14. The outlet

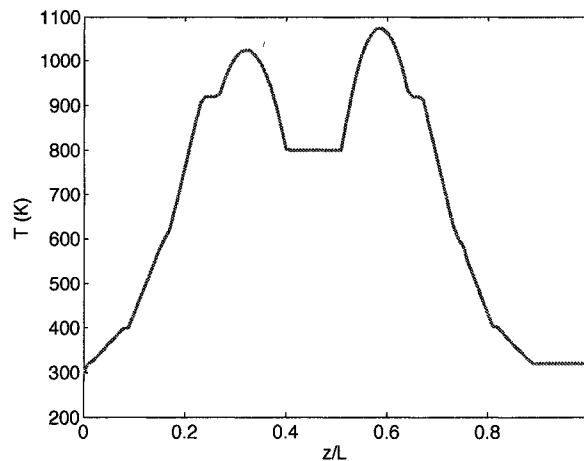


Figure 2.12: Initial temperature distribution along the reactor centerline.

methane conversion and the rate of energy removed from reactor midsection are shown in Figure 2.15 (top) and (bottom), respectively.

From the dynamic behaviour of the system, the following observations are important:

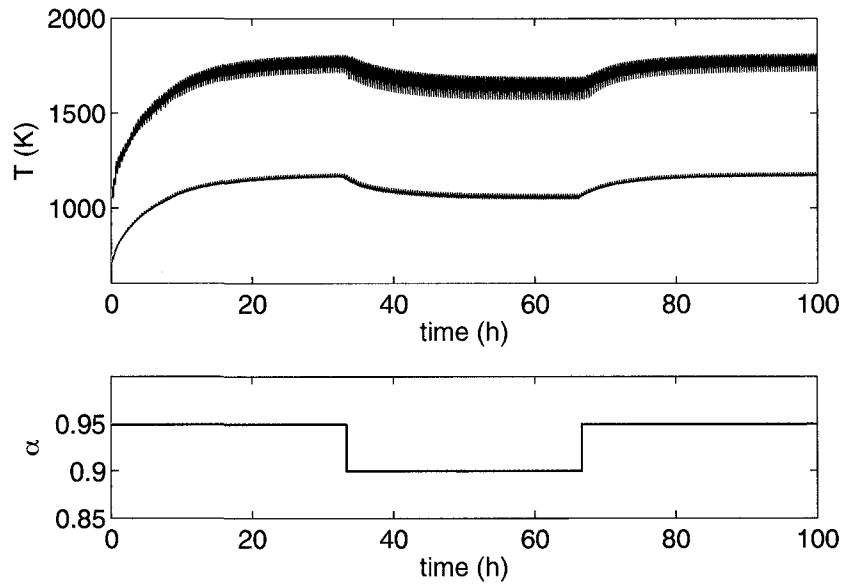


Figure 2.13: Evolution of the maximum and average temperature along the reactor centerline (top) and trajectory of the mass extraction from the reactor midsection (bottom).

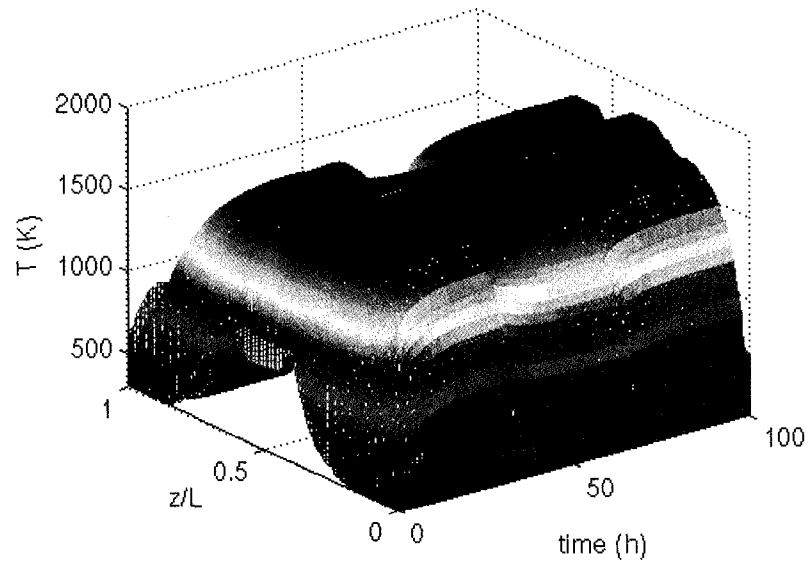


Figure 2.14: Evolution of the temperature distribution along the reactor centerline.

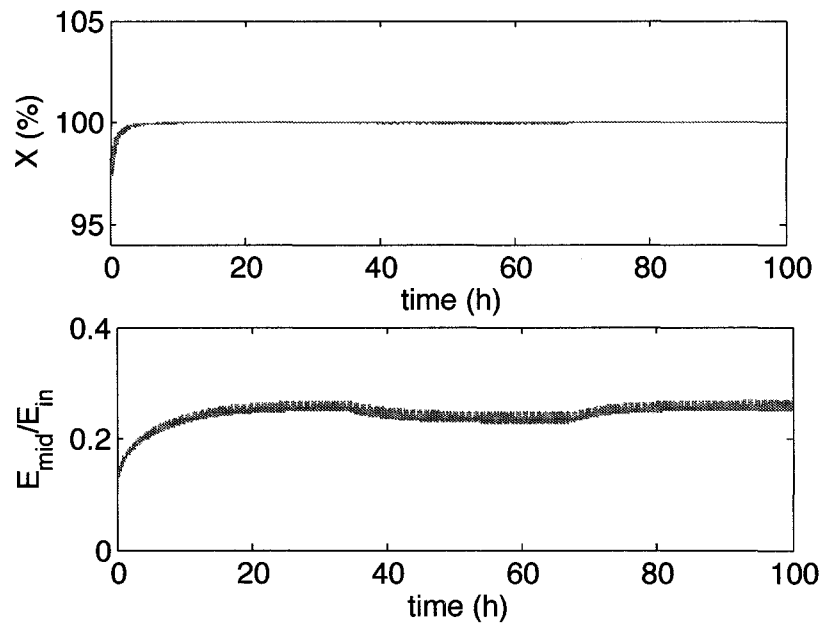


Figure 2.15: Outlet methane conversion (top) and rate of energy removed from reactor midsection (E_{mid}) relative to the total energy fed to the reactor (E_{in}).

- the temperature dynamics has a settling time of the order of hours;
- the maximum temperature follows the same trend as the average temperature;
- the long term dynamic behaviour of the system is time-invariant as the stationary state values for the same operating conditions are the same regardless of the path taken;
- for the long switching time considered ($T_{cycle} = 20$ min), a large fraction of the energy released by the reaction leaves the reactor through the reactor outlet, i.e., $1 - E_{mid}/E_{in}$.

The dynamic behaviour of the reactor in response to changes in the inlet mole fraction of reactant is shown next. Starting from the final stationary state achieved in Figure 2.14, a trajectory of the inlet mole fraction of reactants given by that in Figure 2.16 (bottom) leads to a maximum and average temperature trajectory shown in Figure 2.16 (top). The outlet methane conversion and the rate of energy removed from reactor midsection are shown in Figure 2.17 (top) and (bottom), respectively.

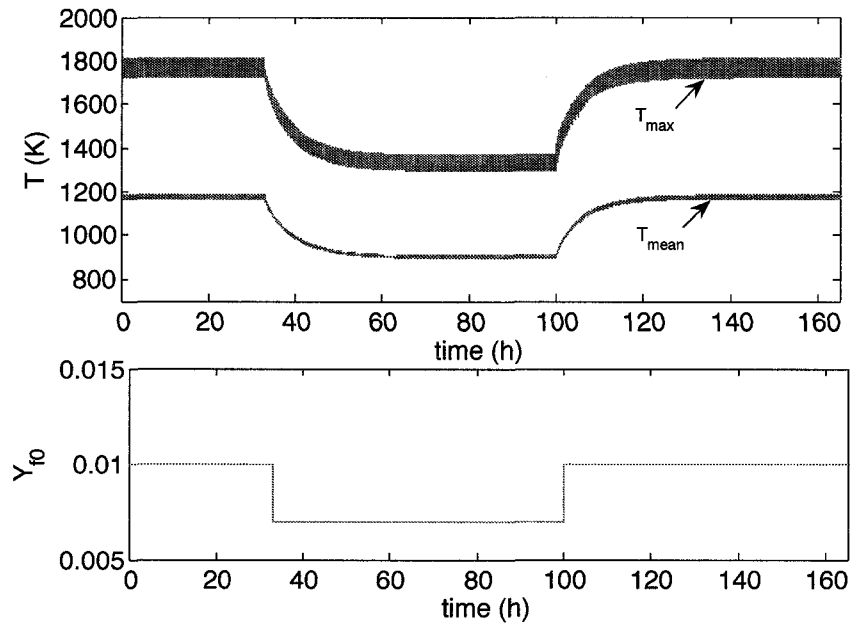


Figure 2.16: (Top) Evolution of the maximum and average temperature along the reactor centerline. (Bottom) trajectory of the inlet mole fraction of reactants.

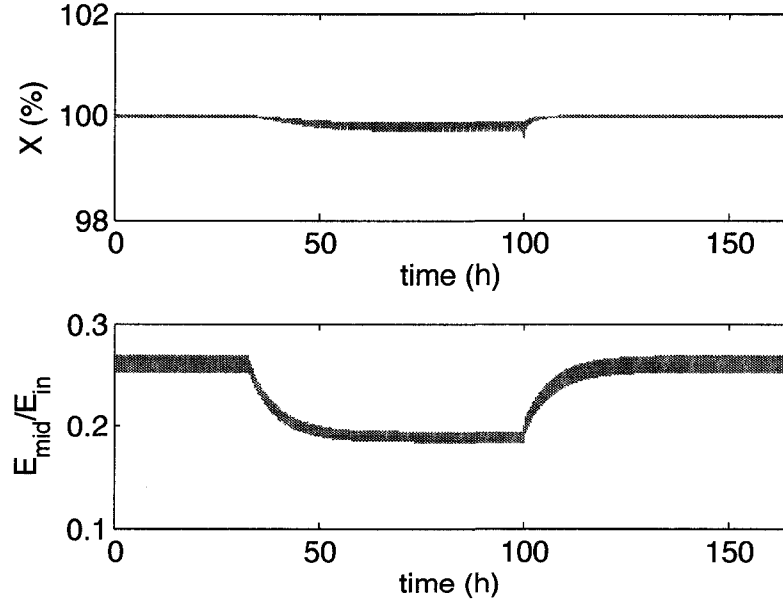


Figure 2.17: (Top) Outlet methane conversion. (Bottom) Rate of energy removed from reactor midsection (E_{mid}) relative to the total energy fed to the reactor (E_{in}).

From the dynamic behaviour of the system, the same conclusions as those stated for changes in the fraction of gas extracted can be drawn for changes in the inlet mole fraction of reactants.

The dynamic behaviour of the reactor to changes in the inlet gas velocity is shown next. Starting from the final stationary state achieved in Figure 2.14, a trajectory in the inlet gas velocity given that in Figure 2.18 (bottom) leads to a maximum and average temperature trajectory shown in Figure 2.18 (top). The outlet methane conversion and the rate of energy removed from reactor midsection are shown in Figure 2.19 (top) and (bottom), respectively.

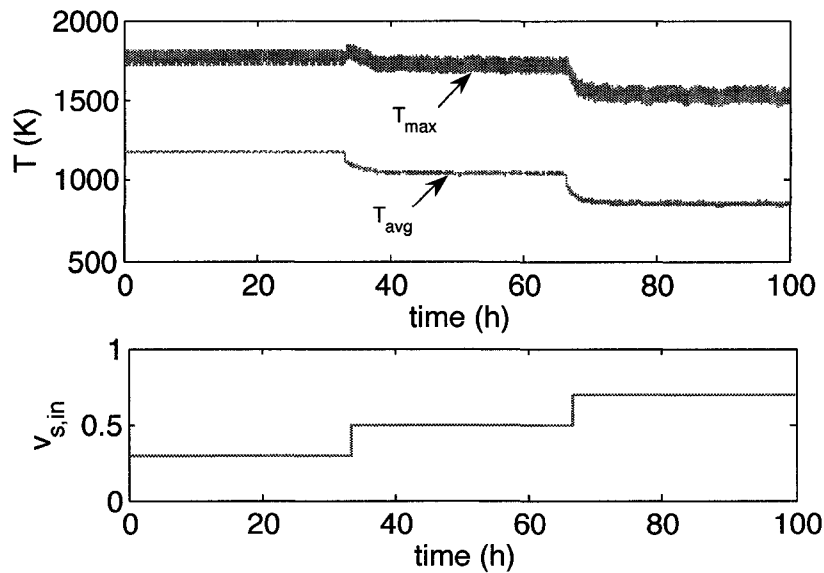


Figure 2.18: Evolution of the maximum and average temperature along the reactor centerline (top) and trajectory of the inlet superficial gas velocity (bottom).

From the dynamic behaviour of the system, it is observed observe that

- the dynamic behaviour of the temperature to changes in the inlet flow velocity is much faster than that for changes in the inlet mole fraction and the fraction of gas removed from the reactor midsection;
- the maximum temperature reacts in one direction right after the changes in the inlet flow velocity are applied and then it evolves towards a stationary state that is in the opposite direction.

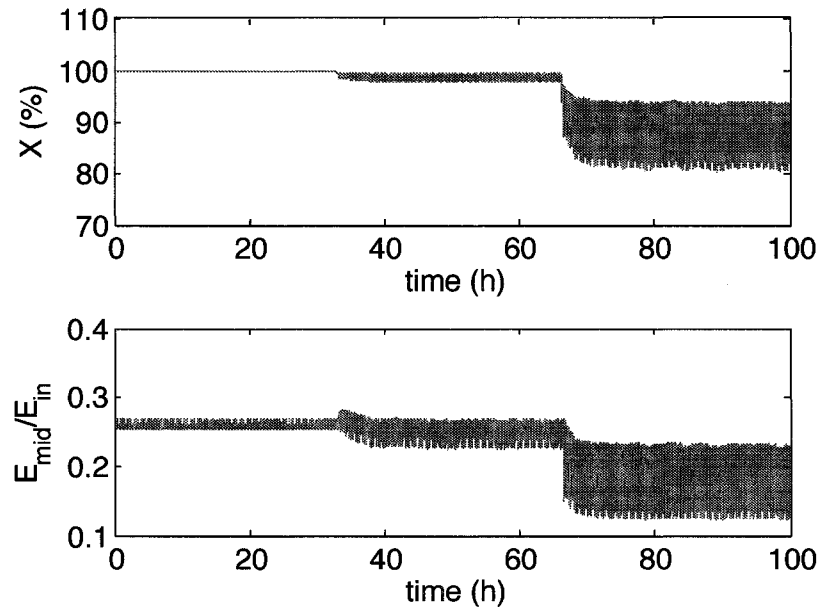


Figure 2.19: Outlet methane conversion (top) and rate of energy removed from reactor midsection (E_{mid}) relative to the total energy fed to the reactor (E_{in}).

Not only operating conditions that are likely to change during normal operation are important to analyze, but also conditions that may remain constant (such as the frequency of flow reversal) can be useful to fully understand the reactor behaviour. Starting from the initial condition given in Figure 2.14, the temperature evolution for two different frequencies of flow reversal is given in Figure 2.20. The outlet methane conversion and the rate of energy removed from reactor midsection are shown in Figure 2.21 (top) and (bottom), respectively.

From the dynamic behaviour of the system, it is observed that

- longer switching times lead to shorter settling times;
- longer switching times leads to large amounts of energy leaving the reactor through the end instead of through the stream at the reactor midsection.

The use of the frequency of flow reversal to control the catalytic reactor is a possible option; however, in practice there are physical limits for the frequency of opening and closing of the valves used to change the flow direction.

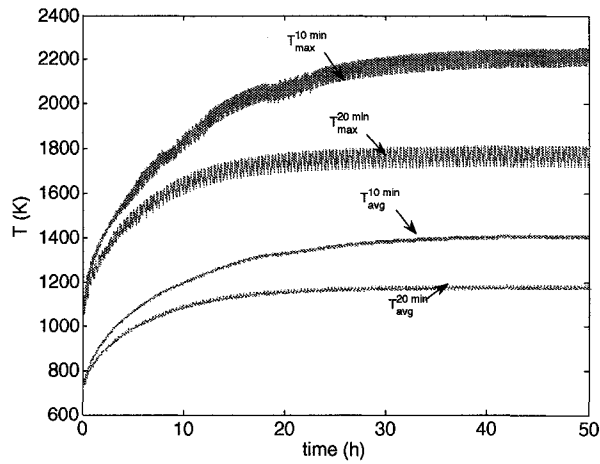


Figure 2.20: Start-up simulation for different switching times.

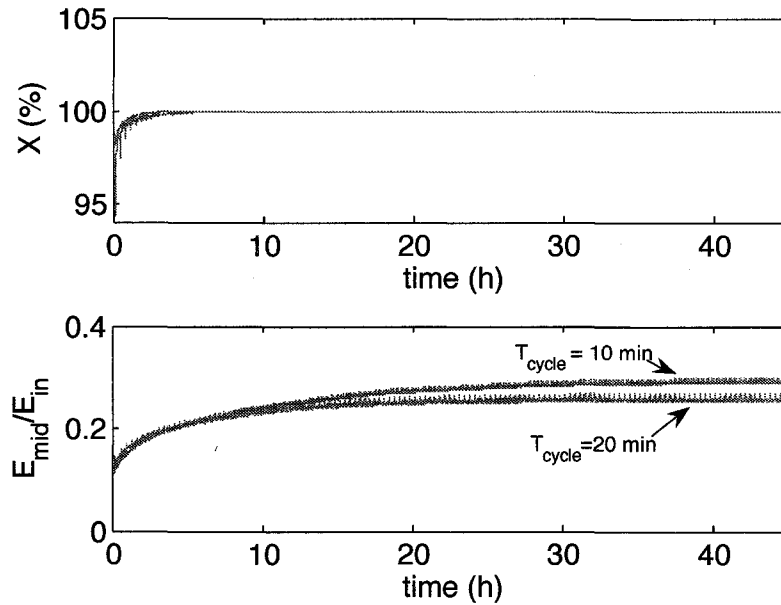


Figure 2.21: Outlet methane conversion (top) and rate of energy removed from reactor midsection (E_{mid}) relative to the total energy fed to the reactor (E_{in}).

2.11.4 Validation of the Pseudo-Homogeneous Model

Studying the dynamics of the 2-D heterogeneous model helps to understand the type of behaviour expected in the actual catalytic reverse flow reactor; however, the 2-D heterogeneous model is too complex for control design and even more for incorporation

into a model-based control algorithm. Therefore, a simpler 1-D pseudo homogeneous model was derived for control purposes.

To assess the suitability of the model to predict the behaviour of the pilot CFRR unit, a wide range of simulations were performed for the reactor configuration given in Figure 2.22.

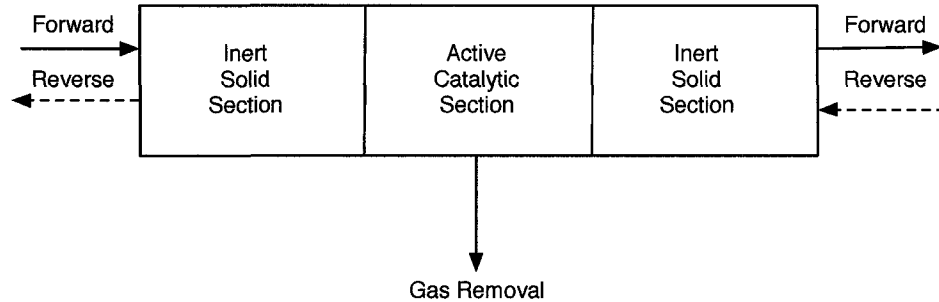


Figure 2.22: Illustration of the CFRR unit used for simulation in the case studies. Inert Sections: solid support without any catalyst material; Active Section: solid support with a catalyst material

One of the main assumptions in the 1-D pseudo-homogeneous model is that the transport phenomena is in plug flow (no axial mixing). Theoretically, this assumption is justified by looking at the Peclet number in the 2-D heterogeneous model in the axial direction:

$$Pe_h = \frac{L_c v_s \rho_f C p_f}{k_{af,eff}}, \quad Pe_m = \frac{L_c v_s}{D_{a,eff}}, \quad (2.26)$$

where L_C is the characteristic length of each of the reactor sections. The Peclet number distribution in the reactor for a typical operating condition is shown in Figure 2.23. In turbulent flow, the maximum value of the particle Peclet number for packed beds ($L_c = D_H$) tends to a constant value independent of the Reynolds number. For gases, the constant for the axial Peclet number is about 2, see Pe definition in Table A.1. Therefore, we can observe from Figure 2.23 that plug flow assumption is justified. In the monolith sections, the Peclet number ($L_c = L$) is large and therefore, mass and heat diffusion can be neglected. The plug flow assumption might not be accurate after the first few seconds that follows the flow reversal process; however, this time is usually short compared to the total of time of each semi-cycle.

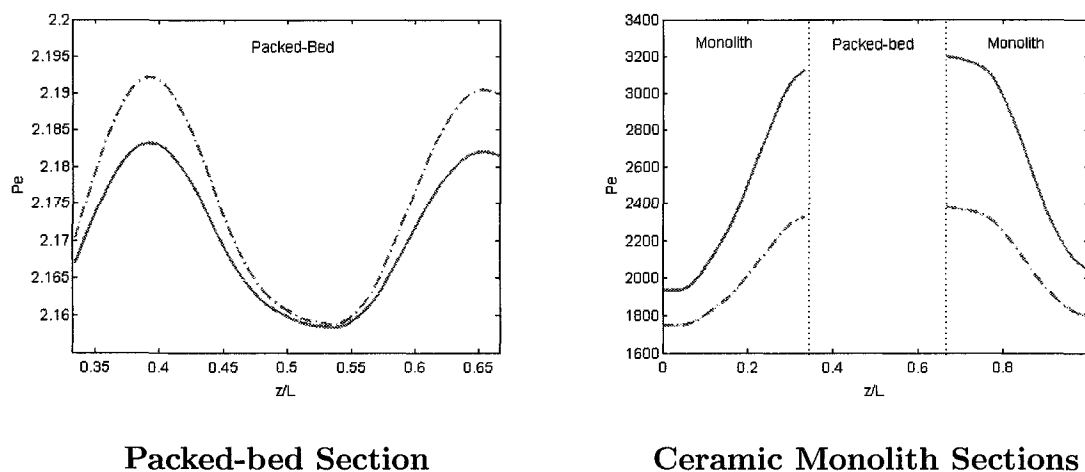


Figure 2.23: Distribution of the Peclet number along the reactor centerline. Solid line: Pe_m ; dashed-dot line Pe_h . Operating conditions: $v_{sin} = 0.3 \text{ m} \cdot \text{s}^{-1}$, $T_{f0} = 298 \text{ K}$, $Y_{f0} = 0.5 \%$ and $\alpha = 1$.

Another assumption made in the 1-D pseudo-homogeneous model is that the process variables in the fluid and solid phase are the same. Figure 2.24 shows the difference between the fluid and solid temperature along the centreline of the reactor for a typical operation. Although the difference is small for the simulated case, and for a wide range of operating conditions, we cannot rule out the possibility that larger differences may occur; however, modelling such differences, if they occur at all, comes at the expense of a more complex heterogeneous model.

An overall assessment of the difference between the 2-D heterogeneous model and the 1-D pseudo-homogeneous model indicates that the output variables of both models agree in the short term, but they differ in the long term, see Figure 2.25. Figure 2.25 shows a comparison of the solid-phase temperature, T_s , of the 2-D model and the homogeneous T for the 1-D model.

For design and simulation, plant/model mismatch might not be tolerable, but for control purposes mild mismatch is tolerable because the missing information can be recovered by feedback control schemes.

To improve the accuracy of the 1-D model in an effective but simple way, a heat dissipation term can be added to model the heat transfer in the radial direction. An effective heat transfer coefficient would have to be computed to model the effective

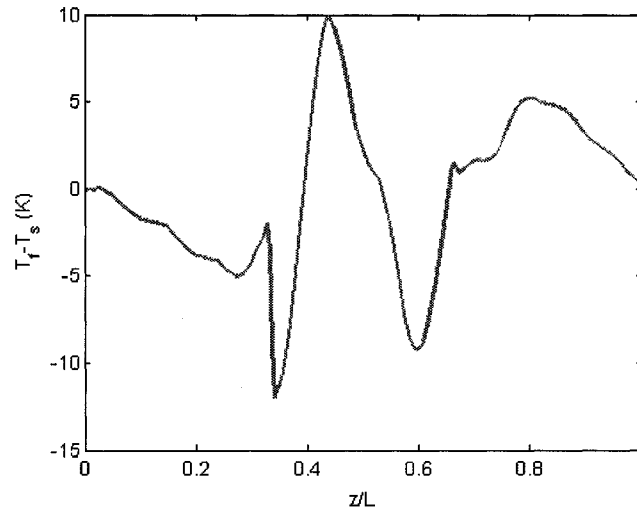


Figure 2.24: Temperature difference between fluid and solid phase along the reactor centerline. Operating conditions: $v_{sin} = 0.3 \text{ m} \cdot \text{s}^{-1}$, $T_{f0} = 298 \text{ K}$, $Y_{f0} = 0.5 \%$ and $\alpha = 1$.

heat transfer between T to a heat source/sink variable that represents the insulation at some distance from the reactor centerline. For illustrative purposes, the 2-dimensional solid temperature distribution in the reactor is shown in Figures 2.26 and 2.27 for two different frequencies of flow reversal.

2.12 Empirical Modelling

It is well known that controllers designed from first principle models offer a wider range of operability. First principle models usually include a great level of detail of process dynamics; however, it is not always possible to find accurate first principle models, and therefore empirical models obtained from process input/outputs are needed.

To the authors knowledge, studies that develop and use empirical dynamical models in a model based control scheme for a catalytic flow reversal reactor have not been published. In this section, a procedure to obtain *empirical discrete linear* models for catalytic reverse flow reactors units is described. The procedure is aimed at finding empirical models for a discrete number of inputs and outputs along the reactor.

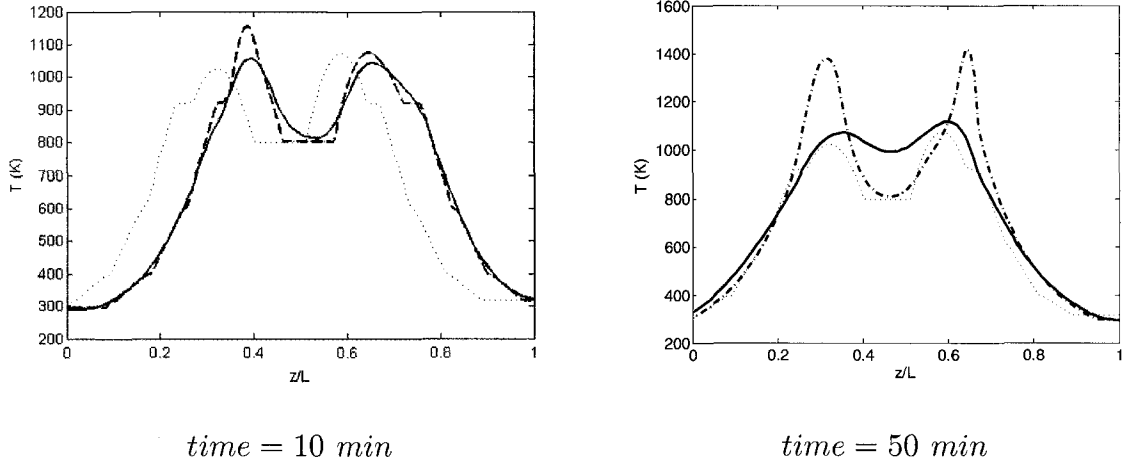


Figure 2.25: Comparison between 1-D pseudo-homogeneous (dashed-dot line) model and 2-D heterogeneous model (solid line). Operating conditions: $v_{sin} = 0.3 \text{ m} \cdot \text{s}^{-1}$, $T_{f0} = 298 \text{ K}$, $Y_{f0} = 0.5 \%$, $\alpha = 1$ and $T_{cycle} = 10 \text{ min}$.

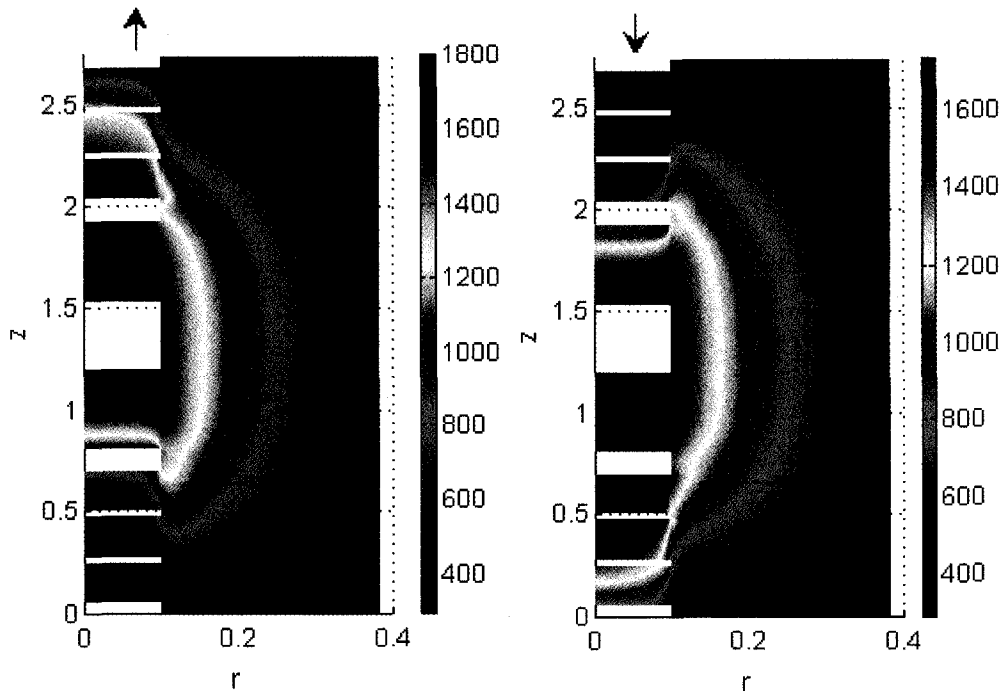


Figure 2.26: 2-D plot of the axial and radial temperature distribution T_s at the stationary state at the end of the semi-cycle and full cycle for $T_{cycle} = 20 \text{ min}$ (flow direction is indicated by the arrows).

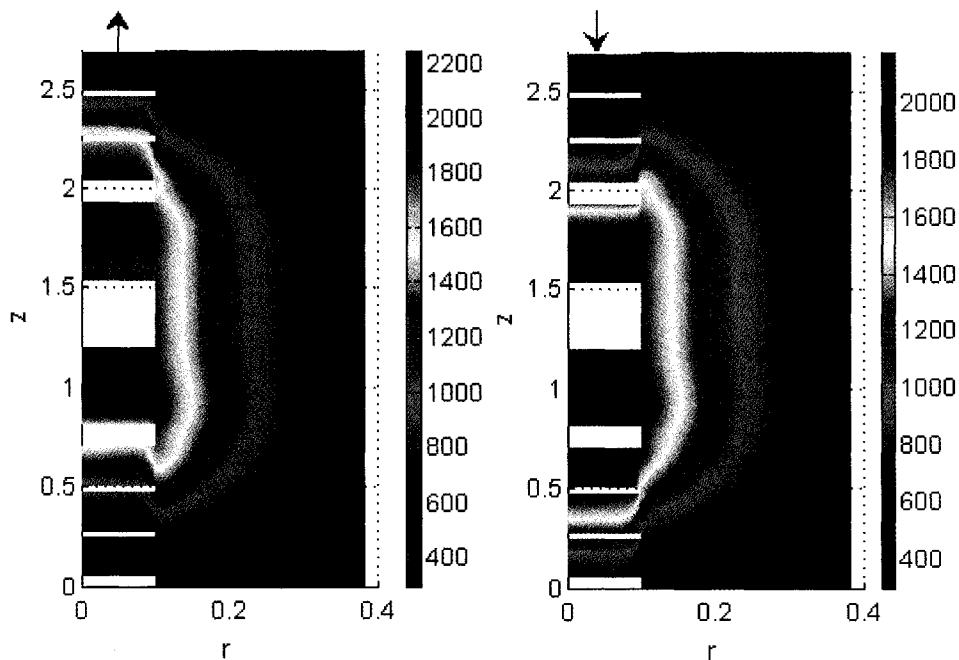


Figure 2.27: 2-D plot of the axial and radial temperature distribution T_s at the stationary state at the end of the semi-cycle and full cycle for $T_{cycle} = 10$ min (flow direction is indicated by the arrows).

The main issue in finding empirical models is that the outputs at discrete spatial points reach a limit cycle at stationary state. Although linear models can be used to describe limit cycles, by for example using a periodic input or by placing the poles on the imaginary axis, modelling the inter-cycle behaviour of the reactor may not be necessary. When the goal is to model the long term behaviour of the output variables, a separation of the time-scales between the switching time and the thermal dynamics can be used. In this way, we can obtain models for the long term input/output behaviour by modelling the reactor dynamics with a sampling rate of, at least, one full cycle.

To obtain empirical models of a catalytic flow reversal reactor, the following procedure is suggested:

1. Bring the CFRR unit to stationary state at the operating conditions that are most likely to occur during normal operation.
2. Perform a step test (or a set of step changes in the manipulated variables)

to obtain a first estimation of the time delay, time constant and gain of the input/output sets. Sample the outputs with a time period equal to the time length of a full cycle.

3. Based on the estimated parameters, design a suitable input signal that excites the range of frequencies where the system has more energy. Measure the outputs at the end of each cycle.
4. Perform typical data conditioning and estimate process models.

2.13 Summary

Catalytic combustion with reverse flow operation is a promising technology for combustion of lean methane emissions and mitigation of greenhouse gases. Moreover, this technology provides an economic incentive because it can be used to generate energy for secondary uses such as heating or power generation.

In this chapter, we developed a computer simulator for a catalytic reactor with reverse flow operation. The computer simulator was based on a 2-D heterogeneous dynamic model. The simulator was used to gain understanding of the reactor dynamics to develop a controller in subsequent chapters.

From the numerical simulations, we observed that the reverse flow reactor considered in this work has a slow time dynamics with a settling time in the order of hours. It was observed that the long term dynamic behaviour of the system is time-invariant as the stationary state values for the same operating conditions are the same regardless of the path taken.

Regarding the energy extracted from the reactor midsection, it was observed that, at long switching (or reverse flow) times, a large fraction of the energy released by the reaction is lost through the reactor outlet.

For control purposes, the dynamic of the temperature to changes in the inlet flow velocity is much faster than that for changes in the inlet mole fraction and in the fraction of gas removed from the reactor midsection. We observed that the maximum temperature reacts in one direction right after the changes in the inlet flow velocity

are applied and then it evolves towards a stationary state that is in the opposite direction. Similar results might be expected, although not observed at the operating conditions considered here, for other operating conditions when the inlet mole fraction or the fraction of gas extracted from the reactor midsection are changed.

Regarding the flow switching time, long switching times lead to short settling times but large amounts of energy are lost through the end of the reactor instead of through the high temperature stream at the reactor midsection. The stream at the reactor midsection has a higher temperature and therefore it can be exploited to easily to recover the energy from this stream.

In this chapter, a 1-D pseudo-homogeneous model was developed and validated so that it could be used in the proceeding chapters for control design. The model was tested against a more detailed 2-D model to assess the sensitivities of the model outputs to the assumptions used in the simplified model.

Having understood the dynamic behaviour of a catalytic flow reversal reactor, we define here the conditions by which reactor is under "ideal" operating conditions.

During *ideal* operation:

- the temperature within the active sections of the reactor is high enough to keep the combustion reaction ignited.
- the maximum temperature within the active sections of the reactor is below the deactivation temperature of the catalyst.
- most the heat produced by the reaction is recovered for use in secondary processes.

Disturbances to the ideal operation mainly occur from changes in the

- inlet concentration;
- inlet fluid flow velocity;

A range of alternatives were proposed in the literature to keep the CFRR system under ideal operation; however, little has been done on control algorithms to achieve automatic control. The next chapters focus specifically on control of CFRR units.

3

Model Predictive Control of a Catalytic Flow Reversal Reactor

In this chapter, the control of catalytic flow reversal reactors (CFRR) is studied. Like any chemical process, these reactors are subject to disturbances in the process variables. The main sources of disturbance in CFRR units are the inlet reactant concentration and inlet gas velocity. Disturbances may lead to operational instability by overheating of the catalyst material or extinction of the reaction. In this chapter, we aim at developing a control scheme that keeps the reactor operating at stable and optimal conditions. The formulation of a model predictive control scheme is studied in this chapter. ¹

3.1 Model Predictive Control: Background

Model Predictive control is a model based control technique that is widely used in the process industry, and is currently receiving much attention in the process control

¹Parts of this chapter are published in Fuxman *et al.* (2006) and Fuxman *et al.* (2007b)

community. In this technique, an explicit model is used to generate predictions of the future plant behaviour. The objective of the MPC control calculations is to determine a sequence of control moves so that the predicted response moves to the desired set point in an optimal manner (Garcia *et al.*, 1989; Camacho and Bordons, 1999; Maciejowski, 2001). In a single input-single output setting, the actual output y , the predicted output \hat{y} , and the manipulated input u are shown in Figure 3.1 (Seborg *et al.*, 1989). At the current sampling instant, denoted by k , the MPC strategy calculates a set of M values of the input $\{u(k+i-1), i = 1, 2, \dots, M\}$. The set consists of the current input $u(k)$ and $M-1$ future inputs. The input is held constant after the M control moves. The inputs are calculated so that a set of P predicted outputs $\hat{\mathbf{y}} = \{\hat{y}(k+i), i = 1, 2, \dots, P\}$ reaches the set point in an optimal manner. The control calculations are based on optimizing an objective function, typically of the form:

$$J = (\mathbf{r} - \hat{\mathbf{y}})^T \mathbf{Q} (\mathbf{r} - \hat{\mathbf{y}}) + \Delta \mathbf{u}^T \mathbf{R} \Delta \mathbf{u}, \quad (3.1)$$

where $\mathbf{r} = \{r(k+i), i = 1, 2, \dots, P\}$ contain the set-point values, $\Delta \mathbf{u} = \{u(k+i) - u(k+i-1), i = 1, 2, \dots, M\}$ and \mathbf{Q} and \mathbf{R} are positive semi-definite time independent weight matrices. The number of predictions P , is referred to as the prediction horizon; while, the number of control moves, M , is called the control horizon.

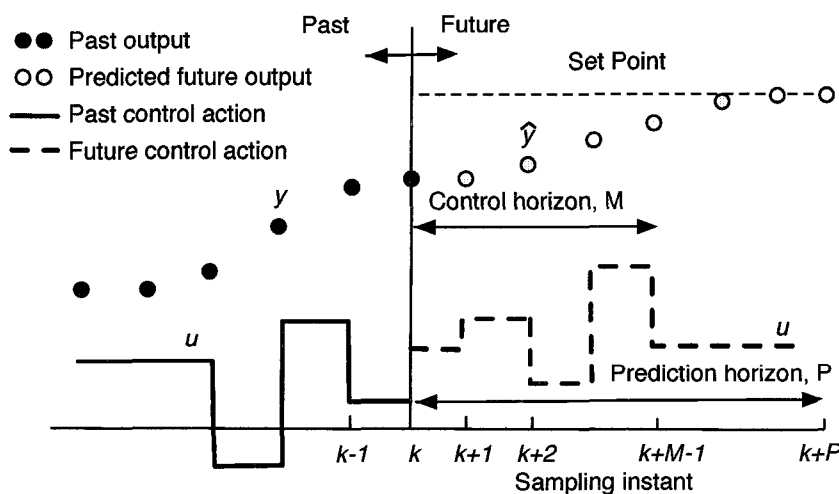


Figure 3.1: Basic concept of Model Predictive Control

Sec. 3.2 Model Predictive Control for Catalytic Flow Reversal Reactors

A distinguishing feature of MPC is its receding horizon approach. Although a sequence of M control moves is calculated at each sampling instant, only the first move calculated in each control interval is implemented. Then a new sequence is calculated at the next sampling instant, after new measurements become available; only the first input move is implemented. This procedure is repeated at each sampling instant.

Model predictive control is becoming increasingly popular (Maciejowski, 2001) because :

- It handles multivariable control problems naturally.
- It can take into account of actuator limitations.
- It allows operation closer to constraints, which frequently leads to more profitable operation.
- Control update rates in the applications where predictive control is successful are relatively low; so there is plenty of time for necessary on-line calculations.

All of the above are of importance for the control of the reverse flow reactor as will become evident in subsequent sections.

3.2 Model Predictive Control for Catalytic Flow Reversal Reactors

From a process control point of view, catalytic reactors with reverse flow operation pose a challenging problem. Many of the inherent characteristics of this type of reactor are the focus of current research within the process control community. The design and modelling of catalytic flow reversal reactors have been thoroughly investigated; however, for a stable and optimal operation of the system, a robust control strategy is required. Control of such systems is an area that has not received much attention until recently.

The control of CFRR units has been approached by different control techniques including feedback PID and feed-forward (Budman *et al.*, 1996); linear quadratic

Sec. 3.2 Model Predictive Control for Catalytic Flow Reversal Reactors

regulator (Edouard *et al.*, 2005) and model predictive control (Dufour *et al.*, 2003; Dufour and Toure, 2004; Balaji *et al.*, 2007).

Within the model predictive control framework, the main challenges in controlling catalytic reactors with reverse flow operation are summarized as follows:

- *Distributed Parameter Nature*: In the area of process control, the bulk of the control theory and control applications deal with lumped parameter systems where ordinary differential equations are used to model the controlled process. Control of distributed parameter systems has been addressed in the literature by various schemes such as *early lumping*, where the distributed parameter system is discretized at the earliest opportunity into an approximate model consisting of a set of ordinary differential equations in time; or *late lumping* that takes advantage of available distributed control theory (Ray, 1981). Despite the advantages of late lumping, it requires greater knowledge of distributed parameter control theory.

Within the model predictive control scheme, Dubljevic *et al.* (2006) and Dubljevic *et al.* (2005) used modal decomposition for parabolic PDE systems to derive a finite-dimensional approximation that captures the dominant dynamics of the infinite-dimensional system. For hyperbolic PDE models, Shang *et al.* (2004), exploited the underlying geometry of hyperbolic PDEs to produce a high performance MPC which was termed characteristics-based model predictive control. In Dubljevic *et al.* (2005) the MPC problem for hyperbolic PDE was approached through finite dimensional approximation of the underlying PDE system.

All published studies on the control of catalytic reverse flow reactors by MPC use the early lumping approach and apply techniques drawn from conventional lumped parameter control theory. In this chapter, we study the application of a what can be considered a late lumping technique in which the method of characteristics for the solution of hyperbolic PDEs is embedded in a MPC scheme. The selection of the technique was inspired in the work of Shang *et al.* (2004), where a high-performance MPC that does not require substantial on-

line computations and provides high accuracy in the prediction of the process output variables can be developed by using the method of characteristics.

- *Dynamic Operation and Nonlinear Dynamics:* A basic feature of model predictive control is that it requires a model of the process dynamics to predict the future process behaviour. One of the main challenges with catalytic reverse flow reactors is that there is, currently, no mathematical model in closed form available to predict the short and long term process behaviour. Mathematical models are usually developed on the basis of a single flow direction, and then the boundary conditions are changed to account for the flow reversal (Matros and Bunimovich, 1996; Marin *et al.*, 2005; Aube and Sapoundjiev, 2000; Salomons *et al.*, 2004). On the basis of a single flow direction model, simulation of the process for a sequence of full cycles would require, for example, an analytical solution of the model equations that can then be assembled to generate the full solution. For complex distributed parameter systems, analytical solutions are generally not possible and thus we need to rely on a numerical approximation. Numerical approximations and their solutions applied to the dynamical models for reverse flow reactors require the solution of a series of PDE equations in a sequential fashion. Such numerical solutions may require, depending on the model fidelity, a high computational time to compute the process dynamics up to the stationary state.

In addition to the dynamic operation, catalytic reverse flow reactors have nonlinear dynamics. There are a variety of MPC schemes that take advantage of nonlinear dynamic models. These schemes range from algorithms that employ a linearized model, which is updated regularly, to schemes that use the full nonlinear model directly (Biegler *et al.*, 2002; Diehl *et al.*, 2002; Bock and Plitt, 1984). In this chapter, a nonlinear MPC algorithm is used. The algorithm employs local linear models, which are computed from integration of characteristic ODEs that model the reactor system. Additional information is provided in the proceeding sections.

- *Manipulated Variables:* In the majority of control studies for plug flow chemical

Sec. 3.2 Model Predictive Control for Catalytic Flow Reversal Reactors

reactors it is considered that the reactor is surrounded by a cooling/heating jacket, see for example (Ray, 1981; Christofides, 2000; Aksikas, 2005), and the entire temperature spatial profile along the reactor is controlled. In general, for catalytic reactors, with reverse flow operation, a manipulated variable that is not distributed in space, but rather located in the reactor midsection is used, (see Section 2.5 for an overview of the different control configurations). Using a single or a set of actuators (manipulated variables) restricts the control achievements and it may not be possible to control the output variables spatial profile; however, it might be possible to control the output variables variables at a single or set of spatial locations along the reactor.

- *Controlled variables:* In all of the studies that approach the control of catalytic reactors with reverse flow operation, the temperature at a single spatial location was controlled, see for example (Dufour *et al.*, 2003; Dufour and Toure, 2004). The spatial point located in the middle section of the reactor or at the entrance of the catalytic sections is chosen on the basis that the maximum and minimum temperature is achieved at that location; however, there is no guarantee that the maximum temperature will be located at a single point if the the frequency of flow reversal is slow and if there is sufficient time for the fluid to shift the temperature profile back and forth by convection. Keeping the minimum temperature at the entrance of the active sections above a minimum value can guarantee that the reaction will not extinguish, but it might not be the optimal way of controlling the system because more energy can be removed without extinguishing the reaction. The main assumption used in (Dufour *et al.*, 2003; Dufour and Toure, 2004) is that the frequency of flow reversal is high and thus the temperature profiles inside the reactor do not move back and forth. High frequencies of flow reversal was justified by the type of application considered for the reactor.

3.3 Contributions

The main contribution of this chapter is the analysis and development of a model predictive control scheme for CFRR units with slow frequency of flow reversal. Slow frequencies are required in the processing of large volumes of gas. Such slow frequency of operation leads to the movement or shifting of the spatial distribution of the state variables back and forth along the reactor. The movement poses a more challenging control problem than that observed when fast frequencies are employed.

Through the development of the model predictive control scheme, the following contributions to the control of CFRR units are addressed:

- Propose a weighted average of the temperature spatial profile along the reactor as the output variable that can be controlled to avoid reactor shutdown due to reaction extinction.
- Use of mass extraction from the reactor midsection section as the manipulated variable. Mass extraction is, from an operational point of view, more advantageous than energy removal via heat exchange and is simpler to implement in practice; however, it poses some challenges for process control.
- Develop a model predictive control scheme that incorporates the method of characteristics to predict the process output variables. Such an MPC approach has been proposed in the literature to produce a method that does not require substantial on-line computations and provides high accuracy in the prediction, but has not been applied to complex catalytic reactors such as CFRR units.
- Discuss in detail the selection of the tuning parameters in an MPC controller for CFRR units.

3.4 Control Objectives

The control objectives for the purposes of this work are summarized, in order of importance, as follows:

1. to avoid reaction extinction by keeping the average temperature in the reactor as constant as possible at an appropriate level and at all times.
2. to reduce or eliminate catalyst overheating by restricting the maximum temperature to be below a threshold value.
3. to maximize the energy extraction from the reactor unit by maximizing the mass of extracted hot gas.

3.5 Selection of Controlled Variables

Under normal operation, it is required that the maximum temperature in the catalytic sections of the reactor remain below a catalyst deactivation temperature. Moreover, the temperature along the active catalytic sections should be such that the reaction does not extinguish. We attempt to achieve this objective by controlling the total energy within the reactor. For this purpose, we use the average temperature of the solid material in the reactor unit as an indication of the total energy.

To show that the average temperature gives an indication of the total energy, an overall energy balance around the reactor system is used:

$$\begin{aligned} \frac{d}{dt} \sum_{i=1}^l \int_{z_i}^{z_{i+1}} \rho_s^i C p_s^i (T_s - T_{f,in}) dz &= v_{s,in} A \Delta H_r C_{in} Y_{CH_4,in} - v_{s,out} A C p_{f,out} \rho_{f,out} \cdot \\ (T_{f,out} - T_{f,in}) - v_{s,mid} A C p_{f,mid} \rho_{f,mid} (T_{f,mid} - T_{f,in}) & \end{aligned} \quad (3.2)$$

In equation (3.2), l represents the total number of solid-bed materials inside the reactor. Other parameters in (3.2) are defined in Appendix A. In equation (3.2), it is assumed that the energy accumulation in the fluid phase (gas) is negligible with respect to the accumulation in the solid phase as the heat capacity of a typical solid bed is about three orders of magnitude larger than the gas. In general, ρ_s and $C p_s$ are a weak function of the temperature and therefore they can be considered constant for each different solid bed material inside the reactor:

$$\begin{aligned} \frac{d}{dt} \sum_{i=1}^l \rho_s^i C p_s^i \left(\int_{z_i}^{z_{i+1}} T_s dz - \int_{z_i}^{z_{i+1}} T_{f,in} dz \right) &= v_{s,in} A \Delta H_r C_{in} Y_{CH_4,in} - \\ v_{s,out} A C p_{f,out} \rho_{f,out} (T_{f,out} - T_{f,in}) - v_{s,mid} A C p_{f,mid} \rho_{f,mid} (T_{f,mid} - T_{f,in}) & \end{aligned} \quad (3.3)$$

By dividing both sides of equation (3.3) by the total length of the reactor L , we obtain:

$$\begin{aligned} \frac{d}{dt} \frac{1}{L} \sum_{i=1}^l \rho_s^i C p_s^i \int_{z_i}^{z_{i+1}} T_s dz = \frac{1}{L} (v_{s,in} A \Delta H_r C_{in} Y_{CH_4,in} - v_{s,out} A C p_{f,out} \rho_{f,out} \cdot \\ (T_{f,out} - T_{f,in}) - v_{s,mid} A C p_{f,mid} \rho_{f,mid} (T_{f,mid} - T_{f,in}) + \sum_{i=1}^l \rho_s^i C p_s^i T_{f,in} (z_{i+1} - z_i) \end{aligned} \quad (3.4)$$

To compute the integral on the left-hand side of equation (3.4), a numerical approximation is needed. If, for example, the trapezoidal method is used (Lapidus, 1962),

$$\int_a^b f(x) dx = h \left(\frac{y_0}{2} + y_1 + y_2 + \cdots + y_{m-1} + \frac{y_m}{2} \right) + O(\Delta h^3), \quad (3.5)$$

where $h = (b - a)/m$, then the left-hand side of equation (3.4) becomes a linear combination of discrete temperature values along the axis of the reactor:

$$\frac{d}{dt} \sum_{i=1}^l \frac{1}{L} \rho_s^i C p_s^i \sum_{j=1}^m v^j T_s^j \quad (3.6)$$

$$\frac{d}{dt} \sum_{k=1}^n \frac{1}{L} w^k T_s^k = \frac{d}{dt} (\mathbf{w} \mathbf{T}_s) = \frac{d}{dt} T_{avg} \quad (3.7)$$

where n is the total number of discrete spatial nodes along the reactor centerline and \mathbf{w} is a vector of appropriate weights. Equation (3.7) is the time derivative of the *weighted average* temperature that will be referred in this chapter as average reactor temperature. By substituting equation (3.7) in (3.4), we obtain

$$\begin{aligned} \frac{d}{dt} (\mathbf{w} \mathbf{T}_s) = \frac{1}{L} (v_{s,in} A \Delta H_r C_{in} Y_{CH_4,in} - v_{s,out} A C p_{f,out} \rho_{f,out} \cdot \\ (T_{f,out} - T_{f,in}) - v_{s,mid} A C p_{f,mid} \rho_{f,mid} (T_{f,mid} - T_{f,in}) + \sum_{i=1}^l \rho_s^i C p_s^i T_{f,in} (z_{i+1} - z_i) \end{aligned} \quad (3.8)$$

From an overall mass balance around the reactor system, we obtain

$$v_{s,in} \rho_{in} A = v_{s,out} \rho_{out} A + v_{s,mid} \rho_{mid} A' \quad (3.9)$$

By assuming that the gas behaves as an ideal gas and that the change in the gas velocity due to changes in the temperature can be approximated by $v_s = v_{s,in}T/T_{in}$ (Salomons *et al.*, 2004), we obtain

$$v_{s,in} = v_{s,out} + v_{s,mid} \frac{A'}{A} \quad (3.10)$$

By defining $\alpha = v_s/v_{s,in}$, where v is the gas velocity at any point within the reactor, we obtain

$$v_{s,in} = \alpha v_{s,in} + v_{s,mid} \frac{A'}{A} \Rightarrow v_{s,in} = \alpha v_{s,in} + (1 - \alpha) v_{s,in} \quad (3.11)$$

and

$$\begin{aligned} \frac{d}{dt} T_{avg} = & \frac{1}{L} (v_{s,in} A \Delta H_r C_{in} Y_{CH_4,in} - \alpha v_{s,in} A C p_{f,out} \rho_{f,out} \cdot \\ & (T_{f,out} - T_{f,in}) - (1 - \alpha) v_{s,in} A C p_{f,mid} \rho_{f,mid} (T_{f,mid} - T_{f,in}) + \\ & \sum_{i=1}^l \rho_s^i C p_s^i T_{f,in} (z_{i+1} - z_i)) \end{aligned} \quad (3.12)$$

By looking at equation (3.12), we observe that by manipulating α , we can control the average temperature which is an indication of the total energy contained in the reactor. By keeping the energy at set-point value, we can be certain that the reaction will maintained and will not extinguish after disturbances in uncontrolled process variables enter the system.

It is important to note that the average temperature is used to control the total energy in the reactor, but does not address the problem of controlling the maximum temperature directly. In fact, a constant average temperature may come at the expense of a lower minimum temperature and a higher maximum temperature. A high maximum temperature can cause overheating and catalyst deactivation. Therefore, an additional control objective is needed to restrict the maximum temperature in the solid material within the reactor to be below a catalyst deactivation temperature.

3.6 Selection of Manipulated Variables

To collect and recover energy from the reaction, and avoid sharp changes in the temperature distribution along the reactor, Aube and Sapoundjiev (2000) suggested

the use of gas extraction from the midsection of the reactor to keep the CFRR under control. Following this suggestion, we studied the formulation of a controller where the gas flow velocity from the reactor midsection is used as manipulated variable.

By means of gas extraction from the reactor midsection, we can fulfill one of the main requirements for ‘ideal’ operation of the CFRR unit: *i.e. recovery of the heat generated by the reaction* for secondary processes. It should be noted that the maximum rate of energy recovered, at stationary state, can only be less or equal to the energy generated by complete depletion of reactants. Otherwise, the system will not reach stationary-state and reaction extinction or reactor overheating will occur.

3.7 MPC Controller Formulation

Conventional approaches to controller design for a distributed parameter systems use lumping techniques that discretize the underlying partial differential equation (PDE) model into a finite number of ordinary equations (ODE’s). Discretization techniques, such as finite difference, finite element and finite volume can be used to discretize the model into a set of ODE’s. Based on the approximate difference equations obtained from discretization, controllers can be designed using control methods for ordinary differential equations (ODE’s).

Recent approaches for control of distributed parameter systems have focused on the development of control methods that directly account for their spatially distributed nature. In this direction, the well known classification of PDE systems into elliptic, parabolic and hyperbolic, according to the properties of the spatial differential operator, essentially determines the approach followed for the solution of the control problem (Christofides, 2000). Christofides and co-workers have provided a considerable amount of work on nonlinear order reduction and control of nonlinear parabolic PDEs for systems where diffusion dominates convection (Christofides (2000) and references therein). Various extensions of nonlinear control techniques can be found in the literature for the control of hyperbolic PDE systems: sliding mode control (Hanczyc and Palazoglu, 1995); geometric control (Christofides, 2000); adaptive control (Hudon *et al.*, 2005) and model predictive control (Shang *et al.*, 2004).

In Shang *et al.* (2004), a characteristics-based model predictive control was proposed and applied to hyperbolic PDE systems with characteristic equations of same order of magnitude. In this chapter, the application of the characteristics based-MPC is extended to catalytic reactor systems. Due to the two time scales of the reactor's dynamics, the system possesses two characteristics, which differ though about three orders of magnitude. To address this issue, two cases were studied: one where both characteristic lines were considered (*multiple characteristics*) and another one where only one characteristic (*single characteristic*) is considered.

The characteristics-based model predictive control consists of three basic steps:

1. The method of characteristics is used to transform the PDE model to an equivalent set of ordinary differential equations (i.e., transform the distributed parameter model to an equivalent lumped parameter model);
2. A nonlinear predictive controller is designed based on the equivalent lumped parameter model.
3. A constrained quadratic program is solved to obtain the optimal input that minimize a control performance objective function.

3.8 Method of Characteristics

In this section, we briefly review the method of characteristics for hyperbolic distributed parameter systems.

Consider the quasi-linear (explicit) first order PDE

$$a(t, z, x) \frac{\partial x}{\partial t} + b(t, z, x) \frac{\partial x}{\partial z} = c(t, z, x). \quad (3.13)$$

Let $x = \vartheta(t, z)$ be a solution of (3.13). A geometrical interpretation of this solution is as follows (Mattheij *et al.*, 2005). The independent variables t and z and the dependent variable x constitute a two-parameter family of vectors $(t, z, x)^T$ that is lying on a surface $\mathcal{S} \subset \mathbb{R}^3$. This surface \mathcal{S} , given by $F(t, z, x) = \vartheta(t, z) - x = 0$, is called integral surface of (3.13). A normal \mathbf{n} on \mathcal{S} is given by

$$\mathbf{n} = \nabla F = \left(\frac{\partial \vartheta}{\partial t}, \frac{\partial \vartheta}{\partial z}, -1 \right)^T. \quad (3.14)$$

Hence, for an infinitesimal displacement $d\mathbf{x} = (dt, dz, dx)^T$ along the surface, we find

$$\mathbf{n} \cdot d\mathbf{x} = \frac{\partial \vartheta}{\partial t} dt + \frac{\partial \vartheta}{\partial z} dz - dx = 0. \quad (3.15)$$

Comparing (3.13) and (3.15), we find that for a solution $x = \vartheta(t, z)$ of (3.13) the following should hold on the integral surface \mathcal{S} :

$$\begin{bmatrix} a & b \\ dt & dz \end{bmatrix} \begin{bmatrix} \frac{\partial \vartheta}{\partial t} \\ \frac{\partial \vartheta}{\partial z} \end{bmatrix} = \begin{bmatrix} c \\ dx \end{bmatrix}. \quad (3.16)$$

The solution of the system is unique if and only if $adz - bdt \neq 0$. This result can be interpreted as follows (see Figure 3.2): suppose we have a smooth, one parameter curve $\mathcal{J} = (t(\sigma), z(\sigma), x(\sigma)) | \sigma \in I \subset \mathbb{R}$ on \mathcal{S} , where the condition $adz - bdt \neq 0$ holds. Then the derivatives x_t and x_z are uniquely determined on \mathcal{J} through (3.16). If, moreover, x is given along \mathcal{J} , then the solution $x = \vartheta(t, z)$ exists and is unique, at least in some neighborhood of \mathcal{J} . The curve \mathcal{J} is referred as a curve of initial values. The actual construction of the solution proceeds as follows. Suppose x is

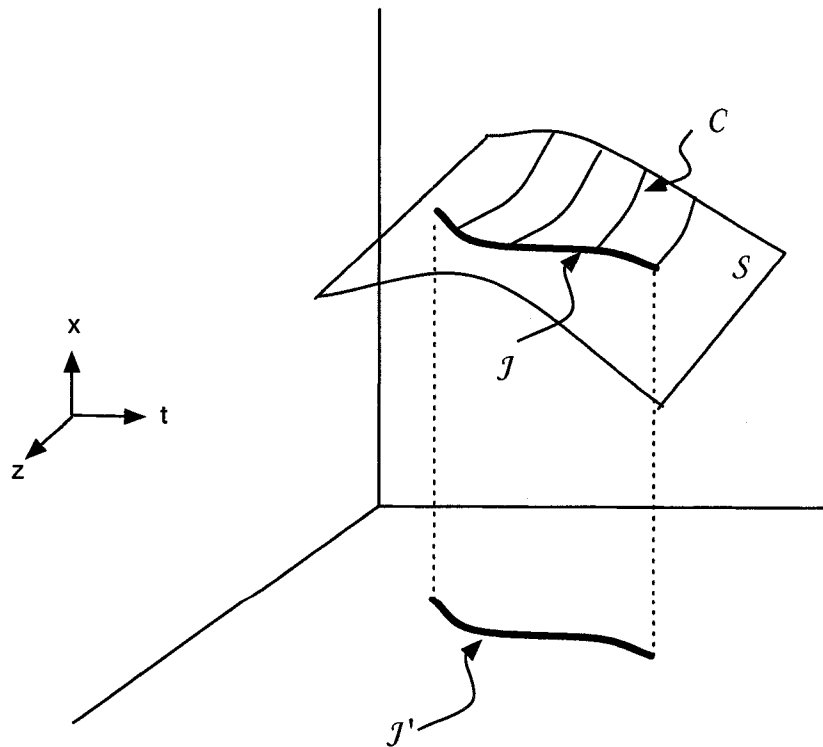


Figure 3.2: Initial curve \mathcal{J} and a characteristic \mathcal{C} on the integral surface \mathcal{S} .

given along an initial curve \mathcal{J} . Consider a curve \mathcal{C} on \mathcal{S} for which $a dz - b dt = 0$. Then the system (3.16) has either no solution or infinitely many. In the latter case the relations

$$\frac{dt}{a} = \frac{dz}{b} = \frac{dx}{c} \quad (3.17)$$

should hold along \mathcal{C} . Clearly, the vector $(a, b, c)^T$ is everywhere tangent to \mathcal{C} . We can now introduce a parametrization $\mathcal{C} = (t(s), z(s), x(s))^T | s \in I \subset \mathbb{R}$ such that 1 and $s = 0$ lie on the initial curve \mathcal{J} . This way, we obtain the set of ODEs

$$\frac{dt}{ds} = a, \quad \frac{dz}{ds} = b, \quad \frac{dx}{ds} = c \quad (3.18)$$

coupled with initial condition of the form

$$x(\sigma; 0) = u(z(\sigma, t(\sigma))) \quad \text{for } (z(\sigma, t(\sigma))) \in \mathcal{J}', \quad (3.19)$$

where \mathcal{J}' is the projection of \mathcal{J} on the (t, z) plane. The ODEs (3.18) are referred to as the *characteristic equations* and the curve \mathcal{C} is a solution of (3.18) and is called *the characteristic*.

For quasi-linear hyperbolic partial differential equations of the form (2.16), for which there exist a matrix \mathbf{T} and $\mathbf{\Lambda}$ as defined by Definition 2.10.1, we can premultiply (2.16) by an arbitrary left eigenvector \mathbf{t}_k^T of \mathbf{B} , giving

$$\mathbf{t}_k^T \frac{\partial \mathbf{x}}{\partial t} + \mathbf{t}_k^T \mathbf{B} \frac{\partial \mathbf{x}}{\partial z} = \mathbf{t}_k^T \left(\frac{\partial \mathbf{x}}{\partial t} + \lambda_k \frac{\partial \mathbf{x}}{\partial z} \right) = \mathbf{t}_k^T \mathbf{c} = \tilde{c}_k. \quad (3.20)$$

We can now find an equivalent ODE system of the form

$$\mathbf{t}_k^T \frac{d\mathbf{u}}{ds} = \tilde{c}_k, \quad (3.21)$$

which should hold on some curve $\mathcal{K} = (t(s), z(s)) | s \in I \subset \mathbb{R}$. Since we have

$$\frac{d\mathbf{u}}{ds} = \frac{\partial \mathbf{u}}{\partial t} \frac{dt}{ds} + \frac{\partial \mathbf{u}}{\partial z} \frac{dz}{ds} \quad (3.22)$$

we thus find by comparing (3.20) and (3.21) and using relation $d\tilde{\mathbf{u}} = \mathbf{T}d\mathbf{u}$ that

$$\frac{dt}{ds} = 1, \quad \frac{dz}{ds} = \lambda_k, \quad \frac{d\tilde{u}_k}{dt} = \tilde{c}_k. \quad (3.23)$$

The curve \mathcal{K} is the characteristic \mathcal{C}_k corresponding to the k^{th} eigenvalue λ_k . If the system (2.16) is hyperbolic, there exist m such characteristics, see Definition 2.10.1.

3.8.1 2-Characteristics Model

To predict the dynamic behaviour of the catalytic reactor, the PDE model equations (2.6) and (2.7) can be used for accurate short term predictions. According to the definition of hyperbolic PDE equations, it is easy to see that the model equations are hyperbolic since

$$\mathbf{\Lambda} = \begin{bmatrix} \frac{\alpha v_{s,in}}{L\epsilon} & 0 \\ 0 & \frac{\alpha v_{s,in}\rho}{L\eta} \end{bmatrix} \quad \mathbf{T} = \begin{bmatrix} 1 & 0 \\ 0 & 1 \end{bmatrix}$$

The equations can be transformed into a set of ODEs by using the method of characteristics. The resulting characteristic curves ξ_1 and ξ_2 are

$$\xi_1 = \frac{dz}{dt} = \frac{\alpha v_{s,in}}{L\epsilon} \quad (3.24)$$

$$\xi_2 = \frac{dz}{dt} = \frac{\alpha v_{s,in}\rho}{L\eta}; \quad (3.25)$$

along which, the state variables Y and T are described by:

$$\frac{dY}{dt} = -k_0 \exp\left(\frac{-E}{R_g T}\right) Y \quad (3.26)$$

$$\frac{dT}{dt} = (-\Delta H_r) k_0 C \exp\left(\frac{-E}{R_g T}\right) Y \quad (3.27)$$

To predict the future state variables at any spatial point, simultaneous integration of equations (3.26) and (3.27) along the two non-parallel characteristic curves (3.24) and (3.25) is required. Predictions of future state values can be obtained by discretizing the initial state at a finite number of spatial points (n) and then projecting the characteristic curves from each of these points and by computing the values of the state variables at the intersection points (Shang *et al.*, 2004). Figure 3.3, illustrates the calculation of the state variables at a point C from the the values at point A and point B. As seen in Figure 3.3, the state variables at any future time is approximated by two points.

The approximation of the state variable value within a segment AC by that at point A and B reflects the true solution of hyperbolic PDE systems more closely than other numerical methods (Shang *et al.*, 2004); however, the spatial discretization of the initial solution affects the accuracy of the predictions. By varying point C and repeating the procedure, the values of the state variables at different grid points and

different future times can be calculated. These predictions of the state variables are then used to compute the optimal control input in the MPC scheme.

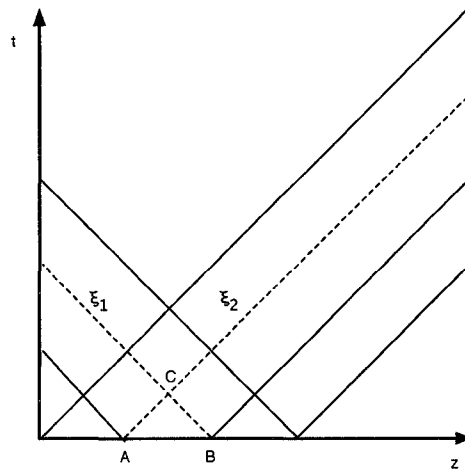


Figure 3.3: Illustration of the computation of future state variables using the method of characteristics

The main advantage of using the method of characteristics is that it allows for the conversion of the underlying PDE model into an ODE model and that the conversion does not require any numerical approximation; however, this advantage can be lost if the model consists of multiple characteristics.

For multiple characteristics models, a numerical approximation is required; however, the method of characteristics can accommodate the use of larger spatial grids and time steps with minimal loss of accuracy (Shang *et al.*, 2004).

In Shang (2002), the method of characteristics for a system with multiple characteristics was applied to a counter flow plug-flow reactor. For such reactor model, it was observed that control performance was satisfactory and that it increased with an increasingly finer discretization. Nevertheless, the characteristic equations in the reactor model had non-homogeneous parts with similar order of magnitude. Application of the method to a system with widely different magnitudes in the non-homogeneous part of the characteristic equations presents some computational issues. Application of the method to a complex process like a catalytic reactor modeled by a system with two characteristics, can provide useful information about possible extensions and limitations of the method in a model predictive control scheme. In

Section 3.10.1, we discuss the limitations of the practical application method for a catalytic reactor.

To provide a computational efficient MPC scheme that uses the advantage of the method of characteristics, the quasi-steady state assumption (typical in catalytic reactor models) is used in the next section.

3.8.2 1-Characteristic Model

To predict the dynamic behaviour of the catalytic reactor, the model equations (2.6) and (2.7) can be further simplified by the assumption that the dynamic behaviour of the mole balance is at quasi-steady state when compared to the energy balance.

Equation (2.7) can be described by a system of DAEs along the characteristic curves ξ :

$$\xi = \frac{dz}{dt} = \frac{\alpha v_{s,in} \rho}{L \eta} \quad (3.28)$$

Along the characteristic curves, ξ , the state variables T is described by:

$$\frac{dT}{dt} = (-\Delta H_r) k_0 C \exp\left(\frac{-E}{R_g T}\right) Y \quad (3.29)$$

Using equations (3.28) and (3.29), we can predict the dynamic behaviour of the temperature without any numerical approximation other than the integration of equation (2.13). For hyperbolic PDE systems with a single characteristic, the method of characteristics can be advantageous for an MPC scheme if, the sampling time used in the control calculations is dictated by the characteristic equation of the system and the controlled outputs are located at the end of the spatial coordinate (Shang, 2002). Under these conditions, no approximation is required to predict the dynamic behaviour of the states in the system.

For the catalytic reactor under study, integration of (3.28) and (3.29) can be performed from a given initial condition. Because the average and maximum temperature are required, a sampling time dictated by the characteristic equation can be used and in this way the full advantage of the method of characteristics in an MPC scheme can be used; however, if the states are required at fixed points in a mesh, then a numerical interpolation can be used to obtain the solutions at fixed mesh points.

3.8.3 MPC problem formulation

A nonlinear version of the traditional model predictive control technique is used in this chapter. The following approximations are necessary in order for the on-line optimization to be a QP at each sampling interval.

- **Effect of Past Manipulated Variables on Predicted Outputs:** The model is described in the form of nonlinear differential equations. The contribution of the effect of past manipulated variables on the predicted outputs is defined as the value of the outputs if there are no input (manipulated variable) changes in the future. This is obtained by integrating the model differential equations from the current state over the prediction horizon with constant inputs.
- **Effect of Future Manipulated Variables on Predicted Outputs:** The contribution of the future manipulated variables to the predicted output is represented with the use of a step model. A linear model obtained by linearization of the nonlinear model at each sampling time is used to compute the step response coefficients.
- **Effect of Future Disturbances on Predicted Outputs:** The unmodeled effects at the current sampling time are computed as the difference between the plant measurements and the model outputs. In the absence of any information on unknown disturbances in the future, it is assumed that the future predicted values of the disturbances are equal to the current values.

To use the predictions from either section 3.8.2 or 3.8.1 in the MPC scheme, an output vector is defined:

$$\mathbf{y} = \mathbf{C}\mathbf{x}$$

where \mathbf{C} is an observation matrix, $\mathbf{x}_{n \times 1}$ is a vector of state variables at the discrete spatial points. The future values of the outputs ($\hat{\mathbf{y}}$) are expressed, at each control

interval, in a locally linear form (Shang *et al.*, 2004):

$$\begin{aligned} \hat{\mathbf{y}} &= \mathbf{C} \cdot \begin{bmatrix} [\hat{\mathbf{x}}(1, 1), \hat{\mathbf{x}}(1, 2), \dots, \hat{\mathbf{x}}(1, H_P)]^T \\ [\hat{\mathbf{x}}(2, 1), \hat{\mathbf{x}}(2, 2), \dots, \hat{\mathbf{x}}(2, H_P)]^T \\ \vdots \\ [\hat{\mathbf{x}}(2n, 1), \hat{\mathbf{x}}(n, 2), \dots, \hat{\mathbf{x}}(n, H_P)]^T \end{bmatrix} \\ &= \mathbf{C} \cdot \begin{bmatrix} [\hat{\mathbf{x}}_0(1, 1), \hat{\mathbf{x}}_0(1, 2), \dots, \hat{\mathbf{x}}_0(1, H_P)]^T \\ [\hat{\mathbf{x}}_0(2, 1), \hat{\mathbf{x}}_0(2, 2), \dots, \hat{\mathbf{x}}_0(2, H_P)]^T \\ \vdots \\ [\hat{\mathbf{x}}_0(n, 1), \hat{\mathbf{x}}_0(n, 2), \dots, \hat{\mathbf{x}}_0(n, H_P)]^T \end{bmatrix} + \mathbf{S}\Delta\mathbf{u} \end{aligned} \quad (3.30)$$

where \mathbf{C} is a $(1 \times n)$ matrix, $\hat{\mathbf{x}}$ is a matrix of dimensions $(n \times H_P)$ of the predicted states for a prediction horizon H_P , $\hat{\mathbf{x}}_0$ is a matrix of dimensions $(n \times H_P)$ of predicted states in the absence of further control actions (u_{-1}), $\Delta\mathbf{u}$ is the vector of future control changes for a control horizon H_c

$$\Delta\mathbf{u} = [u_0 - u_{-1}, u_1 - u_{-1}, \dots, u_{H_c-1} - u_{-1}]^T,$$

and \mathbf{S} is the rate of variation of the states about past control actions (u_{-1})

$$\begin{aligned} \mathbf{S} &= [\mathbf{S}_1, \mathbf{S}_2, \dots, \mathbf{S}_n]^T \\ \mathbf{S}_i &= \begin{bmatrix} \mathbf{s}(i, 1) & 0 & \dots & 0 \\ \mathbf{s}(i, 2) & \mathbf{s}(i, 1) & \dots & 0 \\ \vdots & \vdots & \dots & \vdots \\ \mathbf{s}(i, H_P) & \mathbf{s}(i, H_P - 1) & \dots & \mathbf{s}(i, H_P - H_c - 1) \end{bmatrix} \quad i = 1, \dots, n \end{aligned}$$

where the elements of \mathbf{S} are updated at each control interval and are computed via perturbation:

$$\mathbf{s} = \left(\frac{\partial \hat{\mathbf{x}}}{\partial u} \right)_0 = \frac{\hat{\mathbf{x}}|_{u_{-1+\delta}} - \hat{\mathbf{x}}|_{u_{-1}}}{\delta} \quad (3.31)$$

where δ is a numerical perturbation on past input u_{-1} , $\hat{\mathbf{x}}|_{u_{-1+\delta}}$ and $\hat{\mathbf{x}}|_{u_{-1}}$ are the predicted future states under the control actions $u_{-1+\delta}$ and u_{-1} , respectively.

The control actions are calculated at each control interval by solving an optimization problem with a quadratic objective:

$$\min_{\Delta\mathbf{u}} [(\mathbf{r} - \hat{\mathbf{y}})^T \mathbf{Q}(\mathbf{r} - \hat{\mathbf{y}}) + \Delta\mathbf{u}^T \mathbf{R}\Delta\mathbf{u} + \epsilon^T \mathbf{T}\epsilon] \quad (3.32)$$

subject to equations (3.24) to (3.27) and input constraints

$$\begin{aligned} \mathbf{u}_{min} &\leq \mathbf{u} \leq \mathbf{u}_{max} \\ \Delta \mathbf{u}_{min} &\leq \Delta \mathbf{u} \leq \Delta \mathbf{u}_{max} \\ \epsilon &\geq \mathbf{0} \end{aligned}$$

where \mathbf{r} is the vector of set-points, ϵ is a vector of slack variables used to soften the output constraints and \mathbf{Q} , \mathbf{R} and \mathbf{T} are symmetric positive definite weighting matrices.

To take into account possible plant/model mismatch and/or unknown disturbances, the locally linearized model is modified by adding a mismatch compensation term:

$$\hat{\mathbf{y}}_c = \mathbf{C} \{[\hat{\mathbf{x}}_0 + \mathbf{S}\Delta \mathbf{u}] + \mathbf{e}\} \quad (3.33)$$

where \mathbf{e} is a mismatch term

$$\mathbf{e} = \mathbf{e}_{-1} + (\mathbf{y}_m - \hat{\mathbf{y}}_{-1}), \quad (3.34)$$

where \mathbf{e}_{-1} is the mismatch term computed at the previous control interval, \mathbf{y}_m is the measured controlled output at the current control interval and $\hat{\mathbf{y}}_{-1}$ is the predicted controlled output at the previous control interval for the current control interval. \mathbf{e} is taken to be zero initially and is updated iteratively at every control interval. It is assumed that the value of the state variable T , at all discrete spatial points, is measured.

To address the problem of keeping the maximum temperature below a specified upper bound, an additional output constraint is added:

$$\hat{\mathbf{y}}_{T_{max}} \leq \mathbf{T}_{max} + \epsilon$$

To model the future value of the maximum temperature, $\hat{\mathbf{y}}_{T_{max}}$, as a function of the manipulated variable, two methods were considered. The reason for considering two different methods is that the 1-D pseudo-homogeneous model used to predict the future reactor behaviour might not be accurate enough for predicting the long term maximum temperature.

Method 1: In the first approach, a local linear model computed from a linearization of the 1-D pseudo homogeneous around the current value of the manipulated variable was used:

$$\hat{\mathbf{y}}_{T_{max}} = [\hat{\mathbf{x}}_{0,T_{max}} + \mathbf{S}_{T_{max}} \Delta \mathbf{u}] \quad (3.35)$$

$$\mathbf{S}_{T_{max}} = \left(\frac{\partial \hat{\mathbf{x}}_{T_{max}}}{\partial \mathbf{u}} \right)_0 = \frac{\hat{\mathbf{x}}_{T_{max}}|_{u_{-1+\delta}} - \hat{\mathbf{x}}_{T_{max}}|_{u_{-1}}}{\delta} \quad (3.36)$$

where $\hat{\mathbf{x}}_{0,T_{max}}$ is a vector of predicted values in the absence of further control actions (u_{-1}), δ is a numerical perturbation on past input u_{-1} , $\hat{\mathbf{x}}_{T_{max}}|_{u_{-1+\delta}}$ and $\hat{\mathbf{x}}_{T_{max}}|_{u_{-1}}$ are the predicted future states under the control actions $u_{-1+\delta}$ and u_{-1} , respectively. To update the model and compensate for plant/model mismatch, an additive mismatch term computed from the measured maximum temperature at the current sampling time and the predicted value from previous sampling time was used.

Method 2: In the second approach, the future values of the maximum temperature, $\hat{\mathbf{y}}_{T_{max}}$, used were predicted values at stationary state, $\hat{\mathbf{y}}_{T_{max,ss}}$. A linear model obtained from linearization of equation (2.24) about the manipulated variable was used. To update the model and correct for possible plant/model mismatch, the linear input-output model in (3.35) was used. The model was used to predict the behaviour of the maximum temperature in the *near* future, that is one step ahead, and the difference between current process output information and the predicted values was considered as an additive model mismatch term for the linear model used to predict the maximum temperature at stationary state.

3.9 Controller Tuning

For implementation of an MPC controller, the selection of the prediction horizon (H_p) is one of the most important parameters. In a typical MPC application, where linear lumped parameter models are used, a prediction horizon that approximates the time to steady-state of the process is usually chosen. In this way, most of the dynamic behaviour of the controlled process is known to the controller. This type of prediction horizon is not possible for a reverse flow reactor. Mathematical models are usually developed on the basis of a single flow direction, and then the boundary

conditions and flow sign are changed to account for the flow reversal. On the basis of a single flow direction model, simulation of the process for a sequence of full cycles would require, for example, an analytical solution of the model equations that can then be assembled to generate the full solution. For complex distributed parameter systems, analytical solutions are generally not possible and thus we need to rely on a numerical approximation. Numerical approximations and their solutions applied to the dynamical models for reverse flow reactors require the solution of a sequence of PDE model problems.

In catalytic flow reversal reactors, the dynamic behaviour of the temperature with uni-directional flow is changed by the reversal of the flow direction and the dynamic behaviour is a function of the number of cycles. Thus, even if a sequential solution is used, the number of cycles required to capture the whole dynamic behaviour of a catalytic flow reversal reactor may be large.

A long prediction horizon in the MPC would capture the whole dynamic behaviour and would give a smooth regulation and tracking of temperature within the reactor; however, the computational time for a long prediction may be prohibitive. On the other hand, a short prediction horizon would be computationally feasible, but it would give an aggressive control of the temperature. For MPC control of a reverse flow reactor, the computation of the control input is more tractable using a short prediction horizon that covers the reactor behaviour during either direct or reverse flow direction or a few full cycles.

Two MPC formulations were considered. In the first formulation, we use a prediction horizon that covers only the dynamics of a semi-cycle (*shrinking horizon*). By using a shrinking horizon, we acknowledge that we may lose some control performance. As time progress during each semi-cycle, the prediction horizon shrinks until next flow reversal occurs. This type of implementation of MPC is similar to that used in batch applications. While conventional MPC employs a receding horizon framework and is suited for continuous processes, batch processes require a shrinking horizon because the time available for control shrinks as the end of the batch approaches (Soni and Parker, 2004). In the second formulation, we use the traditional *receding horizon* where we use an even number of full cycles as the prediction horizon.

The selection of the control interval (sampling interval) is another parameter for the MPC that needs to be selected. The control interval should be carefully chosen so that enough time is available for the control calculation. In general, for complex PDE-based reactor models, a long prediction horizon has a higher computational time. With a longer control interval, the control of fast processes may not be satisfactory. For the control of the temperature in a catalytic flow reactor, the control interval required to perform all the computations in an MPC, with a prediction horizon that shrinks until the next flow reversal, is usually much smaller than the settling time of the temperature dynamics.

3.10 Numerical Simulations

In this section, closed-loop numerical simulations are provided to show the performance of the formulated MPC controller. The section begins with short study of the control performance obtained with a shrinking horizon MPC that employs a 2-characteristics internal model. A discussion of the challenges faced in using such controller is provided. A receding horizon MPC controller that employs a 1-characteristic internal model is presented in Section 3.10.1. The MPC controller with the 1-characteristic internal model allows for a faster online computation of the control algorithm and improved control performance.

For all simulations presented in the proceeding sections, the controlled-plant outputs were computed using the model in (2.2) to (2.5); which in turn was solved using the finite element method in the COMSOL[®] Multi-physics simulation software. The combined simulation of the reactor and the MPC controller, including the solution of the optimization problem, was executed in MATLAB[®].

3.10.1 Shrinking Horizon MPC with 2-Characteristics Internal Model

In this section, closed-loop simulations of a CFRR unit controlled with a shrinking horizon MPC with an internal model given by equations (3.24) to (3.27) is presented. A schematic of the reactor configuration is given in Figure 2.22. For simulation of

the closed-loop system, the following nominal operating conditions were used:

$$Y(0, t) = 0.1\%$$

$$T(0, t) = 298 \text{ K}$$

$$v_{s,in} = 1 \text{ m} \cdot \text{s}^{-1}$$

$$T_{cycle} = 10 \text{ min}$$

Using the nominal operating conditions and a nominal manipulated variable $\alpha(t) = u(t) = 0.95$, the stationary state was computed and is given in Figure 3.4.

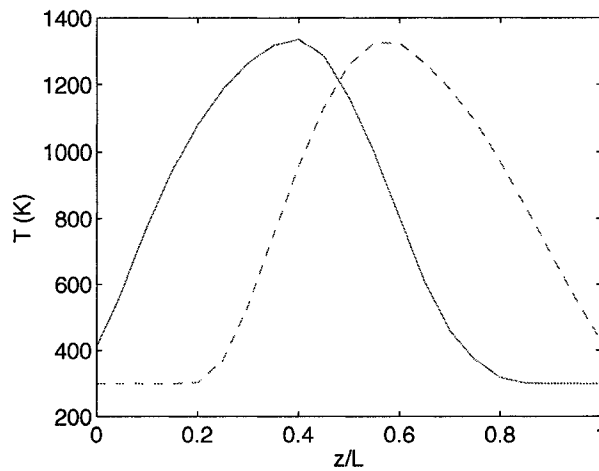


Figure 3.4: Spatial distribution of the temperature along the reactor centerline at stationary state. Solid line: temperature distribution at the beginning of the forward direction. Dashed line: temperature distribution at the beginning of the reverse direction.

The controller was formulated to track a specified set-point trajectory for the average temperature along the reactor centerline. In this section, the set-point is chosen arbitrarily. No constraints were considered for the maximum temperature. A spatial domain discretization, $n = 21$, was used in the computation of the output predictions.

The controller was tuned using the following parameter values

$$\begin{aligned} T_s &= (1/6)T_{cycle} \\ H_c &= 1 \\ \mathbf{R} &= 1 \\ \mathbf{Q} &= \mathbf{I}_{H_p \times H_p} \\ \mathbf{r} &= 1100 \mathbf{I}_{H_p \times 1} \end{aligned}$$

and the following constraint parameters

$$\begin{aligned} \Delta u_{max} &= 0.05 \\ u_{max} &= 0.95 \\ u_{min} &= 0.1 \end{aligned}$$

Figure 3.5 shows the control performance for a closed-loop simulation with disturbances in the inlet mole fraction of reactants (Y_{f0}). As seen in Figure 3.5 (top), the controlled temperature is driven towards the specified set-point. Even when disturbances enter the system, Figure 3.5 (middle), the controller drives the controlled variable to the set-point. Figure 3.5 (bottom), shows the trajectory of the manipulated variable, which in turn indicates the gas extraction required to keep the average temperature along the specified set-point.

The main issue regarding the closed-loop simulations with the 2-characteristics internal model was the computational time. To solve the model equations (3.24) to (3.27), the approach presented in Section 3.8.1 was used; however, this method required the solution of a set of nonlinear algebraic equations. Due to the wide difference in the time scale of (3.24) and (3.25), a fine discretization in the time domain was needed to reach the selected prediction horizon with good accuracy. The discretization not only increased with the prediction horizon, but also with the spatial discretization of the initial condition.

Even when a model that includes the dynamics of both the fluid and solid phase would be more accurate, solution of the model equations by the method of characteristics is computationally intensive and limits the achievable control performance.

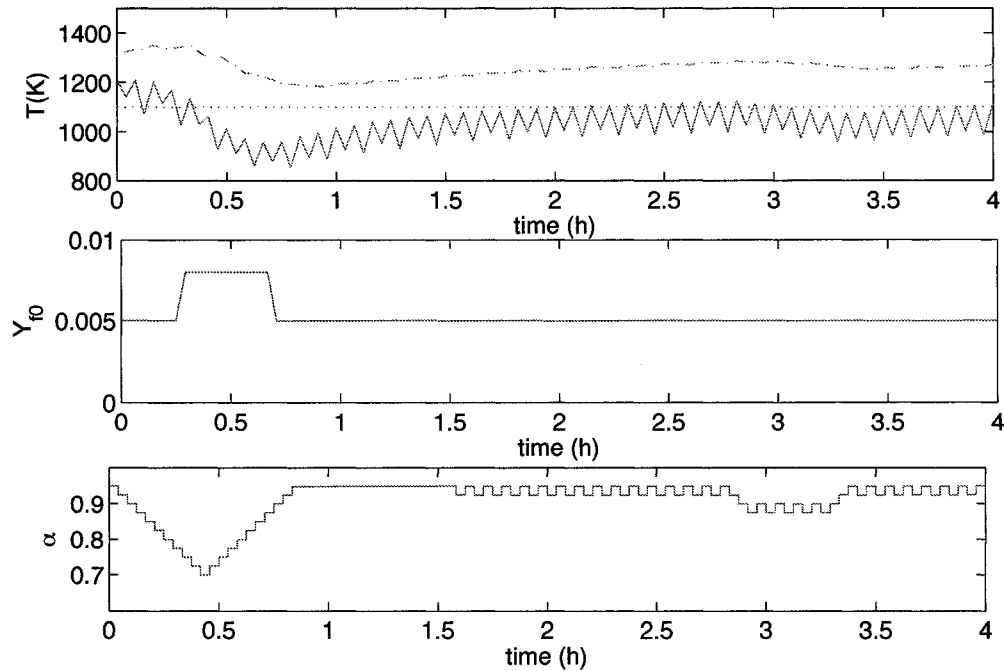


Figure 3.5: Top: trajectory of the maximum (dashed-dot line) and average temperature (solid line) along the reactor centerline. Set-point trajectory is indicated by a dotted-line. Middle: trajectory of the disturbance, i.e. Y_{f0} . Bottom: trajectory of the manipulated variable $\alpha = u$.

A few important points deserve to be noted at this stage:

- The control performance is satisfactory; i.e. the average temperature is driven towards the desired set-point but is too aggressive. The aggressiveness arises from the short prediction horizon used and sensitivity of the output process variable to changes in manipulated variable. To obtain a smoother closed-loop behaviour, two measures will be considered in the next section: a longer prediction horizon and a larger weight for changes in the manipulated variable.
- The maximum temperature follows the same trend as the average temperature. Therefore, it is possible to use the average and maximum temperature together to uniquely characterize the spatial distribution of the output variables at stationary state. Gas extraction from the reactor midsection can be used to drive the reactor system to a unique set of outputs without the need to control

the complete spatial distribution of the temperature, which is by nature an infinite dimensional variable and would require an infinite dimensional input. In the next section, the maximum temperature along the reactor centerline is controlled so that it is kept below an upper bound that would be represented by the deactivation temperature of the catalyst material.

3.10.2 Receding Horizon MPC with 1-Characteristic Internal Model

In this section, the reactor model given in equations (3.28) and (3.29) is used as the internal model in the MPC scheme to improve the computational time required to predict future output behavior. With a reduced computational load, it is possible to use longer predictions times, and thus a receding horizon formulation was used. The control formulation used in this section, not only includes the control of the average temperature but also a constraint for the maximum temperature.

The average temperature that corresponds to a given maximum temperature and that is below the selected upper bound is, in general, not known in advanced. To overcome this issue, we use a simple logic scheme where, if the maximum temperature constraint is violated, the set-point value is adjusted to the value of the average temperature reached at the point where the maximum temperature reaches the upper bound.

The MPC controller was tuned with a prediction horizon H_p , where each H_p interval contains an even number of full cycles. The elements of \mathbf{Q} that corresponds to predicted errors early in the prediction horizon were weighted more heavily than the predicted errors at the end of the horizon. The tuning parameters used in the

MPC controller were:

$$\begin{aligned}
 T_s &= 4T_{cycle} \\
 H_c &= 1 \\
 H_p &= 4 \\
 \mathbf{R} &= 500 \\
 \mathbf{Q} &= \begin{bmatrix} 100 & 0 & 0 & 0 \\ 0 & 1 & 0 & 0 \\ 0 & 0 & 1 & 0 \\ 0 & 0 & 0 & 1 \end{bmatrix}
 \end{aligned}$$

and the input/output constraints used were:

$$\begin{aligned}
 \Delta u_{max} &= 0.025 \\
 u_{max} &= 1 \\
 u_{min} &= 0.1 \\
 T_{max} &= 1300 \text{ K}
 \end{aligned}$$

The spatial domain discretization used in the internal MPC model was $n = 100$. To perform the simulation of the closed-loop system, the following nominal operating conditions were used:

$$\begin{aligned}
 Y(0, t) &= 1\% \\
 T(0, t) &= 298 \text{ K} \\
 v_{s,in} &= 0.3 \text{ m} \cdot \text{s}^{-1} \\
 T_{cycle} &= 10 \text{ min}
 \end{aligned}$$

The reactor configuration used in all simulations presented in this section is shown in Figure 2.4. The reactor was started from the initial condition given in Figure 2.12. The initial condition does not correspond to the stationary state; and therefore, it allows for evaluation of the control performance during start-up of the reactor unit.

We begin by studying the effect on control performance of disturbances in the inlet mole fraction of reactants. Without any control acting on the system (open-loop operation), the evolution of the output variables is shown in Figure 3.6 a) for

an open-loop operation with a disturbance trajectory, Y_{f0} , given in Figure 3.6 b). Clearly, the maximum temperature exceeds the selected upper bound if the reactor is operated in open-loop, i.e. the manipulated variable is constant as shown Figure 3.6 c). Temperatures as high as 2000 – 3000 K might never be achieved in practice due to catalyst overheating and deactivation. Overheating and subsequent catalyst deactivation can be expected, but a mechanism for the catalyst deactivation was not included in the reactor model.

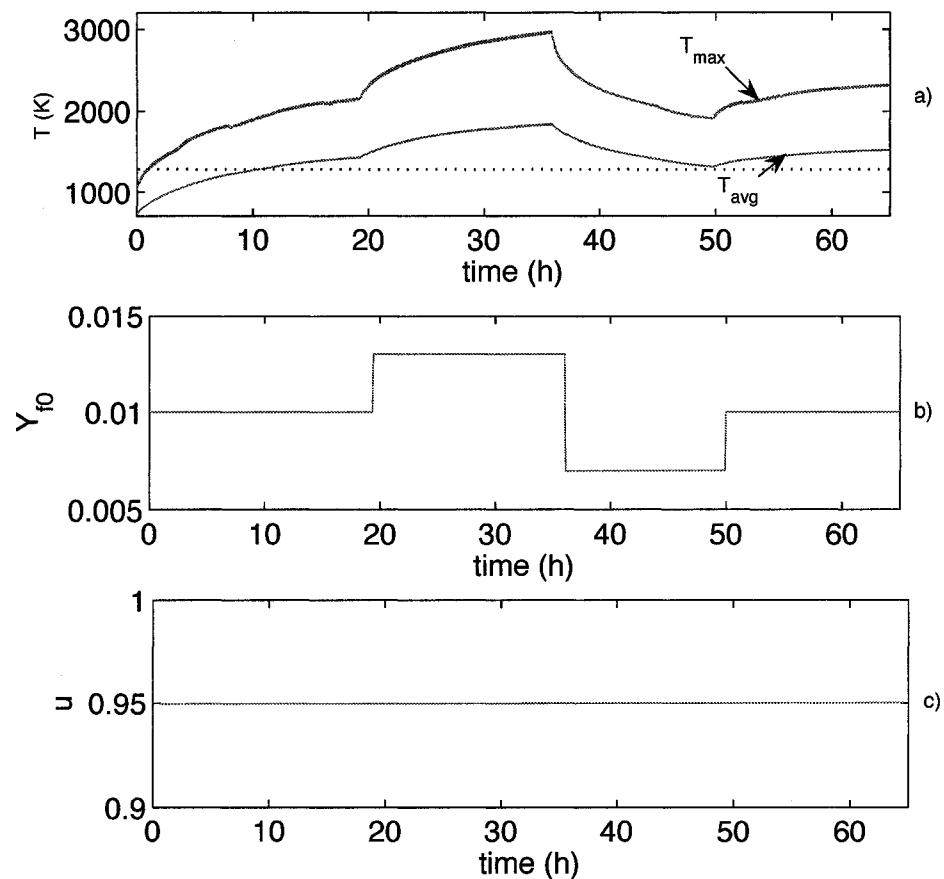


Figure 3.6: a) Trajectory of the maximum and average temperature along the reactor centerline; b) trajectory of the inlet mole fraction of reactant and c) trajectory of the manipulated variable, u . The dotted line in a) indicates the maximum allowable temperature.

When the reactor is operated in closed-loop, the control performance achieved is shown in Figure 3.7. Two cases were simulated to show the improvement in

control performance obtained by using a receding horizon formulation and adding a constraint for the maximum temperature. The method identified as *method 2* in Section 3.8.3, was used, in what follows, to predict the future values of the maximum temperature in the MPC scheme. In one of the simulated cases, the controller used included a constraint for the maximum temperature (solid line), while in the other one the constraint was not included (dashed line). Figures 3.7 a) and b) show the progression of the maximum and average temperature along the reactor centerline, respectively. Figures 3.7 c) and d) show the trajectory of the inlet mole fraction used in the simulation and the trajectory of the manipulated variable, respectively. For the case where the maximum temperature constraint is included in the controller, it is observed that as the system evolves from the initial conditions, the controller drives the maximum temperature below the selected upper bound. Once the maximum temperature is below the upper bound, the set-point value is automatically adjusted. The system is kept at that set-point until a disturbance that leads to an increase in the maximum temperature above the upper bound enters the system. The controller drives the system back to a maximum temperature that is below the upper bound. The simulation results indicate that the controller provides good control performance, as the maximum temperature is kept below the chosen upper bound and stable operation is achieved during times of low inlet reactant concentration.

To better study the closed-loop operation, Figure 3.8 a) shows the evolution of the outlet reactant conversion for closed-loop operation with disturbances in the inlet mole fraction. The controller used was the one that included a constraint for the maximum temperature. It is observed that as the average temperature is kept at a constant set-point value, the conversion achieves a constant value that is independent of the inlet reactant concentration. Figure 3.8 b) shows the ratio of the heat extracted from the reactor midsection and the total energy fed to the reactor. It is observed that more energy than that fed to the reactor ($E_{in} = v_{in}A\Delta H_rCY_{f0}$) is removed from the reactor midsection ($E_{mid} = \dot{m}_{removed}Cp_f(T_{mid} - T_{in})$) during periods of high reactant concentrations. A ratio of extracted energy (E_{mid}/E_{in}) larger than 1 is kept until the maximum temperature is driven below the upper bound. Figure 3.8 indicates that it might be possible to improve process operation by achieving higher conversions and

higher yields of heat recovery from the reactor midsection.

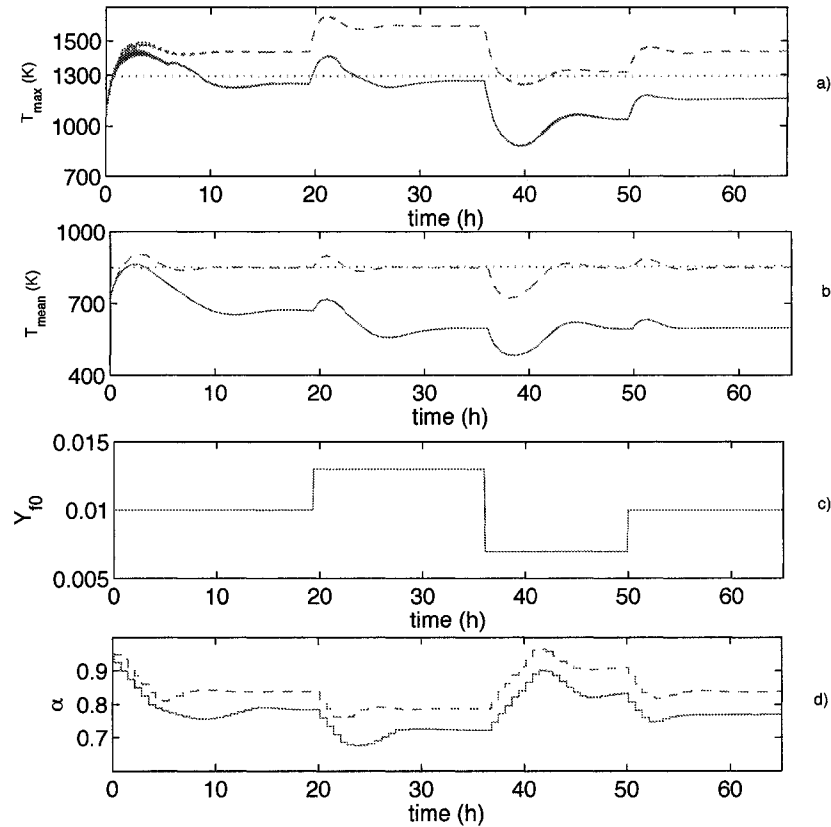


Figure 3.7: a) Trajectory of the maximum and b) average temperature along the reactor centerline. c) Trajectory of the inlet mole fraction of reactant. d) Trajectory of the manipulated variable, $u = \alpha$. The dotted line in a) indicates the maximum allowable temperature. Solid lines: closed-loop simulation of MPC with maximum temperature constraint; dashed lines: closed-loop simulation of MPC without maximum temperature constraint.

Even though the method used to predict future values of the maximum temperature (*method 2*, see Section 3.8.3) can be used to achieve good control performance, it is always desired to have a simpler controller that does not require the identification and formulation of a steady-state model. In what follows, *method 1* as defined in Section 3.8.3 was used to predict future values of the maximum temperature in the MPC scheme. Nevertheless, similar control performance was observed with both methods.

The closed-loop control performance for disturbances in inlet gas velocity is shown in Figure 3.9. As seen in Figure 3.9 (top), the maximum temperature is kept below

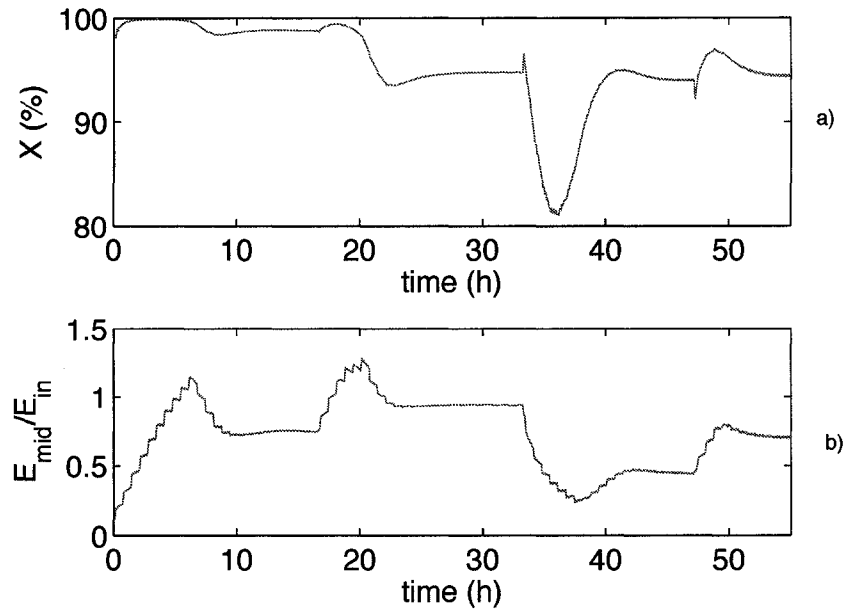


Figure 3.8: Top: reactant conversion at $z/L = 1$. Bottom: ratio of the heat extracted from the reactor midsection and the total energy fed to the reactor.

the selected upper bound and the average temperature tracks a set-point value which guarantees stable operation despite disturbances. As inlet gas velocity disturbances enter the system, Figure 3.9 (middle), an optimal input trajectory is computed, Figure 3.9 (bottom), to achieve specified control objectives. It is observed from Figure 3.9 that rejection of disturbances in the inlet gas velocity is faster than those disturbances in the inlet mole fraction. This behaviour was expected as it was found in the open-loop numerical simulations in Section 2.11.3 that a shorter settling time is obtained for step changes in the inlet gas velocity. The closed-loop simulation reveals that, for the trajectory of the inlet gas velocity considered (which comprise the range of expected values in practical applications), small deviations in the input and output variables are observed to keep the reactor under stable operation.

Figure 3.10 (top) shows the evolution of the outlet reactant conversion. Even though it was observed that the deviation of the output as well as the input variables is small for the range of disturbances considered, large deviations in the reactant concentration are observed. Figure 3.10 (bottom) shows the ratio of the heat extracted from the reactor midsection and the total energy fed to the reactor. Heat removal as

well as reactant conversion show fast changes after the disturbances enter the system, while recovery to a new stationary state show a relatively slower dynamic transition.

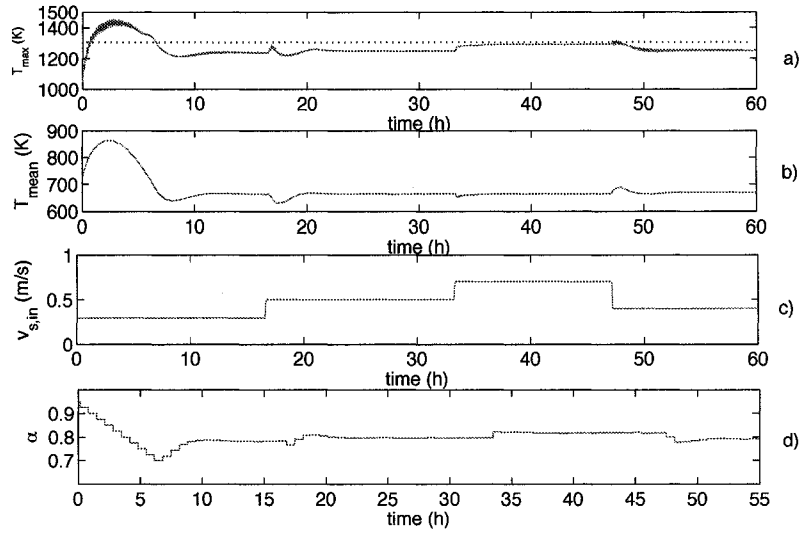


Figure 3.9: a) Trajectory of the maximum temperature and b) trajectory of the average temperature. c) Trajectory of the disturbance (inlet gas velocity). c) Trajectory of the manipulated variable $\alpha = u$. The dotted-line in a) indicates the maximum allowable value for the temperature.

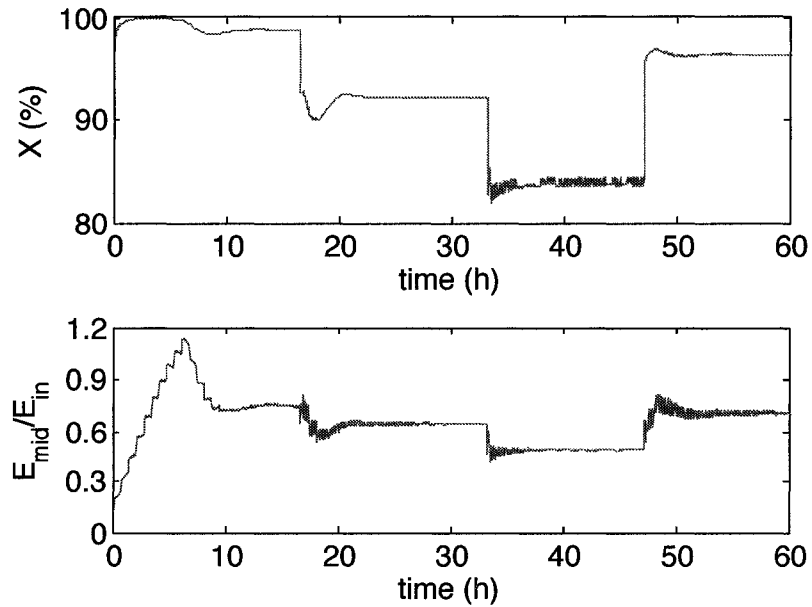


Figure 3.10: Top: reactant conversion at $z/L = 1$. Bottom: ratio of the heat extracted from the reactor midsection and the total energy fed to the reactor.

The closed-loop control performance for tracking specified set-points in the average temperature is shown in Figure 3.11. As seen in Figure 3.11 (top), the average temperature tracks the specified set-point well. The input trajectory is shown in Figure 3.11 (bottom). Figure 3.12 (top) shows the evolution of the outlet reactant conversion. Figure 3.12 (bottom) shows the ratio of the heat extracted from the reactor midsection and the total energy fed to the reactor.

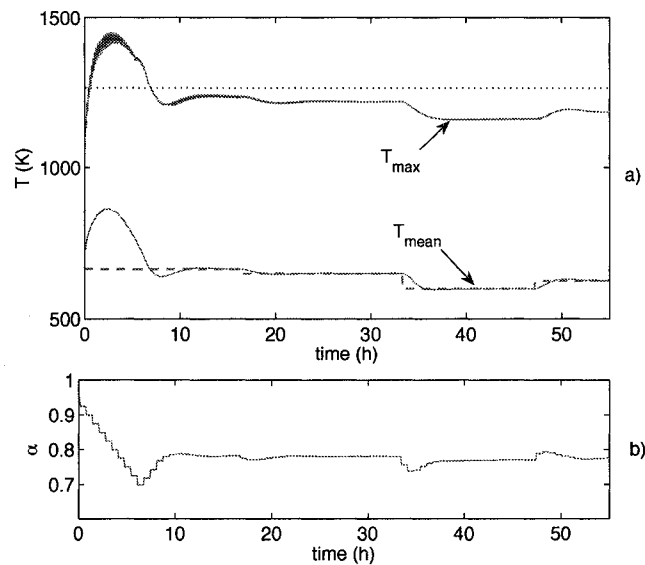


Figure 3.11: a) Trajectory of the maximum and average temperature for the set-point trajectory indicated by the dashed-line. The dotted-line indicates the maximum allowable value for the temperature. b) Trajectory of the manipulated variable $\alpha = u$.

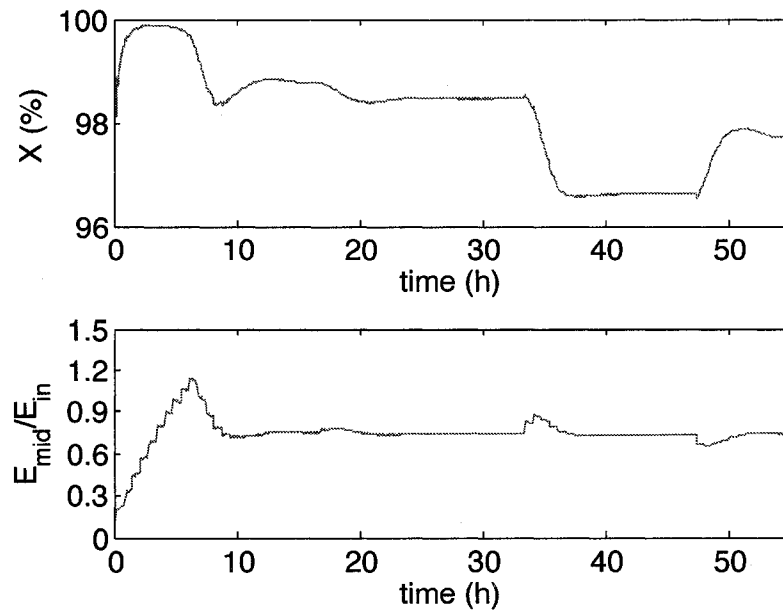


Figure 3.12: Top: reactant conversion at $z/L = 1$. Bottom: ratio of the heat extracted from the reactor midsection and the total energy fed to the reactor.

3.11 Dealing with Manipulated Variable Saturation

While operating in closed-loop, large disturbances in the inlet (boundary) conditions may lead to two extreme situations:

1. *High inlet reactant concentration:* when high inlet concentrations occur, the rate of gas extraction from the midsection of the reactor must be increased to achieve stationary-state without burning the catalytic material. Under highly-concentrated feed stream conditions, a large part of the flowing gas might need to be removed through the reactor midsection; and eventually, only half of the reactor will be effectively used.
2. *Low inlet reactant concentration:* when low inlet concentrations occur, the rate of gas extraction from the midsection of the reactor must be decreased to achieve stationary-state without extinguishing the reaction. Under highly-dilute feed stream conditions, that persist for long periods of time, and without any additional control measure, nothing else can be done to keep a high temperature in the active catalyst sections to avoid reaction extinction.

Additional control measures can be added to the reactor system to allow efficient operation under extreme conditions. Such measures include adding, through the reactor midsection, a hot air stream to increase the reactor temperature during lean inlet conditions or a cold air stream to reduce the reactor temperature during rich inlet conditions. In any case, these additional measures can be implemented using a logic control scheme. The MPC controller would be used to drive and keep the reactor operation within a stable and smooth operating region using mass extraction. Outside the operating region for which mass extraction is not sufficient, then the MPC controller will be turned off and the new measures will become active until a temperature reaches a level that allows the system to be controlled by mass extraction.

3.12 Summary

In this chapter, the development of a model-based controller for a catalytic flow reversal reactor was presented. The controller was formulated to drive and to keep the reactor within stable operating conditions. An MPC scheme that uses the method of characteristics to predict future outputs values was employed.

The formulation of the control scheme was aimed at CFRR units with slow frequency of flow reversal. Slow frequencies are required in the processing of large volumes of gas, and the movement or shifting of the spatial distribution of the state variables along the reactor is a inherent characteristic.

In this chapter, we propose to use an average of the temperature profile along the reactor as the output variable that needs to be controlled to avoid reactor shutdown due to reaction extinction. In addition to the average temperature, the maximum temperature is constraint to be below an upper bound that represents the catalyst deactivation energy. Through the controller formulation and simulation, it is shown that the two variables can be used to keep the reactor within stable operating conditions despite disturbances in the most common uncontrolled variables, i.e. the inlet mole fraction of reactant and inlet gas velocity. It is shown that the use of the heat extraction by means of mass extraction in an MPC scheme can be used to control the reactor system.

Detailed discussion about the selection of the tuning parameters in an MPC controller is provided. The selection of the prediction horizon is addressed in detail, since its selection is essential for the application of a model predictive control to a reverse flow reactor. We studied the formulation of model predictive controller where during each semi-cycle, the prediction horizon begins to shrink as time progress until the next flow reversal occurs *shrinking horizon*. This formulation is proposed to overcome the need of predicting a large number of full-cycles, which would become computational expensive; however, we observe that the controller is too aggressive. We also considered a second approach, where we used the traditional *receding horizon* and an even number of full cycles is used as prediction horizon. The receding horizon formulation along with a 1-characteristic model of the reactor system was shown to

provide satisfactory control performance in the numerical simulations of the closed-loop system.

4

LQ-feedback Control of a Catalytic Flow Reversal Reactor

In this chapter, the control of catalytic flow reversal reactors is studied by means of a linear quadratic (LQ) regulator for infinite-dimensional systems. The goal of this chapter is to study a control technique that can give a control performance benchmark for a catalytic reverse flow reactor with mass extraction. The formulation of a LQ-feedback scheme to control the temperature profile along the reactor centerline is the goal of this chapter. The theory behind analysis and control of infinite dimensional systems is complex and practical applications are rare. This chapter provides an insight into the advantages and limitations of the technique for plug-flow catalytic reactors. ¹

¹Parts of this chapter are published in Fuxman *et al.* (2007a) and in Fuxman *et al.* (n.d.)

4.1 Introduction

The typical approach to the control of PDE systems is based on the spatial discretization, by either finite difference or finite-element method, to transform a PDE system into a lumped parameter system amenable for the well-established control techniques for ordinary differential equations. The fact that the spatial discretization neglects the distributed nature of the original system may lead to false conclusion about conditions of controllability and observability or even erroneous conclusions concerning the stability properties of the open-loop and/or closed-loop system (Ray, 1981; Christofides, 2000). Motivated by these reasons, there has been great interest in the control of infinite-dimensional systems by using a functional analysis framework.

In the functional analysis framework, systems modeled by partial differential equations can be formulated in a state space form similar to that for lumped parameter systems. This requires the introduction a suitable infinite-dimensional space and suitable operators instead of the usual matrices. Control theory for infinite-dimensional linear time-invariant systems is well documented, e.g., (Curtain and Zwart, 1995); however, application of the theory to control of chemical reactors are rare.

For reactor systems modeled by parabolic partial differential equations, and within the framework of geometric and model predictive control, Christofides and co-workers, develop an order reduction by partitioning of the eigenspectrum of the spatial operator to derive a finite-dimensional approximation that captures the dominant dynamics of the infinite-dimensional system (Christofides, 2000; Dubljevic *et al.*, 2005; Dubljevic *et al.*, 2006).

Linear-Quadratic (LQ) optimal temperature and reactant concentration regulation problem was studied in (Aksikas *et al.*, 2007a; Aksikas *et al.*, 2007b) for a hyperbolic partial differential equation model of a nonisothermal plug flow tubular reactor by using a nonlinear infinite dimensional Hilbert state space description.

In this chapter, we study the application of control theory for infinite-dimensional systems to a catalytic reactor through the formulation of an LQ-feedback controller

for a catalytic flow reversal reactor. The LQ-feedback control problem for a catalytic reverse flow reactor was treated in Edouard *et al.* (2005) by using the traditional LQ solution for finite dimensional systems to control of the temperature at a single spatial point along the axis of the reactor.

4.2 Contributions

In this chapter, we use a plug-flow catalytic reactor model with unidirectional flow and develop an LQ controller based on an infinite dimensional representation of the model equations. Conditions for the existence of a solution of the optimal LQ problem are proved for the linear infinite dimensional model. An LQ-controller is developed for catalytic reactor model with unidirectional flow and conditions for stability of the reverse flow reactor are provided. Numerical simulations of the closed-loop system are used to illustrate the behavior of the catalytic reactor with the formulated controller. This chapter helps to provide an insight into the advantages and limitations of the technique for convection dominated catalytic reactors.

We begin this chapter with a brief introduction of some fundamental concepts related to infinite-dimensional linear systems theory. Basic mathematical definitions used throughout the introductory material are given in Appendix B. Extensions to the introductory material can be found in, for example, (Atkinson and Han, 2001; Curtain and Zwart, 1995; Aksikas, 2005).

4.3 Background

The theory of infinite dimensional systems is a complex one and it requires important mathematical background. In this section, we show through an example the formulation of a PDE model as an infinite-dimensional system. Consider the following heat equation

$$\frac{\partial x}{\partial t} = \frac{\partial^2 x}{\partial z^2} \quad x \in (0, 1), \quad t \leq 0 \quad (4.1)$$

with boundary conditions $x(0, t) = x(1, t) = 0$ and initial condition $x(z, 0) = x_0(z)$. The abstract approach to this problem is to recast it as an ordinary differential equation in an infinite-dimensional function space. For this purpose, one defines a

space Z which consist of functions of z defined on the interval $(0,1)$. We then regard x as a function $x(t)$, which, for every given t , takes values in X . That is, $x(t)$ is still a function of z ; to avoid ambiguous notation, we shall use square brackets to denote the z dependence: $x(z, t) = x(t)[z]$. The infinite-dimensional space X replaces R^n in lumped parameter systems. There are many possible choices for this function space; the one most commonly employed is the space of square integrable functions: $X = L^2(0, 1)$. The abstract version of the heat equation is

$$\frac{dx}{dt} = Ax \quad x(0) = x_0 \quad (4.2)$$

where the operator A maps the function $x[z]$ to the function $x''[z]$ (i.e. $x''[z] = \frac{d^2x[z]}{dz^2}$). In contrast to the case of ordinary differential equations, A is not defined on the whole space X . First of all, $x''[z]$ does not exist, at least not as an element of X , unless we assume some smoothness of x . The appropriate space is defined as the space of all functions on $(0, 1)$, which have a second derivative which lies in $L^2(0, 1)$. Even more importantly, the boundary conditions are viewed as a restriction on the domain of the operator A . The reason for incorporating the boundary conditions as a restriction on the domain of A is the objective of defining a meaningful eigenvalue problem $Ax = \sigma x$. The eigenvalue problem solution gives the eigenvalues $\sigma = -n^2\pi^2$, and the associated eigenfunctions $x_n[z] = \sin(n\pi z)$.

The solution of equation (4.2) is available in many introductory books of partial differential equations (Jeffrey, 2003, page 242), and can then be written as a linear combination of the eigenfunctions

$$x(z, t) = \sum_{n \in N} x_n(t) \sin(n\pi z) \quad (4.3)$$

Substitution of (4.3) into (4.2) and using $Ax = \sigma x$, we can rewrite the heat equation in the form

$$\frac{dx_n}{dt} = -n^2\pi^2 x_n \quad (4.4)$$

In this form, the abstract system $\frac{dx}{dt} = Ax$ in (4.2) appears explicitly as an *infinite system* of ODEs, and we can read off the eigenvalues $-n^2\pi^2$.

4.3.1 Semigroup Theory

The solution structures of many PDE systems can be expressed by semigroup operators (Curtain and Zwart, 1995). For the solution of linear infinite-dimensional systems, consider the abstract initial value problem

$$\begin{cases} \dot{x}(t) &= Ax(t) & t \leq 0 \\ x(0) &= x_0 \in D(A), \end{cases} \quad (4.5)$$

in the more general Hilbert space \mathcal{H} . The linear operator A is defined in some subset $D(A)$ of \mathcal{H} . For finite dimensional systems of the form of equation (4.5), the solution is well known: $x(t) = e^{At}x_0$. For infinite dimensional systems, we want to identify a class of operators A which, in some sense, define a ‘solution’ e^{At} and the abstract formulation of the solution on \mathcal{H} becomes

$$x(t) = S(t)x_0 \quad (4.6)$$

To see how the concept of strongly continuous semigroup is closely related to that of a dynamical system with no inputs, suppose that $x_0 \in X$ is the state of a dynamical system defined on a Hilbert space X at time zero, and that the state at time t is $x(t)$. If we assume the dynamics that govern the evolution from x_0 to $x(t)$ are linear, time-invariant, and autonomous, then for each time t we can define a linear operator $S(t)$ such that

$$S(t) : X \rightarrow X, \quad S(0) = I, \quad (4.7)$$

$$x(t) = S(t)x_0 \quad (4.8)$$

Let also assume that the state of the dynamical system satisfies the well-posedness conditions:

- it is unique;
- it varies continuously with the initial state.

An operator $S(t)$ that fulfills the above requirements is called in the semigroup theory, a *strongly continuous semigroup*. In mathematical terms, a strongly continuous semigroup is defined as follows

Definition 4.3.1 *a strongly continuous semigroup (usually abbreviated as C_0 -semigroup) is an operator-valued function $S(t)$ from \mathbb{R}^+ to $\mathcal{L}(\mathcal{H})$ that satisfies the following properties (Curtain and Zwart, 1995):*

1. $S(0) = I$;
2. $S(t+s) = S(t)S(s)$, $t \geq 0, s \geq 0$;
3. $S(t)x_0 \rightarrow x_0$, as $t \rightarrow 0^+ \forall x_0 \in \mathcal{H}$.

The conditions under which A generates a C_0 -semigroup $S(t)$ are given by the Hille-Yosida Theorem (Curtain and Zwart, 1995, Theorem 2.1.12), which characterizes the semigroup generation. Although, the theorem provides necessary and sufficient conditions, it is not, in general, possible to use the theorem to assess whether or not an operator generates a semigroup.

A linear operator of importance for this chapter is

$$Ax = -\frac{dx}{dz} + kx \quad \forall x \in D(A) \quad (4.9)$$

where the domain of A is given by

$$D(A) = \{x \in \mathcal{H} : x \text{ is a.c., } \frac{dx}{dz} \in \mathcal{H} \text{ and } x(0) = 0\},$$

and kI is a bounded function. The operator A is an infinitesimal C_0 -semigroup on \mathcal{H} . A proof can be found in Aksikas (2005).

4.4 Stability Analysis of Infinite-Dimensional Systems

The growth of a C_0 -semigroups plays an important role in the analysis of the stability of an infinite-dimensional system. A strongly continuous semigroup on a Hilbert space \mathcal{H} has the following property:

$$\forall \omega > \omega_0, \text{ there exist a constant } M_\omega \text{ such that } \forall t \geq 0, \|S(t)\| \leq M_\omega e^{-\omega t}.$$

The constant ω_0 is called growth bound of the semigroup (Curtain and Zwart, 1995, page 18). A C_0 -semigroup on a Hilbert space is exponentially stable if there exist

positive constants M and ω such that

$$\|S(t)\| \leq Me^{-\omega t} \quad \forall t \geq 0, \quad (4.10)$$

where ω is called decay rate. If $S(t)$ is exponentially stable, then the solution to problem (4.5) tends to zero exponentially as $t \rightarrow \infty$.

In finite dimensional problems, one usually examines exponential stability via the eigenvalues of the operator or matrix A . For any matrix $A \in \mathbb{R}^{n \times n}$, the finite-dimensional linear system $\dot{x}(t) = Ax(t)$ is exponentially stable if and only if the number $\omega_0 = \sup_{1 \leq i \leq n} \operatorname{Re}(\lambda_i)$, where $\sigma(A) = \{\lambda_i : 1 \leq i \leq n\}$ is the set of eigenvalues of A , is negative. For infinite dimensional systems, however, this is not possible because

$$\sup(\operatorname{Re}(\lambda), \lambda \in \sigma(A)) \leq \omega, \quad (4.11)$$

where $\sigma(A)$ is the spectrum of A (Curtain and Zwart, 1995, page 223).

The exponential stability of C_0 -semigroups can be characterized by a Lyapunov-type criterion (Curtain and Zwart, 1995, page 217):

Theorem 4.4.1 [Lyapunov Criterion for Stability] *Suppose that A is the infinitesimal generator of the C_0 -semigroup $S(t)$ on the Hilbert space \mathcal{H} . Then $S(t)$ is exponentially stable if and only if there exist a positive operator $P \in \mathcal{L}(\mathcal{H})$ such that:*

$$\langle Ax, Px \rangle + \langle Px, Ax \rangle = -\langle x, x \rangle \quad \forall x \in D(A) \quad (4.12)$$

4.5 Linear Quadratic Regulator

A classical problem in optimal control theory of finite dimensional systems is the well known Linear Quadratic Regulator (LQR). LQR is an optimal state feedback controller for linear systems of the form

$$\dot{\mathbf{x}} = \mathbf{A}\mathbf{x} + \mathbf{B}\mathbf{u}, \quad \mathbf{x}(t_0) = \mathbf{x}_0 \quad (4.13)$$

with a control performance objective of the form

$$J(\mathbf{u}) = \frac{1}{2} \mathbf{x}^T(t_f) \mathbf{H} \mathbf{x}(t_f) + \frac{1}{2} \int_0^{t_f} (\mathbf{x}(t)^T \mathbf{Q} \mathbf{x}(t) + \mathbf{u}(t)^T \mathbf{R} \mathbf{u}(t)) dt. \quad (4.14)$$

where \mathbf{H} is positive definite, \mathbf{Q} is positive semi-definite and \mathbf{R} is positive definite. There are several ways to solve optimal control, among which the most commonly used is the variational method for optimal control. Although it is possible to find a solution for the general problem in equations (4.13)-(4.14) by solving a matrix Riccati differential equation, we consider the particular case where the terminal time approaches infinity. Without loss of generality, we assume that the steady state is the origin. Since the linear quadratic regulator gives a stable closed-loop dynamics under the condition that the open-loop system is controllable, then cost at the terminal moment lacks significance and it does not appear in the cost function, i.e., $\mathbf{H} = \mathbf{0}$.

The cost function for an infinite time regulator problem is

$$J(\mathbf{u}) = \frac{1}{2} \int_0^{\infty} (\mathbf{x}(t)^T \mathbf{Q} \mathbf{x}(t) + \mathbf{u}(t)^T \mathbf{R} \mathbf{u}(t)) dt \quad (4.15)$$

and the optimal control law is

$$\mathbf{u}(t) = -\mathbf{R} \mathbf{B}^T \mathbf{K} \mathbf{x}(t) \quad (4.16)$$

where the constant symmetric square matrix \mathbf{K} may be obtained by the following algebraic Riccati equation (Ray, 1981):

$$\mathbf{K} \mathbf{A} + \mathbf{A}^T \mathbf{K} - \mathbf{K} \mathbf{B} \mathbf{R}^{-1} \mathbf{B}^T \mathbf{K} + \mathbf{Q} = \mathbf{0} \quad (4.17)$$

The solution of the algebraic Riccati equation may not be unique. The desired solution is obtained by enforcing the requirement that \mathbf{K} is positive definite.

For a linear time-invariant infinite-dimensional linear system of the form

$$\dot{x}(t) = \mathbf{A}x(t) + \mathbf{B}u(t), \quad x(t_0) = x_0 \quad (4.18)$$

$$y(t) = \mathbf{C}x(t) \quad (4.19)$$

where the following assumptions hold:

1. the state $x(t) \in \mathcal{H}$, a real separable Hilbert space, the input $u(t) \in U$ and the output $y(t) \in Y$, where U and Y are real separable Hilbert spaces;
2. $\mathbf{A} : D(\mathbf{A}) \subset \mathcal{H} \rightarrow \mathcal{H}$ is the infinitesimal generator of a C_0 -semigroup;

3. B and C are bounded linear operators,

the optimal control problem is defined by using the following cost function:

$$J(u) = \int_0^{\infty} \langle y(s), y(s) \rangle + \langle u(s), u(s) \rangle ds. \quad (4.20)$$

The objective of the control problem is to minimize this cost functional along all trajectories. First note that if the system $\Sigma(A, B, C)$ is exponentially stabilizable then for all $x_0 \in H$, there exists an input $u \in L^2([0, \infty); U)$ such that the cost functional J is finite, see (Curtain and Zwart, 1995, page 292). Therefore, the exponential stabilizability guarantees the well-posedness of the minimization problem.

The solution of this problem can be obtained by finding the positive self-adjoint operator $Q_0 \in \mathcal{L}(\mathcal{H})$ that solves the following optimal Riccati algebraic equation (ORAE) (Aksikas, 2005):

$$[A^*Q_0 + Q_0A + C^*C + Q_0BB^*Q_0]x = 0 \quad \forall x \in D(A), \quad (4.21)$$

where $Q_0(D(A)) \subset D(A^*)$.

Theorem 4.5.1 [(Aksikas, 2005)] *Consider an infinite-dimensional system $\Sigma(A, B, C)$. Assume that (A, B) is exponentially stabilizable and (C, A) is exponentially detectable. Then the ORAE 4.21 has a unique positive self-adjoint solution $Q_0 \in \mathcal{L}(\mathcal{H})$ and for any initial state $x_0 \in \mathcal{H}$, the quadratic cost 4.20 is minimized by the unique control given on $t \geq 0$ by*

$$u_{opt}(t) = K_0x(t), \quad x(t) = e^{(A+BK_0)t}x_0, \quad (4.22)$$

where the optimal feedback

$$K_0 = -B^*Q_0 \in \mathcal{L}(\mathcal{H}, U) \quad (4.23)$$

is stabilizing, i.e. the feedback semigroup $e^{(A+BK_0)t}$ is exponentially stable. In addition, the optimal cost is given by $J(x_0, u_{opt}) = \langle x_0, Q_0x_0 \rangle$.

The conditions for exponential stabilizability and detectability can be defined as follows:

Definition 4.5.1 (*Aksikas, 2005*) Let $\Sigma(A, B, C)$ be an infinite-dimensional linear system given by (4.18).

1. (A, B) is exponentially stabilizable if there exists a state feedback operator $F \in \mathcal{L}(\mathcal{H}, U)$ such that $A + BF$ generates an exponentially stable C_0 -semigroup
2. (C, A) is exponentially detectable if there exists an output operator $G \in \mathcal{L}(Y, \mathcal{H})$ such that $A + GC$ generates an exponentially stable C_0 -semigroup

If exponential stability can be proved for a given linear operator, then by Theorem 4.5.1 the existence of a solution of the ORAE can be guaranteed.

4.5.1 LQ-Control of a Catalytic Flow Reversal Reactor

In this section, a linear-quadratic optimal controller is formulated for a catalytic flow reversal reactor. As shown in Section 2.9.2, a catalytic reactor can be modeled by a set of first order hyperbolic PDEs. A controller is developed on the basis of the catalytic reactor model with unidirectional flow and is formulated to regulate the distribution of the temperature along the axis of the reactor by using the fluid flow velocity.

To formulate the controller, a linear infinite dimensional state space description of the PDE model is used. We take advantage of the two-time scale characteristic of catalytic tubular reactors to develop a controller that requires only the measurement of the temperature along the axis of the reactor. Using the infinite dimensional model, a state LQ-feedback operator is computed via the solution of a Riccati differential equation.

4.5.2 Dimensionless Model

In this subsection the dynamics of the catalytic reactor are described by means of an infinite-dimensional system description derived from an equivalent dimensionless nonlinear partial differential equation model. Such an approach is standard in tubular reactor models. Let us consider the reactor model given in (2.6)-(2.7) and the following state transformation:

$$\theta_1 = \frac{Y_{in} - Y}{Y_{in}}, \quad \theta_2 = \frac{T - T_{in}}{T_{in}} \quad (4.24)$$

Then we obtain the following equivalent representation of the model:

$$\frac{\partial \theta_1}{\partial t} = \phi v_1 \frac{\partial \theta_1}{\partial z} + k_1 (1 - \theta_1) \exp\left(\frac{\mu}{1 + \theta_2}\right) \quad (4.25)$$

$$\frac{\partial \theta_2}{\partial t} = \phi v_2 \frac{\partial \theta_2}{\partial z} + k_2 (1 - \theta_1) \exp\left(\frac{\mu}{1 + \theta_2}\right), \quad (4.26)$$

where $\theta = \alpha$ and the dimensionless v_1, v_2, ν, k_1 and k_2 are related to the original parameters as follows:

$$v_1 = -\frac{v_{in}}{\epsilon}, \quad v_2 = -\frac{v_{in}\rho}{\eta}, \quad \mu = \frac{-E}{R_g T_{in}},$$

$$k_1 = \frac{k_0}{\epsilon}, \quad k_2 = \frac{(-\Delta H_r) C k_1 \epsilon}{\eta} \left(\frac{Y_{in}}{T_{in}}\right)$$

A typical feature of catalytic reactors where fluid and solid phases coexist is that the reactant wave propagates through the reactor with a significant larger speed than the heat wave. The different dynamics implies that the system of equations (4.25)-(4.26) possess an inherent two-time-scale property, that is, the dynamics of the mole variable are much faster than the temperature dynamics. For catalytic combustion of methane, the mole fraction dynamics is typically three orders of magnitude faster than the temperature dynamics. In section 2.9.2, it is show that the fast dynamics in equation (2.6) are exponentially stable and they can be neglected in the controller design. Since we are interested in controlling the temperature, we neglect the dynamic term in equation (4.25) which reduces the equation to:

$$\frac{d\theta_1}{dz} = -\left(\frac{1}{\phi v_1}\right) k_1 (1 - \theta_1) \exp\left(\frac{\mu}{1 + \theta_2}\right) \quad (4.27)$$

An analytical solution of equation (4.27) is possible

$$\theta_1(z) = 1 - (1 - \theta_1(0)) \cdot \exp\left(\int_0^z \frac{1}{\phi v_1} k_1 \exp\left(\frac{\mu}{1 + \theta_2}\right) dz\right) \quad (4.28)$$

Remark: The reduction in the dimensionality of the original model of the reactor using the fact that the process exhibits a two-time scale property eliminates the need for measurements of concentration of reactant; which greatly facilitates its practical implementation (Christofides, 2000).

Substituting (4.28) in (4.26) gives

$$\begin{aligned} \frac{\partial \theta_2}{\partial t} &= \phi v_2 \frac{\partial \theta_2}{\partial z} + k_2(1 - \theta_1(0)) \cdot \\ &\quad \exp\left(\int_0^z \frac{1}{\phi v_1} k_1 \exp\left(\frac{\mu}{1 + \theta_2}\right) dz\right) \exp\left(\frac{\mu}{1 + \theta_2}\right) \end{aligned} \quad (4.29)$$

4.5.3 Infinite Dimensional Linearized Model

Let us denote by $\theta_{2,e}$ and ϕ_e the dimensionless profile of the model (4.29) at the operating point. Let us consider the state transformation

$$x(t) := \theta_2(t) - \theta_{2,e}, \quad (4.30)$$

and new input $u(t) := \phi(t) - \phi_e$. Then, linearization of the system (4.25)-(4.26) around its operating profile leads to the following linear infinite-dimensional system on the Hilbert space \mathcal{H} :

$$\begin{cases} \dot{x}(t) &= Ax(t) + Bu(t) \\ x(0) &= x_0 \in \mathcal{H}. \end{cases} \quad (4.31)$$

Here A is the linear operator defined on its domain:

$$D(A) = \{x : x \text{ is a.c.}, \frac{dx}{dz} \in \mathcal{H} \text{ and } x(0) = 0\}, \quad (4.32)$$

by

$$Ax = \alpha \frac{dx}{dz} + \beta x \quad (4.33)$$

where the functions α and β are given by

$$\begin{aligned} \alpha(z) &= \phi_e(z)v_2, \\ \beta(z) &= k_2(1 - \theta_1(0)) \exp\left(\frac{\mu}{1 + \theta_{2,e}}\right) \exp\left(\int_0^z \frac{1}{\phi_e v_1} k_1 \exp\left(\frac{\mu}{1 + \theta_{2,e}}\right) dz\right) \cdot \\ &\quad \left[\int_0^z \frac{1}{\phi_e v_1} k_1 \left(\frac{-\mu}{(1 + \theta_{2,e})^2}\right) \exp\left(\frac{\mu}{1 + \theta_{2,e}}\right) dz + \left(\frac{-\mu}{(1 + \theta_{2,e})^2}\right) \right] \end{aligned}$$

The operator $B \in \mathcal{L}(L^2(0, 1), \mathcal{H})$ is the linear bounded operator given by

$$B = \gamma I, \quad (4.34)$$

where the function γ is given by

$$\begin{aligned} \gamma(z) = & v_1 \frac{d\theta_{2,e}}{dz} + k_2(1 - \theta_1(0)) \exp\left(\frac{\mu}{1 + \theta_{2,e}}\right) \cdot \\ & \left(- \int_0^z \frac{1}{(\phi_e)^2 v_1} k_1 \exp\left(\frac{\mu}{1 + \theta_{2,e}}\right) dz \right) \cdot \\ & \exp\left(\int_0^z \frac{1}{\phi_e v_1} k_1 \exp\left(\frac{\mu}{1 + \theta_{2,e}}\right) dz\right) \end{aligned}$$

The following proposition deals with the exponential stability of the linearized model for the catalytic reactor with unidirectional flow. This property plays an important role in LQ-control design, especially the existence and the uniqueness of a solution.

Proposition 4.5.1 Let us consider the operator A defined by (4.32)-(4.33). Then A generates an exponentially stable C_0 -semigroup on \mathcal{H} .

Proof: By Theorem 4.4.1, it suffices to prove that there exists a positive definite operator $P \in \mathcal{L}(\mathcal{H})$ that satisfies the following Lyapunov equation (Curtain and Zwart, 1995, Theorem 5.1.3)

$$P(D(A)) \subset D(A^*) \text{ and } PA + A^*P + I = 0. \quad (4.35)$$

In view of the form of the operator A , it seems natural to look for a solution of the form $P = p(z)I$, where $p \in \mathbb{R}$. By a straightforward calculation, it can be shown that if the function p is a solution of

$$\begin{aligned} \frac{d(\alpha p)}{dz} &= 2\beta p + 1, \quad p(1) = 0 \\ \Rightarrow \alpha \frac{dp}{dz} &= \left(2\beta - \frac{d\alpha}{dz}\right) p + 1, \quad p(1) = 0 \end{aligned} \quad (4.36)$$

then $P = pI$ is a solution of equation (4.35), since the final condition $p(1) = 0$ implies that $P(D(A)) \subset D(A^*)$. Moreover equation (4.36) admits a positive solution on $[0, 1]$, then $P = pI$ is positive definite (Abou-Kandil *et al.*, 2003, Corollary 6.7.36). A detailed derivation of equation (4.36) is given in Appendix B.2.

□

4.6 Controller Design

In this section, we are interested in the linear-quadratic optimal (LQ) problem in order to design a state LQ-optimal controller for the linearized catalytic flow-reversal reactor described by (4.31)-(4.34). First let us define an output function $y(\cdot)$ by

$$y(t) = Cx(t) := w x(t), t \geq 0, \quad (4.37)$$

Now let us consider the LQ-optimal control problem: for any initial state $x_0 \in \mathcal{H}$, find a square integrable control $u_{opt} \in L^2[[0, \infty); L^2(0, 1)]$ which minimizes the cost functional

$$J(x_0, u) = \int_0^\infty (\langle Cx(t), Cx(t) \rangle + \langle u(t), ru(t) \rangle) dt,$$

where r is a coercive operator (see Appendix B). The solution of this problem can be obtained by finding the positive self-adjoint operator $Q_o \in \mathcal{L}(\mathcal{H})$ which solves the operator Riccati equation (4.21).

By the Theorem 4.5.1, it is required that (A, B) be exponential stabilizable and that (C, A) be exponential detectable for the operator Riccati equation to admit a unique positive self-adjoint solution. In the proof of proposition 4.5.1, it is shown that the unique solution exists. Therefore, we can establish the following theorem:

Theorem 4.6.1 Let us consider the linearized catalytic reactor model (4.31)-(4.33), with control operator B given by (4.34) and observation operator C given by (4.37). Let ψ be the solutions of the system equations:

$$\begin{cases} \frac{d(\alpha\psi)}{dz} = 2\beta\psi + w^2 - \gamma^2 r^{-1} \psi^2, \\ \psi(1) = 0. \end{cases} \quad (4.38)$$

Then the optimal LQ-feedback operator is given for all $x \in \mathcal{H}$ by

$$K_o x = -r^{-1} \gamma \psi x. \quad (4.39)$$

Proof: Let us solve the operator Riccati equation (4.21). Assume that this equation admits a solution under the form $Q_o = \psi(z)I$. Our concern is to find, if possible, a function ψ such that $Q_o = \psi(z)I$ is the unique self-adjoint positive semi-definite

solution of equation (4.21). First, let us substitute the expression for Q_o into the equation (4.21), which yields:

$$\begin{aligned} -\frac{d}{dz} \cdot \alpha\psi \cdot I + \beta\psi \cdot I + \psi\alpha \cdot \frac{d}{dz} + \psi\beta \cdot I + w^2 \cdot I - \gamma^2 r^{-1} \psi^2 \cdot I &= 0 \\ \implies \frac{d(\alpha\psi)}{dz} = 2\beta\psi + w^2 - \gamma^2 r^{-1} \psi^2, \psi(1) = 0. \end{aligned} \quad (4.40)$$

The final condition $\psi(1) = 0$ was deduced from the condition $Q_o(D(A)) \subset D(A^*)$. A detailed derivation of equation (4.40) is given in Appendix B.3. On the other hand, equation (4.38) admits a unique positive solution ψ , see e.g. (Abou-Kandil *et al.*, 2003, Corollary 6.7.36). Hence the operator $Q_o = \psi I$ is positive. Consequently, the optimal control and the optimal cost are given by

$$u_{opt}(t, z) = -\gamma(z)\psi(z)x(t, z)$$

and

$$J(x_0, u_{opt}) = \psi x_0^2.$$

□

Remark 4.6.1 *The LQ-feedback operator guarantees stability of the catalytic reactor model with unidirectional flow (4.31) for any initial state $x_0 \in \mathcal{H}$ and boundary condition $x(0) = 0$. For the catalytic reactor model with reverse flow operation, we can look at the system as an impulsive dynamical system where the state distribution $x(t) \in \mathcal{H}$ is periodically reversed with a time period T at $t_k = kT$, $k = 1, 2, \dots$, but where the boundary condition $x(0) = 0$ remains unchanged. Then the LQ-feedback operator provides stability of the catalytic reactor with reverse flow operation because after each flow reversal (t_k), the LQ operator designed for the catalytic reactor model with $x(0) = 0$ guarantees stability from any initial condition. Therefore, the switching time does not affect the stability of the closed-loop reverse flow reactor system.*

We note, that the LQ-controller is designed to drive the reactor system asymptotically ($t \rightarrow \infty$) to the operating point around which the nonlinear model was linearized. The optimal solution obtained from solving the ORAE satisfies the Lyapunov equation $A_{cl}^* Q_0 + P A_{cl} = -\hat{Q}$, where $A_{cl} = A - B K_0$ and $\hat{Q} = C^* C + K_0^* r K_0$.

Since the Lyapunov function $V = \langle x, Q_0x \rangle$ is positive semi-definite, and the Lyapunov equation guarantees that V is non-increasing, then it is guaranteed that the closed-loop system is driven towards the operating point. At the flow reversal instant, the value of the Lyapunov function does not change. Since V decreases throughout each semi-cycle, it can be concluded that the reactor system approaches the operating point asymptotically, even when the flow direction is changed periodically. It should be noted that the controller guarantees that the reactor system is driven towards the operating point for which it was designed only if the system is started from an initial condition away from the stationary state or if disturbances in the boundary condition are temporary; otherwise, an offset will remain.

4.7 Numerical Simulations

To simulate the operation of the catalytic flow reversal reactor, we use the one-dimensional model given in equation (2.6)-(2.7). Model parameters are given in Table A.2. A scheme of the reactor configuration used in the numerical simulations is given in Figure 2.4. A full cycle time of 600 s was considered.

Removal of gas from the reactor was used to control the temperature of the system. Removal of gas was shown to be to be advantageous over cooling by heat exchanger, see (Aube and Sapoundjiev, 2000), and was an effective means of control in Chapter 3. Associated with the gas removed, energy is removed from the system and therefore the temperature is kept under control. At the spatial points where gas is removed, the velocity of the flowing gas changes. In theory, manipulation of the gas velocity at an infinite number of spatial points leads to the best control performance. We first study this theoretical situation to obtain an upper bound in the best achievable control performance.

Using the nominal operating conditions,

$$Y(0, t) = 0.3\%, \quad T(0, t) = 298K, \quad v_{in} = 1 \text{ m} \cdot \text{s}^{-1},$$

and the model given in equation (2.6)-(2.7), the stationary state was computed, see Figure 4.1.

An LQ-feedback operator was computed using the linearized model, equation (4.31). Linearization was performed around the temperature distribution at the stationary state.

The LQ-control operator that results from solving the system of equations (4.38) is given in Figure 4.2 for $w(z) = 1$ and $r(z) = 10$. For the numerical simulations, the

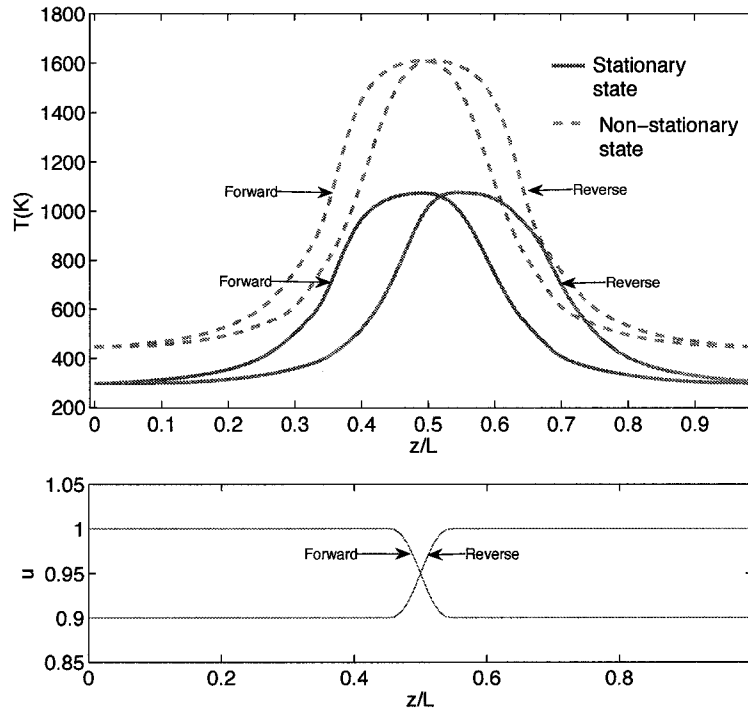


Figure 4.1: Top: temperature distributions at stationary state (solid lines) and initial temperature distribution for closed-loop numerical simulations (dashed-lines). Bottom: spatial distribution of the manipulated variable in the forward and reverse flow direction.

control action was computed every 100 seconds (*i.e.* 1/6 of a full cycle). The time between the calculation of the control action is short compared to the slow dynamics of the temperature variable. For the controller calculations, the temperature along the axis of the reactor is assumed to be available. A total of 100 discrete points were used as the spatial locations where the outputs are measured and the manipulated variable is changed.

To evaluate the control performance to regulate the system, we computed the closed-loop response of the nonlinear model and the LQ-controller from an initial

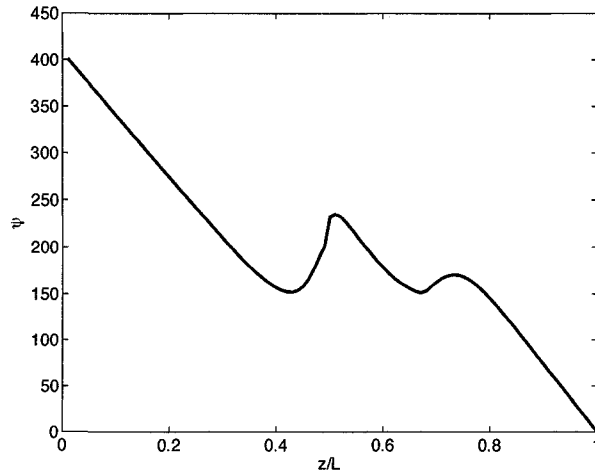


Figure 4.2: LQ-feedback function ψ for $w(z) = 1$ and $r(z) = 10$.

state that is not the stationary state, see Figure 4.1. Such a situation is encountered during reactor start-up and during impulsive disturbances affecting the system. The resulting closed-loop behavior is shown in Figure 4.3. It can be observed that the state converges to the stationary state, as expected. Distribution of the difference between the current temperature and the temperature at stationary state is shown in Figure 4.4. The trajectory of the manipulated variable at the beginning of the the beginning of each full cycle is shown in Figure 4.5. It can be observed that for the optimal regulation of the system, a faster velocity than that at stationary state is needed in the first half of the reactor and a slower velocity is needed in the second half. A comparison of the closed-loop, the open loop and the stationary state maximum temperature for the reactor system started from the same initial conditions is shown in Figure 4.6. As expected, it is observed that the closed-loop system drives the temperature to the stationary state much faster rate than the open-loop. The open-loop system is expected to evolve towards the stationary state (if no persistent disturbances affect the system) because the linear spatial operator A of the infinite dimensional representation of the catalytic model in (4.31) is exponentially stable, the B operator is bounded and the remark used in 4.6.1. To evaluate the ability of the controller to achieve stable operation, the closed-loop behaviour of the system with disturbance in the inlet mole fraction of reactant was simulated. The performance of the closed-loop system is shown in Figure 4.7 for a disturbance trajectory given at the

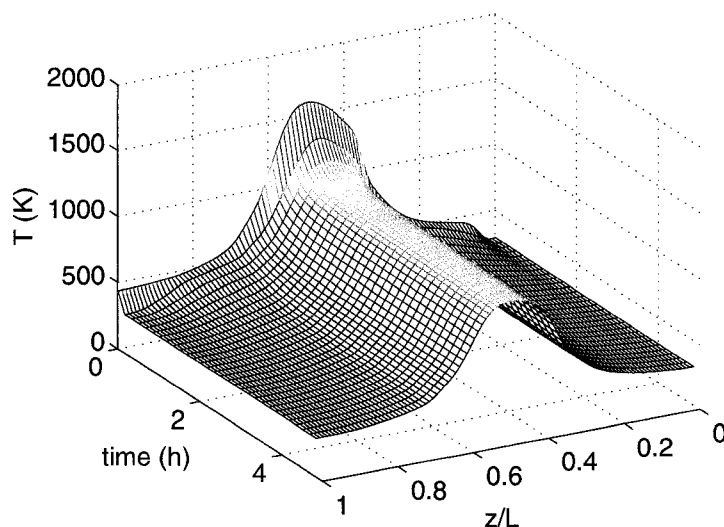


Figure 4.3: Closed-loop distribution of the temperature along the reactor centerline.

bottom of the figure. For comparison, we included the open-loop dynamics in Figure 4.8 for the same disturbance trajectory. It is observed that the open loop operation leads to extinction of the reaction, while the closed-loop keeps stable operation.

Although manipulation of the fluid flow velocity along the axis of the reactor at a large (or infinite) number of points gives the best achievable control performance that is interesting to study and can be used as a benchmark for the maximum achievable performance, it is not practical for real operation. Since it is not practical to manipulate the fluid flow velocity along the axis of the reactor, we approximate the optimal spatial distribution of the manipulated variable by averaging its value as follows:

$$u_{sub}(t) = \frac{1}{z_{out} - z_{mid}} \int_{z_{mid}}^{z_{out}} -r(z)^{-1} \gamma(z) \psi(z) \cdot x(t, z) dz \quad (4.41)$$

where subscripts *mid* and *out* denote midsection ($z = 0.5$) and outlet section of the reactor ($z = 1$), respectively. The fluid flow velocity is constant in the first half of the reactor, after which the fluid flow velocity is manipulated by using a control valve.

Using equation (4.41) as input variable, we computed the closed-loop response of the system from an an initial state that is not the stationary state, see Figure 4.1. The closed-loop temperature response along the axis of the reactor is shown in Figure

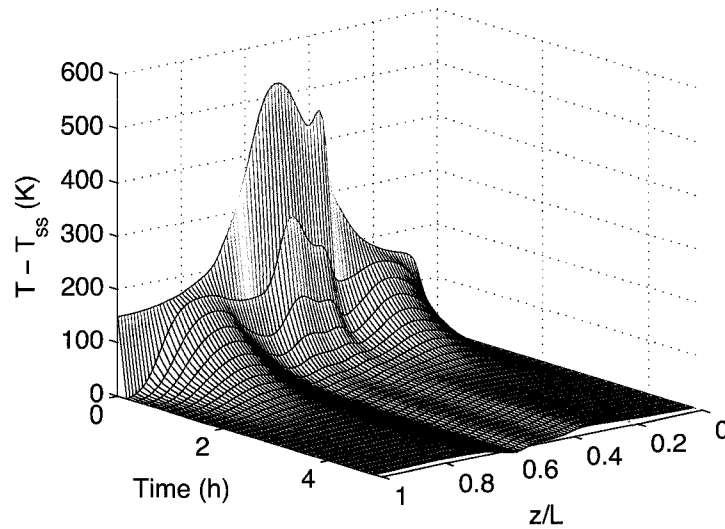


Figure 4.4: Distribution of the difference between the current temperature and the temperature at stationary state, T_{ss} .

4.9. The trajectory of the manipulated variable, $u_{sub}(t)$, is shown in Figure 4.10. We observe that the controller performs well, as the temperature distribution is driven towards the stationary state values.; however, when compared to the closed-loop system with the optimal LQ, see Figure 4.11, some control performance is lost.

To evaluate the ability of the sub-optimal controller to achieve stable operation, we simulate the closed-loop behavior of the system to step disturbances in the inlet mole fraction. The performance of the closed-loop system is shown in Figure 4.12. Figure 4.13 shows the trajectory of the manipulated variable $u_{sub}(t)$. It is observed that the closed-loop system quickly reaches the stationary state for some inlet disturbances, but for very lean inlet reactant concentration the reaction is extinguished. It is noted that the suboptimal controller was arbitrarily selected and no stability properties were verified.

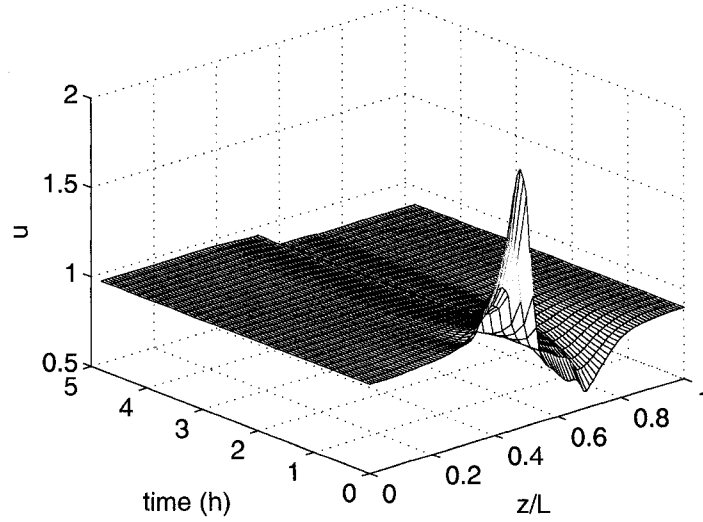


Figure 4.5: Evolution of the the manipulated variable spatial profile along the reactor centerline.

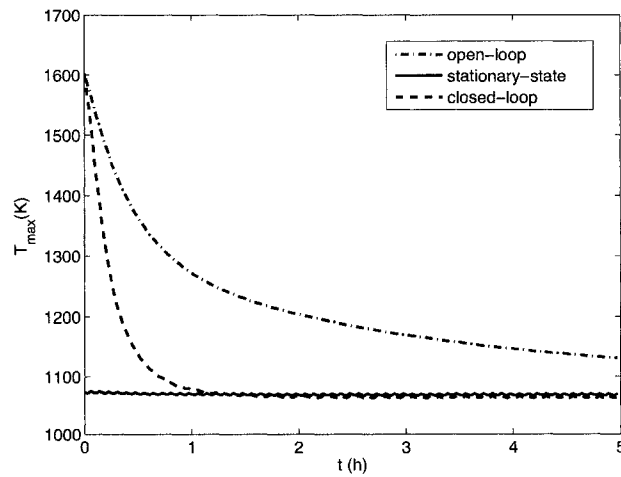


Figure 4.6: Trajectory of the maximum temperature along the axis of the reactor for open- and closed-loop simulations.

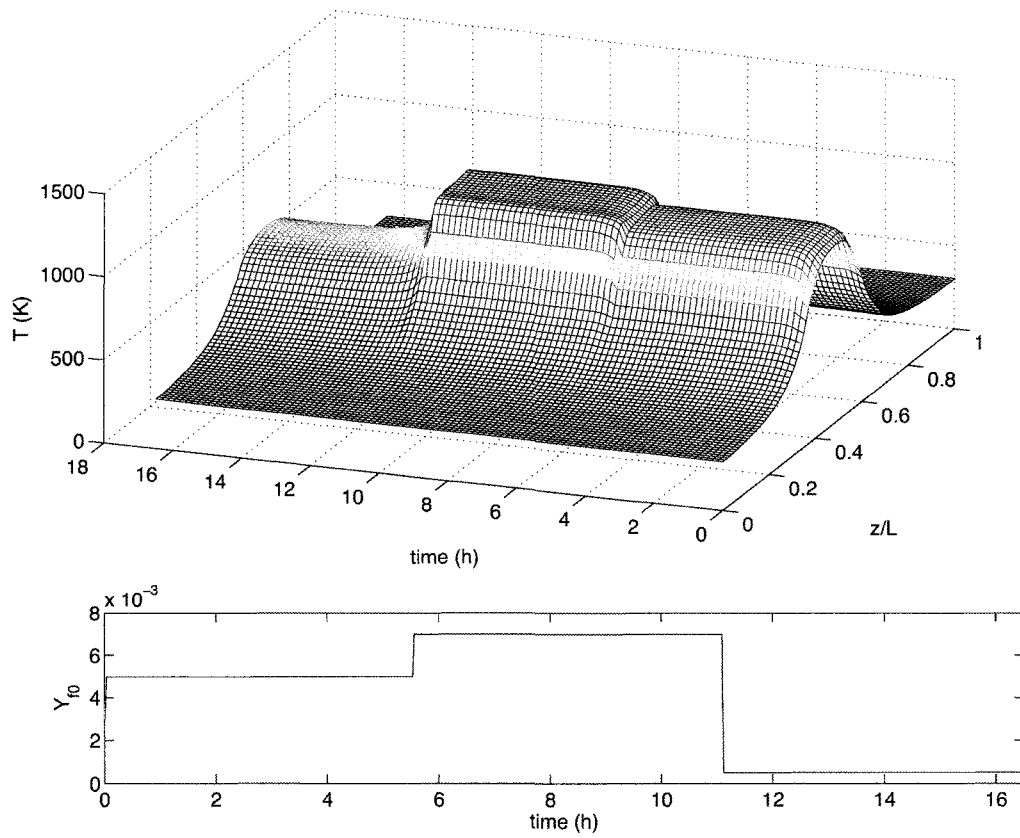


Figure 4.7: Evolution of the closed-loop temperature distribution along the axis of the reactor for step disturbances in the inlet mole fraction of reactant

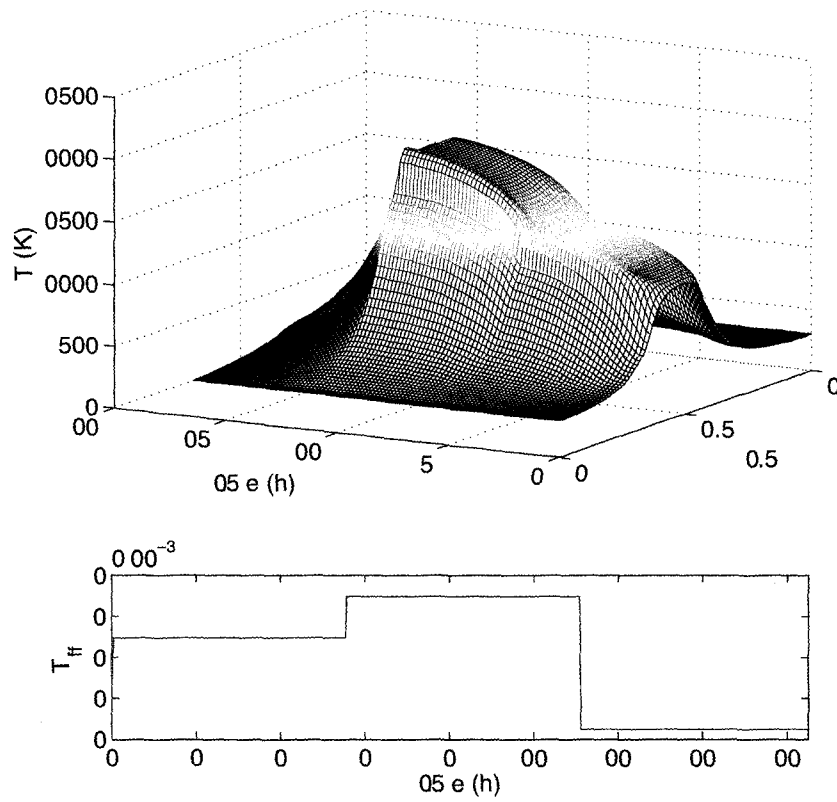


Figure 4.8: Evolution of the open-loop temperature distribution along the axis of the reactor for step disturbances in the inlet mole fraction of reactant

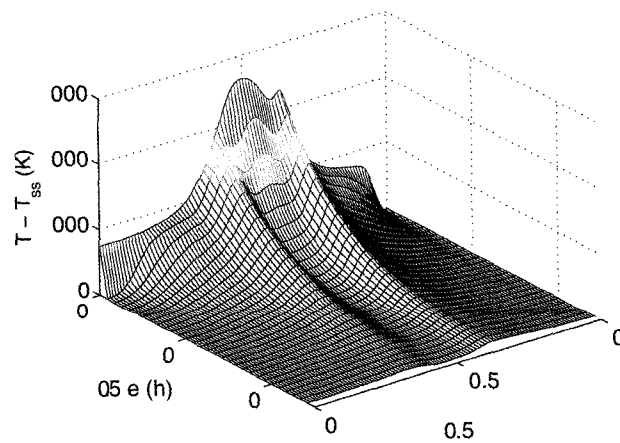


Figure 4.9: Closed-loop distribution of the temperature along the reactor centerline with suboptimal controller, $u_{sub}(t)$.

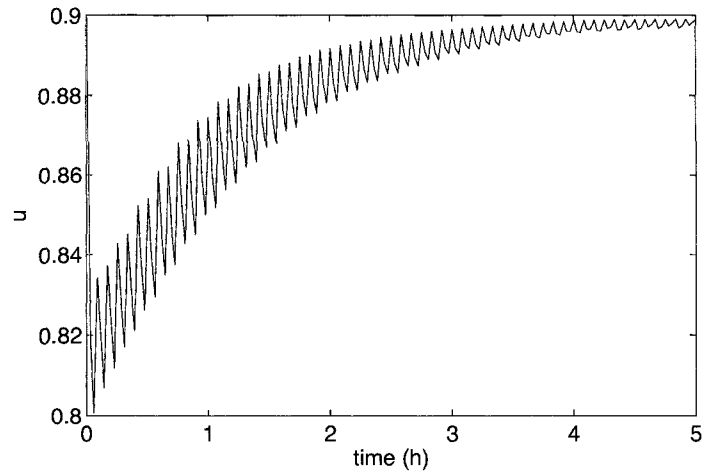


Figure 4.10: Trajectory of the manipulated variable with suboptimal controller, $u_{sub}(t)$.

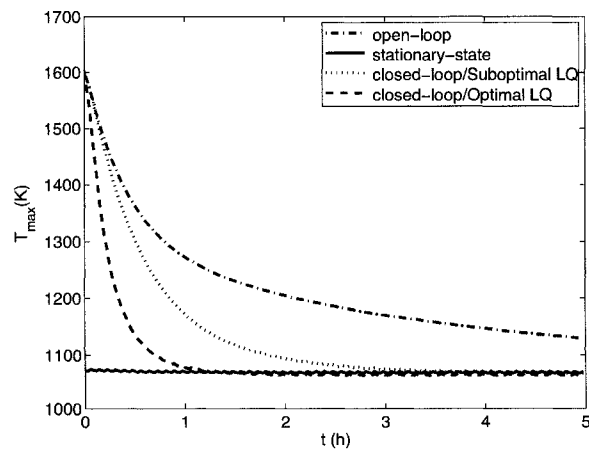


Figure 4.11: Trajectory of the maximum temperature along the axis of the reactor for different cases.

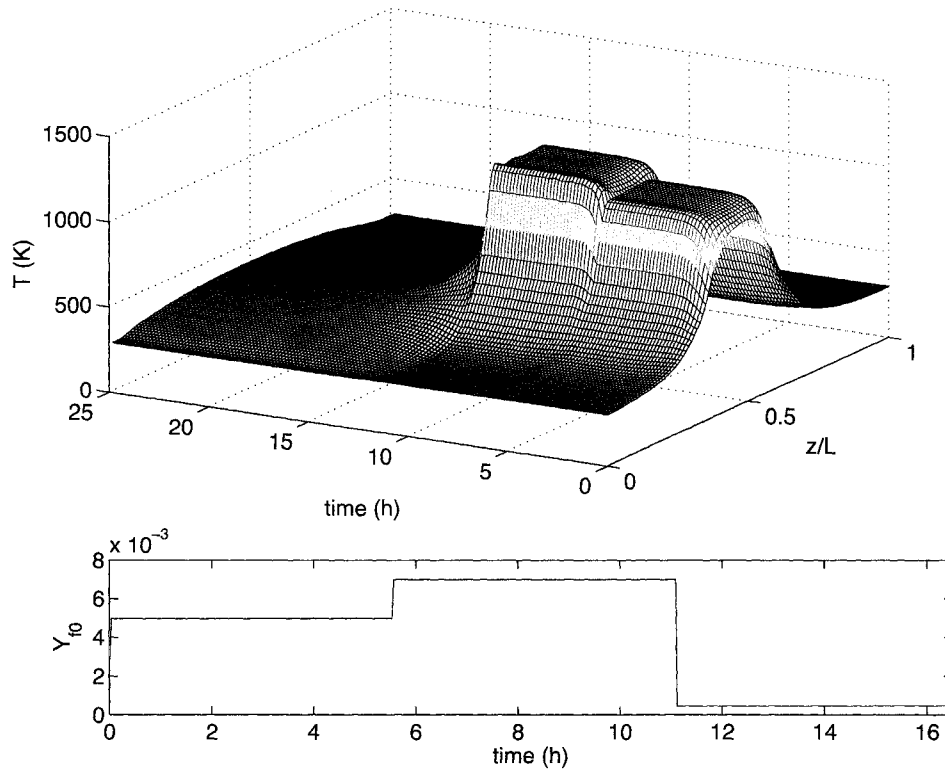


Figure 4.12: Closed-loop distribution of the temperature along the reactor centerline with suboptimal controller, $u_{sub}(t)$ and mole fraction disturbance.

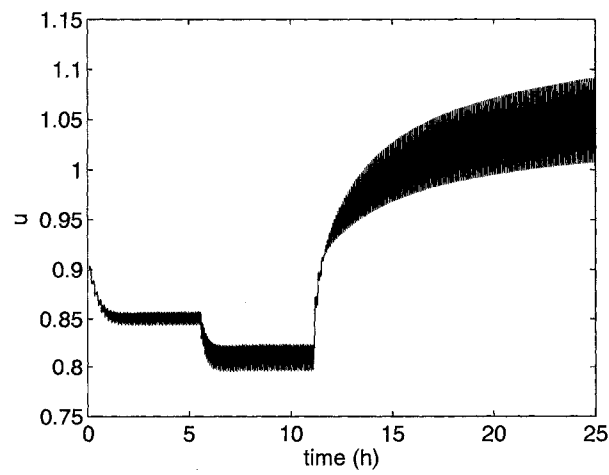


Figure 4.13: Trajectory of the manipulated variable with suboptimal controller, $u_{sub}(t)$.

4.8 Summary

In this chapter, we presented the formulation of an LQ-feedback controller for a catalytic reactor with reverse flow operation using an infinite dimensional state space description of the system.

The LQ-controller was formulated by following the traditional approach to control systems design; i.e. linearization of the system around a desired operating distribution of the state variables, analysis of the resulting linear system for control purposes and finally the design of the controller using the linear model. More specifically, the controller was developed on the basis of a plug-flow pseudo-homogeneous catalytic reactor model with unidirectional flow and it was formulated to keep the temperature along the axis of the reactor at the stationary state values.

The catalytic reactor studied is better controlled by an input variable whose distribution can be manipulated. A spatially distributed input variable, namely gas flow velocity, was considered to control the temperature distribution along the axis of the reactor and derive an upper bound on the best achievable control. Although manipulation of the fluid flow velocity along the axis of the reactor at a large (or infinite) number of points gives the best achievable control performance, it can be used as a benchmark for the maximum achievable performance. Since it is not practical to manipulate the fluid flow velocity along the axis of the reactor, we approximate the optimal distribution of the manipulated variable by averaging its values.

From the results of this chapter, we can conclude that a proportional controller, such as computed and used in this chapter, can be used to drive the reverse flow reactor system to stationary state and to achieve reactor stability while inlet disturbances affect the system; however, control objectives such as offset elimination or temperature excursions above a maximum threshold cannot be fulfilled.

The closed-loop control performance was tested numerically for the catalytic combustion of lean methane streams. The LQ-controller is shown to lead to stable operation for inlet concentration disturbances which comprise the main source of process disturbance. The ability of the controller to drive the system to stationary state is simulated and compared with suboptimal controllers formulated by averaging

the spatially distributed input variable.

5

Open-Loop Nonlinearity Assessment for Hyperbolic PDE Models

Most processes, including the catalytic flow reversal reactor, are nonlinear. For analysis and control, it is important to understand the extent of process nonlinearity so that its impact on control design and closed-loop operation can be assessed. A wide range of measures have been proposed to quantify process nonlinearity to aid in the selection of suitable control techniques. While published results in this area are limited to lumped parameter systems, we focus in this chapter on distributed parameter systems. Specifically, we look at gain nonlinearity quantification of systems modeled by hyperbolic partial differential equations. The measure can help to identify operating regions in distributed parameter systems where process nonlinearity is significant and nonlinear control might need to be considered. The method to quantify open-loop nonlinearity is applied to a tubular chemical reactor and a catalytic flow reversal reactor. ¹

¹Parts of this chapter are published in the proceedings of the European Control Conference (ECC), Kos Island, Greece, 2007.

5.1 Motivation

In general, the dynamics of catalytic reactors are nonlinear. Nonlinearities present themselves in different forms, i.e. chemical process characteristics (e.g., Arrhenius rate expressions), input saturation (e.g., valve limits), and output saturation (physical limits on output variables - e.g., mole fractions) (Guay *et al.*, 1995). A wide range of nonlinear control techniques have been used for tubular and catalytic reactors, see for example (Hanczyc and Palazoglu, 1995; Christofides, 2000; Shang, 2002; Dubljevic *et al.*, 2005). On the other hand, linear control techniques have been successfully applied, see for example (Ray, 1981; Aksikas, 2005); however, no systematic approach has been developed to assess the impact of process nonlinearity in control design. The impact of nonlinearities on closed-loop stability and performance depends on: 1) the degree of nonlinearity of the process, 2) the intended range and direction of operation and 3) the control objectives.

Despite the advantages of nonlinear control, development, implementation and operation becomes more complex than linear control methods. From a practitioner's perspective, it is important to be able to assess when a process is sufficiently nonlinear to justify using a nonlinear control law (Guay *et al.*, 1995).

In this chapter, we address the following issues by developing a suitable measure of process nonlinearity:

- How nonlinear is the steady-state map of a process for a given set of inputs?
- How does the degree of nonlinearity change as a function of the operating point?
- Is it possible to select a linear control law that will achieve satisfactory performance for the nonlinear process?

5.2 Introduction

In general, most physical processes as well as their associated mathematical models are nonlinear. The derivation of systematic methods to evaluate the degree of nonlinearity inherent to a process, and its impact on the design of suitable control systems, has been the focus of many research studies.

Initial steps towards a measure of nonlinearity were concerned with the open-loop ‘nonlinearity quantification’. Nonlinearity quantification is used to indicate whether linear control may be adequate for a nonlinear process (Nikolaou and Misra, 2003).

Operator-based approaches have been proposed in the literature to assess process nonlinearity (Desoer and Wang, 1980; Nikolaou, 1993; Schweickhardt and Allgower, 2004). In operator-based approaches, the nonlinearity is computed as the distance between a nonlinear operator from a suitably defined linear operator.

A linear operator or transformation, L , is defined (see for example Ramkrishna and Amundson (1985)) as a mapping of the elements of a vector space \mathcal{L} into elements of the same space that satisfies the conditions:

$$\begin{aligned} L(x + y) &= L(x) + L(y) & \forall x, y \in \mathcal{L} \\ L(\alpha x) &= \alpha L(x) & \alpha \in \mathbb{R}, x \in \mathcal{L} \end{aligned}$$

Nonlinearity measures appeared for the first time in Desoer and Wang (1980), where a nonlinearity measure was defined as the difference between a nonlinear system and its best linear approximation:

$$v = \inf_{L \in \Lambda} \|N[u] - L[u]\|. \quad (5.1)$$

The dynamic behaviour of the nonlinear and linear systems are described by the operators (mappings)

$$\begin{aligned} N : \mathcal{U} &\rightarrow \mathcal{Y} :, u \mapsto y = N[u] \\ L : \mathcal{U} &\rightarrow \mathcal{Y} :, u \mapsto \tilde{y} = L[u] \end{aligned}$$

The minimization in (5.1) is performed over all linear operators in the set Λ , and the norm function can be any suitable norm. The norm of the error itself, v is not the best quantity to look at, as it heavily depends on the problem scaling (i.e., if the output of the nonlinear system is multiplied by a constant factor, then the nonlinearity measure is magnified by the same factor). Thus, the degree of the nonlinearity seems to get worse while there is no qualitative change in the behavior of the nonlinear system.

To compute the nonlinearity measure in (5.1), Nikolaou (1993) constructed an inner product which can be iteratively computed to a desired accuracy. Ogunnaike *et al.*

(1993) proposed a different operator-based nonlinearity measure, where the degree of nonlinearity is computed by locally approximating the given nonlinear system by a set of linear systems and by computing the maximum distance between any pair of systems within such a set.

Allgower (1995a) proposed the following nonlinearity measure

$$\phi = \inf_{L \in \Lambda} \sup_{u \in \mathcal{U}} \frac{\|N[u] - L[u]\|}{\|u\|}. \quad (5.2)$$

The measure quantifies the largest difference between the output of the nonlinear operator and its best linear approximations for the worst-case input sequence. Allgower (1995a) tackled the computational problem by parametrizing the input signal u and the linear operator L in (5.2) through finite dimensional approximation and convex optimization.

To overcome the scaling problems in (5.1) and (5.2), Allgower (1995b) proposed a new nonlinearity measure

$$\phi = \inf_{L \in \Lambda} \sup_{u \in \mathcal{U}} \frac{\|N[u] - L[u]\|}{\|N[u]\|}. \quad (5.3)$$

The measure ϕ gives the ‘relative error’ of the output of the linear model L that best approximates the nonlinear system N . In other words, the value of ϕ corresponds to the fractional deviation of the output of the best linear approximation L from the output of the nonlinear system N . An important property of the measure ϕ is that its value is bounded by one, a value close to one corresponding to a highly nonlinear system.

The computation of the nonlinearity measure ϕ is performed by parametrization of the input signal u and the linear operator L through finite dimensional approximation, simulation and optimization.

A lower bound on the nonlinearity measure ϕ can be computed if a family of sinusoids is selected, $\{A \sin(\omega t) | \omega \in \Omega, A \in \mathcal{A}\}$ as the space of admissible inputs (Allgower, 1995b). The Fourier series expansion of the system’s stationary-state response is then computed,

$$y = A_0 + \sum_{k=1}^{\infty} A_k \sin(k\omega t + \rho_k),$$

where the A_k are the expansion coefficients and ρ_k is the response phase lag, and the lower bound, χ , becomes

$$\chi = \sup_{A \in \mathcal{A}, \omega \in \Omega} \sqrt{1 - \frac{A_1^2(\omega, A)}{2A_0^2(\omega, A) + \sum_{k=1}^{\infty} \frac{A_k^2(\omega, A)}{2}}}$$

Helbig *et al.* (2000) generalized the approach of Allgower (1995a) and proposed a measure that can be applied both to the analysis of steady-state operating points of continuously operated processes as well as to trajectory dependent analysis of batch or other transient process. The nonlinearity measure proposed is the following:

$$\phi = \inf_{L \in \Lambda} \sup_{u \in U, x_{N,0} \in X_{N,0}} \inf_{x_{L,0} \in X_{L,0}} \frac{\|N[u, x_{N,0}] - L[u, x_{L,0}]\|}{\|N[u, x_{N,0}]\|}$$

The measure focuses on the difference between the output of N and L as a function of both the initial conditions and inputs. It takes values between 0 and 1, thus allowing easy nonlinearity assessment for a value of ϕ . An approximate computational strategy similar to that in Allgower (1995b) was proposed by Helbig *et al.* (2000) to transfer the infinite dimensional nested optimization problem into a convex finite dimensional minimization problem.

Common to all the techniques that have been introduced is the reliance on numerical simulations. The algorithms can be computationally intensive, requiring elaborate optimization schemes and simulations. To overcome the need of intensive numerical computations, various approaches have been proposed.

Sun and Hoo (2000) define a nonlinearity measure for single-input-single-output nonlinear systems by

$$\phi = \max \left\{ \sup_{u \in \mathcal{U}} \|N[u] - L_{up}[u]\|, \sup_{u \in \mathcal{U}} \|N[u] - L_{lo}[u]\| \right\}$$

where L_{up} and L_{lo} are linear systems such that the output y (in the time domain) of N lies at all times between the outputs y_{up} and y_{lo} of L_{up} and L_{lo} , $(y_{lo} - y)(y_{up} - y) \leq 0$.

Harris *et al.* (2000), presented a method to derive lower and upper bounds for the nonlinearity measure ϕ in (5.2) and (5.3) using functional expansion models instead of the calculating the exact nonlinearity measure, which is often computationally intensive. Kihias and Marquez (2004) looked at measuring the distance in the \mathcal{L}_2 -sense

between the state of a nonlinear system and that obtained by Jacobian linearization. A different approach was taken by Guay *et al.* (1995) who quantified steady state nonlinearities by using curvature metrics of the steady-state locus.

The basic idea behind the open-loop nonlinearity measures is that a ‘fairly’ nonlinear operator would require nonlinear control. Nevertheless, they can be used to locate operating regions and input directions where nonlinearity is significant and may pose a challenge for linear control.

5.3 Contributions

All nonlinearity measures available in the literature and discussed in the preceding section were formulated and applied to lumped parameter models; however, there is no specific development nor application of open-loop nonlinearity measure for distributed parameter systems.

In this chapter, we develop a measure of open-loop nonlinearity for systems modelled by quasi-linear hyperbolic PDE equations. Such models typically arise in modeling of chemical engineering processes, including chemical plug flow reactors, packed-bed reactors and heat exchangers, among others.

Drawing from the results for lumped parameter systems, we extend an open-loop nonlinearity measure based on local geometry to hyperbolic distributed parameter systems. The approach used is based on the measure proposed by Guay *et al.* (1995) to assess the degree of nonlinearity of open-loop lumped parameter systems at steady-state.

The goal is to develop a nonlinearity measure that is easy to compute and that can provide information about the gain nonlinearity of the system under study.

5.4 Nonlinearity Assessment based on Local Curvature

The measure of nonlinearity proposed in this work to quantify open-loop nonlinearity employs a Taylor series approximation of the process model. By using a Taylor series approximation, the relative contribution of second or higher order terms can be used

to quantify nonlinearity around an operating point.

In Guay *et al.* (1995), an open-loop nonlinearity assessment framework is proposed for nonlinear lumped parameter systems. The framework is based on the curvature of the steady-state locus obtained from the inputs $\mathbf{u} \in \mathbb{R}^P$ to the states $\mathbf{x} \in \mathbb{R}^n$ or outputs $\mathbf{y} \in \mathbb{R}^m$ map. The geometry of the steady-state locus is described by considering the first and second order derivatives of the states with respect to the P -inputs of the process. To analyze and quantify the steady-state input to state nonlinearity, the first order derivatives are computed by evaluating the tangent space of the steady-state locus, $\Xi(\mathbf{u})$, at a given operating point of the input space (\mathbf{u}_0):

$$\dot{\mathbf{v}}_i = \frac{\partial \Xi(\mathbf{u})}{\partial u_i}, \quad 1 \leq i \leq P \quad (5.4)$$

which forms a set of P n -dimensional *velocity vectors*. The extent of departure from linearity at any point \mathbf{u}_0 can be assessed by evaluating the magnitude of the second order derivatives

$$\ddot{\mathbf{v}}_{ij} = \frac{\partial^2 \Xi(\mathbf{u})}{\partial u_i \partial u_j}, \quad 1 \leq i, j \leq P \quad (5.5)$$

which form a set of $P \times P$ n -dimensional vectors, called *acceleration vectors*.

The second-order information can be decomposed into tangential and normal components; each of which gives different information regarding the nonlinearity of the process. The nonlinearity that results from tangential and normal acceleration components are called tangential curvature and normal curvature, respectively (Bates and Watts, 1988; Guay *et al.*, 1995). The nonlinearity of a system can be assessed by the relative contribution of the second order terms of the Taylor series approximation of the steady-state locus at given operating conditions.

5.5 Classification of PDE systems

As opposed to lumped parameter systems, where model equations are either linear or nonlinear, partial differential equations with nonlinear terms are classified according to the following classification (Jeffrey, 2003):

1. A PDE satisfied by a suitably differentiable function x of the independent variables z_1, \dots, z_n is said to be *linear* if x and its partial derivatives only occur

linearly and, possibly, with coefficients that are functions of the independent variables. This PDE may, or may not, contain a function f that depends only on the independent variables.

2. A PDE satisfied by a suitably differentiable function x of the independent variables z_1, \dots, z_n is said to be *semilinear* when all derivatives of x occur linearly, with coefficients that may be a functions of the independent variables, but x itself occurs nonlinearly.
3. A PDE of order k satisfied by a suitably differentiable function x of the independent variables z_1, \dots, z_n is said to be *quasilinear* if its partial derivatives of order k appear linearly, possibly with coefficients that are functions of x and derivatives of x of order less than k and also the independent variables.
4. A PDE that belongs to none of the above categories is said to be *nonlinear*.

The definitions given above extend in an obvious way to systems of PDEs. We have chosen to analyze quasilinear types of PDEs because they are common in chemical engineering problems.

5.6 Open-Loop Nonlinearity Assessment for Hyperbolic PDE models

Consider the following type of quasi-linear n -first order hyperbolic partial differential equations:

$$\mathbf{A}(z, \mathbf{x}, \mathbf{u}) \frac{\partial \mathbf{x}}{\partial t} + \mathbf{B}(z, \mathbf{x}, \mathbf{u}) \frac{\partial \mathbf{x}}{\partial z} = \mathbf{d}(z, \mathbf{x}, \mathbf{u}) \quad (5.6)$$

with initial and boundary conditions

$$I.C. \mathbf{x}(0, z) = \mathbf{x}_0(z)$$

$$B.C. \mathbf{x}(t, 0) = \mathbf{x}_{in}$$

where t and z are the independent variables, $\mathbf{x} = [x_1(t, z), x_2(t, z), \dots, x_n(t, z)]^T$ is the state function vector and $\mathbf{u} = [u_1(t, z), u_2(t, z), \dots, u_l(t, z)]^T$ is an input function vector.

Consider the output variables to be defined as follows:

$$y_j = C_j h(x) = \int_{z_j}^{z_{j+1}} c_j(z) h(x(t, z)) dz \quad j = 1, 2, \dots, m \quad (5.7)$$

where $c_j(z)$ is a known smooth function of z . The operator C_j is typically used for practical applications in control design of distributed parameter systems (Ray, 1981; Christofides, 2000). For most of the practical applications, the input space is discretized in the space variable leading to a finite number of control actuators (Christofides, 2000):

$$u_i(t, z) = \sum_{j=1}^P b_j(z) u_j(t) \quad i = 1, 2, \dots, l \quad (5.8)$$

where $b_j(z)$ is a known smooth function of z . An schematic representation of the inputs and outputs is illustrated in Figure 5.1. To simplify notation, we consider

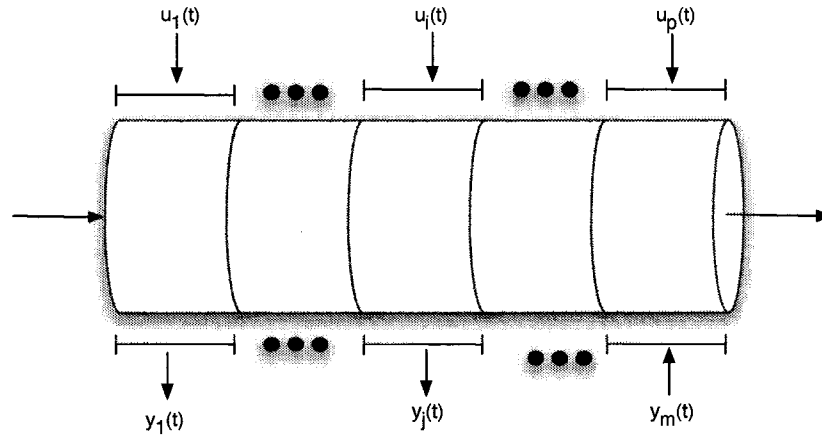


Figure 5.1: Illustration of the input/output specification.

in what follows, a single spatially distributed input ($l = 1$). We use the following notation to represent the discretization of the inputs and outputs:

$$\mathbf{u} = [u_1(t), u_2(t), \dots, u_P(t)]^T, \quad (5.9)$$

$$\mathbf{y} = \mathbf{C} \mathbf{h}(\mathbf{x}) = [y_1(t), y_2(t), \dots, y_m(t)]^T. \quad (5.10)$$

where

$$\mathbf{C} = [(H(z - z_1) - H(z - z_2))\mathbf{C}_1 \cdots (H(z - z_j) - H(z - z_{m+1}))\mathbf{C}_m] \quad (5.11)$$

and H is the heaviside function. Extension to multi-input case, $l > 1$, is straightforward.

To study the geometry of the steady-state input-output map, we find the first order partial derivative of the steady-state locus, $\Xi(\mathbf{u})[z]$, with respect to the inputs (velocity vectors). The notation $[z]$ is used to indicate that the steady-state locus is a function of the independent variable, z .

Remark 5.6.1 *Differentiation of a vector functions (Harville, 1997, Page 291):*

Suppose that there is a (column) vector $\mathbf{f} = (f_1, \dots, f_p)'$ of p functions to be differentiated and that the domain of all of these functions is a set S in $\mathbb{R}^{m \times 1}$. By letting $\mathbf{x} = (x_1, \dots, x_p)'$ represent a vector of m variables and writing $\frac{\partial \mathbf{f}}{\partial \mathbf{x}^T}$ for the $p \times m$ matrix whose s_j^{th} element is $\frac{\partial f_s(\mathbf{x})}{\partial x_j}$. In this context, $\frac{\partial \mathbf{f}(\mathbf{x})}{\partial \mathbf{x}^T}$ is called the first order derivative of $\mathbf{f}(\mathbf{x})$ with respect to \mathbf{x} .

To compute the velocity vectors, we set the system of equations (5.6) to its steady state:

$$\mathbf{B}(z, \mathbf{x}, \mathbf{u}) \frac{d\mathbf{x}}{dz} - \mathbf{d}(z, \mathbf{x}, \mathbf{u}) = \mathbf{g}(z, \mathbf{x}, \mathbf{s}, \mathbf{u}) = \mathbf{0}_{n \times 1} \quad (5.12)$$

where $\mathbf{s} = \frac{d\mathbf{x}}{dz}$. Then, we compute the total derivative of \mathbf{g} with respect to the inputs:

Theorem 5.6.1 *Assume that \mathbf{g} and all its partial derivatives $\frac{\partial \mathbf{g}}{\partial \mathbf{x}^T}$, $\frac{\partial \mathbf{g}}{\partial \mathbf{s}^T}$ and $\frac{\partial \mathbf{g}}{\partial \mathbf{u}^T}$ are continuous, and that $\mathbf{x} = \mathbf{x}(z, \mathbf{u})$ and $\mathbf{s} = \mathbf{s}(z, \mathbf{u})$ are themselves differentiable functions of \mathbf{u} . Let $\mathbf{g}(z, \mathbf{u}) = \mathbf{g}(z, \mathbf{x}(z, \mathbf{u}), \mathbf{s}(z, \mathbf{u}), \mathbf{u})$. Then \mathbf{g} is differentiable and*

$$\frac{d\mathbf{g}}{d\mathbf{u}^T} = \frac{\partial \mathbf{g}}{\partial \mathbf{u}^T} + \frac{\partial \mathbf{g}}{\partial \mathbf{x}^T} \frac{\partial \mathbf{x}}{\partial \mathbf{u}^T} + \frac{\partial \mathbf{g}}{\partial \mathbf{s}^T} \frac{\partial \mathbf{s}}{\partial \mathbf{u}^T} = \mathbf{0}_{n \times P}. \quad (5.13)$$

The term

$$\frac{\partial \mathbf{s}}{\partial \mathbf{u}^T} = \frac{\partial}{\partial \mathbf{u}^T} \left(\frac{d\mathbf{x}}{dz} \right) \quad (5.14)$$

is equivalent to

$$\frac{\partial}{\partial \mathbf{u}^T} \left(\frac{d\mathbf{x}}{dz} \right) = \frac{d}{dz} \left(\frac{\partial \mathbf{x}}{\partial \mathbf{u}^T} \right). \quad (5.15)$$

Proof: The solution of equation (5.12) is a mapping $[0, 1] \times \mathbb{R}^P \rightarrow \mathbb{R}^n$

$$\mathbf{x} = \mathbf{f}(z, \mathbf{u}). \quad (5.16)$$

The partial derivative of (5.16) with respect to the inputs is given by

$$\frac{\partial \mathbf{x}}{\partial \mathbf{u}^T} = \frac{\partial \mathbf{f}}{\partial \mathbf{u}^T}. \quad (5.17)$$

and the total derivative of (5.17) with respect to the independent variable, z , gives

$$\frac{d}{dz} \left(\frac{\partial \mathbf{x}}{\partial \mathbf{u}^T} \right) = \frac{\partial^2 \mathbf{f}}{\partial \mathbf{u} \partial \mathbf{u}^T} \frac{d\mathbf{u}}{dz} + \frac{\partial}{\partial z} \left(\frac{\partial \mathbf{f}}{\partial \mathbf{u}^T} \right). \quad (5.18)$$

Since the inputs \mathbf{u} , as defined in (5.9) are independent of z , then $\frac{d\mathbf{u}}{dz} = \mathbf{0}_{P \times 1}$.

Therefore,

$$\begin{aligned} \frac{d}{dz} \left(\frac{\partial \mathbf{x}}{\partial \mathbf{u}^T} \right) &= \frac{\partial}{\partial z} \left(\frac{\partial \mathbf{f}}{\partial \mathbf{u}^T} \right) \\ &= \frac{\partial}{\partial z} \left(\frac{\partial \mathbf{x}}{\partial \mathbf{u}^T} \right) = \frac{\partial}{\partial \mathbf{u}^T} \left(\frac{\partial \mathbf{x}}{\partial z} \right) \\ \Rightarrow \frac{d}{dz} \left(\frac{\partial \mathbf{x}}{\partial \mathbf{u}^T} \right) &= \frac{\partial}{\partial \mathbf{u}^T} \left(\frac{d\mathbf{x}}{dz} \right) \end{aligned}$$

□

Using (5.15) in eq. (5.13) we obtain

$$\left(\frac{\partial \mathbf{g}}{\partial \mathbf{s}^T} \right) \frac{d}{dz} \left(\frac{\partial \mathbf{x}}{\partial \mathbf{u}^T} \right) + \left(\frac{\partial \mathbf{g}}{\partial \mathbf{x}^T} \right) \frac{\partial \mathbf{x}}{\partial \mathbf{u}^T} + \frac{\partial \mathbf{g}}{\partial \mathbf{u}^T} = \mathbf{0}_{n \times P}. \quad (5.19)$$

Equation (5.19) is a set of ordinary differential equations that can be solved simultaneously with (5.12) to obtain the velocity vectors,

$$\frac{\partial \mathbf{x}}{\partial \mathbf{u}^T} [z] = \frac{\partial \Xi(\mathbf{u})}{\partial \mathbf{u}^T} [z]. \quad (5.20)$$

The initial conditions for (5.19) depend on the type of boundary condition in (5.6), i.e. for Dirichlet boundary conditions, $\frac{\partial \mathbf{x}}{\partial \mathbf{u}} [0] = \mathbf{0}_{n \times P}$.

From the solution of (5.19), we obtain the velocity vectors for the input-output map:

$$\frac{\partial \mathbf{y}}{\partial \mathbf{u}^T} = \mathbf{c} \left\{ \frac{\partial \mathbf{h}}{\partial \mathbf{x}^T} \Big|_{\Xi(\mathbf{u}_0)[z]} \frac{\partial \Xi(\mathbf{u})}{\partial \mathbf{u}^T} [z] \right\}. \quad (5.21)$$

To compute the acceleration vectors, the second total derivative of (5.13) with respect to the inputs is evaluated:

$$\frac{d}{d\mathbf{u}} \left(\frac{d\mathbf{g}}{d\mathbf{u}^T} \right) = \frac{\partial}{\partial \mathbf{u}} \left[\frac{\partial \mathbf{g}}{\partial \mathbf{u}^T} + \frac{\partial \mathbf{g}}{\partial \mathbf{x}^T} \frac{\partial \mathbf{x}}{\partial \mathbf{u}^T} + \frac{\partial \mathbf{g}}{\partial \mathbf{s}^T} \frac{\partial \mathbf{s}}{\partial \mathbf{u}^T} \right] = \mathbf{0}_{n \times P} \quad (5.22)$$

Remark 5.6.2 *Differentiation of a matrix functions:*

Suppose that there is a $p \times q$ matrix \mathbf{F} of pq functions to be differentiated and that the domain of all these functions is a set S in $\mathbb{R}^{m \times 1}$ (that contains at least some interior points). Each of the elements of \mathbf{F} can be regarded as a function of a vector $\mathbf{x} = (x_1, \dots, x_m)'$ of m independent variables. All mpq partial derivatives (of the elements of \mathbf{F}) can be presented in the form of $m \times (p \times q)$ three dimensional array where each face (of the m faces) is a $p \times q$ matrix of partial derivatives.

From (5.22), we obtain

$$\begin{aligned} & \frac{\partial}{\partial \mathbf{x}} \left(\frac{\partial \mathbf{g}}{\partial \mathbf{u}^T} \right) \frac{\partial \mathbf{x}}{\partial \mathbf{u}^T} + \frac{\partial^2 \mathbf{g}}{\partial \mathbf{u} \partial \mathbf{u}^T} + \frac{\partial}{\partial \mathbf{x}} \left(\frac{\partial \mathbf{g}}{\partial \mathbf{x}^T} \frac{\partial \mathbf{x}}{\partial \mathbf{u}^T} \right) \frac{\partial \mathbf{x}}{\partial \mathbf{u}} + \frac{\partial}{\partial \mathbf{u}} \left(\frac{\partial \mathbf{g}}{\partial \mathbf{x}^T} \frac{\partial \mathbf{x}}{\partial \mathbf{u}^T} \right) + \\ & \frac{\partial}{\partial \mathbf{x}} \left(\frac{\partial \mathbf{g}}{\partial \mathbf{s}^T} \frac{\partial \mathbf{s}}{\partial \mathbf{u}^T} \right) \frac{\partial \mathbf{x}}{\partial \mathbf{u}} + \frac{\partial}{\partial \mathbf{u}} \left(\frac{\partial \mathbf{g}}{\partial \mathbf{s}^T} \frac{\partial \mathbf{s}}{\partial \mathbf{u}^T} \right) = \mathbf{0}_{n \times P}. \end{aligned} \quad (5.23)$$

Remark 5.6.3 *Product of a three-dimensional matrix and a two-dimensional matrix:*

The product of a three-dimensional matrix $m \times (p \times q)$ and a two-dimensional matrix $p \times q$ is a $p \times m$ matrix for which the i^{th} column is obtained by multiplying the i^{th} face of the three-dimensional matrix and the i^{th} column of the two-dimensional matrix.

Expanding the partial derivatives in (5.23) and using (5.15), we obtain

$$\begin{aligned} & \frac{\partial^2 \mathbf{g}}{\partial \mathbf{x} \partial \mathbf{u}^T} \left(\frac{\partial \mathbf{x}}{\partial \mathbf{u}} \right) + \frac{\partial^2 \mathbf{g}}{\partial \mathbf{u} \partial \mathbf{u}^T} + \frac{\partial^2 \mathbf{g}}{\partial \mathbf{x}^2} \left(\frac{\partial \mathbf{x}}{\partial \mathbf{u}^T} \right) \left(\frac{\partial \mathbf{x}}{\partial \mathbf{u}} \right) + \frac{\partial^2 \mathbf{g}}{\partial \mathbf{u} \partial \mathbf{x}^T} \left(\frac{\partial \mathbf{x}}{\partial \mathbf{u}^T} \right) + \\ & \frac{\partial \mathbf{g}}{\partial \mathbf{x}^T} \left(\frac{\partial^2 \mathbf{x}}{\partial \mathbf{u} \partial \mathbf{u}^T} \right) + \frac{\partial^2 \mathbf{g}}{\partial \mathbf{x} \partial \mathbf{s}^T} \frac{d}{dz} \left(\frac{\partial \mathbf{x}}{\partial \mathbf{u}^T} \right) \left(\frac{\partial \mathbf{x}}{\partial \mathbf{u}} \right) + \frac{\partial^2 \mathbf{g}}{\partial \mathbf{u} \partial \mathbf{s}^T} \frac{d}{dz} \left(\frac{\partial \mathbf{x}}{\partial \mathbf{u}^T} \right) + \\ & \frac{\partial \mathbf{g}}{\partial \mathbf{s}^T} \frac{d}{dz} \left(\frac{\partial^2 \mathbf{x}}{\partial \mathbf{u} \partial \mathbf{u}^T} \right) = \mathbf{0}_{n \times P}. \end{aligned} \quad (5.24)$$

In (5.24), we used the following equality

$$\frac{\partial^2 \mathbf{s}}{\partial \mathbf{u} \partial \mathbf{u}^T} = \frac{\partial^2}{\partial \mathbf{u} \partial \mathbf{u}^T} \left(\frac{d\mathbf{x}}{dz} \right) \quad (5.25)$$

$$= \frac{d}{dz} \left(\frac{\partial^2 \mathbf{x}}{\partial \mathbf{u} \partial \mathbf{u}^T} \right). \quad (5.26)$$

Proof: The solution of equation (5.12) is a mapping $[0, 1] \times \mathbb{R}^P \rightarrow \mathbb{R}^n$

$$\mathbf{x} = \mathbf{f}(z, \mathbf{u}). \quad (5.27)$$

The first and second partial derivative of (5.27) with respect to the inputs is given by

$$\frac{\partial \mathbf{x}}{\partial \mathbf{u}} = \frac{\partial \mathbf{f}}{\partial \mathbf{u}} \quad (5.28)$$

$$\frac{\partial^2 \mathbf{x}}{\partial \mathbf{u} \partial \mathbf{u}^T} = \frac{\partial^2 \mathbf{f}}{\partial \mathbf{u} \partial \mathbf{u}^T}, \quad (5.29)$$

and the total derivative of (5.29) with respect to the independent variable, z , gives

$$\frac{d}{dz} \left(\frac{\partial^2 \mathbf{x}}{\partial \mathbf{u} \partial \mathbf{u}^T} \right) = \frac{\partial}{\partial \mathbf{u}} \left(\frac{\partial^2 \mathbf{f}}{\partial \mathbf{u} \partial \mathbf{u}^T} \right) \frac{d\mathbf{u}}{dz} + \frac{\partial}{\partial z} \left(\frac{\partial^2 \mathbf{f}}{\partial \mathbf{u} \partial \mathbf{u}^T} \right). \quad (5.30)$$

Since the inputs \mathbf{u} , as defined in (5.9) are independent of z , then $\frac{d\mathbf{u}}{dz} = \mathbf{0}$. Therefore,

$$\frac{d}{dz} \left(\frac{\partial^2 \mathbf{x}}{\partial \mathbf{u} \partial \mathbf{u}^T} \right) = \frac{\partial}{\partial z} \left(\frac{\partial^2 \mathbf{f}}{\partial \mathbf{u} \partial \mathbf{u}^T} \right) \quad (5.31)$$

$$\begin{aligned} &= \frac{\partial}{\partial z} \left(\frac{\partial^2 \mathbf{x}}{\partial \mathbf{u} \partial \mathbf{u}^T} \right) = \frac{\partial^2}{\partial \mathbf{u} \partial \mathbf{u}^T} \left(\frac{\partial \mathbf{x}}{\partial z} \right) \\ \Rightarrow \frac{d}{dz} \left(\frac{\partial^2 \mathbf{x}}{\partial \mathbf{u} \partial \mathbf{u}^T} \right) &= \frac{\partial^2}{\partial \mathbf{u} \partial \mathbf{u}^T} \left(\frac{d\mathbf{x}}{dz} \right) \end{aligned} \quad (5.32)$$

□

Substituting (5.19) in (5.24), we obtain

$$\begin{aligned} &\frac{\partial^2 \mathbf{g}}{\partial \mathbf{x} \partial \mathbf{u}^T} \left(\frac{\partial \mathbf{x}}{\partial \mathbf{u}} \right) + \frac{\partial^2 \mathbf{g}}{\partial \mathbf{u} \partial \mathbf{u}^T} + \frac{\partial^2 \mathbf{g}}{\partial \mathbf{x}^2} \left(\frac{\partial \mathbf{x}}{\partial \mathbf{u}^T} \right) \left(\frac{\partial \mathbf{x}}{\partial \mathbf{u}^T} \right)^T + \frac{\partial^2 \mathbf{g}}{\partial \mathbf{u} \partial \mathbf{x}^T} \left(\frac{\partial \mathbf{x}}{\partial \mathbf{u}^T} \right) + \\ &\frac{\partial \mathbf{g}}{\partial \mathbf{x}^T} \left(\frac{\partial^2 \mathbf{x}}{\partial \mathbf{u} \partial \mathbf{u}^T} \right) + \frac{\partial^2 \mathbf{g}}{\partial \mathbf{x} \partial \mathbf{s}^T} \left[\left(\frac{\partial \mathbf{g}}{\partial \mathbf{s}^T} \right)^{-1} \left(- \left(\frac{\partial \mathbf{g}}{\partial \mathbf{x}^T} \right) \left(\frac{\partial \mathbf{x}}{\partial \mathbf{u}^T} \right) - \frac{\partial \mathbf{g}}{\partial \mathbf{u}^T} \right) \right] \left(\frac{\partial \mathbf{x}}{\partial \mathbf{u}} \right) + \\ &\frac{\partial^2 \mathbf{g}}{\partial \mathbf{u} \partial \mathbf{s}^T} \left[\left(\frac{\partial \mathbf{g}}{\partial \mathbf{s}^T} \right)^{-1} \left(- \left(\frac{\partial \mathbf{g}}{\partial \mathbf{x}^T} \right) \left(\frac{\partial \mathbf{x}}{\partial \mathbf{u}^T} \right) - \frac{\partial \mathbf{g}}{\partial \mathbf{u}^T} \right) \right] + \frac{\partial \mathbf{g}}{\partial \mathbf{s}^T} \frac{d}{dz} \left(\frac{\partial^2 \mathbf{x}}{\partial \mathbf{u} \partial \mathbf{u}^T} \right) = \mathbf{0}_{n \times P}. \end{aligned} \quad (5.33)$$

Theorem 5.6.2 *For systems modelled by quasilinear hyperbolic PDE, the inverse of the matrix $\frac{\partial \mathbf{g}}{\partial \mathbf{s}^T}$ exists.*

Proof: For systems of quasilinear hyperbolic PDE, proving that $\frac{\partial \mathbf{g}}{\partial \mathbf{s}^T}$ exists reduces to prove that \mathbf{B} has an inverse. By the definition of hyperbolic PDE, see Definition 2.10.1, there exists a set of distinct and real eigenvalue matrix, $\mathbf{\Lambda}(z, \mathbf{x}, \mathbf{u})$, and orthogonal eigenvectors, $\mathbf{T}(z, \mathbf{x}, \mathbf{u})$, such that

$$\mathbf{B}(z, \mathbf{x}, \mathbf{u}) = \mathbf{T}^{-1}(z, \mathbf{x}, \mathbf{u})\mathbf{\Lambda}(z, \mathbf{x}, \mathbf{u})\mathbf{T}(z, \mathbf{x}, \mathbf{u}) \quad (5.34)$$

$$\mathbf{B}^{-1}(z, \mathbf{x}, \mathbf{u}) = (\mathbf{T}(z, \mathbf{x}, \mathbf{u})^{-1}\mathbf{\Lambda}(z, \mathbf{x}, \mathbf{u})\mathbf{T}(z, \mathbf{x}, \mathbf{u}))^{-1} \quad (5.35)$$

$$= \mathbf{T}(z, \mathbf{x}, \mathbf{u})^{-1}\mathbf{\Lambda}^{-1}(z, \mathbf{x}, \mathbf{u})\mathbf{T}(z, \mathbf{x}, \mathbf{u}). \quad (5.36)$$

Since there must exist a distinct eigenvalue for each dependent variable and each dependent variable depends on all independent variables, then the set of eigenvalues must be different from zero. Therefore, $\mathbf{\Lambda}^{-1}(z, \mathbf{x}, \mathbf{u})$ exists and thus $\mathbf{B}^{-1}(z, \mathbf{x}, \mathbf{u})$ also exists. □

Equation (5.33) becomes a system of ordinary differential equations that can be solved simultaneously with the system given in (5.12) and (5.19) to yield the second-order derivatives of the steady-state locus with respect to the inputs (acceleration vectors):

$$\frac{\partial^2 \mathbf{x}}{\partial \mathbf{u} \partial \mathbf{u}^T} [z] = \frac{\partial^2 \Xi(\mathbf{u})}{\partial \mathbf{u} \partial \mathbf{u}^T} [z]. \quad (5.37)$$

In general, the solution of the system of equations (5.12), (5.19) and (5.33) is obtained numerically. The initial conditions for (5.33) depend on the type of boundary condition in (5.6), i.e. for Dirichlet boundary conditions, $\frac{\partial^2 \mathbf{x}}{\partial \mathbf{u} \partial \mathbf{u}^T} [0] = \mathbf{0}_{P \times (n \times P)}$.

From the solution of (5.33), we obtain the acceleration vectors for the input-output map:

$$\frac{\partial^2 \mathbf{y}}{\partial \mathbf{u} \partial \mathbf{u}^T} = \mathbf{c} \left\{ \frac{\partial^2 \mathbf{h}}{\partial \mathbf{x} \partial \mathbf{x}^T} \Big|_{\Xi(\mathbf{u}_0)[z]} \left(\frac{\partial \Xi(\mathbf{u})}{\partial \mathbf{u}} [z] \right)^T \frac{\partial \Xi(\mathbf{u})}{\partial \mathbf{u}^T} [z] + \frac{\partial \mathbf{h}}{\partial \mathbf{x}^T} \Big|_{\Xi(\mathbf{u}_0)[z]} \frac{\partial^2 \Xi(\mathbf{u})}{\partial \mathbf{u} \partial \mathbf{u}^T} [z] \right\} \quad (5.38)$$

The relative contribution of the acceleration vectors with respect to the velocity vectors can be used to assess the nonlinearity of the system. The larger the magnitude of the acceleration vectors are relative to the velocity vectors, the more

significant is the nonlinearity. The second order derivative information can be decomposed into tangential and normal constituents. The tangential component depends on the parametrization of the model and presents itself as unequally spaced curves of constant input-parameter values on the steady-state locus. The normal component depends on the form of the steady-state locus, and presents itself as the curvature of the steady-state locus relative to its surrounding space (Bates and Watts, 1988; Guay, 1996).

To separate the acceleration vectors into their tangential and normal components, we look for an orthogonal basis for the velocity and acceleration vectors (Bates and Watts, 1988). P basis vectors will span the tangent space, and P^N basis vectors span the space normal to the tangent space. Note that P^N is not necessarily equal to $(n - P)$. The orthogonal basis is defined by first taking the velocity and *nonredundant* acceleration vectors, and arranging them in an $n \times (P(P+3)/2)$ matrix, $[\mathbf{V}, \mathbf{W}]$, given by

$$[\mathbf{V}, \mathbf{W}] = [\dot{\mathbf{v}}_1 \dot{\mathbf{v}}_2 \dots \dot{\mathbf{v}}_P \ddot{\mathbf{v}}_{1,1} \ddot{\mathbf{v}}_{1,2} \ddot{\mathbf{v}}_{2,2} \dots \ddot{\mathbf{v}}_{1,P} \dots \ddot{\mathbf{v}}_{P,P}] \quad (5.39)$$

The **QR** decomposition of $[\mathbf{V}, \mathbf{W}]$ yields an orthonormal basis, $\mathbf{Q}_{n \times n}$, for the tangent space and the space normal to the tangent:

$$[\mathbf{V}, \mathbf{W}] = \mathbf{QR} = [\mathbf{Q}_{1,T} \mathbf{Q}_{1,N} \mathbf{Q}_2] \begin{bmatrix} \mathbf{R}_1 & \mathbf{A}_T \\ \mathbf{0} & \mathbf{A}_N \\ \mathbf{0} & \mathbf{0} \end{bmatrix} \quad (5.40)$$

$\mathbf{R}_1(P \times P)$ contains the projections of \mathbf{V} onto the first P columns of \mathbf{Q} which span the tangent space to the steady state locus ($\mathbf{Q}_{1,T}$), \mathbf{A}_T contains the projections of \mathbf{W} onto ($\mathbf{Q}_{1,T}$) and \mathbf{A}_N contains the projections of \mathbf{W} onto the P_N columns that follow the first P columns of \mathbf{Q} and span the normal space to the steady state locus ($\mathbf{Q}_{1,N}$).

To remove the scale-dependence of the curvature on the output variables, scaling can be performed to reflect the intended region of operation on the output space (Guay *et al.*, 1995)

$$\Delta \mathbf{y}^T \mathbf{S}_y^T \mathbf{S}_y \Delta \mathbf{y} = 1, \quad (5.41)$$

where \mathbf{S}_y is an invertible scaling matrix whose elements reflect the expected range of operation for the outputs and $\Delta \mathbf{y}$ is the deviation of the output variables from the

steady-state point of interest. Alternatively, one could specify an elliptical region in the input space. The equation for the ellipse in the input space is:

$$\Delta \mathbf{u}^T \mathbf{S}_{in}^T \mathbf{S}_{in} \Delta \mathbf{u} = 1. \quad (5.42)$$

This elliptical region is then mapped into the state space or output space, where it becomes non-elliptical due to nonlinearity.

The corresponding elliptical approximation in the output space of the region defined in the input space is

$$\Delta \mathbf{y}^T \mathbf{S}_{eq}^T \mathbf{S}_{eq} \Delta \mathbf{y} = 1, \quad (5.43)$$

where $\mathbf{S}_{eq} = \mathbf{S}_{in} \mathbf{V}^{-1}$. By using \mathbf{S} to represent the output \mathbf{S}_y , or the equivalent output scaling matrix, \mathbf{S}_{eq} , the velocity and acceleration arrays can be scaled using the \mathbf{S} matrix

$$\tilde{\mathbf{V}} = \mathbf{S} \mathbf{V} \quad (5.44)$$

$$\tilde{\mathbf{W}} = \mathbf{S} \mathbf{W}, \quad (5.45)$$

where the tilde indicates a scaled quantity. If scaled quantities are used, then the **QR** decomposition should be performed on the $[\tilde{\mathbf{V}}, \tilde{\mathbf{W}}]$.

A unit independent curvature measure can be defined in the basis defined by \mathbf{Q} (Bates and Watts, 1988; Guay *et al.*, 1995). The curvature of the steady-state locus or input-output map, is defined along a direction $\mathbf{u} = \mathbf{u}_0 + b\mathbf{e}$ as the ratio of the norm of the acceleration vector to the squared norm of the corresponding velocity vector

$$C_e = \frac{\|\mathbf{e}^T \mathbf{A}_r \mathbf{e}\|}{\|\mathbf{R}_1 \mathbf{e}\|^2}, \quad (5.46)$$

where \mathbf{A}_r is a n -dimensional array of $P \times P$ matrices obtained from the $n \times P(P+1)/2$ matrix $\mathbf{A} = [\mathbf{A}_T, \mathbf{A}_N]^T$. The array \mathbf{A}_r has the form

$$\mathbf{A}_r = [\mathbf{a}_1, \mathbf{a}_2, \dots, \mathbf{a}_n], \quad (5.47)$$

where each \mathbf{a} is a complete $P \times P$ second derivative matrix or Hessian of the i^{th} coordinate on the rotated state space, see Figure 5.2 (Benda, 2000).

Pre-multiplication and post-multiplication by \mathbf{e} in (5.46) is performed on each $P \times P$ submatrix (face) of \mathbf{A}_r . The tangential and normal contributions to the

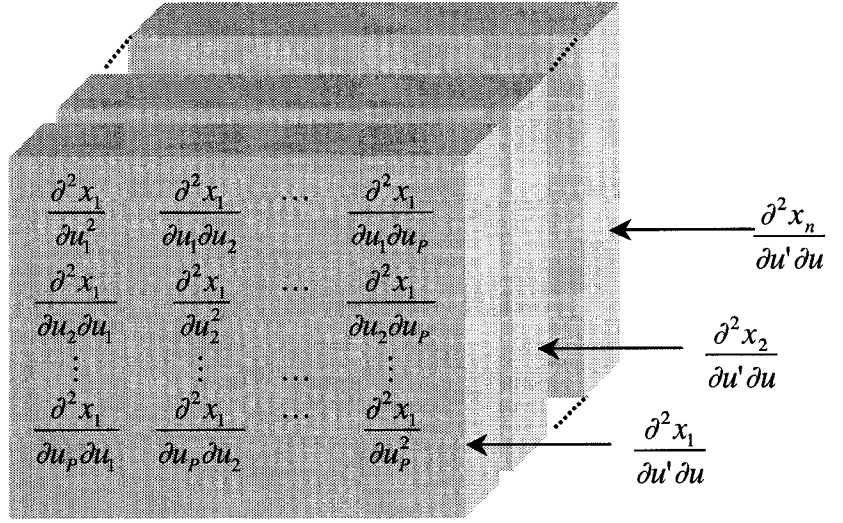


Figure 5.2: Representation of the structure of \mathbf{A}_r . Each face represents the Hessian of the i^{th} coordinate of the rotated space.

overall curvature can be separated by evaluating the curvature for the first P and the next P^N faces of \mathbf{A}_r , respectively.

Remark 5.6.4 *An important case that is not considered in (Guay et al., 1995) is the case where the $\dot{\mathbf{v}} = \mathbf{0}_{n \times P}$. In such cases, there is no need to scale the norm of the acceleration vector in (5.46).*

To simplify the calculation of the curvature measure (5.46), we transform \mathbf{u} to orthogonal inputs given by

$$\Phi = \mathbf{R}_1(\mathbf{u} - \mathbf{u}_0) = \mathbf{R}_1\mathbf{e}. \quad (5.48)$$

such that the denominator of $\|\mathbf{R}_1\mathbf{e}\|^2 = 1$ for any θ (an arbitrary direction in the Φ -space) of unit length (Bates and Watts, 1988).

The curvature becomes an array

$$\mathbf{C}_r = (\mathbf{R}_1^{-1})\mathbf{A}_r(\mathbf{R}_1^{-1}), \quad (5.49)$$

which consists of $P \times P \times P$ tangential curvature array, given by the first P faces of \mathbf{C}_r and a $P^N (\leq n - P) \times P \times P$ normal curvature array given by the last $P^N (\leq n - P)$

faces of \mathbf{C} . When the scaling \mathbf{S} is used, \mathbf{C}_r is the relative curvature array for the region defined by \mathbf{S} .

5.6.1 Overall Measure of Curvature

In Section 5.6, it was shown how model nonlinearity can be qualified in terms of its effect on the geometry of the steady-state locus or steady-state input-output map, which can be quantified by each term of the relative curvature array.

Although the decomposition of the second order effects can be used to characterize many aspects of nonlinear behaviour of a process, it is desirable to have a unique measure of process nonlinearity. An overall measure of nonlinearity has been developed by Bates and Watts (1988) and used in (Guay *et al.*, 1995) to obtain a measure of curvature averaged over all possible input directions. The overall measure is referred as the root mean square curvature measure (RMS), c , is given by:

$$c^2 = \frac{1}{P(P+2)} \sum_{i=1}^n \left[2 \sum_{j=1}^P \sum_{k=1}^P (c_{ijk})^2 + \left(\sum_{j=1}^P c_{ijj} \right)^2 \right]$$

where c_{ijk} is the i^{th} face, j^{th} row, k^{th} element of the relative curvature array C_r . A convenient scale for the root mean square curvature c has been proposed in Bates and Watts (1988). The RMS measure quantifies the degree of deviation between a second-order approximation of a properly scaled model and a linear approximation, where the nonlinear steady-state locus is locally approximated by a sphere of radius $1/c$. The magnitude of the deviation from the tangent plane approximation can be measured at the boundary of the region of interest to be:

$$|deviation| = \left(\frac{1}{c} - \left(\frac{1}{c^2} - 1 \right)^{0.5} \right) \times 100\% \quad (5.50)$$

An illustration of the meaning of the scaling measure is given in Figure 5.3 As a benchmark value, Bates and Watts (1988) and Guay *et al.* (1995) suggest that an RMS curvature of 0.3 or greater indicates considerable nonlinearity. This RMS curvature value of 0.3 corresponds to a 15% deviation between the second order approximation and the linear approximation, measured at a unit distance in the z-coordinates from the point of linearization. This measure of deviation can be conveniently compared to the size of the region of interest, which has been scaled to unity.

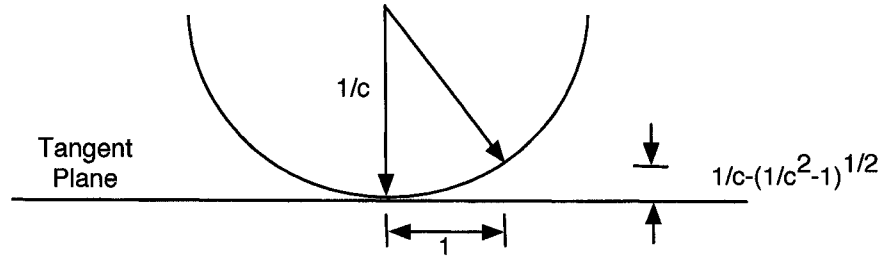


Figure 5.3: Scale fused or measuring the extent of nonlinearity. The steady-locus is approximated by a surface of constant curvature $1/c$ where c is the RMS curvature.

5.7 Case Study: Plug-flow Reactor

In this section, we study the nonlinearity of a non-isothermal plug-flow reactor with a heat exchanger. The control of such reactor system has been studied in a large number of publications (Smets *et al.*, 2002; Christofides, 2000; Hudon *et al.*, 2005; Aksikas *et al.*, 2007c). A first order Arrhenius law rate of reaction is considered. The mathematical model used for the reactor system consists of a set of quasi-linear first-order hyperbolic PDEs of the following form (Smets *et al.*, 2002):

$$\frac{\partial x_1}{\partial t} + v \frac{\partial x_1}{\partial z} = -k \exp\left(\frac{-\alpha_1}{x_2}\right) x_1 \quad (5.51)$$

$$\frac{\partial x_2}{\partial t} + v \frac{\partial x_2}{\partial z} = \alpha_2 k \exp\left(\frac{-\alpha_1}{x_2}\right) x_1 - \alpha_3(x_2 - u) \quad (5.52)$$

$$\text{Initial Conditions : } \begin{cases} x_1(0, z) = x_{1,0}(z) \\ x_2(0, z) = x_{2,0}(z) \end{cases} \quad (5.53)$$

$$\text{Boundary Conditions : } \begin{cases} x_1(t, 0) = x_{1,in} \\ x_2(t, 0) = x_{2,in} \end{cases} \quad (5.54)$$

where u is the jacket temperature (input variable) and x_1 and x_2 are the state variables which correspond to the concentration and temperature in the reactor, respectively. Model parameters are given in Table 5.1.

We begin this case study by considering the case where the input is spatially uniformly distributed, *i.e.* $u(t, z) = \cdot u(t)$. In order to get a first qualitative impression

Table 5.1: Model Parameters for the Tubular Reactor Model

Parameter	Value
v	$0.1 \text{ m} \cdot \text{s}^{-1}$
k	$1\text{E}6 \text{ s}^{-1}$
α_1	$5,665 \text{ K}$
α_2	$4,250 \text{ K} \cdot \text{l} \cdot \text{mol}^{-1}$
α_3	0.2 s^{-1}
$x_{1,in}$	$0.02 \text{ mol} \cdot \text{l}^{-1}$
$x_{2,in}$	340 K
L	1 m

of the nonlinearity of the system at steady-state, the steady-state locus is plotted in Figure 5.4 and 5.5 for equally spaced input values: $u_0 \in \{260, 280, \dots, 440\}$. From the

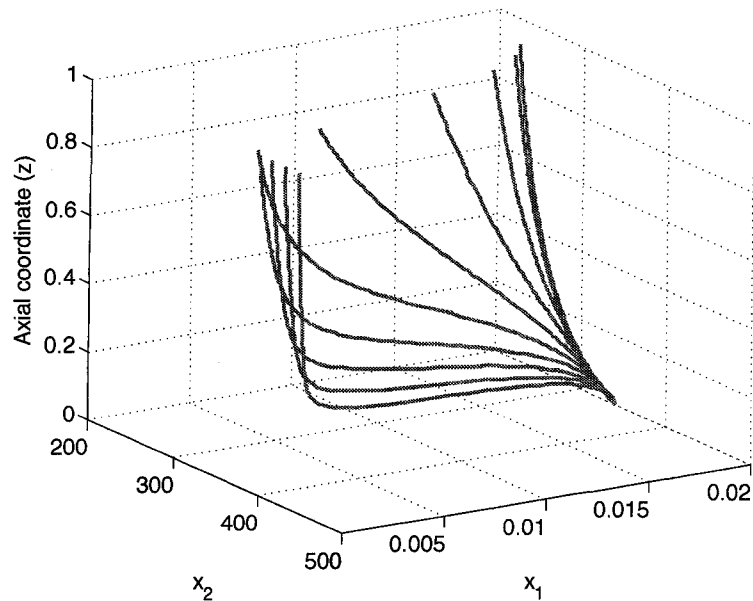


Figure 5.4: 3-dimensional plot of the steady-state locus for equally spaced input $u_0 \in \{260, 280, \dots, 440\}$.

steady-state locus, it can be observed that the states are unequally spaced when the input values are equally spaced. Such behavior will be quantified by the tangential curvature. It can also be observed that there is some curvature in the steady-state locus and that the curvature of the steady-state locus relative to its surrounding space changes with the operating conditions (\mathbf{u}_0).

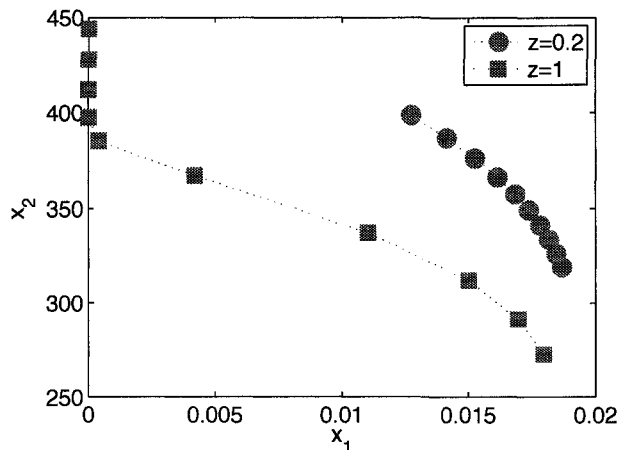


Figure 5.5: 2-dimensional steady-state locus for equally spaced input $u_0 \in \{260, 280, \dots, 440\}$.

To quantify the nonlinearity of the system, we choose as output variables the values of the states at $z = 1$, i.e. $\mathbf{y} = \mathbf{x}(z = 1)$. The reason for choosing such an output is that typical control objectives in plug-flow reactors is the control of the outlet temperature and concentration. The velocity and acceleration vectors are computed using equations (5.19) and (5.33), respectively, and the projected velocities and acceleration matrices are scaled using

$$\mathbf{S} = \begin{bmatrix} 500 & 0 \\ 0 & 0.1 \end{bmatrix} \quad (5.55)$$

Both the tangential and normal components of the curvature or nonlinearity measure are shown in Figures 5.6 and 5.7, respectively. It can be observed that the reactor steady-state nonlinearity is significant around $u_0 = 360 \text{ K}$. Such behavior is the result of the relative contribution of the linear and nonlinear terms in the reactor model. At low jacket operating temperatures, the temperature of the fluid in the reactor (x_2) is low and the effect of the nonlinear term is relatively small. At high jacket temperatures, the nonlinear term $\exp\left(\frac{-\alpha_1}{x_2}\right)$ is significant but its effect is not important at $z = 1$ because $x_1 \rightarrow 0$. Therefore, at high and low values of the jacket temperature, the reactor steady-state behavior is almost linear.

To study how the nonlinearity changes for outputs located at different positions along the reactor, Figures 5.8 and 5.9 show the distribution of the tangential and

normal curvature, respectively, at a given input value for different value of the independent variable z . As expected, it can be observed that at low operating jacket temperatures the nonlinearity is small due the small contribution of the nonlinearity term, i.e. $\exp\left(\frac{-\alpha_1}{x_2}\right)$ is small when x_2 is small. At high operating temperatures, the nonlinearity is significant near the inlet section of the reactor.

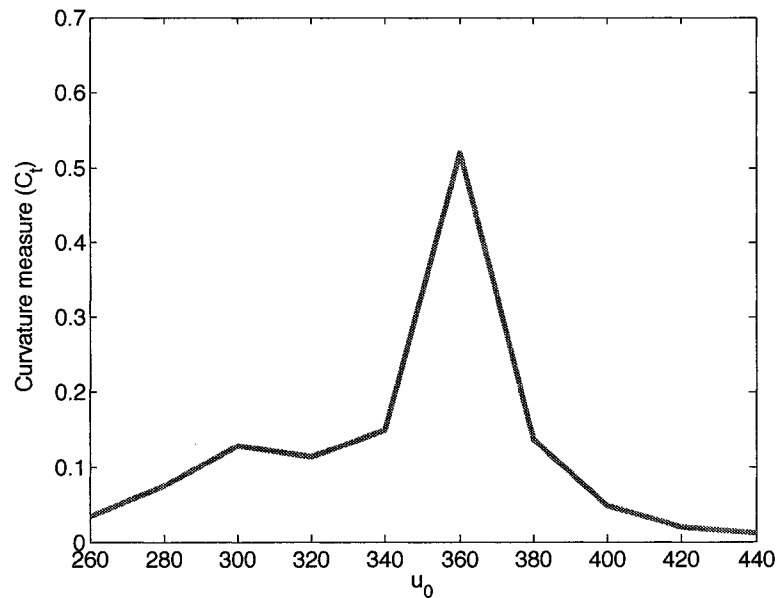


Figure 5.6: Tangential curvature for $y = [x_1(z = 1), x_2(z = 1)]^T$.

To study the effect of process nonlinearity on closed-loop operation, an input-output linearizing controller was designed following the technique proposed in Christofides (2000). The formulation of the controller is given in Appendix C. Two controllers were formulated; one using the full nonlinear hyperbolic PDE model and another one using a local linearization of the PDE model. Both controllers were designed to drive the output, $y = x_2(z = 1)$ to a specified set-point value and keep it at that value. The closed-loop dynamic behavior of the input /output system is chosen to be the same for both controllers, i.e. same eigenvalues. Figure 5.10 shows a comparison of the closed-loop performance at three different operating points. As expected, the closed-loop trajectory of the output of the system with the linear controller resembles that of the nonlinear one at high and low operating values

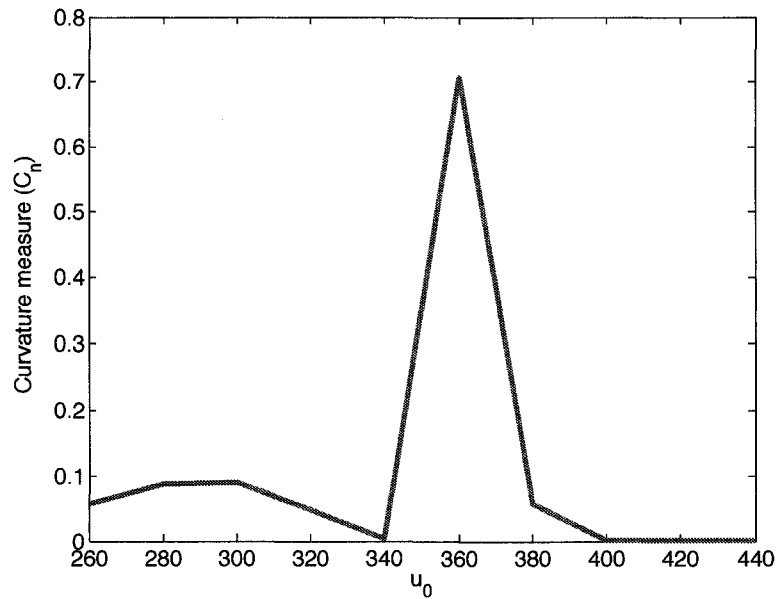


Figure 5.7: Normal curvature for $y = [x_1(z = 1), x_2(z = 1)]^T$.

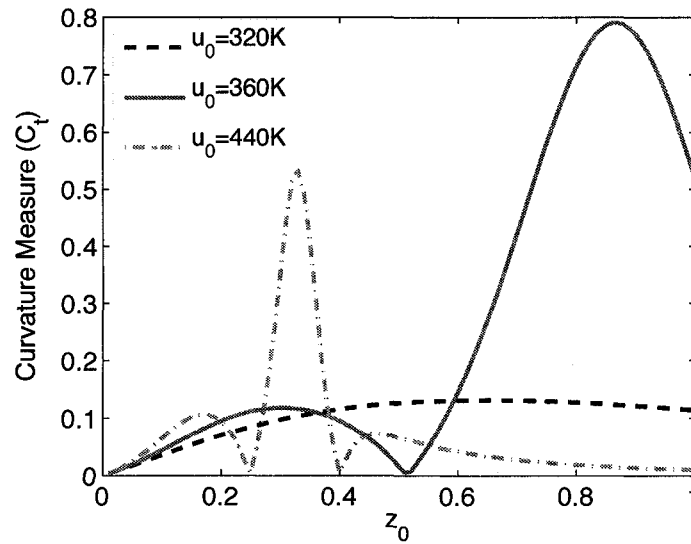


Figure 5.8: Distribution of the tangential curvature for $y = [x_1(z_0), x_2(z_0)]^T$ at three different operating conditions.

(u_0); however, at intermediate values, $u_0 = 360\text{K}$, the linear controller does not give good control performance. Nevertheless, a different linear controller may give better performance. The impact of nonlinearity on closed-loop operation is studied in more detail in the next chapter.

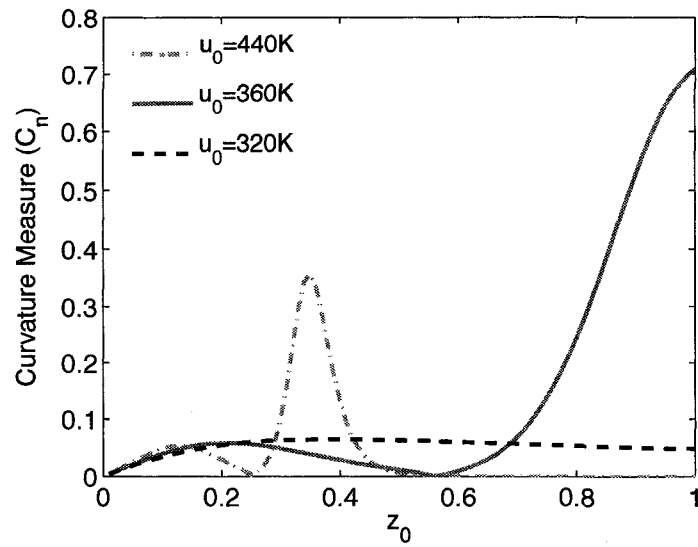


Figure 5.9: Distribution of the normal curvature for $y = [x_1(z_0), x_2(z_0)]^T$ at three different operating conditions.

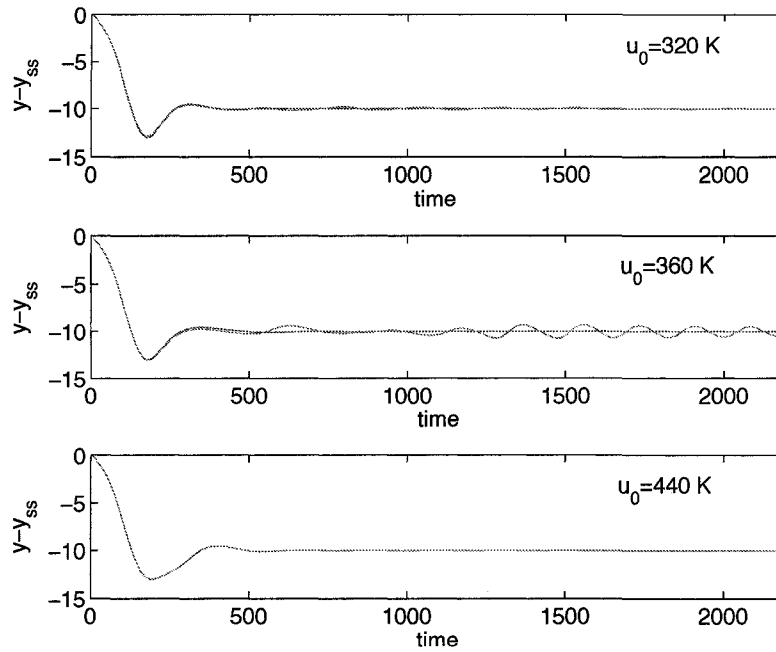


Figure 5.10: Closed-loop trajectories of $y = x_2(z = 1)$ for set-point changes about three different operating points.

5.8 Case Study: Catalytic Flow Reversal Reactor

In this section, the open-loop nonlinearity of a catalytic flow reversal reactor is studied. The mathematical model of the catalytic reactor is given in equations (2.6) and (2.7).

In order to get a first qualitative impression of the nonlinearity of the system at steady-state, the steady-state locus is plotted for equally spaced input values: $\alpha_0 \in \{0.8, 0.82, \dots, 1\}$ and, for easy visualization, for only two selected points along the axis of the reactor, see Figures 5.11 and 5.12. The two points represent sections of the reactor where the mole fraction at stationary-state changes significantly ($z = 0.65L$), and where the change is minimal or null due to low temperatures or complete conversion ($z = 0.4L$).

The operating conditions used to obtain the steady-state locus of the CFRR reactor unit are the following:

$$Y_{f0} = 5E^{-3}; T_{f0} = 298 \text{ K}; v_{s,in} = 1 \text{ m/s}$$

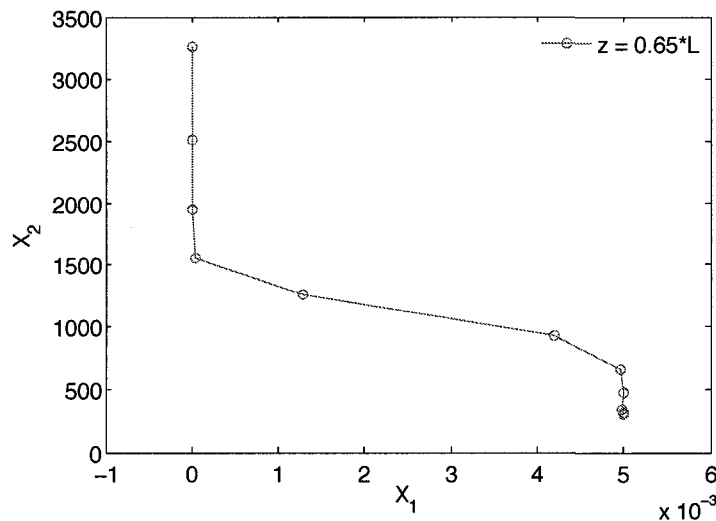


Figure 5.11: Steady-state locus for $z = 0.65L$ and for equally spaced input values: $\alpha_0 \in \{0.8, 0.82, \dots, 1\}$. x_1 represents the mole fraction Y and x_2 represents the reactor temperature T .

From the steady-state locus, it can be observed that for equally spaced input values, the value of the states at stationary-state are not equally spaced. Such behavior can

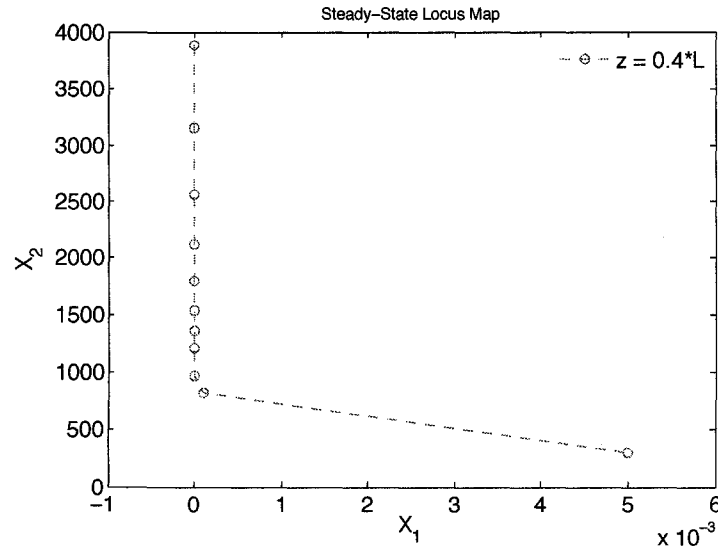


Figure 5.12: Steady-state locus for $z = 0.4L$ and for equally spaced input values: $\alpha_0 \in \{0.8, 0.82, \dots, 1\}$. x_1 represents the mole fraction Y and x_2 represents the reactor temperature T .

be quantified by the tangential curvature. It can also be observed that there is some curvature in the steady-state locus and that the curvature of the steady-state locus relative to its surrounding space changes with the operating conditions (α_0).

To quantify the nonlinearity of the system, the states at equally spaced spatial points are chosen. The velocity and acceleration vectors are computed by numerical simulation of the stationary-state under different operating conditions and subsequent numerical approximation of the first and second order derivatives. The velocities and acceleration matrices are scaled using

$$\mathbf{S} = \begin{bmatrix} 500 & 0 \\ 0 & 0.01 \end{bmatrix} \quad (5.56)$$

Both the tangential and normal components of the curvature or nonlinearity measure are shown in Figures 5.13 and 5.14, respectively. It can be observed that the reactor steady-state nonlinearity is significant at low values of the input variable. It is noted that as the input values are lowered, less reaction occurs and the reactor temperature decreases.

To study how the nonlinearity changes for outputs located at different positions along the reactor, we plotted in Figures 5.15 the distribution of the tangential and normal curvature at $u_0 = 0.9$ for outputs located at different value of independent

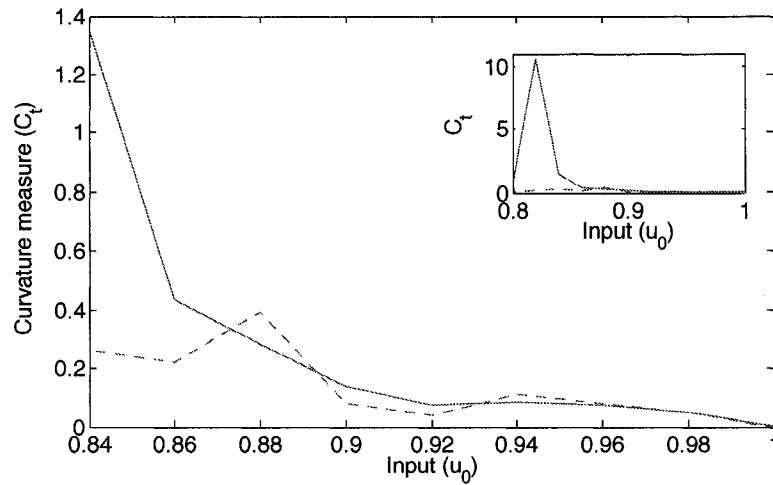


Figure 5.13: Tangential curvature for $y = [x_1(z = 0.4L), x_2(z = 0.4L)]^T$ (dashed-line) and $y = [x_1(z = 0.65L), x_2(z = 0.65L)]^T$ (solid-line).

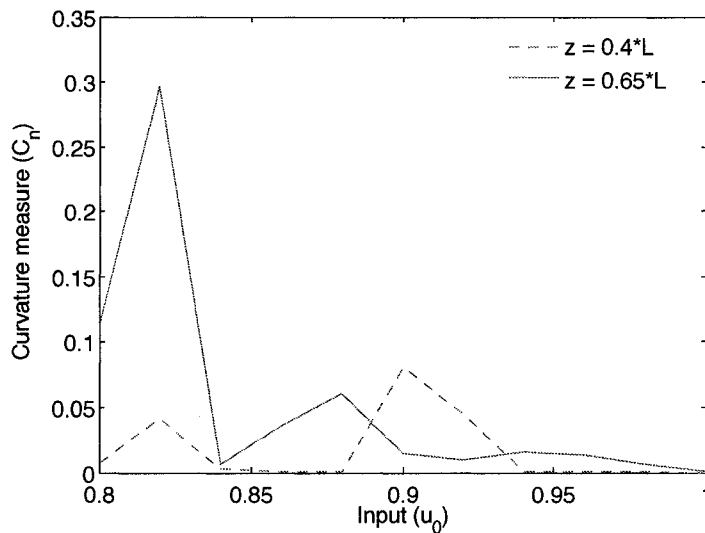


Figure 5.14: Normal curvature for $y = [x_1(z = 0.4L), x_2(z = 0.4L)]^T$ (dashed-line) and $y = [x_1(z = 0.65L), x_2(z = 0.65L)]^T$ (solid-line).

variable z within the catalytic section of the reactor. Near the section of the reactor where most of the reaction occurs ($z \approx 0.6$), it can be observed that the normal curvature becomes more significant. Everywhere else in the catalytic section, the normal curvature is negligible and the nonlinearity is mainly due to tangential curvature which is caused by the nonuniform spacing of the reactor temperature for uniform spacing of the input variable.

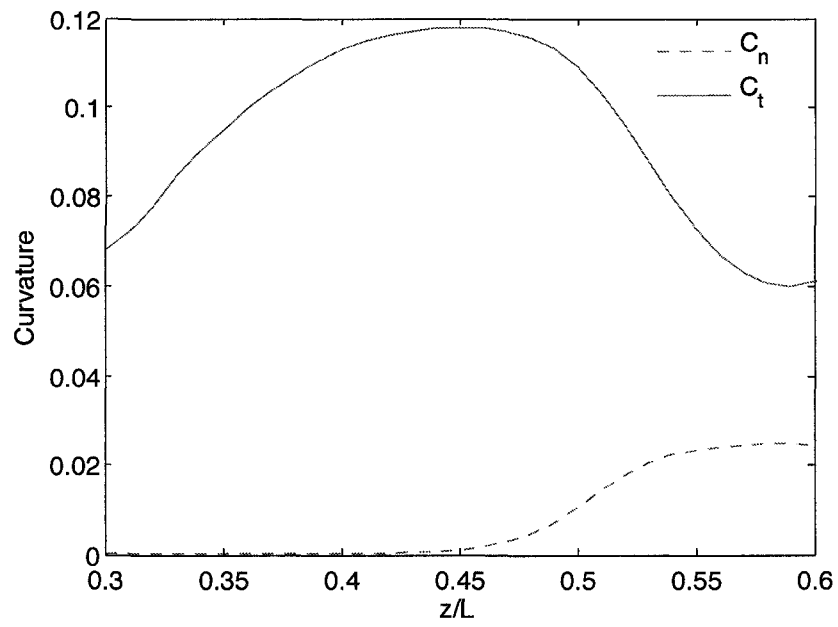


Figure 5.15: Spatial distribution of the tangential and normal curvature for $y = [x_1(z_0), x_2(z_0)]^T$ at $u_0 = 0.9$.

5.9 Summary

In this chapter, we presented a measure of nonlinearity for processes modeled by quasilinear hyperbolic partial differential equations. The measure of nonlinearity proposed here is based on the geometric properties of the steady-state locus of the model equations. The measure is an extension to distributed parameter systems of the open-loop measure of nonlinearity proposed by (Guay *et al.*, 1995) for lumped parameter models.

This measure of nonlinearity can be used to characterize many aspects of nonlinear behavior of a hyperbolic PDE system. The measure quantifies the gain nonlinearity and can be used to locate regions of the output space where the nonlinearity is significant. This aspects of nonlinearity can be used as a preliminary information for the design of a controller for the system under study.

Using a tubular reactor with heat exchanger as case study, the application of the measure of nonlinearity was illustrated. Operating regions were mapped to the nonlinearity measure so that regions with a larger degree of nonlinearity can be identified for control uses. Comparison of closed-loop control performance around the different operating regions using linear and nonlinear control was shown to highlight the application of the nonlinearity measure.

The application of the nonlinearity measure was also shown on a catalytic flow reversal reactor. Due to the lack of a closed-form mathematical model of the process for direct computation of the stationary-state of the reactor, computer simulations were used to find the stationary state and use it to numerically approximate the first and second order derivatives. Operating regions that covered a significant range of input values were mapped to the nonlinearity measure proposed for quantifying gain nonlinearity. It was observed that normal curvature due to the combination of mole fraction and temperature in the reactor model was minimal. The main source of nonlinearity, i.e. nonuniform spacing of the reactor temperature, was successfully quantified by the tangential curvature.

6

Control Relevant Nonlinearity Assessment for Hyperbolic PDE Models

For the catalytic flow reversal reactor studied in this thesis, control techniques that employ linear models, both online and offline, were used to compute control actions. For mildly nonlinear problems, one can attempt to use linear models and linear controller design methods; however, this approach requires a rigorous justification in order to guarantee the proper operation of a linear controller in presence of the nonlinear system behavior. Due to the diverse and complex behavior of nonlinear systems, tools for nonlinear control design exhibit a much lower level of generality than their linear counterpart. In this chapter, we focus on developing tools to assess whether or not linear control of systems modelled by quasi-linear hyperbolic partial differential equations can provide satisfactory level of control performance, or if nonlinear control is required. Specifically, we focus on quantifying the sensitivity of a control performance index to linear control. The sensitivity quantification is studied for a tubular chemical reactor and a catalytic flow reversal reactor.

6.1 Introduction

In general, most processes as well as their associated mathematical models are nonlinear. Process nonlinearity is one of the most relevant factors for process analysis and controller design. Very often the formulation of controllers for nonlinear processes is addressed by first linearizing the nonlinear plant model equations around a steady-state operating point or a nominal trajectory. Then a controller is designed using the well-developed techniques for linear systems.

For systems where the range of linearity is small (highly nonlinear processes) or for processes that are operated over a large range of operating conditions, a controller must be designed in such a way that it is aware of the process nonlinearity. The controller must compensate the effects of the nonlinearity. Nonlinear control techniques are more complex than their linear counterpart and are mathematically more involved. Quantification of the extent and severity of a process inherent nonlinearity is crucial in order to decide whether linear system analysis and controller synthesis methods are adequate (Schweickhardt and Allgower, 2006).

Open-loop nonlinearity measures were presented in Chapter 5. Different methods proposed in the literature to quantify the degree of open-loop nonlinearity were shown. The main assumption related to the use of open-loop nonlinearity measures in controller design is that highly nonlinear systems require nonlinear controllers. Although this may be true in a significant number of applications, proximity of a nonlinear process to a linear one is neither necessary nor sufficient for good closed-loop linear control performance (Nikolaou and Misra, 2003).

As discussed in Chapter 5, open-loop nonlinearity measures can be used to locate operating conditions where nonlinearity might be significant; but they do not directly address the question of whether linear controller design is suitable despite the nonlinear process behavior. In an effort to provide a more precise description of nonlinearity in control systems, a number of authors proposed *control-relevant* nonlinearity measures (Guay, 2006).

In the area of control-relevant nonlinearity, the intended range of operation and the control performance objective are used to specifically address the question of

whether or not nonlinear control is needed. The main objective of a control-relevant nonlinearity assessment is to avoid unnecessary nonlinear control design.

In Guay (1996) the idea of control-law nonlinearity was introduced. Control-law nonlinearity was defined as the degree of nonlinear compensation in a controller, a system property distinct from open-loop nonlinearity. As the inverse of the process steady-state map can be used to achieve perfect set-point tracking, Guay (1996) proposed to analyze the inverse of the steady-state map in order to obtain a measure of control law nonlinearity.

To assess the effect of nonlinearity on closed-loop systems, the "Optimal Control Structure" was introduced to examine the nonlinearity of suitable controllers for a given nonlinear plant (Stack and Doyle III, 1995; Stack and Doyle III, 1997*b*; Stack and Doyle III, 1997*a*). A control operator, called the optimal control structure, was derived using Lagrangian optimization. The nonlinearity of the optimal control structure is defined as the degree of nonlinear compensation in the controller, and is determined by a performance objective, the region of operation and the nature of the open-loop system. The degree of nonlinearity of the control operator provides an indication of whether or not a nonlinear controller may be required. This approach is, as described in Guay (2006), counterproductive since one needs to design a nonlinear controller structure to find out if such structure is indeed needed. The main advantage of the approach is that it provides a very accurate description of the nonlinear control structure. Furthermore, it is not restricted to open-loop stable nonlinear systems.

In Schweickhardt and Allgower (2004), the optimal control structure concept is combined with the nonlinearity measure proposed in (Allgower, 1995*b*). The combination addresses the question of whether nonlinear control is needed. From a practical perspective, it is unclear whether the measurement of control law nonlinearity precludes the successful application of a linear controller.

Hernjak and Doyle III (2003) used the open-loop nonlinearity measure proposed in (Allgower, 1995*a*; Helbig *et al.*, 2000) to find correlations between nonlinearity and the achievable performance of a variety of control structures for two benchmark processes: a quadruple tank process and a bioreactor system.

In Eker and Nikolaou (2002), the internal model control framework (IMC) of Garcia

and Morari (1982) was used to place bounds on an appropriately defined closed-loop nonlinearity measure. Two measures were proposed, the first measure was based on the difference (in terms of weighted incremental norm over set) between a linear control system with linear controller and linear model and a nonlinear control system with linear controller and nonlinear plant. The second measure was based on the difference between a linearly controlled nonlinear plant and a nonlinearly controlled plant.

A different approach to assess control-relevant nonlinearity was taken by Guay and coworkers (Guay and Forbes, 2004; Guay *et al.*, 2005; Guay, 2006) who developed a performance sensitivity measure to assess the effect of nonlinearity on linear quadratic regulator control performance. The measure in (Guay *et al.*, 2005) and (Guay, 2006) is based on quantification of initial conditions on the performance of optimal closed-loop systems. The main principle of the approach is that the nominal performance is invariant to the choice of initial conditions, if the underlying control system is nearly linear. Thus, the sensitivity of the nominal performance to changes in initial conditions provides an effective means of investigating the nonlinearity effects in control systems.

6.2 Contributions

All control-relevant nonlinearity measures available in the literature have been formulated and tested on lumped parameter models. There is no specific development nor application of a control-relevant nonlinearity assessment for distributed parameter systems to aid in the formulation of a suitable controller.

In this chapter, we focus on systems modeled by hyperbolic partial differential equations, and we address the problem of control-relevant nonlinearity. To address the problem, the approach studied by Guay and coworkers (Guay and Forbes, 2004; Guay *et al.*, 2005; Guay, 2006) was extended. The approach is motivated by the general approach to the design of control systems, where one seeks a local linear approximation of the process and designs a linear controller to locally achieve control performance objectives. The degree to which these objectives are realizable depend

on the underlying structure of the process. Therefore, it seems natural to look into a method that allows quantification of the control performance lost due to linear control based on a process model obtained from, for example, a Jacobian linearization.

To show the applicability of the proposed measure developed in this chapter, a plug-flow reactor and a catalytic flow reversal reactor are used. The conclusions reached in this chapter from a closed nonlinearity assessment are compared to those obtained from the open-loop nonlinearity assessment .

6.3 Control Relevant Nonlinearity Assessment of Hyperbolic PDE Models

A common approach to the design of control systems consists of the development of linear models of the process (*i.e.* by Taylor Series expansion) and the design of a suitable controller to regulate its local behavior. Nevertheless, nonlinear control techniques that are based on the original nonlinear model, such as nonlinear model predictive control, Lyapunov-based design and geometrical control, have been shown to provide improved control performance (Guay, 2006); however, their implementation is sometimes impeded by a considerable degree of mathematical sophistication or computational requirements.

Guay and Forbes (2004) proposed the idea of a sensitivity measure to assess the performance degradation in a closed-loop system with a controller designed using a local linear model. The idea is to develop an index that measures the effect of process nonlinearity on linear controller performance. Then, such index would indicate whether sufficient benefit is available to warrant investment in a nonlinear controller (Guay *et al.*, 2005). This approach to assessing the effect of process nonlinearity has the advantage over other methods proposed in the literature, that it does not require the solution of an optimization problem, as in (Schweickhardt and Allgower, 2004), nor the computation of a nonlinear optimal structure, as in (Stack and Doyle III, 1997*b*), or intensive computational effort as in (Eker and Nikolaou, 2002).

The goal of this chapter is to formulate a measure of nonlinearity for processes

modeled by quasi-linear hyperbolic partial differential equations. The measure is used to quantify the control performance degradation when linear control is used for nonlinear hyperbolic distributed parameter systems.

6.4 Performance Sensitivity Measure

In this chapter, we focus on systems modelled by quasi-linear first order hyperbolic partial differential equations of the form

$$\mathbf{A} \frac{\partial \mathbf{x}}{\partial t} + \mathbf{B}(z, \mathbf{x}, \mathbf{u}) \frac{\partial \mathbf{x}}{\partial z} = \mathbf{f}(z, \mathbf{x}, \mathbf{u}) \quad (6.1)$$

with initial (*I.C.*) and boundary (*B.C.*) conditions

$$I.C.: \mathbf{x}(0, z) = \mathbf{x}_0(z)$$

$$B.C.: \mathbf{x}(t, 0) = \mathbf{x}_{in}$$

where t and z are the independent variables, $\mathbf{x} = [x_1(t, z), x_2(t, z), \dots, x_n(t, z)]^T$ is the state function vector and $\mathbf{u} = [u_1(t, z), u_2(t, z), \dots, u_P(t, z)]^T$ is an input function vector. Without loss of generality, it is considered in equation (6.1) that $\mathbf{A} = \mathbf{I}$, and it is assumed that the equilibrium profile of system of equations (6.1) is given by $\mathbf{x}_{eq} = \mathbf{0}_{n \times 1}$. The inputs and outputs variables for the system in (6.1) are defined in the the same way as in Section 5.6.

We re-write the system (6.1) in the following form

$$\frac{\partial \mathbf{x}}{\partial t} = \mathbf{g}(z, \mathbf{x}, \mathbf{s}, \mathbf{u}) + \mathbf{f}(z, \mathbf{x}, \mathbf{u}), \quad (6.2)$$

where $\mathbf{s} = \frac{\partial \mathbf{x}}{\partial z}$. The jacobian linearization of the system (6.2) about the equilibrium spatial profiles is given by the following linear system of equations

$$\begin{aligned} \frac{\partial \mathbf{x}}{\partial t} &= \mathbf{A}_1(z) \frac{\partial \mathbf{x}}{\partial z} + \mathbf{A}_0(z) \mathbf{x} + \mathbf{B}(z) \mathbf{u} \\ \left\{ \begin{array}{l} I.C. : \mathbf{x}(t, 0) = \mathbf{x}_{in} \\ B.C. : \mathbf{x}(0, z) = \mathbf{x}_0(z) \end{array} \right. \\ \mathbf{y}(t) &= \mathbf{C} \{ \mathbf{C}(z) \mathbf{x}(t, z) \}, \end{aligned} \quad (6.3)$$

where,

$$\begin{aligned}\mathbf{A}_1(z) &= \frac{\partial \mathbf{g}}{\partial \mathbf{s}^T} \Big|_{\mathbf{x}=0, \frac{\partial \mathbf{x}}{\partial z}=0, \mathbf{u}=0}, \\ \mathbf{A}_0(z) &= \left[\frac{\partial \mathbf{g}}{\partial \mathbf{x}^T} + \frac{\partial \mathbf{f}}{\partial \mathbf{x}^T} \right] \Big|_{\mathbf{x}=0, \frac{\partial \mathbf{x}}{\partial z}=0, \mathbf{u}=0}, \\ \mathbf{B}(z) &= \left[\frac{\partial \mathbf{g}}{\partial \mathbf{u}^T} + \frac{\partial \mathbf{f}}{\partial \mathbf{u}^T} \right] \Big|_{\mathbf{x}=0, \frac{\partial \mathbf{x}}{\partial z}=0, \mathbf{u}=0}, \\ \mathbf{C}(z) &= \frac{\partial \mathbf{h}}{\partial \mathbf{x}^T} \Big|_{\mathbf{x}=0, \frac{\partial \mathbf{x}}{\partial z}=0, \mathbf{u}=0}\end{aligned}$$

and \mathbf{C} is defined in equation (5.11).

For the linear system in equation (6.3), a general linear feedback controller is given by

$$u_i(t, z) = \mathbf{b}^T(z) \psi(\mathbf{K}_0(z) + \mathbf{K}(z)\mathbf{x}(t, z)) \quad i = 1, \dots, l \quad (6.4)$$

where

$$\mathbf{K}(z) = \mathbf{K}_1(z) + \mathbf{K}_2(z) \frac{\partial}{\partial z}, \quad (6.5)$$

and

$$\mathbf{b}(z) = [(H(z - z_1) - H(z - z_2))b_1(z), \dots, (H(z - z_j) - H(z - z_{m+1}))b_m(z)]^T \quad (6.6)$$

$$\psi = [(H(z - z_1) - H(z - z_2))\psi_1 \cdots (H(z - z_j) - H(z - z_{m+1}))\psi_P] \quad (6.7)$$

$$\psi_j(\cdot) = \int_{z_j}^{z_{j+1}} (\cdot) dz \quad j = 1, 2, \dots, P \quad (6.8)$$

The controller gains, $\mathbf{K}_0(1 \times 1)$, $\mathbf{K}_1(1 \times n)$, $\mathbf{K}_2(1 \times n)$, are computed according to the linear control technique selected. To quantify the sensitivity of the closed-loop control performance to process nonlinearity, the following performance index J is chosen:

$$\begin{aligned}J &= \int_0^\infty \mathbf{y}(t)^T \mathbf{Q} \mathbf{y}(t) dt \\ &= \int_0^\infty \sum_{i=1}^m \sum_{j=1}^m \mathbf{C}_i x(t, z) Q_{i,j} \mathbf{C}_j x(t, z) dt.\end{aligned} \quad (6.9)$$

The matrix \mathbf{Q} is used to weight the importance of specific outputs in the overall control performance of the distributed parameter system. The performance index J is commonly used in practice to evaluate closed-loop performance of a given controller.

As in Guay and Forbes (2004), the sensitivity of the control performance index to changes in the initial conditions is evaluated. The idea is that the nominal performance will be invariant to the choice of initial conditions if the underlying control system is nearly linear. The sensitivity of the performance index J to changes in the inlet conditions can be analyzed for any linear controller that gives stable closed-loop operation of the nonlinear PDE system around the nominal operation.

To assess the effect of initial conditions on the performance of the closed-loop system, equation (6.9) is differentiated with respect to $\mathbf{x}_0(z) = [x_{01}(z), x_{02}(z), \dots, x_{0n}(z)]^T$ in a neighborhood of the the nominal operation:

$$\frac{\partial J}{\partial x_{0l}} = \int_0^\infty \sum_{i=1}^m \sum_{j=1}^m \left(\frac{\partial y_i}{\partial x_{0l}} Q_{i,j} y_j + y_i Q_{i,j} \frac{\partial y_j}{\partial x_{0l}} \right) dt = 0 \quad l = 1, \dots, n \quad (6.10)$$

$$\begin{aligned} \frac{\partial^2 J}{\partial x_{0l} \partial x_{0m}} &= \int_0^\infty 2 \sum_{i=1}^m \sum_{j=1}^m \left(\frac{\partial^2 y_i}{\partial x_{0l} \partial x_{0m}} Q_{i,j} y_j + \frac{\partial y_i}{\partial x_{0l}} Q_{i,j} \frac{\partial y_j}{\partial x_{0m}} \right) dt \\ &= \int_0^\infty 2 \sum_{i=1}^m \sum_{j=1}^m \left(\frac{\partial y_i}{\partial x_{0l}} Q_{i,j} \frac{\partial y_j}{\partial x_{0m}} \right) dt \quad l, m = 1, \dots, n \end{aligned} \quad (6.11)$$

$$\begin{aligned} \frac{\partial^3 J}{\partial x_{0l} \partial x_{0m} \partial x_{0k}} &= \int_0^\infty 2 \sum_{i=1}^m \sum_{j=1}^m Q_{i,j} \left(\frac{\partial^3 y_j}{\partial x_{0k} \partial x_{0l} \partial x_{0m}} y_i + \frac{\partial^2 y_i}{\partial x_{0l} \partial x_{0k}} \frac{\partial y_j}{\partial x_{0m}} + \right. \\ &\quad \left. \frac{\partial^2 y_j}{\partial x_{0l} \partial x_{0m}} \cdot \frac{\partial y_i}{\partial x_{0k}} + \frac{\partial y_i}{\partial x_{0l}} \frac{\partial^2 y_j}{\partial x_{0m} \partial x_{0k}} \right) dt \\ &= \int_0^\infty 2 \sum_{i=1}^m \sum_{j=1}^m Q_{i,j} \left(\frac{\partial^2 y_i}{\partial x_{0l} \partial x_{0k}} \frac{\partial y_j}{\partial x_{0m}} + \frac{\partial^2 y_j}{\partial x_{0l} \partial x_{0m}} \frac{\partial y_i}{\partial x_{0k}} + \right. \\ &\quad \left. \frac{\partial y_i}{\partial x_{0l}} \frac{\partial^2 y_j}{\partial x_{0m} \partial x_{0k}} \right) dt \quad l, m, k = 1, \dots, n \end{aligned} \quad (6.12)$$

All derivatives in (6.10) to (6.12) are evaluated at the spatial distribution of the state variables at the nominal (equilibrium) conditions.

To compute all the derivatives of J , it is required the calculation of the first and second order partial derivative (*sensitivity coefficients*) of $\mathbf{x}(t, z)$ with respect to the initial conditions, \mathbf{x}_0 .

Lemma 6.4.1 Assume that \mathbf{g} , \mathbf{f} and all its partial derivatives $\frac{\partial \mathbf{g}}{\partial \mathbf{x}^T}$, $\frac{\partial \mathbf{g}}{\partial \mathbf{s}^T}$ and $\frac{\partial \mathbf{f}}{\partial \mathbf{x}^T}$ are continuous, and that $\mathbf{x} = \mathbf{x}(z, \mathbf{x}_0)$ and $\mathbf{s} = \mathbf{s}(z, \mathbf{x}_0)$ are themselves

differentiable functions of \mathbf{x}_0 . Let $\mathbf{g}(z, \mathbf{x}_0) = \mathbf{g}(z, \mathbf{x}(z, \mathbf{x}_0), \mathbf{s}(z, \mathbf{x}_0))$ and $\mathbf{f}(z, \mathbf{x}_0) = \mathbf{f}(z, \mathbf{x}(z, \mathbf{x}_0), \mathbf{s}(z, \mathbf{x}_0))$. Then \mathbf{g} and \mathbf{f} are differentiable and

$$\frac{\partial}{\partial t} \left(\frac{\partial \mathbf{x}}{\partial x_{0i}} \right) = \frac{\partial \mathbf{g}}{\partial \mathbf{x}^T} \frac{\partial \mathbf{x}}{\partial x_{0i}} + \frac{\partial \mathbf{g}}{\partial \mathbf{s}^T} \frac{\partial \mathbf{s}}{\partial x_{0i}} + \frac{\partial \mathbf{f}}{\partial \mathbf{x}^T} \frac{\partial \mathbf{x}}{\partial x_{0i}} \quad i = 1, \dots, n \quad (6.13)$$

Lemma 6.4.2 Assume that all second order partial derivatives $\frac{\partial^2 \mathbf{g}}{\partial \mathbf{x}^2}$ and $\frac{\partial^2 \mathbf{f}}{\partial \mathbf{x}^2}$ are continuous, and that $\mathbf{x} = \mathbf{x}(z, \mathbf{x}_0)$ and $\mathbf{s} = \mathbf{s}(z, \mathbf{x}_0)$ are themselves twice differentiable functions of \mathbf{x}_0 . Then,

$$\begin{aligned} \frac{\partial}{\partial t} \left(\frac{\partial^2 \mathbf{x}}{\partial x_{0j} \partial x_{0i}} \right) &= \frac{\partial}{\partial x_{0j}} \left(\frac{\partial \mathbf{g}}{\partial \mathbf{x}^T} \frac{\partial \mathbf{x}}{\partial x_{0i}} + \frac{\partial \mathbf{g}}{\partial \mathbf{s}^T} \frac{\partial \mathbf{s}}{\partial x_{0i}} + \frac{\partial \mathbf{f}}{\partial \mathbf{x}^T} \frac{\partial \mathbf{x}}{\partial x_{0i}} \right) \quad i = 1, \dots, n \\ &= \frac{\partial^2 \mathbf{g}}{\partial \mathbf{x}^2} \frac{\partial \mathbf{x}}{\partial x_{0j}} \frac{\partial \mathbf{x}}{\partial x_{0i}} + \frac{\partial \mathbf{g}}{\partial \mathbf{x}^T} \frac{\partial^2 \mathbf{x}}{\partial x_{0j} \partial x_{0i}} + \frac{\partial \mathbf{g}}{\partial \mathbf{s}^T} \frac{\partial^2 \mathbf{s}}{\partial x_{0j} \partial x_{0i}} + \frac{\partial^2 \mathbf{f}}{\partial \mathbf{x}^2} \frac{\partial \mathbf{x}}{\partial x_{0j}} \\ &\quad \frac{\partial \mathbf{x}}{\partial x_{0i}} + \frac{\partial \mathbf{f}}{\partial \mathbf{x}^T} \left(\frac{\partial^2 \mathbf{x}}{\partial x_{0j} \partial x_{0i}} \right) \quad i, j = 1, \dots, n \end{aligned} \quad (6.14)$$

The solution of the equations (6.13) and (6.14) can be obtained by solving the system of PDEs numerically and simultaneously.

To solve equations (6.13) and (6.14), the following initial and boundary conditions are needed:

$$\frac{\partial \mathbf{x}}{\partial \mathbf{x}_0}(0, z) = \mathbf{I}_{n \times n} \quad (6.15)$$

$$\frac{\partial^2 \mathbf{x}}{\partial \mathbf{x}_0 \partial \mathbf{x}_0^T}(0, z) = \mathbf{0}_{n \times (n \times n)} \quad (6.16)$$

$$\frac{\partial \mathbf{x}}{\partial \mathbf{x}_0}(t, 0) = \mathbf{I}_{n \times n} \quad (6.17)$$

$$\frac{\partial^2 \mathbf{x}}{\partial \mathbf{x}_0 \partial \mathbf{x}_0^T}(t, 0) = \mathbf{0}_{n \times (n \times n)} \quad (6.18)$$

Remark 6.4.1 Since the initial condition chosen to evaluate the sensitivity of the linear control performance is independent of the spatial distribution, then

$$\begin{aligned} \frac{\partial^2 \mathbf{s}}{\partial x_{0j} \partial x_{0i}} &= \frac{\partial^2}{\partial x_{0j} \partial x_{0i}} \left(\frac{\partial \mathbf{x}}{\partial z} \right) \\ &= \frac{\partial}{\partial z} \left(\frac{\partial^2 \mathbf{x}}{\partial x_{0j} \partial x_{0i}} \right) \end{aligned} \quad (6.19)$$

If one computes the first and second order sensitivities about the equilibrium solution for a linear hyperbolic PDE system, then one finds that the second order

sensitivity coefficients, $\left(\frac{\partial^2 \mathbf{x}}{\partial x_{0j} \partial x_{0i}}\right)$, are identically zero. The following proof was derived to prove that the second order coefficients are indeed identically zero:

Proof: For linear hyperbolic PDE models, equation (6.14) becomes

$$\begin{aligned} \frac{\partial}{\partial t} \left(\frac{\partial^2 \mathbf{x}}{\partial x_{0j} \partial x_{0i}} \right) &= \frac{\partial \mathbf{g}}{\partial \mathbf{x}} \frac{\partial^2 \mathbf{x}}{\partial x_{0j} \partial x_{0i}} + \frac{\partial \mathbf{g}}{\partial \mathbf{s}} \frac{\partial^2 \mathbf{s}}{\partial x_{0j} \partial x_{0i}} + \frac{\partial \mathbf{f}}{\partial \mathbf{x}} \left(\frac{\partial^2 \mathbf{x}}{\partial x_{0j} \partial x_{0i}} \right) \\ &= \left[\frac{\partial \mathbf{g}}{\partial \mathbf{x}} + \frac{\partial \mathbf{f}}{\partial \mathbf{x}} \right] \frac{\partial^2 \mathbf{x}}{\partial x_{0j} \partial x_{0i}} + \frac{\partial \mathbf{g}}{\partial \mathbf{s}} \frac{\partial}{\partial z} \left(\frac{\partial^2 \mathbf{x}}{\partial x_{0j} \partial x_{0i}} \right) \end{aligned} \quad (6.20)$$

Since

$$\frac{\partial \mathbf{g}}{\partial \mathbf{s}} = -\mathbf{B}(z, \mathbf{x}|_{eq}) \Rightarrow \frac{\partial \mathbf{g}}{\partial \mathbf{s}} = -\mathbf{B}(z, \mathbf{0}),$$

and $\mathbf{B}(z, \mathbf{x})$ admits diagonalization, then there exists a real diagonal matrix $\Lambda(z, \mathbf{x})$ and a nonsingular matrix $\mathbf{T}(z, \mathbf{x})$ such that

$$\mathbf{T}(z, \mathbf{0})\mathbf{B}(z, \mathbf{0}) = \Lambda(z, \mathbf{0})\mathbf{T}(z, \mathbf{0}). \quad (6.21)$$

Pre-multiplication of (6.20) by an arbitrary left eigenvector \mathbf{t}_k^T of \mathbf{B} , gives

$$\mathbf{t}_k^T \frac{\partial}{\partial t} \left(\frac{\partial^2 \mathbf{x}}{\partial x_{0j} \partial x_{0i}} \right) + \mathbf{t}_k^T \mathbf{B}(z, \mathbf{0}) \frac{\partial}{\partial z} \left(\frac{\partial^2 \mathbf{x}}{\partial x_{0j} \partial x_{0i}} \right) = \mathbf{t}_k^T \left[\frac{\partial \mathbf{g}}{\partial \mathbf{x}} + \frac{\partial \mathbf{f}}{\partial \mathbf{x}} \right] \left(\frac{\partial^2 \mathbf{x}}{\partial x_{0j} \partial x_{0i}} \right) \quad (6.22)$$

$$\mathbf{t}_k^T \left\{ \frac{\partial}{\partial t} \left(\frac{\partial^2 \mathbf{x}}{\partial x_{0j} \partial x_{0i}} \right) + \lambda_k(z) \frac{\partial}{\partial z} \left(\frac{\partial^2 \mathbf{x}}{\partial x_{0j} \partial x_{0i}} \right) \right\} = \mathbf{t}_k^T \left[\frac{\partial \mathbf{g}}{\partial \mathbf{x}} + \frac{\partial \mathbf{f}}{\partial \mathbf{x}} \right] \left(\frac{\partial^2 \mathbf{x}}{\partial x_{0j} \partial x_{0i}} \right) \quad (6.23)$$

An equivalent form of (6.23) is:

$$\mathbf{t}_k^T \frac{d\mathbf{v}}{ds} = \mathbf{t}_k^T \left[\frac{\partial \mathbf{g}}{\partial \mathbf{x}} + \frac{\partial \mathbf{f}}{\partial \mathbf{x}} \right] \mathbf{v} \quad (6.24)$$

for each k . Since

$$\frac{d\mathbf{v}}{ds} = \frac{\partial \mathbf{v}}{\partial t} \frac{dt}{ds} + \frac{\partial \mathbf{v}}{\partial x} \frac{dx}{ds}, \quad (6.25)$$

it can be obtained, by comparing (6.23) and (6.24), that

$$\frac{dt}{ds} = 1 \quad (6.26)$$

$$\frac{dx}{ds} = \lambda_k \quad (6.27)$$

$$\frac{d\mathbf{v}}{ds} = \mathbf{t}_k^T \left[\frac{\partial \mathbf{g}}{\partial \mathbf{x}} + \frac{\partial \mathbf{f}}{\partial \mathbf{x}} \right] \mathbf{v} \quad (6.28)$$

The solution of equation (6.28) is given by

$$\mathbf{v} = \exp \left(\mathbf{t}_k^T \left[\frac{\partial \mathbf{g}}{\partial \mathbf{x}} + \frac{\partial \mathbf{f}}{\partial \mathbf{x}} \right] t \right) \mathbf{v}_0. \quad (6.29)$$

The solution \mathbf{v} can be linearly combined by $\mathbf{t}_k^T \mathbf{v}$ to obtain the solution v_k along the characteristic curve given by λ_k . By equation (6.16), we obtain $\mathbf{v} = \mathbf{0}$. For each λ_k , we find that $v_k = 0$ and therefore, it is proven that the second order sensitivity coefficients $\mathbf{v} = \frac{\partial^2 \mathbf{x}}{\partial x_{0j} \partial x_{0i}}$ are identically zero.

□

Since the second order sensitivities are zero for linear hyperbolic PDE systems with linear controller, the third order derivative of the performance index can be used to assess the effect of nonlinearity on local controller performance by assessing the magnitude of the third order term.

The third order Taylor Series approximation of the performance index about $\mathbf{x}_0 = \mathbf{0}$ is given by

$$\begin{aligned} J(\mathbf{x}_0) &\approx J(\mathbf{x}_0 = \mathbf{0}) + dJ_{\mathbf{x}_0} + \frac{1}{2}d^2 J_{\mathbf{x}_0} + \frac{1}{6}d^3 J_{\mathbf{x}_0} \\ &\approx \frac{1}{2}d^2 J_{\mathbf{x}_0} + \frac{1}{6}d^3 J_{\mathbf{x}_0} \end{aligned} \quad (6.30)$$

where $d^k J_{\mathbf{x}_0}$ is defined as (Callen, 1985),

$$d^k J_{\mathbf{x}_0} = \left(x_{01} \frac{\partial}{\partial x_{01}} + x_{02} \frac{\partial}{\partial x_{02}} + \cdots + x_{0n} \frac{\partial}{\partial x_{0n}} \right)^k J(\mathbf{x}_0) \quad k = 2, 3$$

The second-order differential of J in equation (6.30) can be written in matrix form as:

$$d^2 J_{\mathbf{x}_0} = \mathbf{x}_0^T \nabla_{\mathbf{x}_0}^2 J_{\mathbf{x}_0} \quad (6.31)$$

where $\nabla_{\mathbf{x}_0}^2 J$ is the Hessian of $J(x_0)$. $\nabla_{\mathbf{x}_0}^2 J$ is a symmetric positive definite matrix that is formed using the partial derivatives given in equation (6.11). $\nabla_{\mathbf{x}_0}^2 J$ is a real square symmetric matrix for which we consider the spectral decomposition

$$\nabla_{\mathbf{x}_0}^2 J = 2\mathbf{U}^T \mathbf{\Lambda}_d \mathbf{U} \quad (6.32)$$

where $\mathbf{\Lambda}_d$ is a diagonal matrix with the eigenvalues of $\nabla_{\mathbf{x}_0}^2 J$ and \mathbf{U} is an orthogonal matrix ($\mathbf{U}^T = \mathbf{U}^{-1}$) containing the eigenvectors. The decomposition in (6.32) can be

used to obtain a simplified measure to assess the effect of nonlinearity on linear controller performance. For a meaningful measure, we define, as in (Guay and Forbes, 2004), a quadratic operating region:

$$\Omega = \{\mathbf{x}_0 \in R^n | \mathbf{x}_0^T \mathbf{S}^T \mathbf{S} \mathbf{x}_0 = 1\} \quad (6.33)$$

and we parametrize \mathbf{x}_0 as follows

$$\mathbf{w} = \mathbf{U} \mathbf{S} \mathbf{x}_0 \quad (6.34)$$

to obtain

$$\frac{1}{2} d^2 J_{\mathbf{x}_0} = \frac{1}{2} \mathbf{w}^T \mathbf{U} \nabla_{\mathbf{x}_0}^2 J \mathbf{U}^T \mathbf{w} = \mathbf{w}^T \mathbf{\Lambda}_d \mathbf{w}$$

Along \mathbf{w} and for any given value of \mathbf{w} (such that $\|\mathbf{w}\| = 1$), we can convert \mathbf{w} into \mathbf{x}_0 through equation (6.34). The relative contribution of the third-order differential contribution can then be quantified by the ratio of the third-order differential to the second order differential:

$$\Theta(\mathbf{w}) = \frac{(1/6) d^3 J_{\mathbf{w}}}{\mathbf{w}^T \mathbf{\Lambda} \mathbf{w}} \quad (6.35)$$

The quantity $\Theta(\mathbf{w})$ provides a measure of the degree of departure of the linear controller performance in the actual nonlinear control system.

By using the same definition used in Guay and Forbes (2004), we call $\Theta(\mathbf{w})$ the *performance sensitivity measure* (PSM) and the *root mean squared performance sensitivity measure* (RMSPSM) is defined as $RMSPSM = \sqrt{PSM}$. If the system behaves linearly, then we expect that the root mean square measure to be small. As the value increases, the contribution of the nonlinear terms to the closed-loop performance will become significant and the intended nominal performance will not be achieved.

6.5 Case study: Chemical Tubular Reactor

In this section, we study the application of the performance sensitivity measure to a chemical tubular reactor. To model the reactor system, the model equations (2.6) and (2.7) were considered.

The first step towards the computation of the sensitivity measure is the selection of a linear control technique. To formulate the linear controller, the geometric state-feedback control technique for hyperbolic PDE systems proposed in Christofides (2000) is used.

For the controller formulation, it is assumed that there are P actuators available, each of which has a unity distribution function, that is, $b_j(z)u_j = u_j$ for all $j = 1, \dots, P$, which act over equispaced intervals. The desired control objective is selected as the control of the temperature, x_2 , at the end of each spatial interval, i.e. $y_j = \int_{z_j}^{z_{j+1}} \delta(z - z_{j+1})x_2(t, z)dz$.

Using the specified inputs and outputs, the model that is used for synthesis of the state feedback controller is given by:

$$\frac{\partial x}{\partial t} = A \frac{\partial x}{\partial z} + f(x) + g(x) \sum_{j=1}^m (H(z - z_j) - H(z - z_{i+1}))u_j \quad (6.36)$$

$$y_j = \int_{z_j}^{z_{j+1}} \delta(z - z_{j+1})x_2(t, z)dz \quad (6.37)$$

where

$$A = \begin{bmatrix} -v & 0 \\ 0 & -v \end{bmatrix}, \quad f(x) = \begin{bmatrix} -ke^{\left(\frac{-\alpha_1}{x_2}\right)}x_1 \\ \alpha_2 ke^{\left(\frac{-\alpha_1}{x_2}\right)}x_1 - \alpha_3 x_2 \end{bmatrix},$$

$$g(x) = \begin{bmatrix} 0 \\ \alpha_3 \end{bmatrix}, \quad h(x) = [x_2].$$

Using the model given above, the linear controller is derived in Appendix C. The controller has the following form:

$$\tilde{u}(t) = \frac{1}{C_j d_2} \left[-\varphi_j - C_j(x_2 - x_2^{ss}) - C_j \left(a_2 \frac{\partial x_2}{\partial z} + b_2 x_1 + c_2 x_2 \right) \right] \quad (6.38)$$

To study the application of the performance sensitivity measure, a set of three different operating conditions, i.e. $u^{ss}(z) = [300 K, 360 K, 440 K]$, were selected. The open-loop equilibrium distribution of the state variables is shown in Figure 6.1.

As a first approach to the study of the closed-loop nonlinearity of the tubular reactor, we study the control of the outlet temperature, i.e. $y(t) = x_2(t, z = 1)$. Such an approach is chosen because it the most common control requirement for tubular reactors is control of the outlet variables.

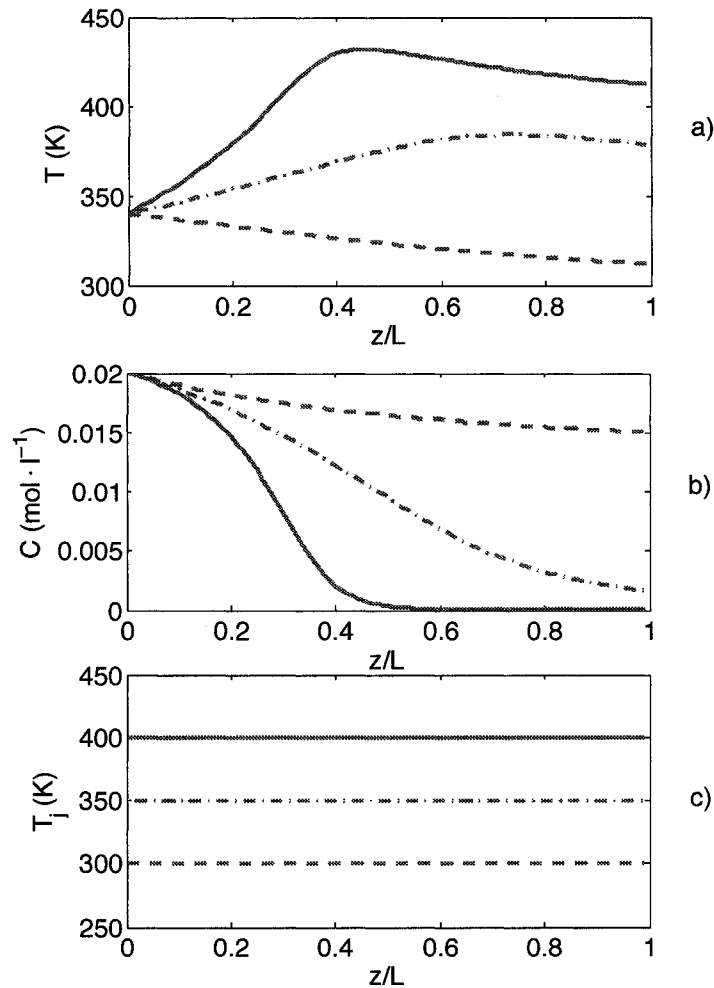


Figure 6.1: Equilibrium profiles of a) x_2^{ss} , b) x_1^{ss} , c) u^{ss} , for selected operating conditions: $u^{ss}(z) = 300K$ (dashed line), $u(z) = 360K$ (dashed-dot line) and $u(z) = 440K$ (solid line).

The second step towards the performance sensitivity measure is to compute the first and second order sensitivities for the set of equilibrium profiles shown in Figure 6.1. The sensitivities are shown on Figures 6.2 and 6.3.

The resulting performance sensitivity measure (RMSPSM) is given in Figure 6.4. Figure 6.4 indicates that locally, the impact of nonlinearity in linear control performance becomes more important as u^{ss} increases. Local linear and nonlinear control performance are compared in Figure 6.5 for different operating conditions.

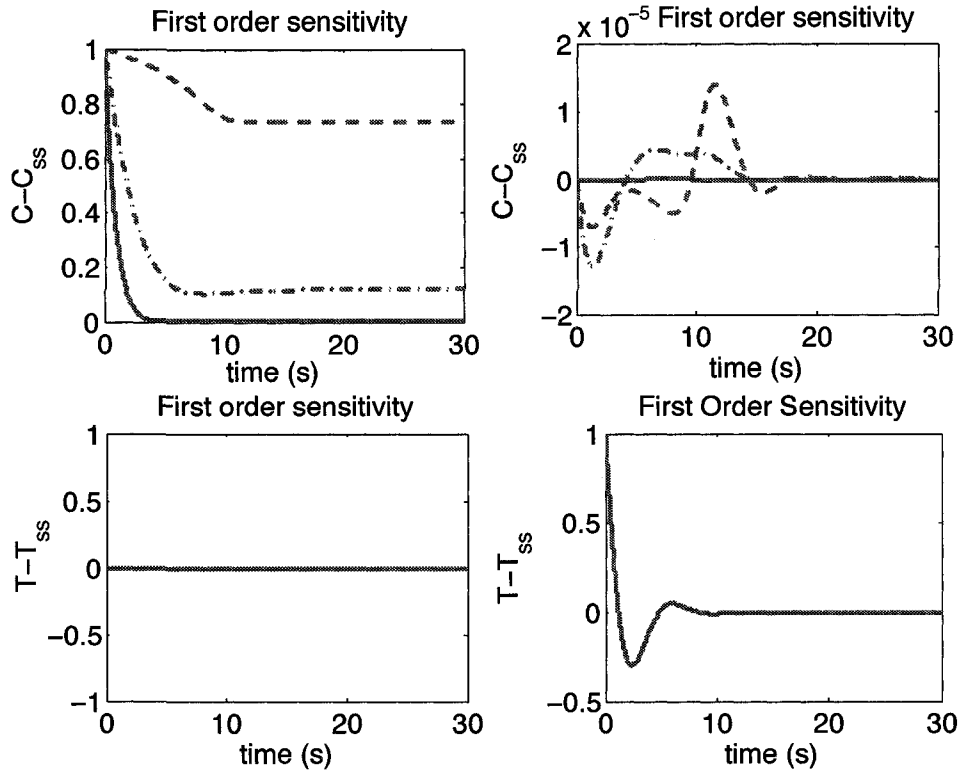


Figure 6.2: First order sensitivity for selected operating conditions: $u(z) = 300K$ (dotted line), $u(z) = 350K$ (dashed-dot line) and $u(z) = 400K$ (solid line). Top-left figure: $\frac{\partial x_1}{\partial x_{1,0}}$ vs. *time*; top-right figure: $\frac{\partial x_1}{\partial x_{2,0}}$ vs. *time*; bottom-left figure: $\frac{\partial x_2}{\partial x_{1,0}}$ vs. *time*; bottom-right figure: $\frac{\partial x_2}{\partial x_{2,0}}$ vs. *time*.

Initial conditions away from the steady-state conditions were selected, i.e. $\mathbf{x}(0, z) = [0.01, 10]^T$. From the closed-loop dynamics in Figure 6.5, it can be observed that the RMSPSM correctly quantifies the local linear control performance difference at the different operating conditions.

It is interesting to note that in the open-loop nonlinearity assessment, it was observed that the nonlinearity was significant at $u^{ss}(z) = 360K$ but small at $u^{ss}(z) = 440K$. When the closed-loop dynamics in Figure 6.5 are compared to that observed in Figure 5.10, it is observed that when the system is driven from an operating condition to another by a set-point change, control performance follows the observations made from the open-loop nonlinearity assessment. The comparison between the information given by the two measures gives valuable information as it shows that the effect of process nonlinearity can affect control performance in different

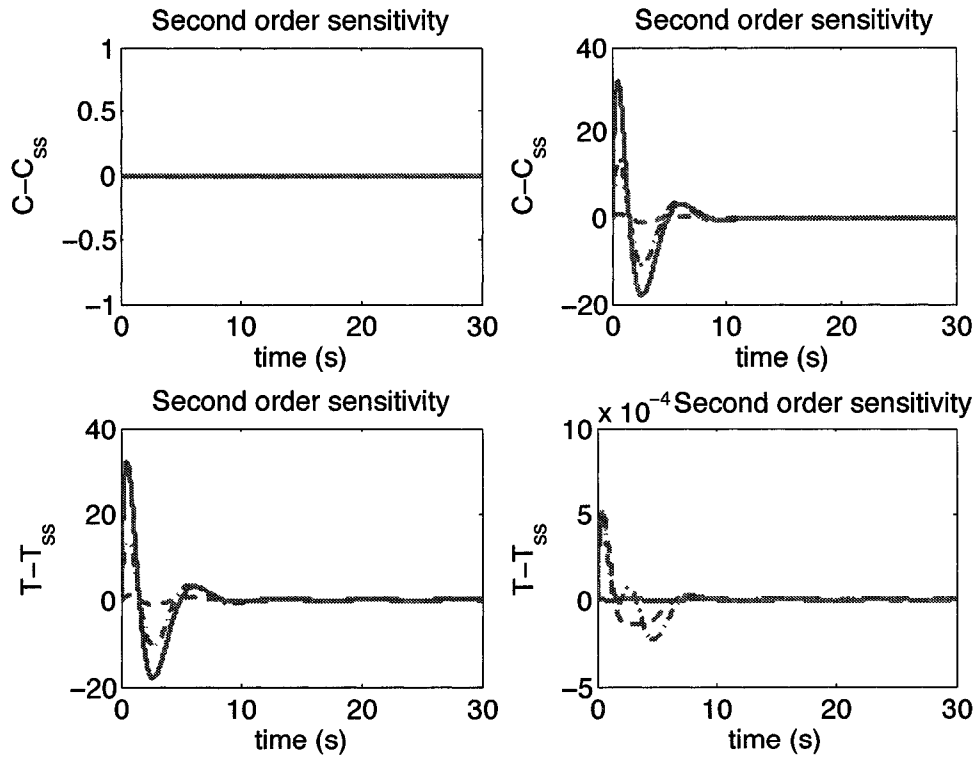


Figure 6.3: Second order sensitivity for selected operating conditions: $u(z) = 300K$ (dotted line), $u(z) = 350K$ (dashed-dot line) and $u(z) = 400K$ (solid line). Top-left figure: $\frac{\partial^2 x_2}{\partial x_{1,0}^2}$ vs. *time*; top-right figure: $\frac{\partial^2 x_2}{\partial x_{1,0} \partial x_{2,0}}$ vs. *time*; bottom-left figure: $\frac{\partial^2 x_2}{\partial x_{2,0} \partial x_{1,0}}$ vs. *time*; bottom-right figure: $\frac{\partial^2 x_2}{\partial x_{2,0}^2}$ vs. *time*.

ways. Therefore, the open-loop nonlinearity measure and the performance sensitivity measure can be computed and used to assess the impact of nonlinearity on linear control design without the need to formulate a nonlinear control law.

To further analyze the effect of the nonlinearity of the tubular reactor, we studied the effect of multiple control actuators along the axis of the reactor. For tubular reactors, it is often required that the spatial temperature distribution is controlled along the reactor length. We study two problems: the control of the temperature at five and ten spatial points using five and ten heat exchangers, respectively. The operating (equilibrium) profiles selected are those given in Figure 6.1. The resulting performance sensitivity measure (RMSPSM) is given in Figure 6.6. It is observed that as the number of controlled outputs increases, the the effect of process nonlinearity on linear control increases as well. It should be noted that the increase is small indicating

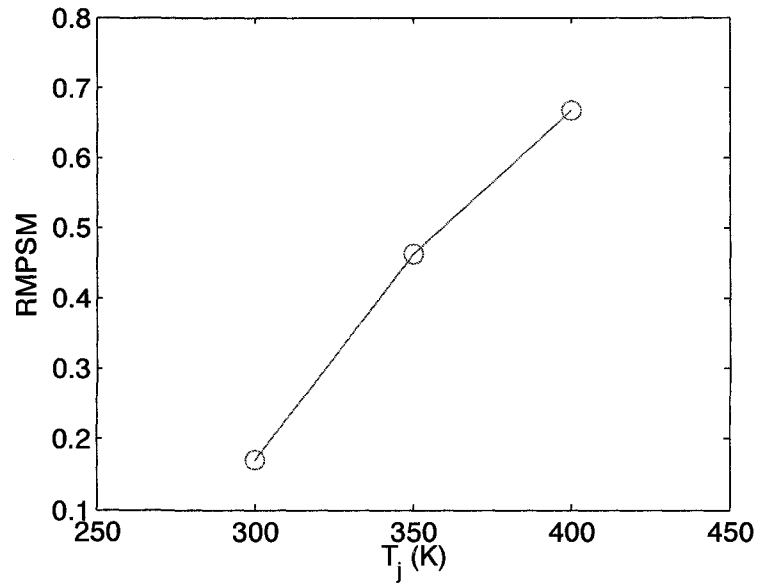


Figure 6.4: RMPSM for selected operating conditions.

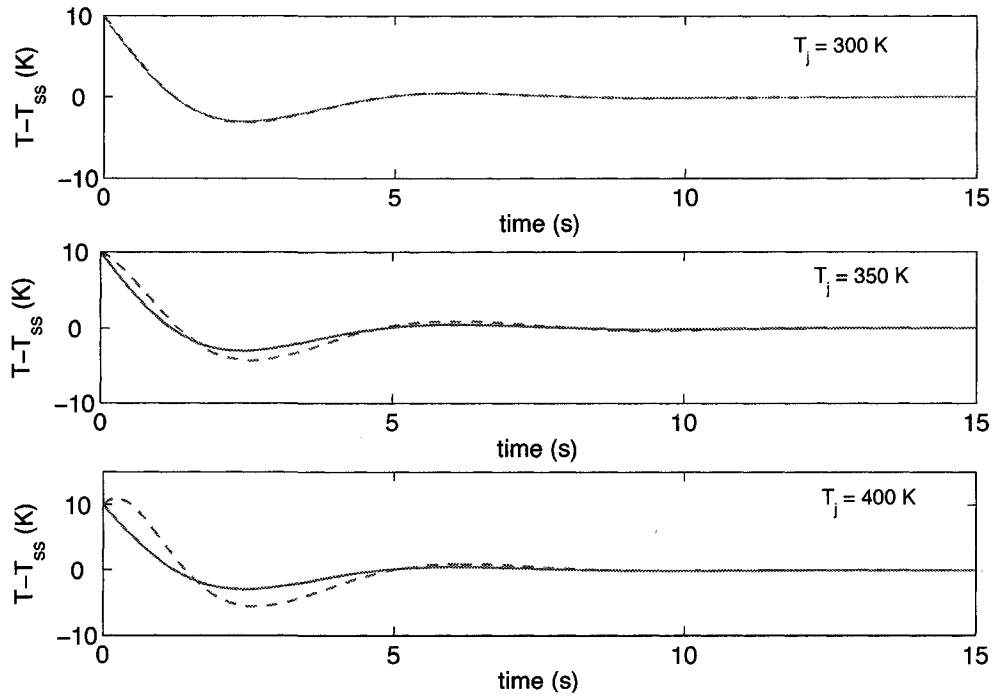


Figure 6.5: Closed-loop temperature at $z/L = 1$ for $\tilde{x}_0 = [0.01, 10]^T$ with linear (dashed line) and non-linear control (solid line).

that, for the reactor under study, the effect of nonlinearity is more sensitive to the operating conditions than the spatial location of the controlled temperature.

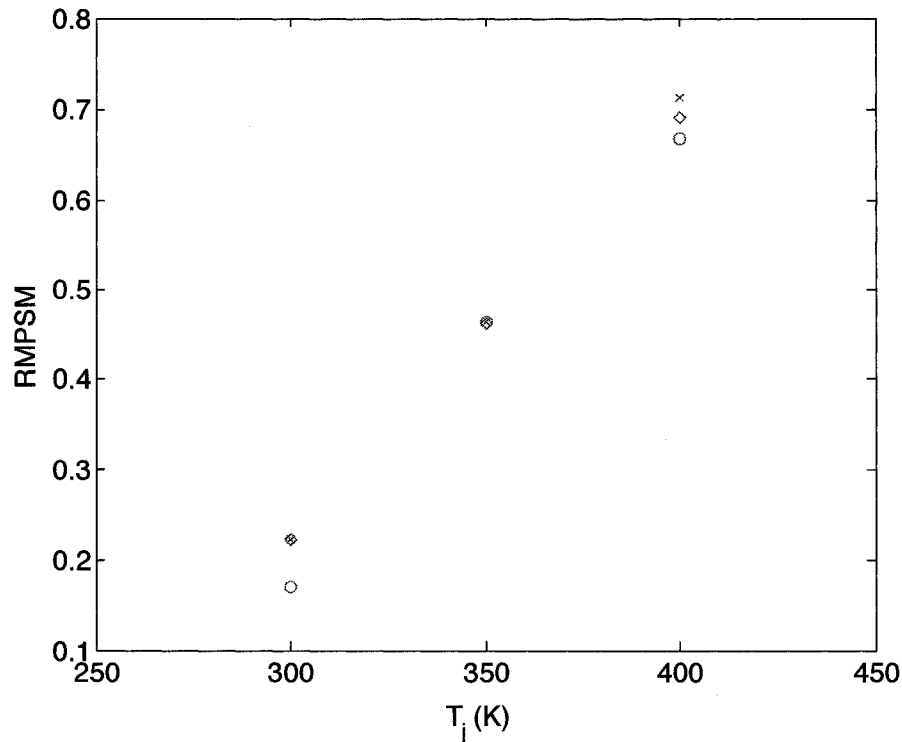


Figure 6.6: RMSPSM vs. operating condition (T_j) for the case where one (circles), five (diamonds) and ten (crosses) heat exchangers are used to control the reactor system.

6.6 Case study: Catalytic Flow Reversal Reactor

In this section, we study the application of the performance sensitivity measure to a catalytic flow reversal reactor.

To model the reactor system, we consider the model equations in (5.51) to (5.52). To formulate the linear controller, the linear quadratic controller developed in Section 4, and given in equation (4.41), was used. For the controller formulation, it was assumed that only one control input was available (i.e. removed gas from the reactor mid-section) and that the outputs were the temperatures at 100 equally-spaced spatial points along the axis of the reactor.

Due to the complexity of the reactor model, numerical solutions were used. The first and second order sensitivities of the temperature with respect to the initial values were computed by numerical simulation of the closed-loop system under different initial conditions and subsequent numerical approximation of the first and second

order derivatives.

To study the application of the performance sensitivity measure, a set of three different operating conditions, *i.e.* $u_{ss} = [0.9, 0.92, 0.94]$, were selected and the open-loop equilibrium distribution of the state variables were computed. The first and second order sensitivities for the set of operating conditions were then computed.

For $u_{ss} = 0.92$, the first and second order sensitivities of the outputs with respect to the initial temperature values are shown in Figure 6.7 for three different spatial points along the axis of the reactor.

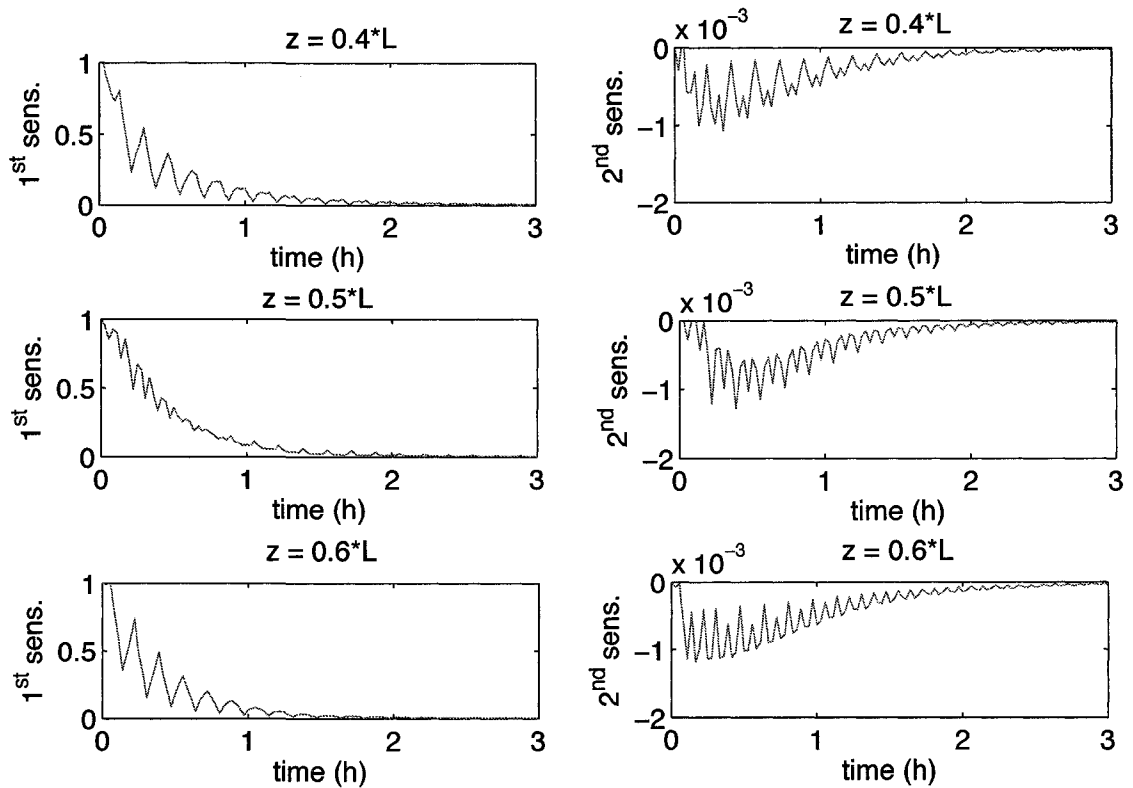


Figure 6.7: First and second order sensitivity for $u_{ss} = 0.92$ at three different spatial points along the axis of the reactor.

The performance sensitivity measure (RMSPSM) for the selected operating conditions is given in Figure 6.8. Figure 6.8 indicates that locally, the impact of nonlinearity in linear control performance becomes more important as u_{ss} increases.

Comparison of local linear and nonlinear control performance for the different operating conditions would give a definite answer to whether nonlinear control would

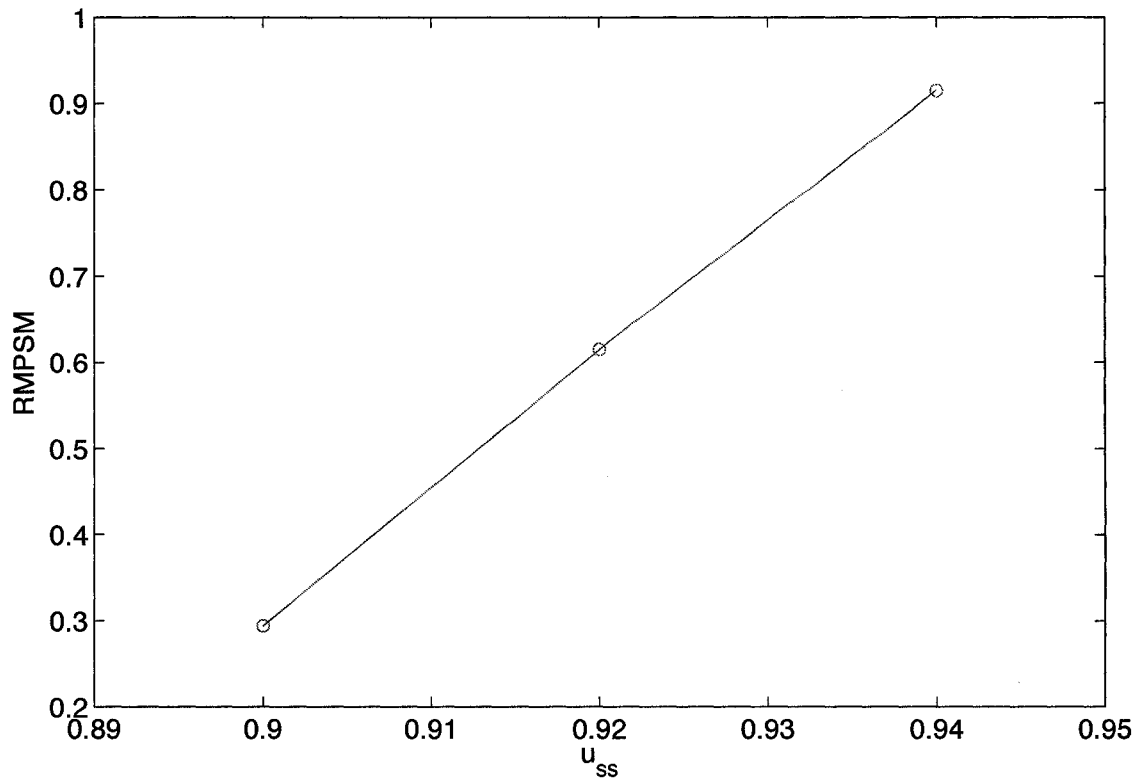


Figure 6.8: RMSPM for selected operating conditions for the CFRR unit.

provide a significant benefit. The formulation of a nonlinear controller, however, is not within the scope of this chapter. The goal of this case study is to infer whether or not linear control is sufficient without designing a nonlinear controller. Based on the RMSPM values, it can be said that for the control the complete temperature profile along the reactor, the higher the operating value of mass extraction is, the higher will be the performance of the linear controller.

6.7 Summary

In this chapter, we presented a performance sensitivity measure to assess the impact of nonlinearity in linear control of processes modeled by quasilinear hyperbolic partial differential equations.

The measure developed in this chapter is an extension for distributed parameter

systems of the work in Guay *et al.* (2005). The main principle of the performance sensitivity measure is that the nominal performance is invariant to the choice of initial conditions if the underlying control system is nearly linear. Thus, the sensitivity of the nominal performance to changes in initial conditions provides an effective means of investigating the nonlinearity effects in control systems.

Using a tubular reactor with heat exchanger as a case study, the application of the performance sensitivity measure was illustrated. It was observed that the performance sensitivity measure gives useful information about the impact of nonlinearity for local control and that it can be combined with the open-loop nonlinearity measure developed in Chapter 5 to assess the impact of nonlinearity for control systems that not only regulates the process but also drives it from one operating point to another.

The performance sensitivity measure was also applied to a catalytic flow reversal reactor. Due to the lack of a closed form amenable for the computation of analytical derivatives, sensitivities of the output variables with respect to the initial conditions were computed using numerical approximations using closed-loop data from numerical simulations. The reactor temperature along a fixed number of spatial points was considered as output variable. It was observed that using the linear quadratic controller developed in Section 4 and given in equation (4.41), the higher the operating value of mass extraction was, the higher is the expected level of linear control performance. Nevertheless, the gas extraction cannot be increased without limit as the reaction within the reactor will extinguish. This indicates that there is an optimum value of gas removal from the reactor midsection for best linear control of the 1-D pseudo-homogeneous model representation of the catalytic flow reversal reactor.

7

Conclusions and Recommendations

7.1 Conclusions

Catalytic flow reversal reactor is a promising technology for efficient and economic processing of chemical reactants with low heats of reaction. Dynamic operation of catalytic reactors is not the most common or preferred mode of operation. Even though design and modeling of catalytic reactors with reverse flow operation have been thoroughly investigated, control of such reactors has not received much attention.

In this thesis, tools were developed to address the control problem of catalytic flow reversal reactors. The tools were applied to a catalytic reactor for combustion of lean methane emissions. Such an application can have a great impact on the reduction greenhouse gas emissions from oil and gas transportation facilities and coal mines.

The concept of catalytic reactor with reverse flow operation, as well as its application for the combustion of lean methane streams was introduced in Chapter 2. Due to the complex reactor dynamics, computer simulations were needed to understand the main dynamic characteristics.

In Chapter 2, a 2-D heterogenous mathematical model of a reactor pilot unit was implemented to obtain high fidelity numerical simulations of the reactor dynamics. Many interesting conclusions were drawn from the simulation results.

In particular, it was observed that the reverse flow reactor considered had a slow time dynamics with a settling time that was in the order of hours. Moreover, the temperature response to changes in the inlet gas velocity was observed to be much faster than to changes in the inlet mole fraction. Since the inlet mole fraction and inlet gas velocity are the most important sources of reactor disturbance, it would be interesting to study in future research a control scheme where the inlet concentration is controlled by, for example, an external air stream. In this way, the reactor temperature distribution would only be disturbed by the inlet gas velocity. As the dynamic behaviour of the temperature for changes in the gas velocity is fast, regulation of the reactor temperature can be achieved at a much faster rate.

To assist in the formulation and testing of control schemes for catalytic reactors with reverse flow operation, a mathematically simple 1-D pseudo-homogeneous model was developed and validated for use in an online control strategy and a linear quadratic regulator controller. It was observed that under the 1-D pseudo-homogeneous model assumptions, the short term dynamic behaviour of the reactor was accurately modeled. The long term (or multi-cycle) behaviour could not be predicted with sufficient accuracy. Nevertheless, it was observed that even when the simple model neglected some characteristics of the reactor, it can be used for process control as the feedback control techniques selected in this thesis compensate for unmodeled plant/model mismatch.

In Chapter 3, the development of a model predictive control for a catalytic flow reversal reactor for large volumes of lean methane emissions was addressed. An average of the temperature along the axis of the reactor reactor was proposed as the output variable to be controlled to avoid reactor shutdown due to low reactor temperatures and reaction extinction. In addition to the average temperature, the maximum temperature was constrained with an upper bound that represented the temperature at which the catalyst deactivates at a fast rate.

A model predictive control scheme that incorporates the method of characteristics to predict the process output variables was developed. The idea of using the method of characteristics in a model predictive control scheme had been proposed in the literature, but not applied to a complex catalytic reactor. Based on the results

obtained in Chapter 3, it can be concluded that the method can be efficient for catalytic reactors that have two widely different dynamic time-scale.

Through closed-loop simulations, it was shown that two output variables, i.e. average temperature and maximum temperature, can be used to keep the reactor within stable operating conditions despite disturbances in uncontrolled process variables, i.e. inlet mole fraction of reactants and inlet gas velocity. It was shown that, at least theoretically, the use of the heat extraction by means of mass extraction in a model predictive control scheme can be used to control the reactor system.

Chapter 4 presented the formulation of feedback control scheme for a catalytic reactor with reverse flow operation. A linear quadratic feedback operator was formulated from a infinite-dimensional representation of the catalytic reactor with unidirectional flow. As applications of the selected control technique are rare in the literature, this chapter provides an interesting and novel application. The application of the technique for the catalytic reactor unit can provide a theoretical threshold for the best achievable control performance. A spatially distributed input variable, namely gas flow velocity, was considered for control of the the temperature distribution along the axis of the reactor and derive an upper bound on the achievable control performance.

Numerical simulations showed that a feedback proportional controller, such as the one computed in Chapter 4, can be used to drive the reverse flow reactor system to stationary state and to achieve reactor stability while inlet disturbances affect the system; however, control objectives such as offset elimination or temperature excursions above a maximum threshold cannot be fulfilled. Nevertheless, the technique provides a theoretical foundation for optimal optimal control and leads to a simple control law. Issues like practical implementation and robustness need to be further investigated.

The control schemes developed in Chapters 3 and 4 were proven to be adequate for the control of the reverse flow reactor unit; however, we overlooked the fact that the system had a nonlinear dynamic. A major issue that control engineers face while selecting of a control technique for a given process is the impact of process nonlinearity on the closed-loop system. A wide range of measures have been proposed

to quantify process nonlinearity. While published results in this area are limited to lumped parameter systems, measures of nonlinearity were developed in Chapter 5 and 6 for distributed parameter systems; in particular for systems modeled by hyperbolic partial differential equations.

Chapter 5 presented a measure to quantify the magnitude of open-loop process nonlinearity in hyperbolic partial differential equation models. The measure quantifies the gain nonlinearity and can be used to locate regions of the output space where nonlinearity is significant. The gain nonlinearity can be used as preliminary information for the design of a controller for the system under study.

A plug flow reactor was used to show the application of the proposed measure and to study the relation between the measure and the observed control performance. Operating regions were mapped to a nonlinearity measure so that regions with a larger degree of nonlinearity could be identified for control uses. Comparison of closed-loop control around the different operating regions using linear and nonlinear controllers was shown to be an effective way to highlight the importance of the measure.

The open-loop nonlinearity measure was also applied to a catalytic flow reversal reactor. Unfortunately, the analytical method developed in Chapter 5 could not be used to derive the nonlinearity measure due to the lack of a closed-form mathematical model of the reactor for direct computation of the stationary-state. Computer simulations were used to find the stationary state and use it to numerically approximate the first and second order derivatives. From the results obtained, it was observed that normal curvature due to the combination of mole fraction and temperature in the reactor model was minimal. Moreover, the main source of nonlinearity, i.e. nonuniform spacing of the reactor temperature, was successfully quantified by the tangential curvature. Curvature profiles at different operating conditions can be created to analyze with great detail the operating regions where the nonlinearity might be significant.

Even though an open-loop nonlinearity measure provides meaningful information, the main assumption related to the use of open-loop nonlinearity measures in controller design is that highly nonlinear systems will require nonlinear controllers. Although this may be true in a significant number of applications, proximity of a

nonlinear process to a linear one is neither necessary nor sufficient for good closed-loop linear control performance.

Chapter 6 presented a performance sensitivity measure to assess the impact of nonlinearity in linear control of processes modeled by quasilinear hyperbolic partial differential equations. The measure is an extension to distributed parameter systems of the sensitivity measure available in the literature for lumped parameter systems. The main principle of the performance sensitivity measure is that the nominal performance is invariant to the choice of initial conditions if the underlying control system is nearly linear. Thus, the sensitivity of the nominal performance to changes in initial conditions provides an effective means of investigating the nonlinearity effects in control systems.

A tubular reactor with heat exchanger was used to show the application of the performance sensitivity measure. It was observed that the performance sensitivity measure gives useful information about the impact of nonlinearity for local control and that it can be combined with the open-loop nonlinearity measure developed in Chapter 5 to assess the full impact of nonlinearity, not only for regulation but also for set point-tracking.

The performance sensitivity measure was also applied to a catalytic flow reversal reactor. Due to the lack of a closed form model amenable for the computation of analytical derivatives, sensitivities of the output variables with respect to the initial conditions were computed using closed-loop data from numerical simulations and numerical approximations. The reactor temperature along a fixed number of spatial points was considered as output variable. It was observed that using the linear quadratic controller developed in Section 4 (equation (4.41)), the higher the operating value of mass extraction is, the higher is the expected level of linear control performance. The study indicates that there is an optimum value of gas removal from the reactor midsection for best linear control of the 1-D pseudo-homogeneous model representation of the catalytic flow reversal reactor.

7.2 Recommendations

7.2.1 Modeling of Catalytic Flow Reversal Reactors

In Chapter 2, a 1-D pseudo-homogeneous low fidelity model was used to represent the catalytic reactor dynamics and to develop control strategies. The model was observed to provide good short term predictions, but it failed to provide long term estimations of the reactor dynamics. It is suggested to improve the reactor model by including a third dependent variable to model the temperature of the insulation and to add an effective heat transfer coefficient to model the heat transfer between the reactor temperature and the insulation. Moreover, experimental data would be beneficial for validation of the model predictions; specially the long term predictions.

Although a first principle model can provide extensive information about the dynamic behavior of the reactor system, it would be interesting to evaluate empirical models that can be used directly into commercial MPC software packages. Until now, there has been no research work that studies exclusively the identification of empirical models for CFRR units. It is recommended to perform such a study by modeling the cycle-by-cycle dynamic behaviour and neglecting the inter-cycle dynamics; i.e., a sampling time of one full cycle.

7.2.2 Control Design for CFRR units

The main issue regarding model predictive control is that a good mathematical representation of the the controlled system is required. While the vast majority of the MPC implementations employ a linear lumped parameter dynamic model of the controlled process, most chemical processes, and especially catalytic reactors, are nonlinear distributed parameter systems. Despite the advantage of accuracy of a nonlinear model, nonlinear models have the disadvantage of necessitating online nonlinear optimization, which may require large computational effort and might not provide significant improvement in the control performance. .

In Chapters 3, a model predictive control scheme was used to control the simulated pilot catalytic flow reversal reactor unit. A linear approximation of the reactor dynamics was used to predict the future output behavior in the MPC scheme. Periodic

updating of the linear model was used and good control performance was observed in the numerical simulations results. The good control performance observed indicates that the system behaves linearly in the region of operation selected, i.e. the changes in the operating conditions used were small enough to keep the reactor within a linear region. Even though experimental results would be needed to provide a definite answer about the suitability of the linear models in the model based control scheme, the measures developed in Chapters 5 and 6 can be used to quantify the impact of nonlinearity on the closed-loop system. Numerical simulations and approximations can be used to compute first and second order derivatives or sensitivities, although an extension of the analytical methods developed in Chapters 5 and 6 to processes that operate under unsteady-state conditions would provide a more precise answer to the problem.

Application of the control schemes developed in this thesis, more specifically the MPC scheme, in the pilot reactor unit can provide the much needed control scheme for industrial application and can help to improve the control scheme by the identification potential problems that are not evident in the design stage. In this thesis, there was significant model/plant mismatch and the controller provided satisfactory control in the numerical simulations, so it can be expected that it will be sufficiently robust in practice; however, other issues such as stochastic components have not been considered or tested.

An important issue that was briefly discussed in Chapters 3 was the possibility of saturation of the manipulated variable during extreme conditions, i.e. lean or concentrated inlet stream. If such cases exist, then a logic control scheme can be added. Using the mass extraction as manipulated variable, the MPC controller would be used to drive and keep the reactor operation within a stable operating region. If that is not possible due to saturation of the manipulated variable and extreme conditions, then the temperature of the reactor will be driven outside the stable operating region. A solution for that situation would be to automatically turn off the MPC and to use new control measures such as injection of hot or cold air stream through the reactor midsection. Once the temperature is driven back to safe operating conditions, then the system will be again controlled by the MPC through

mass extraction.

7.2.3 Nonlinearity Assessment of Hyperbolic PDE

In Chapters 5 and 6, open-and closed-loop nonlinearity measures for quasi-linear hyperbolic PDE models were developed. To show the application of the measures, a plug flow reactor and a catalytic reactor with reverse flow operation were used.

For the study of the catalytic reactor with reverse flow operation, numerical simulations were required to compute the nonlinearity measures. Further extension of the method proposed in this thesis would be required for such a complex system. Nevertheless, numerical simulations and approximation helped to obtain the measures of nonlinearity and gain deeper insight into the impact of process nonlinearity on the control of such system.

It is recommended to apply the concept of performance sensitivity assessment to the closed-loop system composed of the 2-D heterogeneous model and the model predictive control. Even though this performance assessment can only be performed by using numerical simulations at this time, it can give a definite answer about the impact of nonlinearity on linear control performance of the catalytic flow reversal reactor.

It is recommended to extend the application to other types of PDEs. An interesting extension would be to parabolic PDE equations. Parabolic PDE models arise in catalytic reactors when dispersive transport phenomena is significant. Issues like the effect of diffusive transport phenomena on the process nonlinearity measures would be interesting for future study.

This thesis is a starting point in the area of nonlinearity quantification in distributed parameter systems. Further study is required to gain full understanding of the strengths and limitations of the methods.

Bibliography

- Abou-Kandil, H., G. Freiling, V. Ionescu and G. Jank (2003). *Matrix Riccati Equations*. Birkhauser.
- Agency, United States Environmental Protection (2007). Inventory of u.s. greenhouse gas emissions and sinks: 1990-2005. Technical report. EPA.
- Aksikas, I. (2005). Analysis and LQ-Optimal Control of Infinite Dimensional Semilinear Systems, Application to a Plug Flow Reactor. PhD thesis. University Catholique of Louvain. Belgium.
- Aksikas, I., J.J. Winkin and D. Dochain (2007a). Optimal lq-feedback control for a class of first-order hyperbolic distributed parameter systems, in press. *ESAIM: Control, Optimisation and Calculus of Variations*.
- Aksikas, I., J.J. Winkin and D. Dochain (2007b). Optimal LQ-feedback regulation of a nonisothermal plug flow reactor model by spectral factorization. *IEEE Transactions on Automatic Control* **52**(7), 1179 – 1193.
- Aksikas, I., J.J. Winkin and D. Dochain (2007c). Optimal LQ-feedback regulation of a nonisothermal plug flow reactor model by spectral factorization. *IEEE Transactions on Automatic Control*.
- Allgower, F. (1995a). Definition and computation of a nonlinearity measure. In: *Proc. of Nonlinear Control System Desgn Symp. NOLCOS95*. pp. 257 – 262.
- Allgower, F. (1995b). Definition and computation of a nonlinearity measure and application to approximate i/o linearization. Technical report. University of Stuttgart.

- Atkinson, K. and W. Han (2001). *Theoretical Numerical Analysis: A Functional Analysis Framework*. Springer Verlag.
- Aube, F. and H. Sapoundjiev (2000). Mathematical model and numerical simulations of catalytic flow reversal reactors for industrial applications. *Computers and Chemical Engineering* **24**, 2623 – 2632.
- Balaji, S., A. Fuxman, S. Lakshminarayanan, J.F. Forbes and R.E. Hayes (2007). Repetitive model predictive control of a reverse flow reactor. *Chemical Engineering Science* **62**, 2154 – 2167.
- Bates, D. and D. Watts (1988). *Nonlinear Regression Analysis and its Applications*. John Wiley and Sons, Inc.. New York.
- Benda, M.A. (2000). Nonlinearity and controller performance for product property control in a gas-phase polyethylene reactor. Master's thesis. Queen's University. Kingston, Ontario, Canada.
- Bhatia, S.K. (1991). Analysis of catalytic reactor operation with periodic-flow reversal. *Chemical Engineering Science* **46**(1), 361 – 367.
- Biegler, L.T., A.M. Cervantes and A. Wachter (2002). Advances in simultaneous strategies for dynamic process optimization. *Chemical Engineering Science* **57**, 575 – 593.
- Bock, H.G. and K.J. Plitt (1984). A multiple shooting algorithm for direct solution of optimal control problems. In: *Ninth IFAC World Congress*. Budapest.
- Budman, H., M. Kzyonsek and P. Silveston (1996). Control of nonadiabatic packed-bed reactor under periodic flow reversal. *Canadian Journal of Chemical Engineering* **74**, 751 – 759.
- Callen, H.B. (1985). *Thermodynamics and an Introduction to Thermostatistics*. John Wiley and Sons, Inc.
- Camacho, E.F. and C. Bordons (1999). *Model Predictive Control*. 2nd ed.. Springer. Berlin.

- Christofides, P.D. (2000). *Nonlinear and Robust Control of PDE Systems*. Birkhauser. Boston.
- Curtain, R.F. and H.J. Zwart (1995). *An introduction to infinite-dimensional linear systems theory*. Springer Verlag. New York.
- Desoer, C.A. and Y.T. Wang (1980). Foundations of feedback theory for nonlinear dynamical systems. *IEEE Transactions on Circuits and Systems CAS-27*(2), 104.
- Devals, C., A. Fuxman, F. Bertrand, J.F. Forbes and R.E. Hayes (2006). Combustion of lean methane in a catalytic flow reversal reactor. In: *Proceedings of the COMSOL Users Conference*. Boston.
- Diehl, M., H. G. Bock, J.P. Schlöder, R. Findeisen, Z. Nagy and F. Allgower (2002). Real-time optimization and nonlinear model predictive control of processes governed by differential-algebraic equations. *Journal of Process Control* **12**, 577 – 585.
- Dochain, D., J.P. Babary and N. Tali-Maamar (1992). Modelling and adaptive control of nonlinear distributed parameter bioreactors via orthogonal collocation. *Automatica* **28**(5), 873 – 883.
- Dubljevic, S, N.H. El-Farra, P. Mhaskar and P.D. Christofides (2006). Predictive control of parabolic pdes with state and control constraints. *International Journal of Robust and Nonlinear Control* **16**, 749 – 772.
- Dubljevic, S, P. Mhaskar, N.H. El-Farra and P.D. Christofides (2005). Predictive control of transport-reaction processes. *Computers and Chemical Engineering* **29**, 2335 – 2345.
- Dufour, P. and Y. Toure (2004). Multivariable model predictive control of a catalytic reverse flow reactor. *Computers and Chemical Engineering* **28**(11), 2259 – 2270.

- Dufour, P., F. Couenne and Y. Toure (2003). Model predictive control of a catalytic reverse flow reactor. *IEEE Transactions on Control Systems Technology* **11**(5), 705 – 714.
- Edouard, D., P. Dufour and H. Hammouri (2005). Observer based multivariable control of a catalytic reverse flow reactor: Comparison between lqr and mpc approaches. *Computers and Chemical Engineering* **29**, 851 – 865.
- Eigenberger, G. and U. Nieken (1988). Catalytic combustion with periodic flow reversal. *Chemical Engineering Science* **43**(8), 2109 – 2115.
- Eker, S.A. and M. Nikolaou (2002). Linear control of nonlinear systems: Interplay between nonlinearity and feedback. *American Institute of Chemical Engineering Journal* **48**(9), 1957 – 1980.
- EPA, US (July 2003). Assessment of the worldwide market potential for oxidising coal mine ventilation air methane. Technical Report EPA 430-R-03-002. United States Environmental Protection Agency.
- Fogler, H.S. (2005). *Elements of Chemical Reaction Engineering*. Prentice Hall.
- Fuxman, A.M., I. Aksikas, J.F. Forbes and R.E. Hayes (2007a). Control of a catalytic flow reversal reactor model by linear quadratic regulator. In: *8th International IFAC Symposium on 8th International IFAC Symposium on Dynamics and Control of Process Systems (DYCOPS)*. Cancun, Mexico.
- Fuxman, A.M., I. Aksikas, J.F. Forbes and R.E. Hayes (n.d.). Lq-feedback control of a catalytic reverse flow reactor. *Journal of Process Control, in press*.
- Fuxman, A.M., J.F. Forbes and R.E. Hayes (2006). Model predictive control of a catalytic flow reversal reactor with heat extraction. In: *International Symposium on Advanced Control of Chemical Processes (ADCHEM)* (F. J. Doyle III, J.O. Trierweiler and A.R. Secchi, Eds.). Vol. 2. pp. 1009 – 1014.

- Fuxman, A.M., J.F. Forbes and R.E. Hayes (2007b). Characteristics-based model predictive control of a catalytic flow reversal reactor. *Canadian Journal of Chemical Engineering* **84**(4), 424 – 432.
- Garcia, C.E. and M. Morari (1982). Internal model control. 1. a unifying review and some new results. *Industrial and Engineering Chemistry Process Design and Development* **21**, 308 – 323.
- Garcia, C.E., D. Prett and M. Morari (1989). Model predictive control: Theory and practice - a survey. *Automatica* **25**, 225 – 248.
- Gawdzik, A. and L. Rakowski (1988). Dynamic properties of the adiabatic tubular reactor with switch flow. *Chemical Engineering Science* **43**(11), 3023 – 3030.
- Grasselli, M. and D. Pelinovsky (2008). *Numerical Mathematics*. Jones and Bartlett Publishers.
- Guay, M. (1996). Measurement of Nonlinearity in Chemical Process Control. PhD thesis. Queen's University. Kingston, Ont., Canada.
- Guay, M. (2006). The effect of process nonlinearity on linear controller performance in discrete-time systems. *Computers and Chemical Engineering* **30**, 381 – 391.
- Guay, M. and J.F. Forbes (2004). Effect of nonlinearity on linear quadratic regulator performance. In: *43rd IEEE Conference on Decision and Control*. Atlantis, Paradise Island, Bahamas.
- Guay, M., J. McLellan and D.W. Bacon (1995). Measurement of nonlinearity in chemical process control systems: The steady state map. *Canadian Journal of Chemical Engineering* **73**, 868.
- Guay, M., R. Dier, J. Hahn and J. McLellan (2005). Effect of nonlinearity on linear quadratic regulator performance. *Journal of Process Control* **15**, 113 – 124.
- Gupta, V.K. and Bhatia S.K. (1991). Solution of cyclic profiles in catalytic reactor operation with periodic flow reversal. *Computers and Chemical Engineering* **15**(4), 229 – 237.

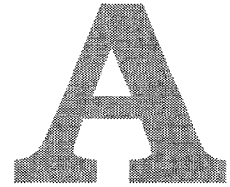
- Hanczyc, E.M. and A. Palazoglu (1995). Sliding mode control of nonlinear distributed parameter chemical processes. *Industrial and Engineering Chemistry Research* **34**, 557 – 566.
- Harris, K.R., M.C. Colantonio and A. Palazoglu (2000). On the computation of a nonlinearity measure using functional expansions. *Chemical Engineering Science* **55**, 2393 – 2400.
- Harville, D.A. (1997). *Matrix Algebra form a Statistician's Perspective*. Springer-Verlag. New York.
- Hayes, R.E. (2004). Catalytic solutions for fugitive methane emissions in the oil and gas sector. *Chemical Engineering Science* **59**(19), 4073 – 4080.
- Hayes, R.E. and S.T. Kolaczkowski (1997). *Introduction to Catalytic Combustion*. Gordon and Breach Science Publishers. UK.
- Helbig, A., W. Marquardt and F. Allgower (2000). Nonlinearity mesures: Definition, computation and applications. *Journal of Process Control* **10**, 113 – 123.
- Hernjak, N. and F. J. Doyle III (2003). Correlation of process nonlinearity with closed-loop disturbance rejection. *Industrial and Engineering Chemistry Research* **42**, 4611 – 4619.
- Hudon, N., M. Perrier, M. Guay and D. Dochain (2005). Adaptive extremum seeking control of non-isothermal tubular reactor with unknown kinetics. *Computers and Chemical Engineering* **29**, 839 – 849.
- Jeffrey, A. (2003). *Applied Partial Differential Equations: An Introduction*. Academic Press.
- Khalil, H.K. (1996). *Nonlinear Systems*. 2 ed.. Prentice-Hall, Inc.
- Kihas, D and H.J. Marquez (2004). Computing the distance between a nonlinear model and its linear approximation: an \mathcal{L}_2 approach. *Computers and Chemical Engineering* **28**, 2659 – 2666.

- Kushwaha, A. (2003). Parametric study of a catalytic flow reversal reactor for combustion of lean methane emissions. Master's thesis. University of Alberta.
- Lapidus, L. (1962). *Digital Computation for Chemical Engineers*. McGraw Hill Inc.
- Levenspiel, O. (1998). *Chemical Reaction Engineering*. Wiley.
- Litto, R., R.E. Hayes, H. Sapoundjiev, A. Fuxman, F. Forbes, B. Liu and F. Bertrand (2006). Optimization of a flow reversal reactor for the catalytic combustion of lean methane mixtures. *Catalysis Today* **117**(4), 536 – 542.
- Maciejowski, J.M. (2001). *Predictive Control: with Constraints*. Prentice-Hall, Inc.
- Marin, P., M.A.G. Hebia, S. Ordonez and F.V. Diez (2005). Combustion of methane lean mixtures in reverse flow reactors: Comparison between packed bed and structured catalyst beds. *Catalysis Today* **105**, 701 – 708.
- Marquez, H.J. (2003). *Nonlinear Control Systems: Analysis and Design*. John Wiley and Sons, Inc.. Hoboken, New Jersey.
- Matros, Y. SH. and G. A. Bunimovich (1996). Reverse-flow operation in fixed bed catalytic reactors. *Catalysis Reviews - Science and Engineering* **38**(1), 1 – 68.
- Matros, Y.S. (1989). *Catalytic Processes Under Unsteady State Conditions*. Elsevier. Amsterdam.
- Mattheij, R.M.M., S.W. Rienstra and J.H.M. ten Thije Boonkkamp (2005). *Partial Differential Equations*. SIAM.
- Moore, S., P. Freund, P. Riemer and A. Smith (June 1998). Abatement of methane emissions. In: *IEA Greenhouse Gas R&D Programme*.
- Morton, K.W. and D.F. Mayers (1994). *Numerical Solution of Partial Differential Equations*. Cambridge University Press.
- Nikolaou, M. (1993). When is nonlinear dynamic modeling necessary. In: *Proc. of American Control Conf.*. pp. 1067 – 1071.

- Nikolaou, M. and P. Misra (2003). Linear control of nonlinear processes: Recent developments and future directions. *Computers and Chemical Engineering* **27**, 1043 – 1059.
- Ogunnaike, B.A., R.K. Pearson and F. J. Doyle III (1993). Chemical process characterization: With applications in the rational selection of control strategies. In: *2nd European Control Conference (ECC)*. Groningen, The Netherlands. pp. 1067 – 1071.
- Ramkrishna, D. and N. R. Amundson (1985). *Linear Operator Methods in Chemical Engineering with Applications to Transport and Chemical Reaction Systems*. Prentice-Hall, Inc.
- Ray, W. H. (1981). *Advanced Process Control*. McGraw Hill Inc.
- Salomons, S., R.E. Hayes, M. Poirier and H. Sapoundjiev (2004). Modelling a reverse flow reactor for the catalytic combustion of fugitive methane emissions. *Computers and Chemical Engineering* **28**, 1599 – 1610.
- Sapundzhiev, C., G. A. Bunimovich, V.I. Drobyshovich, G. Grozev, L.V. Yausheva, Y.S. Matros and D. Elenkov (1988). Effect of heat loss on operation of reactors with periodic reverse gas feed. *Theoretical Foundations of Chemical Engineering* **22**(3), 258 – 263.
- Sapundzhiev, C., G. Grozev and D. Elenkov (1990). Influence of geometric and thermophysical properties of reaction layer on sulphur dioxide oxidation in transient conditions. *Chemical Engineering Technology* **13**, 131 – 135.
- Schweickhardt, T. and F. Allgower (2004). *The Integration of Process Design and Control*. Chap. Quantitative Nonlinearity Assessment - An Introduction to Nonlinearity Measures, pp. 76 – 95. Elsevier B.V.
- Schweickhardt, T. and F. Allgower (2006). Good or bad - when is plant nonlinearity an obstacle for control?. In: *International Symposium on Advanced Control of Chemical Processes (ADCHEM)* (F. J. Doyle III, J.O. Trierweiler and A.R. Secchi, Eds.). Vol. 2. pp. 1009 – 1014.

- Seborg, D.E., T.F. Edgar and D.A Mellichamp (1989). *Process Dynamics and Control*. John Wiley and Sons, Inc.
- Shang, H. (2002). Characteristics-Based Control of Distributed Parameter Systems. PhD thesis. University of Alberta. Edmonton, Alberta, Canada.
- Shang, H., J.F. Forbes and M. Guay (2004). Model predictive control for quasilinear hyperbolic distributed parameter systems. *Industrial and Engineering Chemistry Research* **43**(9), 2140 – 2149.
- Shi, S. and J. Agnew (2006). Catalytic combustion of coal mine ventilation air methane. *Fuel* **85**(9), 1201 – 1210.
- Smets, I.Y., D. Dochain and J.F. Van Impe (2002). Optimal temperature control of a steady-state exothermic plug-flow reactor. *American Institute of Chemical Engineering Journal* **48**, 279 – 286.
- Soni, A.S. and R.S. Parker (2004). Closed-loop control of fed-batch bioreactors: A shrinking-horizon approach. *Industrial and Engineering Chemistry Research* **43**, 3381 – 3393.
- Stack, A. J. and F. J. Doyle III (1995). A measure for control relevant nonlinearity. In: *Proceedings of the American Control Conference, 21-23 June*. pp. 2200 – 2204.
- Stack, A. J. and F. J. Doyle III (1997a). Application of control-law nonlinearity measure to chemical reactor analysis. *American Institute of Chemical Engineering Journal* **43**(2), 425 – 439.
- Stack, A. J. and F. J. Doyle III (1997b). The optimal control structure: An approach to measuring control-law nonlinearity. *Computers and Chemical Engineering* **21**(9), 1009 – 1019.
- Sun, D. and K. Hoo (2000). Non-linearity measures for a class of siso non-linear systems. *International Journal of Control* **73**(1), 29 – 37.

Van de Beld, L. and K.R. Westerterp (1996). Air purification in a reverse-flow reactor: Model simulations vs. experiments. *American Institute of Chemical Engineering Journal* **42**(4), 1139 – 1148.



Appendix A

A.1 Mathematical Model: Parameters

Table A.1: Model Parameters used in the Heterogeneous Model of the Catalytic Reactor

Monolith Sections:		
Parameter	Expression or Value	Units
$D_{r,eff}$	0	$m^2 \cdot s^{-1}$
$D_{a,eff}$	$\epsilon \left(D_{AB} + \frac{(vD_H)^2}{196D_{AB}} \right)$	$m^2 \cdot s^{-1}$
$k_{rf,eff}$	$k_s G$	$W \cdot m^{-1} \cdot K^{-1}$
$k_{af,eff}$	$k_s(1 - \epsilon)$	$W \cdot m^{-1} \cdot K^{-1}$
$k_{rs,eff}$	0	$W \cdot m^{-1} \cdot K^{-1}$
$k_{as,eff}$	$\rho_f C p_f \left(\alpha + \frac{(vD_H)^2}{196\alpha} \right)$	$W \cdot m^{-1} \cdot K^{-1}$
G	0.2	--

Table A.1: Continuation

Monolith Sections:

Parameter	Expression or Value	Units
D_{AB}	$9.86 \times 10^{-10} T_f^{1.75}$	$m^2 \cdot s^{-1}$
D_H	0.00216	m
ϵ	0.75	–
L_C	$\frac{D_H v_s}{(Pe_r)_m}$	1
a_v	$\frac{4\epsilon}{D_H}$	$m^2 \cdot m^{-3}$
k_m	$\frac{D_H v_s}{(Pe_r)_m}$	1
C_s	$\frac{P}{R_g T_s}$	$mol \cdot m^{-3}$
Cp_s	1020	$J \cdot kg^{-1} \cdot K^{-1}$
ρ_s	1683	$kg \cdot m^{-3}$
k_s	1.46	$W \cdot m^{-1} \cdot K^{-1}$
k_m	0	$m \cdot s^{-1}$
h	$\frac{k_f}{D_H} (2.977[1 + 3.6(Gz)^{0.5} \exp(-\frac{50}{Gz})])$	$W \cdot m^{-2} \cdot K^{-1}$

Packed-Bed Sections:

Parameter	Expression or Value	Units
$D_{r,eff}$	$\frac{D_H v_s}{(Pe_r)_m}$	$m^2 \cdot s^{-1}$
$D_{a,eff}$	$\frac{D_H v_s}{(Pe_a)_m}$	$m^2 \cdot s^{-1}$
$(Pe_r)_m$	$[0.1 + \frac{0.66\epsilon}{ReSc}]^{-1}$	–
$(Pe_a)_m$	$[\frac{0.73\epsilon}{ReSc} + \frac{0.5}{1+(9.7\epsilon/ReSc)}]^{-1}$	–
$(Pe_r)_h$	$[0.1 + \frac{0.66\epsilon}{RePr}]^{-1}$	–
$(Pe_a)_h$	$[\frac{0.73\epsilon}{RePr} + \frac{0.5}{1+(9.7\epsilon/RePr)}]^{-1}$	–
Pr	$\frac{C_{p,f}\mu}{k_f}$	–
Gz	$\frac{D_H RePr}{z}$	–
Re	$\frac{v_s D_C \rho_f}{\mu}$	–
Sc	$\frac{\mu}{\rho_f D_{AB}}$	–
C_s	$\frac{P}{R_g T_s}$	$mol \cdot m^{-3}$
D_H	$\frac{D_R}{(3D_R/2D_C)(1-\epsilon)+1}$	m

Table A.1: Continuation

Packed-Bed Sections:

Parameter	Expression or Value	Units
D_C	0.0075	m
L_C	0.00125	m
ϵ	0.51	—
τ	2	—
a_v	$\frac{6(1-\epsilon)}{D_C}$	$m^2 \cdot m^{-3}$
k_m	$\frac{D_{AB}}{D_C} (2 + 1.1Sc^{1/3}Re^{0.6})$	$m \cdot s^{-1}$
h	$\frac{k_f}{D_C} (2 + 1.1Pr^{1/3}Re^{0.6})$	$W \cdot m^{-2} \cdot K^{-1}$
$k_{rf,eff}$	$\frac{v_s D_C \rho_f C_{p,f}}{(Pe_r)_h}$	$W \cdot m^{-1} \cdot K^{-1}$
$k_{af,eff}$	$\frac{v_s D_C \rho_f C_{p,f}}{(Pe_a)_h}$	$W \cdot m^{-1} \cdot K^{-1}$
$k_{rs,eff}$	$\frac{2k_f(1-\epsilon)^{0.5}}{1-(k_f/k_s)B} \left(\frac{1-(k_f/k_s)B}{(1-B(k_f/k_s))^2} \ln\left(\frac{k_s}{Bk_f}\right) - \frac{B+1}{2} - \frac{B-1}{1-(k_f/k_s)B} \right)$	$W \cdot m^{-1} \cdot K^{-1}$
$k_{as,eff}$	$k_{rs,eff}$	$W \cdot m^{-1} \cdot K^{-1}$
B	$1.2 \left(\frac{1-\epsilon}{\epsilon}\right)^{1/0.9}$	—
ρ_s	1240	$kg \cdot m^{-3}$
Cp_s	1020	$J \cdot kg^{-1} \cdot K^{-1}$
k_s	0.5	$W \cdot m^{-1} \cdot K^{-1}$
r_p	5×10^{-9}	m
$-R_{CH_4}$	$k_\infty C_s Y_s$	$mol \cdot s^{-1} \cdot m^{-3}$
ΔH_r	$-806.9 + 1.586 \times 10^{-2} T_s - 8.485 \times 10^{-6} T_s^2 - 3.963 \times 10^{-9} T_s^3 + 2.16 \times 10^{-12} T_s^4$	$kJ \cdot mol^{-1}$
η	$\frac{\tanh(\phi)}{\phi}$	—
ϕ	$L_C \left(\frac{k_R}{D_{eff}}\right)^{1/2}$	—
D_{eff}	$\frac{D_K \epsilon}{\tau}$	$m^2 \cdot s^{-1}$
D_K	$97r_p \left(\frac{T_f}{M}\right)^{0.5}$	$m^2 \cdot s^{-1}$
$k_{inf ty}$	$1.35 \times 10^e \exp\left(\frac{-6543}{T_s}\right)$	$mol \cdot s^{-1}$

Table A.1: Continuation

Insulation:

Parameter	Expression or Value	Units
ρ_s	1240	$kg \cdot m^{-3}$
Cp_s	1020	$J \cdot kg^{-1} \cdot K^{-1}$
k_s	0.5	$W \cdot m^{-1} \cdot K^{-1}$
h_e	3	$W \cdot m^{-2} \cdot K^{-1}$

Stainless steel wall:

ρ_s	7800	$kg \cdot m^{-3}$
Cp_s	460	$J \cdot kg^{-1} \cdot K^{-1}$
k_s	14.3	$W \cdot m^{-1} \cdot K^{-1}$

Open Sections:

$D_{r,eff}$	$100 \times D_{AB}$	$m^2 \cdot s^{-1}$
$D_{a,eff}$	$10 \times D_{AB}$	$m^2 \cdot s^{-1}$
D_H	D_R	m
ϵ	1	–
$k_{rf,eff}$	$100k_f$	$W \cdot m^{-1} \cdot K^{-1}$
$k_{af,eff}$	$10 \times k_f$	$W \cdot m^{-1} \cdot K^{-1}$
k_m	0	$m \cdot s^{-1}$
h	0	$W \cdot m^{-2} \cdot K^{-1}$

Fluid Phase:

v	$\frac{v_s}{\epsilon}$	$m \cdot s^{-1}$
C_f	$\frac{\epsilon P}{R_g T_f}$	$mol \cdot m^{-3}$
ρ_f	$\frac{MP}{R_g T_f}$	$kg \cdot m^{-3}$
μ	$7.701 \times 10^{-6} + 4.166 \times 10^{-8} T_f - 7.531 \times 10^{-12} T_f^2$	$Pa \cdot s$
\overline{M}	0.02896	$kg \cdot mol^{-1}$
k_f	$0.01679 + 5.073 \times 10^{-5} T_f$	$W \cdot m^{-1} \cdot K^{-1}$
α	$\frac{k_f}{\rho_f C_{p,f}}$	–

Table A.2: Model Parameters used in the Pseudo-Homogeneous Model of the Catalytic Reactor

Parameter	Value	Units
k_∞	1.35E5	s^{-1}
ϵ	0.51	
E	54,400	$kg \cdot m^2 \cdot s^{-2} \cdot mol^{-1}$
R_g	8.314	$kg \cdot m^2 \cdot s^{-2} \cdot mol^{-1} \cdot K^{-1}$
ρ_s	1240	$kg \cdot l^{-1}$
Cp_f	1066	$J \cdot kg^{-1} \cdot K^{-1}$
Cp_s	1020	$J \cdot kg^{-1} \cdot K^{-1}$
ΔH_r	-802E3	$J \cdot mol^{-1}$
P	101325	$kg \cdot m^{-1} s^{-2}$
\bar{M}	0.02896	$kg \cdot mol^{-1}$
μ_{eff}	1	
L	3	m

Table A.3: Model Coefficients

a	a_0	a_1	a_2	a_3	a_4	a_{11}	a_{12}
T_{max}	965.88	820.391	-307.538	-235.504	400.918	189.04	-255.868
X	65.0574	52.5745	-23.7093	-26.5325	32.4804	-8.7747	-8.6759
a	a_{13}	a_{14}	a_{22}	a_{23}	a_{24}	a_{33}	a_{34}
T_{max}	-131.974	157.156	6.555	-156.524	-189.822	-50.857	-85.366
X	-10.0481	0.5321	-5.1499	-12.9644	-5.6211	-4.3463	-5.2924
a	a_{44}	a_{112}	a_{113}	a_{114}	a_{221}	a_{223}	a_{224}
T_{max}	-248.346	157.156	6.555	-156.524	-189.822	-50.857	-85.366
X	-29.6010	0.5321	-5.1499	-12.9644	-5.6211	-4.3463	-5.2924
a	a_{331}	a_{332}	a_{334}	a_{441}	a_{442}	a_{443}	a_{1122}
T_{max}	-147.587	-17.931	-29.869	-16.1864	1.597	32.481	-107.967
X	-8.3026	-0.9875	0.2558	-0.3859	4.8699	5.8887	-6.9788
a	a_{1133}	a_{1144}	a_{2233}	a_{2244}	a_{3344}		
T_{max}	-118.639	242.276	44.307	44.828	-11.444		
X	-9.5791	29.7057	9.0768	-0.093	-0.6428		

B

Appendix B

B.1 Mathematical Background

Definition B.1.1 [*Linear Vector Space*] A linear vector space V is a collection of elements called vectors on which two fundamental operations, called sum and scalar multiplication, are defined. V is called linear space if these operations satisfy the following properties for $u, v, w \in V$ and $\alpha, \beta \in \mathbb{K}$:

1. *Commutativity:*

$$u + v = v + u.$$

2. *Associativity:*

$$(u + v) + w = u + (v + w)$$

$$\alpha(\beta u) = (\alpha\beta)u.$$

3. *Distributivity:*

$$(\alpha + \beta)u = \alpha u + \beta u$$

$$\alpha(u + v) = \alpha u + \alpha v.$$

4. There exists a zero element $0 \in V$ such that $u + 0 = u$.
5. For every element $u \in V$ there exists an additive inverse $v \in V$ such that: $u + v = 0$; v is denoted $-u$. Subtraction of a vector v from u , denoted $u - v$, is defined as $u - v = u + (-v)$.
6. Scalar multiplication is such that $1u = u \quad \forall u \in V$, where "1" is the unity element in \mathbb{K} .

A linear vector space is called real vector space if $\mathbb{K} = \mathbb{R}$, where \mathbb{R} is the field of real numbers. If $\mathbb{K} = \mathbb{C}$, where \mathbb{C} is the field of complex numbers, then the vector space is called complex vector space.

Definition B.1.2 [Normed Space] Given a linear space V , a norm $\|\cdot\|$ is a function from V to \mathbb{R} with the following properties.

1. $\|v\| \geq 0$ for any $v \in V$, and $\|v\| = 0$ if and only if $v = 0$;
2. $\|\alpha v\| = |\alpha| \|v\|$ for any $v \in V$ and $\alpha \in \mathbb{K}$;
3. $\|u + v\| \leq \|u\| + \|v\|$ for any $u, v \in V$.

The space V equipped with the norm $\|\cdot\|$ is called normed space.

Definition B.1.3 [Banach Space]

In the finite dimensional space \mathbb{R}^d , any Cauchy sequence is convergent. However, in a general infinite-dimensional space, a Cauchy sequence may fail to converge.

Definition B.1.4 [Inner Product] Let V be a linear space over $\mathbb{K} = \mathbb{R}$ or \mathbb{C} . An inner product (\cdot, \cdot) is a function from $V \times V$ to \mathbb{K} with the following properties.

1. For any $u \in V$, $(u, u) \geq 0$ and $(u, u) = 0$ if and only if $u = 0$.
2. For any $u, v \in V$, $(u, v) = \overline{(v, u)}$.
3. For any $u, v, w \in V$, and $\alpha, \beta \in \mathbb{K}$, $(\alpha u + \beta v, w) = \alpha(u, w) + \beta(v, w)$.

The space V together with the inner product (\cdot, \cdot) is called an inner product space.

Definition B.1.5 [Hilbert Space] Let V be a linear space equipped with the inner product $\langle \cdot, \cdot \rangle$. V is called Hilbert space if it is a Banach space under the norm induced by the inner product.

Definition B.1.6 [L^p Space] For $p \in [1, \infty)$, $L^p(0, 1)$ is the linear space of measurable functions $x : [0, 1] \rightarrow \mathbb{R}$ such that

$$\|x\|_p = \left(\int_0^1 |x(z)|^p dz \right)^{1/p} < \infty \quad (\text{B.1})$$

For $p \in [1, \infty]$, $L^p(0, 1)$ is a Banach space.

Definition B.1.7 [Linear Operator] A linear operator maps elements of a linear space V into elements of a space W , i.e. $L : V \rightarrow W$. The linear operator L further satisfies the conditions

$$L(u + v) = L(u) + L(v) \quad \forall u, v \in V \quad (\text{B.2})$$

$$L(\alpha u) = \alpha L(u) \quad \forall \alpha \in \mathbb{K}, u \in V \quad (\text{B.3})$$

Definition B.1.8 [Bounded Operator] An operator L is called bounded if there exists a constant $\gamma \geq 0$ such that

$$\|Lu\|_W \leq \gamma \|u\|_V \quad \forall u \in V. \quad (\text{B.4})$$

where V and W are two normed linear spaces.

Definition B.1.9 [Adjoint Operator] Let L be a linear operator on a Hilbert space \mathcal{H} . Then L^* , called its adjoint operator, satisfies the relation

$$\langle Lx, y \rangle = \langle x, L^*y \rangle$$

for every pair of elements $x, y \in \mathcal{H}$. If $L^* = L$, we say that L is a self adjoint operator. The notion of an adjoint operator is a generalization of the matrix transpose to infinite-dimensional spaces.

Definition B.1.10 [Coercive Operator] A self-adjoint operator L is called coercive if there exist $c \geq 0$ such that

$$\langle Lx, x \rangle \geq c \|x\|^2.$$

Example: for finite dimensional systems, the quadratic form $Q(x) = x^T Ax$ is coercive iff A is positive definite. If A is positive definite, then it can be shown that $x^T Ax \geq \lambda_{\min}(A)x^T x$

B.2 Exponential Stability of a Linear Operator

The exponential stability of the operator

$$A = \alpha I \frac{d.}{dz} + \beta I \quad (\text{B.5})$$

can be probed by using the Lyapunov criterion 4.4.1.

To show the existence of a positive definite solution of the Lyapunov equation, we begin by replacing A and $P = p(z)I$ into (4.12) to obtain

$$pI \left(\alpha I \frac{d.}{dz} + \beta I \right) + \left(\alpha I \frac{d.}{dz} + \beta I \right)^* pI + I = 0 \quad (\text{B.6})$$

By the adjoint property:

$$(A + B)^* = A^* + B^*, \quad (\text{B.7})$$

we can write

$$p\alpha I \frac{d.}{dz} + p\beta I + \left(\alpha \frac{d.}{dz} \right)^* pI + \beta^* pI + I = 0 \quad (\text{B.8})$$

$$p\alpha I \frac{d.}{dz} + \left(\alpha \frac{d.}{dz} \right)^* pI + 2\beta pI + I = 0 \quad (\text{B.9})$$

By the adjoint property:

$$(AB)^* = B^* A^* \quad (\text{B.10})$$

we can write

$$\left(\alpha I \frac{d.}{dz} \right)^* = \left(\frac{d.}{dz} \right)^* \alpha^* pI \quad (\text{B.11})$$

$$= \left(\frac{d.}{dz} \right)^* \alpha pI \quad (\text{B.12})$$

The adjoint of the operator (d/dz) can be obtained as follows:

Let $X = L_2(0, 1)$ and consider the operator A given by

$$(Ax) = \frac{d}{dz} x \quad (\text{B.13})$$

where $D(A) = \{x \in L^2(0, 1) | x \text{ is absolutely continuous with } dx/dz \in L^2(0, 1), x(0) = 0\}$. By definition, the adjoint is given by $\langle Ax, y \rangle = \langle x, y^* \rangle = \langle x, A^*y \rangle$, where $\langle \cdot, \cdot \rangle$ represents the inner product,

$$\begin{aligned} \langle Ax, y \rangle &= \int_0^1 \frac{dx}{dz}(z)y(z)dz = [x(z)y(z)]_0^1 - \\ &\int_0^1 x(z)\frac{dy}{dz}(z)dz = x(1)y(1) - \int_0^1 x(z)\frac{dy}{dz}(z)dz \end{aligned} \quad (\text{B.14})$$

Equation (B.14) is obtained from the following general mathematical equation

$$f(b)g(b) - f(a)g(a) = \int_a^b \frac{d}{dz}(f(z)g(z))dz \quad (\text{B.15})$$

$$= \int_a^b \frac{df(z)}{dz}g(z)dz + \int_a^b f(z)\frac{dg(z)}{dz}dz. \quad (\text{B.16})$$

Equation (B.14) can be written in the form $\langle x, y^* \rangle$ if and only if $y(1) = 0$ and $A^*y = -dy/dz$ with $D(A^*) = \{y \in L^2(0, 1) | y \text{ is absolutely continuous with } dy/dz \in L^2(0, 1), y(1) = 0\}$. By replacing $A^* = -d/dz$ in equation (B.9), we obtain

$$p\alpha I \frac{d}{dz} - \frac{d(\alpha p I)}{dz} + 2\beta p I + I = 0 \quad (\text{B.17})$$

By the chain rule, we obtain equation (4.36)

$$\frac{d(\alpha p)}{dz} = 2\beta p + 1, \quad p(1) = 0$$

B.3 LQ-Feedback Controller Formulation

The solution of the LQ-control problem in (4.38) can be obtained by finding the positive self-adjoint operator $Q_o \in \mathcal{L}(\mathcal{H})$ which solves the operator Riccati equation (4.21).

To solve the Riccati equation, we look for a solution $Q_o = q(z)I \in \mathcal{L}(\mathcal{H})$. We write

$$A = \left(\alpha I \frac{d}{dz} + \beta I \right) \quad (\text{B.18})$$

and

$$Q_o A = (qI) \left(\alpha I \frac{d}{dz} + \beta I \right) \quad (\text{B.19})$$

Then, we write

$$A^* = \left(\alpha I \frac{d.}{dz} + \beta I \right)^* \quad (\text{B.20})$$

and

$$A^* Q_o = \left(\alpha I \frac{d.}{dz} + \beta I \right)^* (q I) \quad (\text{B.21})$$

By the adjoint properties:

$$(A + B)^* = A^* + B^* \quad (\text{B.22})$$

$$(AB)^* = B^* A^* \quad (\text{B.23})$$

we can write

$$A^* Q_o = \left(\alpha I \frac{d.}{dz} \right)^* (q I) + \beta^* q I \quad (\text{B.24})$$

$$= \left(\frac{d.}{dz} \right)^* (\alpha I)^* (q I) + \beta^* q I \quad (\text{B.25})$$

Since $\alpha^* = \alpha$ and $\beta^* = \beta$, we obtain

$$A^* Q_o = \left(\frac{d.}{dz} \right)^* (\alpha q I) + \beta q I \quad (\text{B.26})$$

The adjoint of the operator $A = (d./dz)$ was obtained in Section B.2 and is given by:

$$(A^* x) = -\frac{d}{dz} x \quad (\text{B.27})$$

where $D(A^*) = \{x \in L^2(0, 1) | x \text{ is absolutely continuous with } dx/dz \in L^2(0, 1), x(1) = 0\}$.

By combining $Q_o A + A^* Q_o$, we obtain

$$Q_o A + A^* Q_o = (\alpha q I) \frac{d.}{dz} - \frac{d.}{dz} (\alpha q I) + 2\beta q I \quad (\text{B.28})$$

By the chain rule, we obtain

$$Q_o A + A^* Q_o = -\frac{d.}{dz} (\alpha q I) + 2\beta q I. \quad (\text{B.29})$$

Combining equation (B.29) with

$$C^* C = w^2 I \quad (\text{B.30})$$

and

$$Q_o B R^{-1} B^* Q_o = q \gamma r^{-1} \gamma q I \quad (\text{B.31})$$

leads to the result in equation (4.38):

$$\frac{d(\alpha q)}{dz} = 2\beta q + w^2 - q \gamma r^{-1} \gamma q. \quad (\text{B.32})$$

C

Appendix C

C.1 Feedback Control of Hyperbolic PDE Systems

For a hyperbolic PDE system of the form

$$\frac{\partial x}{\partial t} = A \frac{\partial x}{\partial z} + f(x) + g(x)u \quad (\text{C.1})$$

$$u(t, z) = \sum_{j=1}^m b_j(z)u(t) \quad (\text{C.2})$$

$$y = \mathcal{C}h(x) \quad (\text{C.3})$$

$$R(t) = C_1x(z_a, t) + C_2x(z_b, t) \quad (\text{C.4})$$

with a finite set of input and output variables

$$u = [u_1 \cdots u_p]^T \quad (\text{C.5})$$

$$y = [y_1 \cdots y_m]^T \quad (\text{C.6})$$

$$b(z) = [(H(z - z_1) - H(z - z_2))b_1 \cdots (H(z - z_j) - H(z - z_{m+1}))b_m] \quad (\text{C.7})$$

$$\mathcal{C} = [(H(z - z_1) - H(z - z_2))\mathcal{C}_1 \cdots (H(z - z_j) - H(z - z_{m+1}))\mathcal{C}_m], \quad (\text{C.8})$$

we followed the input/output linearizing feedback technique proposed in Christofides (2000).

To formulate an input/output linearizing controller, the first step is to compute the characteristic index of the system (Khalil, 1996; Marquez, 2003). For hyperbolic PDEs, Christofides (2000) defined the characteristic index of the output y_j with respect to the input u_j is calculated as the smallest integer σ_j for which

$$\mathcal{C}_j L_g \left(\sum_{i=1}^n \frac{\partial x_i}{\partial z} L_{a_i} + L_f \right)^{\sigma_j - 1} h(x) b_j(z) \neq 0 \quad (\text{C.9})$$

where a_j denotes the j^{th} column vector of the matrix A . For the tubular reactor in (5.51) and (5.52), the resulting index is 1. Therefore, we should check that the zero dynamics of the system (*i.e.* dynamic of the states that are unobservable from the output) are stable. As discussed in Section 2.9.2, equation (5.51) has a stable dynamic behavior around any equilibrium profile.

Christofides (2000) proposed a distributed state feedback law that enforces the input-output response of the closed-loop system. We modify the controller to add integral action in the form of

$$\dot{\varphi}_j = e_j \quad j = 1, \dots, m \quad (\text{C.10})$$

$$e_j = \mathcal{C}_j(x - x^{ss}). \quad (\text{C.11})$$

For the tubular reactor given in (5.51) and (5.52), the model states are shifted so that the zero profile corresponds to the equilibrium profile of the system:

$$\frac{\partial \tilde{x}_1}{\partial t} + v \frac{\partial \tilde{x}_1}{\partial z} = -ke \left(\frac{-\alpha_1}{\tilde{x}_2 + x_2^{ss}} \right) (\tilde{x}_1 + x_1^{ss}) - \left(-ke \left(\frac{-\alpha_1}{x_2^{ss}} \right) x_1^{ss} \right) \quad (\text{C.12})$$

$$\frac{\partial \tilde{x}_2}{\partial t} + v \frac{\partial \tilde{x}_2}{\partial z} = \alpha_2 ke \left(\frac{-\alpha_1}{\tilde{x}_2 + x_2^{ss}} \right) (\tilde{x}_1 + x_1^{ss}) - \alpha_3 (\tilde{x}_2 - \tilde{u}) - \left(\alpha_2 ke \left(\frac{-\alpha_1}{x_2^{ss}} \right) x_1^{ss} \right) \quad (\text{C.13})$$

$$\text{Initial and boundary conditions} \quad \begin{cases} x_1(t, 0) = x_{1,in} & x_1(0, z) = x_{1,0}(z) \\ x_2(t, 0) = x_{2,in} & x_2(0, z) = x_{2,0}(z) \end{cases} \quad (\text{C.14})$$

where

$$\tilde{x}_1 = x_1 - x_1^{ss} \quad (\text{C.15})$$

$$\tilde{x}_2 = x_2 - x_2^{ss} \quad (\text{C.16})$$

$$\tilde{u} = u - u^{ss} \quad (\text{C.17})$$

The nonlinear controller for the tubular reactor becomes

$$\tilde{u}_j(t) = \frac{1}{\mathcal{C}_j g_2(\tilde{x})} \left[-\gamma \varphi_j - \gamma \mathcal{C}_j (\tilde{x}_2 - \tilde{x}_2^{ss}) - \mathcal{C}_j \left(a_2 \frac{\partial \tilde{x}_2}{\partial z} + f_2(\tilde{x}) \right) \right] \quad (\text{C.18})$$

where

$$a_2 = -v \quad (\text{C.19})$$

$$g_2(\tilde{x}) = \alpha_3 \quad (\text{C.20})$$

$$f_2(\tilde{x}) = \alpha_2 k \left(\exp\left(\frac{-\alpha_1}{\tilde{x}_2 + x_2^{ss}}\right) (\tilde{x}_1 - x_1^{ss}) - \exp\left(\frac{-\alpha_1}{x_2^{ss}}\right) x_1^{ss} \right) - \alpha_3 \tilde{x}_2 \quad (\text{C.21})$$

guarantees zero offset and exponentially stable closed-loop dynamics. The closed-loop behavior for each input/output pair is tuned to $\gamma = 1$ which leads to closed-loop eigenvalues located at $\tau = -0.5 \pm 0.866i$. The resulting controller for the tubular reactor in (5.51) and (5.52) with linearized dynamics around an operating (equilibrium) profile is:

$$\tilde{u}_j(t) = \frac{1}{\mathcal{C}_j d_2(z)} \left[-\gamma \varphi_j - \gamma \mathcal{C}_j (\tilde{x}_2 - \tilde{x}_2^{ss}) - \mathcal{C}_j \left(a_2 \frac{\partial \tilde{x}_2}{\partial z} + b_2(z) \tilde{x}_1 + c_2(z) \tilde{x}_2 \right) \right] \quad (\text{C.22})$$

where

$$a_2 = -v \quad (\text{C.23})$$

$$b_2(z) = \alpha_2 k \exp\left(\frac{-\alpha_1}{x_2^{ss}}\right) \quad (\text{C.24})$$

$$c_2(z) = \alpha_2 k \exp\left(\frac{-\alpha_1}{x_2^{ss}}\right) \left(\frac{\alpha_1}{(x_2^{ss})^2} \right) (-x_1^{ss}) - \alpha_3 \quad (\text{C.25})$$

$$d_2(z) = \alpha_3 \quad (\text{C.26})$$

The integral action in (C.22) and (C.18) is obtained from the solution of

$$\dot{\varphi}_j = \mathcal{C}_j (x_2 - x_2^{ss}) \quad j = 1, \dots, m \quad (\text{C.27})$$